Universitat Autònoma de Barcelona

Local Pro-inflammatory or Anti-inflammatory Microenvironments induce alterations in the Neuron-Microglia "On/Off" signalling after Facial Nerve Axotomy

Ariadna Regina Gómez López

ADVERTIMENT. L'accés als continguts d'aquesta tesi queda condicionat a l'acceptació de les condicions d'ús establertes per la següent llicència Creative Commons: http://cat.creativecommons.org/?page_id=184

ADVERTENCIA. El acceso a los contenidos de esta tesis queda condicionado a la aceptación de las condiciones de uso establecidas por la siguiente licencia Creative Commons: http://es.creativecommons.org/blog/licencias/

WARNING. The access to the contents of this doctoral thesis it is limited to the acceptance of the use conditions set by the following Creative Commons license: https://creativecommons.org/licenses/?lang=en

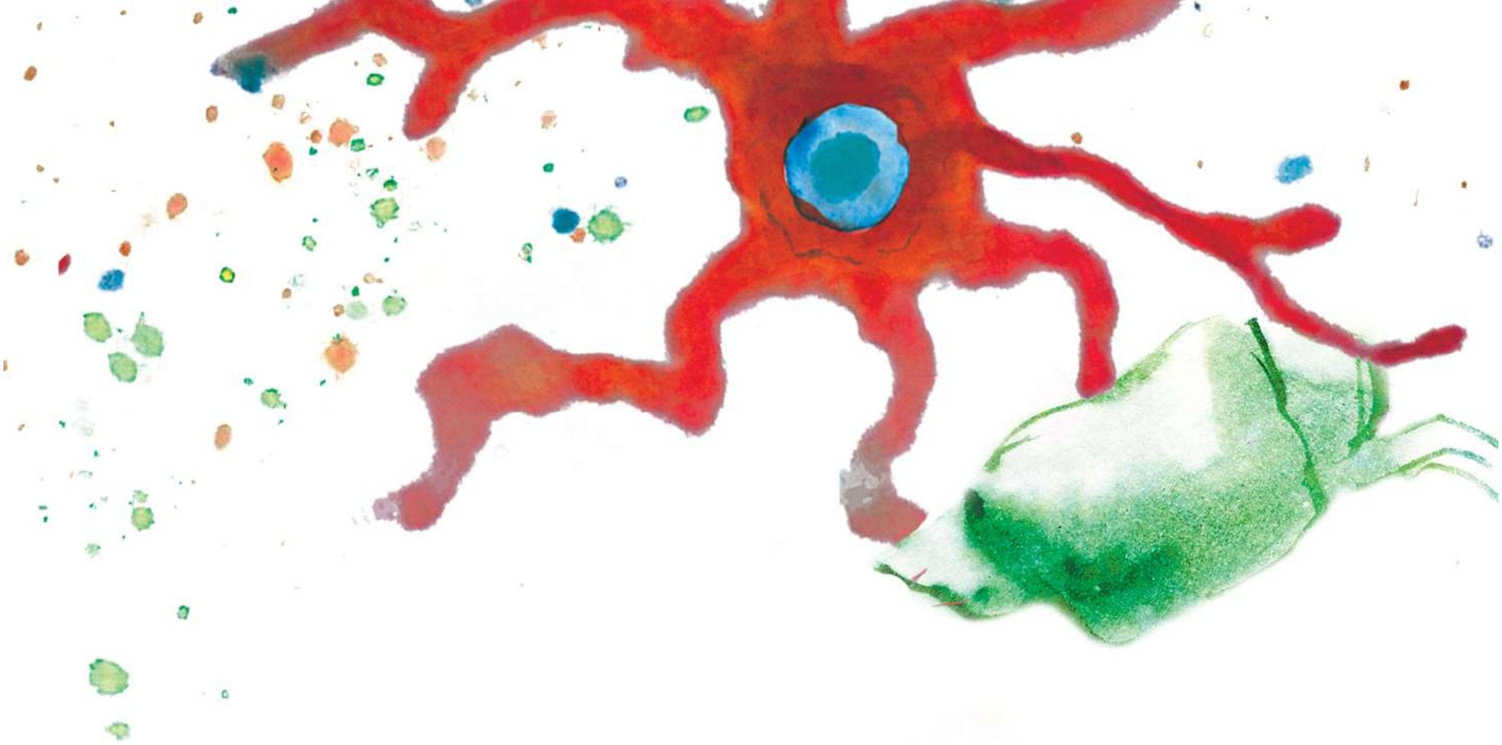

PhD Thesis

LOCAL PRO-INFLAMMATORY OR ANTI-INFLAMMATORY MICROENVIRONMENTS INDUCE ALTERATIONS IN THE NEURON-MICROGLIA "ON/OFF" SIGNALLING AFTER FACIAL NERVE AXOTOMY

Ariadna Regina Gómez López
2022

UAB
Universitat Autònoma
de Barcelona

INc
Institut de
Neurociències

Local Pro-inflammatory or Anti-inflammatory Microenvironments induce alterations in the Neuron-Microglia "On/Off" signalling after Facial Nerve Axotomy

A dissertation to obtain the degree of Doctor in Neuroscience submitted by

Ariadna Regina Gómez López

This work has been done at the "Unitat d'Histologia Mèdica de la Facultat de Medicina" of "Universitat Autònoma de Barcelona" under the direction of Dr. Berta González and Dr. Gemma Manich.

Dr. Berta González de Mingo
Tesis Supervisor and Tutor

Dr. Gemma Manich Raventós
Tesis Supervisor

Ariadna Regina Gómez López
PhD Student

Bellaterra 2022

Als meus pares, Carme i Joan
i a la meva germana Selena

A l’Elisabet

Per ser-hi abans,
per ser-hi ara.
Però no només per això,
sinó per moltes altres coses.

TABLE OF CONTENTS

ABSTRACT......8

I. INTRODUCTION......11

1. Microglia......13

1.1 Origin and differentiation of microglia......13

1.2 Microglial identity and functions in the healthy CNS......15

1.2.1 Transcriptomic profiling: A unique gen signature to identify different subtypes of microglial cells......15

1.2.2 Microglia identity and functions in the developmental CNS......17

1.2.3 Physiological functions of microglia in adult CNS......20

1.3 Microglia in pathological conditions: microglial activation......22

2. On/Off Signalling......28

2.1 CD200-CD200R......30

2.2 CX3CL1-CX3CR1......32

2.3 CD22-CD45......35

2.4 CD47-SIRP-α......36

2.5 TREM2......38

3. Cytokines in the CNS......40

3.1 IL-6 role in CNS and microglial response......42

3.2 IL-10 role in CNS and microglial response......44

4. Facial nerve axotomy model......46

4.1 Microglial and astroglial reaction after FNA......48

4.2 Immune cell infiltration after FNA......50

4.3 GFAP-IL6Tg and GFAP-IL10Tg mice after facial nerve axotomy model......51

II. HYPOTHESIS AND OBJECTIVES......54

III. METHODOLOGY......58

1. Materials and methods......60

1.1 Animals......60

1.2 Construction of GFAP-IL6 fusion gene and production of transgenic mice......60

1.3 Construction of GFAP-IL10 fusion gene and production of transgenic mice......60

1.4 Tissue processing for PCR analysis......60

1.5 Facial nerve axotomy and experimental groups......61

1.6 5’Bromodeoxyuridine injections 61
1.7 Tissue processing for IHC analysis 61
1.8 Single IHC staining 62
1.9 Double and triple IHC..62
1.10 Densitometric analysis 64
1.11 Confocal Microscopy Quantification 65
1.12 Isolation of myelin and fluorescent labelling with pHrodo™ Green STP Ester ..66
1.13 Flow cytometry 66
1.14 Tissue processing for protein analysis 67
1.15 Cytokine analysis 68
1.16 Enzyme-linked adsorbent immunoassay for sTREM2 detection 68
1.17 Statistical analysis 69

IV. RESULTS AND DISCUSSION 71

1. Neuronal-microglial “On/Off” signalling evolution in FNA model 73

1.1 Neuron-microglia “On/Off” expression in the non-lesioned FN.........................74
1.2 Regulation of neuronal-microglial “On/Off” signalling after FNA......................76
1.2.1. Microglia-neuron “Off” signalling protects FMNs during the peak of microgliosis 76
1.2.2. Disruption of microglia-neuron “Off” signalling and appearance of the “On” signalling promote microglial phagocytosis and regulate FMNs death 79
1.2.3 Microglia in clusters show a specific phagocytic phenotype after FNA.......82
1.2.4. “On/Off” signalling in microglia-lymphocyte crosstalk after FNA 84
1.2.5 “On/Off” signalling may affect FMNs repair in the FNA model 85

2. Effects of chronic IL-6 and IL-10 overproduction in neuronal-microglial “On/Off” signalling after FNA 86

2.1 Chronic IL-6, but not IL-10 overproduction alters microglial “On/Off” signalling in homeostasis and after FNA...86
2.2 Chronic IL-6 and IL-10 overproduction only modifies neuronal “Off” CD47 ligand, but no other neuronal “Off” signals were altered after FNA 89
2.3 IL-6 overproduction modifies “Off” signalling present in lymphocytes while IL-10 overproduction does not interfere on it...92

V. CONCLUSIONS 97

VI. BIBLIOGRAPHY **102**

VII. ANNEXES **137**

1. Annex 1: Supplementary Figure 1 139

2. Annex 2: Supplementary Figure 2 140

3. Annex 3: Supplementary Figure 3 141

4. Annex 4 – Article 1: *Alterations in microglial SIRP-α and CD47 signalling modify neuronal survival after Periferal Nerve Injury* 142

5. Annex 5 – Article 2: *Differential Roles of TREM2+ Microglia in Anterograde and Retrograde Axonal Injury Models* 194

6. Annex 6- Article 3: *Evaluation of Myelin Phagocytosis by Microglia/Macrophages in Nervous Tissue Using Flow Cytometry* 220

ABBREVIATIONS

AD	Alzheimer’s disease
ALS	Amyotrophic lateral sclerosis
APP	Amyloid precursor protein
ARM	Activated response microglia
BSA	Bovine serum albumin
CLRs	C-type lectin receptors
CNS	Central Nervous System
DAM	Disease-associated microglia
DAMPs	Damage associated molecular patterns
DAP12	DNAX activation protein of 12kDa
DAPI	4,9,6-diamidino-2-phenylindole
Dpi	Days post-injury
EAE	Experimental autoimmune encephalomyelitis
FMNs	Facial motoneurons
FN	Facial nucleus
FNA	Facial nerve axotomy
GFAP	Glial fibrillary acidic protein
HIV	Human immunodeficiency virus
ICH	Intracerebral haemorrhage
IAP	Integrin-associated protein
IgSF	Immunoglobulin superfamily
IHC	Immunohistochemistry
IL-6	Interleukin-6
IL-10	Interleukin-10
I.p	Intraperitoneally
ITAMs	Immunoreceptor tyrosine-based activation motifs
LDAM	Lipid-droplet-accumulating microglia
LPS	Lipopolysaccharide
MBP	Myelin basic protein

MGnD	Microglia neurodegenerative phenotype
MS	Multiple sclerosis
NAMPs	Neurodegeneration associated molecular patterns
NL	Non-lesioned
P2ry12	P2Y purinoceptor 12
PAM	Proliferative-region-associated microglia
PAMPs	Pathogen associated molecular patterns
PD	Parkinson’s disease
pHH3	Phospho-Histone 3
PRRs	Pattern recognition receptors
RT	Room temperature
SCI	Spinal cord injury
scRNAseq	Single-Cell RNA sequencing
TBI	Traumatic brain injury
TBS	Tris-buffered saline
TL	Tomato lectin
TLRs	Toll-like receptors
WAM	White matter-associated microglia
WT	Wild-type
YS	Yolk sac

ABSTRACT

Microglial cells play a pivotal role during homeostasis and under neuroinflammatory conditions in the central nervous system (CNS). When they detect any disturbance, they rapidly become activated in a process called “microglial activation”. One of the mechanisms involved in microglial activation is the “On/Off” signalling, which consists in the interaction of microglial “Off-receptors” (CD200R, CX3CR1, CD45 and CD47) with their corresponding neuronal ligands (CD200, CX3CL1, CD22 and SIRP-α). Any absence of these interactions, as well as de novo expression of “On” signals like TREM2, trigger microglial activation and phagocytosis. Once activated, microglial response to an injury and this response will be modulated by the microenvironment and the presence of molecules such as cytokines. Research carried out in our group showed that transgenic mice overproducing either pro-inflammatory interleukin (IL)-6 or anti-inflammatory IL-10 (GFAP-IL6Tg and GFAP-IL10Tg) showed reduced or increased facial motoneurons (FMNs) survival after facial nerve axotomy (FNA), respectively, compared to wild-type (WT), together with changes in the microglial activation pattern. Hence, the main goal of this work was to determine if IL-6 or IL-10 overproduction were modifying “On/Off” signalling and triggering differences in microglial activation and neuronal survival after FNA. To address this aim, “On/Off” molecules (CD200-CD200R, CX3CL1-CX3CR1, CD22-CD45, CD47-SIRP-α and TREM2) were analysed by immunohistochemistry and flow cytometry techniques in non-lesioned (NL) and lesioned WT, GFAP-IL6Tg and GFAP-IL10Tg mice. Our results showed that, in steady state, both FMNs and microglia displayed a constitutive expression of “Off” molecules while an inactive TREM2 expression pattern was detected. After FNA, TREM2 and all the “Off” signalling –with the exception of microglial CX3CR1 and CD47– were first upregulated in both FMNs and microglia, protecting injured FMNs. Later, FMNs downregulated “Off” neuronal signals, with the exception of CD47, and showed de novo expression of TREM2 ligands ApoE and Galectin-3. Concomitantly, microglial TREM2 expression peaked and the inhibitory phagocytic receptor SIRP-α was downregulated. Altogether, these changes eased microglial phagocytosis taking place in microglial clusters at the peak of FMNs death. Indeed, expression of “On” and “Off” signals in microglial clusters was intensely regulated, as shown by the exclusive expression of phagocytic receptors TREM2, ApoE and Galectin-3, high levels of the “Off” receptors CD45 and CD200R, and variable levels of SIRP-α and the homeostatic receptor P2RY12. TREM2 expression in microglia clusters promoted an efficient phagocytosis and reparatory microglial profile. Analysis of the effect of pro-inflammatory chronic IL-6 overproduction showed an inhibited upregulation of CD47 in the facial nucleus (FN) and a promotion of a more phagocytic and unresponsive microglial phenotype, with altered SIRP-α, CX3CR1 and CD45 expression and reduced TREM2 expression, all consistent with increased FMNs death. On the other hand, chronic overproduction of anti-inflammatory IL-10 slowed down microglial activation without modifying neither microglial “On” nor “Off” receptors,

but induced CD47 upregulation in the FN at earlier time-points –related to the new formation of synaptic contacts–, which could result in the inhibition of microglial phagocytosis through SIRP-α mechanism. This study demonstrates that “Off” signalling attempted to protect altogether FMNs, while the “On” signal TREM2 facilitated injury damage clearance promoting an efficient reparation. In addition, this study outlines the decisive role of CD47-SIRPα axis in the control of FMNs death through microglial phagocytosis. In this sense, IL-10 has been identified as a cytokine to promote FMNs survival through CD47-SIRPα pathway. In conclusion, this study highlights the modulation of “On” and “Off” signalling as a potential therapeutic approach to protect neurons and control neuroinflammation.

I. INTRODUCTION

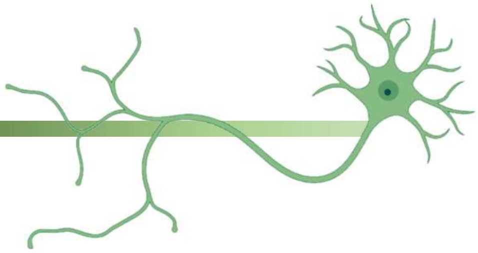

1. MICROGLIA

Microglia, a type of glia, are generally considered the immune cells of the central nervous system (CNS) parenchyma. Not only do they play a fundamental role in homeostasis, but also in pathological conditions where they regulate the inflammatory process (Hanisch and Kettenmann, 2007; Kettenmann et al., 2011; Wake and Fields, 2011).

Rudolf Virchow previously named and introduced the concept of neuroglia in 1856 (Kettenmann et al., 2011; Kierdork and Prinz 2017), which he defined as a glial cell population in the brain distinct from neurons (Kierdorf and Prinz, 2017; Wolf, Bodekke and Kettenmann, 2017). Following Virchow's observations, lots of works were performed to characterize possible differences with glial cells. Although Franz Nissl and Alois Alzheimer reported the presence of rod-shaped cells in the diseased brain (Wolf, Boddeke and Kettenmann, 2017; Menassa and Gomez-Nicola, 2018), and Santiago Ramón y Cajal postulated a new third element different from neurons and astrocytes, it was not until 1919 when Pío del Río Hortega referred to this newly discovered cell class as microglia due to their ramified morphology (Kettenmann et al., 2011; Ginoux and Prinz, 2015; Kierdorf and Prinz, 2017; Wolf, Boddeke and Kettenmann, 2017; Menassa and Gomez-Nicola, 2018). After del Río Hortega, the investigation of microglial cells received little attention from the neuroscience community owing to the limiting techniques available at that time (Kettenmann et al., 2011; Wolf, Boddeke and Kettenmann, 2017; Menassa and Gomez-Nicola 2018).

The modern era of microglial research started in the late 1960s when Georg Kreutzberg introduced the facial nerve lesion model. Kreutzberg's group studied microglial response to injury in tissue, with an intact blood-brain barrier, and these studies stimulated the evolution of research in the field (Blinzinger and Kreutzberg, 1968; Kettenmann et al., 2011; Wolf, Boddeke and Kettenmann, 2017; Menassa and Gomez-Nicola, 2018;). Since then, the study of microglia has developed quickly, and nowadays is one of the most active fields of neuroscience (Colonna and Butovsky, 2017; Stratoulias et al., 2019; Brioschi, Zhou and Colonna, 2020; Tan, Yuan and Tian, 2020; Lee et al., 2021; Xu et al., 2021).

1.1. ORIGIN AND DIFFERENTIATION OF MICROGLIA

Defining the origin of microglia has been an elusive goal for generations of researchers, and a longstanding issue of debate (Ginhoux et al., 2013). Although the origin of microglial cells differs from that of other CNS parenchymal cells, only in the recent years did the scientific community reach a consensus about their exact origin (Rezaie and Male, 2002; Ginhoux et al., 2013; Mosser et al., 2017).

Following their discovery, Pío del Río Hortega together with W. Ford Robertson and Santiago Ramon y Cajal proposed a mesodermal origin for these cells (Ginhoux et al., 2013; Mosser et al., 2017; Wolf, Boddeke and Kettenmann, 2017). During the second half of the 20th century, two dominant hypotheses emerged: on one hand, the neuroectodermal theory argued that microglia shared common origin with neurons and other glial cells (de Groot et al., 1992; Fedoroff, Zhai and Novak et al., 1997; Mosser et al., 2017 - Review; Menassa and Gomez-Nicola, 2018 - Review); on the other hand, the second one postulated that microglial cells derived from hematopoietic cells (i.e. monocytes), which give rise to the macrophages of peripheral tissue (Kaur, Ling and Wong, 1987; Ling, 1994; Ginhoux et al., 2013; Mosser et al., 2017 - Review; Menassa and Gomez-Nicola, 2018 - Review).

In the last decade, it has been convincingly shown the undeniable myeloid nature of microglia (Hume, Perry and Gordon, 1983; Murabe and Sano, 1983; Perry, Hume and Gordon, 1985). Microglial cells arise from embryonic yolk sac (YS) precursors, which also give rise to macrophages in other tissues (Ginhoux et al., 2010 and 2013; Ginhoux and Prinz, 2015; Mosser et al., 2017; Mecca et al., 2018) (Figure 1). Briefly, during development, YS myeloid precursors migrate to the brain, at approximately embryonic day 9.5 (E9.5) in mouse, before the formation of the blood brain-barrier. YS myeloid precursors differentiate into embryonic microglia, a process that is dependent on two myeloid transcription factors: Pu.1 and Irf8 (Kierdorf et al., 2013; Li and Barres, 2018). Upon entering the developing neuroectoderm, the embryonic microglial population expands via proliferation (Dalmau et al., 2003; Kierdorf and Prinz, 2017), and immature microglia display amoeboid morphology and distinct molecular and functional properties (Alliot, Godin and Pessac, 1999; Kierdorf et al., 2013; Li and Barres, 2018). Recent findings using transcriptomic tools also suggest that about 20-25% of brain microglia stem from Hoxb8-positive fetal liver-derived-monocytes, arising from fetal liver hematopoiesis around E12 in mouse (Brioschi, Zhou and Colonna, 2020). Microglial colonization and differentiation occur concurrently with the formation of neurons, and before the generation of astrocytes and oligodendrocytes, which provides microglia with a unique opportunity to take part in numerous developmental events in the CNS, such as neurogenesis (Cunningham, Martínez-Cerdeño and Noctor, 2013), programmed cell death (Marín-Teva et al., 2004), synapse elimination (Schafer et al., 2012) and the establishment and remodelling of neural circuits (Paolicelli et al., 2011). At this stage, microglia quickly adapt to their environment and modify their functions with a broad spectrum of activation states (Ransohoff, 2016).

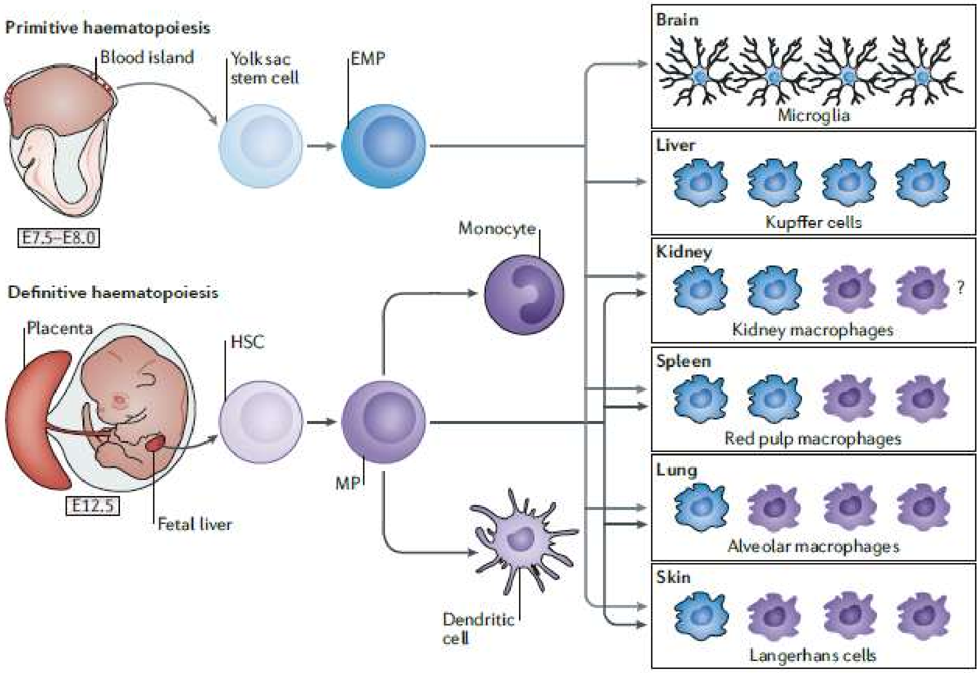
Primitive haematopoiesis
Blood island
Yolk sac stem cell
EMP
E7.5–E8.0
Definitive haematopoiesis
Placenta
HSC
E12.5
Fetal liver
MP
Monocyte
Dendritic cell
Brain
Microglia
Liver
Kupffer cells
Kidney
?
Kidney macrophages
Spleen
Red pulp macrophages
Lung
Alveolar macrophages
Skin
Langerhans cells

Figure 1: Origin and differentiation of microglia. Schematic representation illustrating the origin, entry to the CNS, migration, and differentiation of microglia from embryonic day (E7.5-E8.0) to adult age. Initially, cells with stem cell properties develop in blood islands of the yolk sac. Their progeny (erythromyeloid progenitors (EMPs)) further differentiate and populate several tissues, including the brain, where they become tissue macrophages. Shortly thereafter, myelopoiesis is taken over by progenitors found in the aorta–gonad–mesonephros region (not depicted) and foetal liver (starting at E12.5), where it forms part of the process of definitive haematopoiesis. Maturating myeloid cells derived from definitive haematopoiesis are engrafted in all tissues except the brain, which is already disconnected from any cell recruitment owing to the establishment of the blood–brain barrier, and the liver (Prinz and Priller, 2014).

In light of these discoveries, it is not surprising that microglial activation and dysfunction are increasingly implicated in the etiopathogenesis of most diseases and injuries of the CNS, since they maintain brain homeostasis in every stage of life (Crotti and Ransohoff, 2016; Colonna and Butovsky, 2017; Wolf, Boddeke and Kettenmann, 2017). Further research is still necessary to uncover more details of microglial maturation during development, to completely understand the process that establishes a network of adult steady-state microglia (Kierdorf and Prinz, 2017).

1.2 MICROGLIAL IDENTITY AND FUNCTIONS IN THE HEALTHY CNS

1.2.1 Transcriptomic profiling: A unique gen signature to identify different subtypes of microglial cells

Until recently, the molecular and functional characteristics of homeostatic microglia had not been identified. It was thanks to new technological advances, including RNA-sequencing, quantitative proteomics, epigenetics, and bioinformatics, that a unique transcriptional signature for homeostatic microglia has been identified in adult mice, which offered the possibility to differentiate microglia from peripheral myeloid cells (Gautier et al., 2012; Hickman et al., 2013; Butovsky et al., 2014; Butovsky and Weiner, 2018). Specifically, homeostatic microglia were shown to express *P2ry12, Tmem119, Siglech, Gpr34, Soc3, Hexb, Olfm12* and *Fcrls* genes. The homeostatic microglial transcriptional signature is regulated and maintained by molecular mechanisms (including *Pu.1, TGF-β, Sall1* and *Irf8* genes), which are crucial in determining and establishing microglial genesis and homeostatic regulation (Butovsky and Weiner, 2018).

Those differences are also exemplified by distinct surface protein signature, which also helps to distinguish microglia from CNS macrophages and from other related cell types, like infiltrated monocyte-derived cells and perivascular macrophages. While it is true that microglia express common macrophage markers such as F4/80, CD11b, CD45, CD163, Iba1 and CX3CR1, many of these proteins are expressed in different levels between these cell types. For example, microglia express lower levels of CD45 than monocytes, allowing these two cell types to be discriminated, whereas the expression of scavenger receptor CD163 by microglia enables their distinction from perivascular macrophages (Butovsky and Weiner, 2018; Lee et al., 2021).

Moreover, although microglia have been confirmed to self-renew during the over the course of a lifetime, new approaches have demonstrated that, in some circumstances, peripherally derived macrophages can replace depleted microglia with cells that maintain their own unique identity (distinct from that of microglia) and that these cells may play a distinct role in the progression or resolution of neurological diseases (Butovsky and Weiner, 2018; Brioschi, Zhou and Colonna, 2020). Monocyte-derived microglia were identified as F4/80^{high}Clec12a^{+}, whereas resident microglia were F4/80^{low}Clec12a^{-} underlining these subsets in microglial population rely upon ontogeny as well. Similarly, unlike resident microglia, monocyte-derived counterparts did not express the transcriptional regulator Sall1, as well as other macrophage genes (like MHC-II chains, *Lyz2, Clec12a, Ms4a7, ApoE, Cybb)* that are typically silenced in resident microglia at steady state (Bennett et al., 2018; Lund et al., 2018).

Despite the existence of the molecular signatures described above, the presence of microglial heterogeneity itself has been recognized for many years, and in the last years, different subtypes of microglial population within CNS have been described (Colonna and Butovsky, 2017; Szepesi et al., 2018; Stratoulias et al., 2019). These subtypes would co-exist at steady state and undergo further modulation or phenotypic transformation in response to stimuli. The regional microenvironment has been shown to tightly determine microglial identity at transcriptional level. Direct evidence for microglial regional variability was determined based on panels of pre-selected microglial markers. In one study, the expression of CD11b, CD40, CD45, CD80, CD86, F4/80, TREM2b, CX3CR1 and CCR9 was compared among microglia isolated from different CNS regions of adult mice. Although all these markers were expressed across the CNS, their protein expression varied significantly between areas (de Haas et al., 2008). Similar results were obtained in subsequent studies (Stratoulias et al., 2019; Tan, Yuan and Tian, 2020). For instance, cerebellar microglia appeared skewed towards a more “immune alerted” and “metabolically demanding” phenotype. By contrast, in cortex and striatum, microglia displayed a more homeostatic state while hippocampal microglia had an intermediate phenotype (Brioschi, Zhou and Colonna, 2020). Even in the same region, microglial heterogenicity has been described at steady state, not only into the transcriptional level, but also in morphology, density, and distribution heterogeneity (Stratoulias et al., 2019; Tan, Yuan and Tian, 2020).

When applying a single-cell RNA sequencing study, 47 molecularly distinct cell subtypes were identified in hippocampal tissue (Stratoulias et al., 2019). Interestingly, microglial ablation studies using genetic or pharmacological approach have also revealed that repopulation of microglia in different CNS regions diversify after ablation. These observed differences between microglia could arise from local cues, including interaction with different subtypes of neurons and glial cells, or slight differences in signaling threshold (Stratoulias et al., 2019). Therefore, when we talk about microglial function in the healthy CNS, we are not referring to a unique microglial profile that develop all the possible functions assigned to them. Depending on the region and requirement of the surrounding environment, microglia will develop a unique gene expression that would determine their final role in that region. Furthermore, each microglial subtype will response in a very different way when detecting any disruption or alert signal within CNS.

Numerous studies have demonstrated that microglia have several physiological, non-inflammatory functions that are crucial for CNS development and for regulating neuroplasticity in the adult (Hong, Dissing-Olesen and Stevens et al., 2016; Kierdorf and Prinz, 2017; Salter and Stevens, 2017; Tay et al., 2017). In the following subsections, microglia identity and physiological functions in developmental and adult CNS will be described.

1.2.2 Microglia identity and functions in the developmental CNS

The inherent microglial heterogeneity and their unique signature they display are not only present in mature microglia, but also in developmental stages. Surprisingly, some studies claimed that postnatal microglia showed much higher heterogeneity than adult homeostatic microglia (Matcovitch-Natan et al., 2016; Li et al., 2019).

Different subsets of microglia were identified throughout postnatal development including those involved in cell cycle, differentiation, and proliferation. These subtypes were sorted in the different developmental stages and referred as early microglia, pre-microglia, and adult microglia (Matcovitch-Natan et al., 2016). Of interest is the so-called proliferative-region-associated (PAM), which shared a transcriptional signature with disease-associated microglia (DAM) microglia which is common in aging and neurodegenerative diseases or models (will be explained in “Microglia in pathological conditions” section). This PAM microglia mimicked DAM gene expression pattern probably because they exert similar functions, such as phagocytosis (Hagemeyer et al., 2017; Li et al., 2019). Nevertheless, this PAM microglia found in developing microglia behave very differently than adult activated microglia (Lenz and Nelson, 2018; Li et al., 2019), despite sharing a gene expression profile, since, for instance, PAM microglia expressing CD11c+ are not similar to those expressing the same marker in rodent model of multiple sclerosis (MS) (Lenz and Nelson, 2018). Furthermore, unlike DAM, PAM do not depend on a TREM2-APOE axis, suggesting that different signals may trigger the emergence of these two microglial populations (Li et al., 2019). Developmental microglia are clearly unique and easily distinguishable from adult “activated” microglia when it takes into account their gene expression profile or function (Lenz and Nelson, 2018).

Because microglial progenitors enter the CNS with the onset of functional neuronal network, it could be said that microglia are essential for the correct neuroectoderm developing (Rigato et al., 2011; Kierdorf and Prinz, 2017). Accordingly, animals lacking microglia, exhibited several impairments in brain development with marked structural abnormalities in brain architecture (Erblich et al., 2011). Taking all of this into account, several fundamental functions have been attributed to microglia during development, such as: phagocytosis of dead cells, trophic support of developing neurons, support and refinement of neural circuits, guidance of developing vasculature and myelogenesis in the CNS (Salter and Beggs, 2014; Kierdorf and Prinz, 2017; Salter and Stevens, 2017; Tay et al., 2017; Lenz and Nelson, 2018).

Microglia seem to play a major part in the establishment of the correct number of neurons produced and maintained in the developing CNS by acting on the proliferation, the survival and the death of progenitors and maturing neurons. Microglia regulate neuronal numbers by controlling neuronal precursors, as well as neurons (Salter and Beggs, 2014). Developmental microglia phagocytose viable precursor cells in multiple regions of the developing CNS, thus limiting cell production and ultimately regulating brain size, and lack of this function has been correlated to neurodevelopmental disorders, namely autism and schizophrenia (Cunningham, Martínez-Cerdeño and Noctor, 2013). It has been long assumed that their primary role in CNS development is to remove apoptotic neurons that die as a result of programmed cell death, eliminating the excess of neurons generated in normal development (Marín-Teva et al., 2011; Salter and Beggs, 2014; Kierdorf and Prinz, 2017). However, microglia are also active neuronal killers, by driving programmed cell death in neurons without triggering inflammation (Marín-Teva et al., 2011; Salter and Stevens, 2017; Tay et al., 2017) through the release of superoxide ions, NGF or TNF-α (Frade and Barde, 1998; Marín-Teva et al., 2004; Sedel et al., 2004) and the removal through its receptor TREM2 (Kierdorf and Prinz, 2017).

During CNS development, neurons require trophic support to survive and to be integrated in neuronal circuits. Microglial cells sustain neuronal survival and proliferation (Kierdorf and Prinz, 2017; Mosser et al., 2017), as clearly evidenced in vivo for the microglial-derived insulin growth factor 1 (IGF-1), essential to enhance neuronal survival (Ueno et al., 2013; Mosser et al., 2017).

Microglia have been also shown to play a fundamental role in the refinement of synaptic networks and to the functional maturation of synapses (Kierdorf and Prinz, 2017; Mosser et al., 2017; Salter and Stevens, 2017). Microglia, sculpt immature neuronal circuits by engulfing and eliminating synaptic structures (axons and dendritic spines) in a process known as “synaptic pruning”. Among several mechanisms, complement proteins C1q and C3 serve as identification signals allowing the removal of material by phagocytic cells (Salter and Beggs, 2014; Kierdorf and Prinz, 2017; Mosser et al., 2017; Salter and Stevens, 2017; Tay et al., 2017; Menassa and Gomez-Nicola, 2018). Disruption of microglia pruning, including deficiency of microglial receptor CR3 or neuronal ligands C1q or C3, leads to sustained defects in synaptic development and wiring abnormalities (Stevens et al., 2007; Paolicelli et al., 2011; Schader et al., 2012; Mosser et al., 2017). In addition to synaptic pruning, microglial cells are required for proper maturation of synaptic circuits. For example, microglia expose neurons to signalling factors that regulate the functional expression of glutamate receptors (Béchade, Cantaut-Belarif and Bessis, 2013; Salter and Beggs, 2014; Mosser et al., 2017; Li and Barres, 2018). Once again, a great number of psychiatric brain disorders, such as schizophrenia and autism involve disruptions in synapse number, morphology, or function, with a pathogenesis that is believed to initiate with synapse development (Penzes et al., 2011; Miyamoto et al., 2016), thus highlighting the crucial role of microglia.

Microglia are also involved in the vascularization of the CNS to provide nutrient and oxygen, during development. Growth of blood vessels into the neuroectoderm starts around 10 days post-conception in mice, shortly after the first microglial progenitors enter the CNS. Microglia play a key role in this process of vascular networking by serving as “tip macrophages” that connect growth vessels by secreting soluble guidance factors, rather than by direct contact, with bidirectional communication between them (Rymo et al., 2011; Kierdorf and Prinz, 2017). It has been shown that microglial depletion led to reduced vessel growth and density (Checchin et al., 2006; Kubota et al., 2009).

Lastly, but not least, early post-natal microglia have been identified as vital for oligodendrocyte progenitor maintenance, maturation and subsequent physiological myelinogenesis (Hagemeyer et al., 2017; Wlodarczyk et al., 2017). Even though the importance of microglia during development have been studied for a while, their role in oligodendrogenesis and proper myelination was only hypothesized not long ago (Shigemoto-Mogami et al., 2014; Hagemeyer et al., 2017; Wlodarczyk et al., 2017). Specifically, IGF-1 has been found in different studies to be present in microglia in the developing brain (413, 418). Deficiencies in IGF-1 has been linked to increased neuronal death and myelination impairment, whereas its overexpression increased populations of neurons and oligodendrocytes, and enhanced myelin production (Hagemeyer et al., 2017; Wlodarczyk et al., 2017).

1.2.3 Physiological functions of microglia in adult CNS

Microglia are distributed over the entire CNS parenchyma and can be found in every single region in the adult CNS, accounting for approximately 10% of the total cell number in the healthy brain (Prinz and Priller, 2014; Kierdorf and Prinz, 2017). Several studies have suggested that microglial cells are capable of local self-renewal throughout adult life (Lawson, Perry and Gordon, 1992; Hashimoto et al., 2013; Askew et al., 2017; Zhan et al., 2019). In this sense, adult healthy animals showed very little exchange between blood cells and brain parenchyma (Mildner et al., 2007). Thus, maintenance of their population normally does not depend on the recruitment of circulating progenitors (Lawson, Perry and Gordon, 1992; Hashimoto et al., 2013).

Under physiological conditions, microglia display a very characteristic phenotype with a small cell soma containing few organelles and surrounding elongated processes with secondary branching and lamellipodia (Nolte et al., 1996; Nimmerjahn, Kirchoff and Helmchen, 2005). This ramified morphology was already recognized by Pío del Río Hortega, and hence he named these cells as microglia (Hanisch and Kettenmann, 2007; Lull and Block 2010; Ginhoux et al., 2013; Wolf, Boddeke and Kettenmann, 2017; Zhang, 2019). Ramified morphology and the sparse expression of molecules associated with macrophage function in microglia of the healthy adult CNS have been associated with a homeostatic phenotype (Nakajima and Kohsaka, 2001; Dheen, Kaur and Ling, 2007; Hanisch and Kettenmann, 2007). Contrary to what expected, homeostatic microglia are not dormant cells. Microglia are constantly surveying their environment looking for any danger or signal of CNS disruption by protruding and retracting their processes. Each microglia process seems to have a defined territory and they are able to scan their environment within several hours (Szepesi et al., 2018; Xu et al., 2021). While scanning the whole brain parenchyma, microglia regulate their phenotype to adapt to the CNS microenvironment and are sensitive to any change in the extracellular microenvironment or pathological imbalance (Xu et al., 2021). Microglial processes interact with blood vessels, neurons, ependymal cells, and other glial cells as well as they monitor the functional state of synapses in response to environmental cues (Raivich et al., 1999; Nimmerjahn, Kirchoff and Helmchen, 2005; Ramírez et al., 2005; Salter and Beggs, 2014; Chen and Trapp, 2016; Colonna and Butovsky, 2017; Salter and Stevens, 2017). Microglia express constitutive markers like Iba1, MHC-I, FcR, CD68 that may modify their expression depending on the environmental cues they sense, being involved in antigen presentation, cytotoxic activation, phagocytosis, antibody-associated phagocytosis, etc. (Marín-Teva et al., 2011; Salter and Beggs, 2014; Salter and Stevens, 2017)

First of all, microglia have been described to play a critical role in maintaining persistent synaptic plasticity and in regulating synaptic properties under physiological conditions, which particularly occurs in early adulthood (Salter and Beggs, 2014; Kierdorf and Prinz, 2017; Salter and Stevens, 2017). Changes in microglial number or function during development, for example, through the deletion of TGF-β in the CNS (Butovsky 2014) or by knocking out CX3CR1 (Rogers et al., 2011), resulted in aberrations in neuroplasticity in adulthood. More importantly, eliminating microglia in the adult or blocking the cells' ability to make brain derived BDNF resulted in reduced synaptic structural plasticity associated with learning impairment (Parkhurst et al., 2013). Additionally, loss-of-function mutation or deletion of microglial DAP12 and CD200R or CX3CR1 resulted in reduced synaptic structural plasticity associated with learning (Salter and Beggs, 2014; Kierdorf and Prinz, 2017; Salter and Stevens, 2017).

Another important function of microglia during adulthood is neurogenesis. Neurogenesis is a process that takes place in both development and in the healthy adult brain (Bachstetter et al., 2011; Gemma and Bachstetter, 2013; Kierdorf and Prinz, 2017; Salter and Stevens, 2017). Adult microglia regulate neurogenesis in the subgranular zone of the dentate gyrus in the hippocampal formation and because of their role in the maintenance of the hippocampal neurogenic niche during adulthood, microglia are essential components in learning and memory formation (Gemma and Bachstetter, 2013; Kierdorf and Prinz, 2017). The process of generating new neurons consists in four phases: proliferation, migration, differentiation, and survival (Ming and Song, 2011). One of the critical roles of microglia in modulating hippocampal neurogenesis is the elimination of new-born cells during the first critical period. However, the role of microglia in neurogenesis is not limited to removal of cells. Evidence suggests that microglia can support neurogenesis through the production of neurotrophic factors or other factors that influence proliferation and neuron differentiation as well as survival of the new-born cells (Bachstetter et al., 2011; Gemma and Bachstetter, 2013; Kierdorf and Prinz, 2017). In that process, neurons have been found to communicate with microglia to regulate neurogenesis, confirming the existence of a bidirectional microglia-neuron dialogue in neurogenesis. One of the best-characterized examples of a neuronal signal that regulates microglial function is the neuronal chemokine CX3CL1. It has been described that CX3CL1 supports and regulates adult neurogenesis, through the interaction with its receptor CX3CR1 in microglia (Bachstetter et al., 2011; Gemma and Bachstter, 2013; Kierdorf and Prinz, 2013). Loss of CX3CL1/CX3CR1 signalling not only affects neurogenesis, but also impairs cognitive function and synaptic plasticity (Bachstetter et al., 2011; Rogers et al., 2011; Sellner et al., 2016). Although their clear role in neurogenesis, microglia have also been shown to impair neurogenesis by the secretion of pro-inflammatory cytokines, including IL-1β, IL-6, TNF-α, which directly act on neural progenitor cells. Therefore, the involvement of microglia, likely depends on the activating signals and state of the microglia in the neurogenic niche which determines if microglia will support or impair neurogenesis (Monje, Toda and Palmer, 2003; Iosif et al., 2006; Koo and Duman, 2008).

Microglia are specially in close contact with neurons as well as oligodendrocytes. In the healthy brain, microglia exhibit an active surveying phenotype that is dependent on a dynamic crosstalk between microglia and neurons, especially. It has been proposed that the removal of this neuronal derived inhibitory control represents a type of danger signal for microglia, indicating that neuronal function is impaired and leads to alterations of microglial morphology and function. The reciprocal neuron–microglia communication is mediated by numerous soluble factors, extracellular vesicles as well as contact-dependent mechanisms and is essential for adaptive neuroplasticity and learning (Szepesi et al., 2018). One of this mechanism is the immune checkpoint which is triggered by close contact to healthy neurons and other glial cells via receptors for CX3CL1 (also called fractalkine), CD47, CD200, and CD22 that send a homeostasis signal to microglia. These immune checkpoint mechanisms will be described in future sections since this work is based on them and play a fundamental role in microglial activation in pathological conditions too (Xu et al., 2021).

The entire repertoire of microglial function has not been yet fully elucidated. Newly developed tools and techniques will help to identify more physiological functions in the future. It is worth mentioning that one of the relevant functions of microglia in the adult healthy CNS, which is important for the fully understanding of this work, is the key role that these cells play in the surveillance of the entire CNS to detect any minimum signal of CNS disruption and in maintaining and contributing to brain homeostasis. In the following subsection these functions will be deeply portrayed and their relevance in this thesis work will be highlighted.

1.3 MICROGLIA IN PATHOLOGICAL CONDITIONS: MICROGLIAL ACTIVATION

As pointed out in the previous section, microglia develop several essential functions in non-pathological conditions during development and adulthood. Nevertheless, what has drawn most attention is the role of microglia in neuroinflammation and their implication in the pathology of neurodegenerative diseases (Colonna and Butovsky, 2017).

Microglia, as tissue resident macrophages and members of the monocyte-macrophage family, recognize and scavenge dead cells, pathogens, and several endogenous and exogenous compounds (Hanisch and Kettenmann, 2007; Salter and Stevens, 2017). When microglia detect any disturbance or alteration on the brain homeostasis, that could be triggered by infection, ischemia, trauma, altered neuronal activity, and both acute and chronic neurological injuries and diseases, they evolve from a ramified shape (homeostatic state, previously described) to a heteromorphic one in a process called microglial activation (Raivich et al., 1999; Hanisch and Kettenmann, 2007; Carniglia et al., 2017; Mosser et al., 2017; Wolf, Boddeke and Kettenmann, 2017).

A wide range of molecules promote microglial activation, that can be classified as three main types: pathogen associated molecular patterns (PAMPs), damage associated molecular patterns (DAMPs) and neurodegeneration associated molecular patterns (NAMPs). PAMPs are a diverse set of microbes and other exogenous materials like components of bacterial cell walls and repeats of bacterial or viral nuclei acids that alert the organism to intruding pathogens, whereas DAMPs warn of internal cell damage of the own organism and involve molecules released by injured or altered cells as a consequence of tissue damage, such as oxidized lipoproteins or fragments of extracellular matrix molecules (Bianchi, 2007; Kaur and Ling et al., 2007; Matzinger, 2007; Dheen, Neher et al., 2011; Marín-Teva et al., 2011; Deczkowska et al; 2018). NAMPs, on their part, consist in an analogical model to the peripheral immune system’s pathogen- and damage-associated stress signals (PAMPs and DAMPs) that are commonly present in various CNS conditions. They are recognized by a battery of receptors constitutively expressed on microglia and trigger their transition into DAM, whose primary function is to contain and remove the damage (Deczkowska et al; 2018). Microglia possess an array of cell surface receptors for these kinds of alerting signalling, which include Toll-like receptors (TLRS) (TLR4 and TLR1/2), that belong to the family of pattern recognition receptors (PRRs), and their coreceptors such as CD14 (Bianchi, 2007; Matzinger, 2007; Lehnardt, 2010); scavenger receptors namely CD36, CD91 (Szepesi et al., 2018), SR1 and MARCO (Husemann et al., 2002); NLRs receptors like NLRP3 inflammasome; LDL receptor family member (LDLR, ApoER2 and VLDL); three receptor tyrosine kinases, Tyro3, Axl and Mertk; receptors for nucleic acids, C-type lectin receptors (CLRs) receptors such as Clec7a (Colonna and Butovsky, 2017); and a wide variety of cytokine and chemokine receptors. The interaction between these receptor subsets with DAMPs, PAMPs and NAMPs leads to rapid microglial activation which become motile and contribute to the ongoing inflammation (Kierdorf and Prinz, 2013).

Nonetheless, it would be a great mistake to claim that microglial activation is a simple event that only involve PAMPs, NAMPs and DAMPs signalling. On the contrary, it is complex and implies still unidentified signalling mechanisms. In fact, recent studies have directed their efforts in characterizing a fourth signalling that is essential for regulation of microglial activation and in which this work is focused: "On/Off" signalling. In future sections of this memory, this signalling will be deeper described (Bessis et al., 2007; Hanisch and Kettenmann, 2007; Kierdorf and Prinz, 2013).

Microglial activation implies rapid morphological transformations (Raivich et al., 1999; Nakajima and Kohsaka, 2001; Ju et al., 2018; Zhang, 2019). In addition to changes in microglial phenotype, microglial activation launches a specific program of modifications in gene expression and functional behaviour that include increased migratory ability to accumulate in injured regions, enhanced proliferation, active phagocytosis and the release of cytokines and other factors (Nakajima and Kohsaka, 2001; Nakamura, 2002; Dheen, Kaur and Ling, 2007; Hanisch and Kettenmann, 2007; Marín-Teva et al., 2011; Zhang, 2019).

Activated microglia thereupon migrate to the origin of the damaged site. This microglial recruitment involves several factors, including chemokines released from both neurons, and glial cells. Therefore, it is safe to say that microglial migration is a complex process that involves an intense crosstalk between extended microglial processes and endangered neurons and glial cells. Microglia exhibit two types of motilities classified in two phases: a first phase in which microglia respond within minutes by only enlarging and extending their processes towards the disturbing element, without migration of the soma; and a second phase, where, if the damage is recognised and evaluated as important enough, the microglial whole cell body is translocated (Nimmerjahn, Kirchoff and Helmchen, 2005; Davalos et al., 2005). Activation of CXCR3 receptor by the chemokine CCL21 has been linked to microglial migration, for instance (Rappert et al., 2004). CXCR4 chemokine, as well as integrins like CD11b and CD11c also control migration and positioning of microglia within CNS and enhance their capacity to bind target cells to be phagocytosed and eliminated (Colonna and Butovsky, 2017). Most of these molecules are released as soluble factors that form chemotactic gradients for cell migration, although it is possible to find them as a membrane-anchored molecules too. Other potential candidates proposed as stimulators of microglial motility include ATP, cannabinoids, LPA, bradykinin, ion channels, neurotensin, TGF-β, complement factor C5a, and transporters (Schwab, 2001; Walter et al., 2003; Schilling et al., 2004; Davalos et al., 2005; Ifuku et al., 2007).

Once in the injured site, microglia proliferate, increasing their numbers. In terms of function, they change the expression pattern of many enzymes and receptors, and the production of immune response molecules is induced (Colton, 2009). Without additional damage, microglia gradually decrease in number, lose activation markers, and revert to a homeostatic state. On the other hand, when the damage is strong and persistent, microglia can evolve to a more reactive stage and become phagocytes (Raivich et al., 1999; Schilling et al., 2004). Hence, microglial developing phagocytic function is linked to the pattern gene expression that microglia will acquire after injury. Traditionally, microglia have been defined to develop a classic pro-inflammatory program in the beginning of the response by releasing inflammatory cytokines like TNF-α, IL-6, IL-12, IFN-γ, CCL2, IL-1β; reactive species NO and ROS; proteases like MMP12; and the expression of molecules such as MHC class II, costimulatory molecules, Fc receptors, and integrins. This activated phenotype, referred as pro-inflammatory, are essential for host defence and elimination of the threat. Be that as it may, if there is no regulation, it could also result in collateral damage of healthy tissue. When the noxious stimulus has been dealt with, it is crucial that the inflammatory response be dampened and resolved. This is achieved by active redirection of microglial phenotype towards an alternative immunomodulatory or acquired deactivation profile, characterized by release of anti-inflammatory cytokines such as TGF-β, IL-10, IL-13, IL-4 and AG1. These immunomodulatory mediators inhibit the release of pro-inflammatory factors and promote tissue regeneration, thereby facilitating the return to homeostasis. When the resolution phase of the inflammatory response is altered, excessive damage to the affected tissue may ensue, potentially leading to cell death and neurodegeneration (Colton, 2009; Lull and Block, 2010; Hu et al., 2015; Carniglia et al., 2017;) (Figure 2).

New technologies and approaches like massive transcriptomic analysis, proteomic, and epigenomic are beginning to unravel new other microglial responsivity patterns in health and disease (Martinez and Gordon, 2014; Ransohoff, 2016; Mosser et al., 2017; Salter and Stevens, 2017; Li and Barres, 2018; Zhang, 2019). In a similar way than microglia in homeostasis, activated microglia display a unique gene signature related to specific diseases and to specific stage of diseases which are now being described for the first time (Butovsky and Weiner, 2018; Lee et al., 2021). Under pathological conditions, several microglial subtypes, such as the already mentioned DAM or "disease associated microglia" are reportedly associated with neurodegenerative diseases. This phenotype has been linked to Alzheimer's disease (AD) pathology and other neurodegenerative conditions and overlaps in some extent with the phenotype of what is also referred as MGnD or microglia neurodegenerative phenotype and ARM or activated response microglia (Butovsky and Weiner, 2018; Stratoulias et al., 2019; Boche and Gordon, 2021). DAM show downregulation of homeostatic genes such as *TMEM119*, *P2ry12, Selplg, Tgfbr1, Sall1* and *CX3CR1* and upregulation of specific DAM or MGnD-associated genes, such as *TREM2, Cst7, Lpl, Spp1, ApoE* and *Axl*, among others (Brioschi, Zhou and Colonna, 2020; Lee et al., 2021; Casali and Reed-Geaghan, 2021). TREM2 signalling plays a pivotal role in microglial activation since these DAM microglia were shown to be generated through a two-step activation process in which homeostatic microglia first transition to an intermediate stage (known as stage 1 DAM) in a TREM2-independent manner, followed by a second TREM2-dependent transition to stage 2 DAM (Keren-Shaul et al., 2017; Casali and Reed-Geaghan, 2021). DAM microglia are frequently detected under conditions of accumulating degenerating neurons, myelin debris, or extracellular protein aggregates and reportedly alleviate the damage; however, it is not clear whether they have a protective or disease-inducing function (Brioschi, Zhou and Colonna, 2020; Casali and Reed-Geaghan, 2021; Lee et al., 2021) (Figure 2).

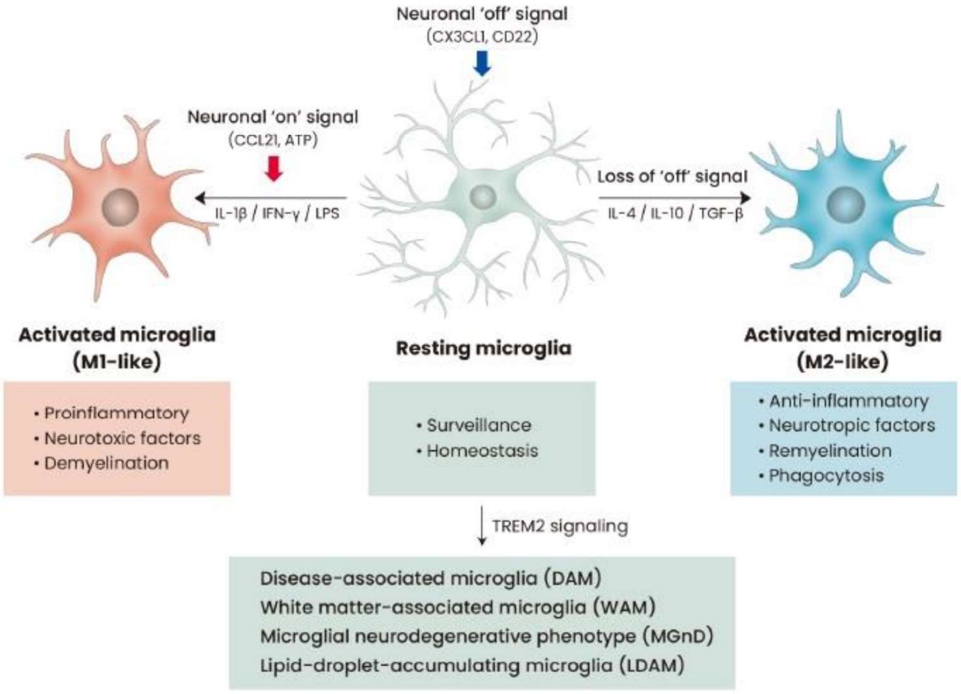
Neuronal 'off' signal
(CX3CL1, CD22)
Neuronal 'on' signal
(CCL21, ATP)
IL-1β / IFN-γ / LPS
Loss of 'off' signal
IL-4 / IL-10 / TGF-β
Activated microglia (M1-like)
• Proinflammatory
• Neurotoxic factors
• Demyelination
Resting microglia
• Surveillance
• Homeostasis
Activated microglia (M2-like)
• Anti-inflammatory
• Neurotropic factors
• Remyelination
• Phagocytosis
TREM2 signaling
Disease-associated microglia (DAM)
White matter-associated microglia (WAM)
Microglial neurodegenerative phenotype (MGnD)
Lipid-droplet-accumulating microglia (LDAM)

Figure 2. Diversity of microglial phenotypes. Neuronal "Off" signals, constantly inhibit microglial activation in physiological conditions. Microglia in this environment show a ramified morphology are referred to as "resting" microglia. Resting microglia can be activated by PAMPs (LPS) or DAMPs (ATP) inside the CNS into M1-like microglia and are characterized by ameboid morphology, high CD68 expression, and proinflammatory phenotypes. Neuronal "On" signals also contribute to M1 microglial polarization. In contrast, loss of "Off" signals or anti-inflammatory cytokine-rich milieu can induce the activation of microglia into neuroprotective M2-like phenotype. Recently, diverse microglial phenotypes have been identified in pathological conditions, such as DAM, white matter-associated microglia (WAM), MGnD and LDAM (Lee et al., 2021).

Altogether, this highlights the importance of the phagocytic role of microglial cells in maintaining homeostasis in the nervous parenchyma and in triggering CNS repair after injury. Nevertheless, both the absence of protective function served by microglia, or their abnormal and excessive proinflammatory activation have been implicated in the pathology of many neurodegenerative disorders, namely AD (von Bernhardi, 2007), Parkinson's disease (PD) (Gao et al., 2003), MS and HIV-associated dementia (Minagar et al., 2002), prion diseases (Perry, Cunningham and Boche, 2002), Amyotrophic lateral sclerosis (ALS) (McGeer and McGeer, 2002) and Huntington's disease (Sapp et al., 2001). Therefore, it is well established that microglial activation could turn out to be neurotoxic or neuroprotective, depending on the pathologic context and the type of stimulation (Mallat and Chamak, 1994; Hanisch and Kettenmann, 2007).

The "negative" or neurotoxic effect of microglial activation has been widely reported to be a decisive factor in different neurodegenerative diseases (Hanisch and Kettenmann, 2007; Lull and Block, 2010; Prinz and Mildner, 2011). Neurodegenerative diseases are characterized by chronic and progressive neuronal loss, and pathological levels of cytotoxic substances, including extracellular debris, elevated levels of pro-inflammatory factors, and production of reactive oxygen species, resulting in oxidative stress (Lull and Block 2010; Salter and Stevens, 2017; Wolf, Boddeke and Kettenmann, 2017; Li and Barres, 2018). In these conditions, microglial activation-derived inflammation is thought to be an amplifier of neurodegeneration. Once early neuronal death is triggered, DAMP signals released by dead neurons contribute to stimulate reactive microgliosis. This process become chronic by further microglial activation associated with persistent neuroinflammation and toxicity (Lull and Block, 2010; Gao et al., 2011). In order to halt this vicious circle, there are mechanisms that mediate the resolution of the inflammation-mediated activation of microglia and their transition to non-activated phenotypes (Colton, 2009; Saijo and Glass, 2011). Undoubtedly, any defect in these mechanisms will contribute to chronic neurodegenerative diseases.

Since microglial activation is involved in the detrimental outcome from most of the neurodegenerative diseases, therapeutic strategies aim to counteract this microglial feature. Be that as it may, recent findings suggesting that DAM microglia could be both beneficial or detrimental in neurodegenerative diseases depending on the type of sickness and stage open up new strategies to treat each disease state in a specific way (Butovsky and Weiner, 2018; Lee et al., 2021).

Microglial activation also plays a role in diseases not related to age. In HIV-associated neurocognitive disorder, activated microglia play a strong part in harbouring the HIV and acting as a site of viral replication. The interaction between microglia, viral replication/proteins, and the production of cytotoxic factor in HIV-associated dementia has strong implications for disease progression (Jordan et al., 1991; Speth, Dierich and Sopper, 2005).

Despite the higher research carried out on the detrimental effects of microglia-mediated neuroinflammation, it is now accepted that self-limited activation of microglia is essential for the structural and functional integrity of the CNS. Phagocytic activity is believed to be one of the putative neuroprotective features of microglia since implies efficient removal of apoptotic cells and clearance of tissue debris at the lesion site (Napoli and Neumann, 2009), thus enhancing an appropriate microenvironment for regeneration and repair (Kotter et al., 2006). Furthermore, microglia have been reported to remove β-amyloid deposits, which are related to malfunction and development and progression of AD, via the secretion of proteolytic enzymes (Schlachetzki and Hüll, 2009; Malm, Jay and Landreth, 2015). Besides, they can also display neuroprotective effects by releasing neurotrophins and cytokines for the survival of injured neurons (Schwartz, 2003). Similarly, in other neurodegenerative diseases, such as ALS, Huntington's disease, and prion disease, it has been also pointed out the role that activated microglia can play in cell damage and death (Sapp et al., 2001; Perry, Cunningham and Boche, 2002; Obst et al., 2017; Christoforidou, Joilin and Hafezparast, 2020). A special case among these neurological disorders is MS, a disease associated with severe inflammation and demyelination of axons. Microglia, by contrast, appear to have a beneficial role, particularly during the remission phase. They clean up myelin debris, aiding in tissue repair (Yamasaki et al., 2014) and may directly promote remyelination by inducing the differentiation of oligodendrocyte precursor cells (Miron et al., 2013; Miron, 2017).

Whether microglia would display a neurotoxic or neuroprotective role after a CNS challenge depend on the balance between the different types of molecules they will release, as well as the microenvironmental context where this microglial activation takes place (Marín-Teva et al., 2011; Colton, 2009; Ramesh, MacLean and Philipp, 2013).

2. ON/OFF SIGNALLING

Currently, lots of works invest their efforts in microglial immune checkpoints mechanisms, which restrain microglial immune activity: the so-called "Off" signalling, which consist in the interaction of some inhibitory receptors ("Off-receptors") located on the microglial membrane, with the corresponding ligands ("Self-associated molecular patterns" or SAMPs) on healthy neurons and glial cells. These constitutive interactions take place in the healthy CNS and keep microglia in the homeostatic state (Kierdorf and Prinz, 2013; Deczkowska, Amit and Schwartz, 2018; Szepesi et al., 2018). Some of the proposed inhibitory receptors in microglia are CD200R, CX3CR1, SIRP-α and CD45, which interact in a direct cell-to-cell contact with their respective ligands CD200, CX3CL1, CD47 and CD22 on the surface of healthy neurons (Hanisch and Kettenmann, 2007; Lull and Block, 2010; Marín-Teva et al., 2011; Kierdorf and Prinz,2013; Szepesi et al., 2018). In addition to these cell-to-cell membrane signals, neurons can also release some soluble “Off-signals” into the extracellular space, such as TGF-β, neurotransmitters and neurotrophins including NGF, BDNF and NT-3 (Biber et al., 2007). If any of these “Off-signals” are lost, due to changes in the microenvironment, or they are downregulated, as may occur on pathological conditions, microglial activation is triggered. Therefore, there is an active and permanent crosstalk between microglia and neurons, indicating that neurons are not merely passive targets of microglia but rather control microglial activity (Biber et al., 2007; Hanisch and Kettenmann, 2007; Lull and Block, 2010; Marín-Teva et al., 2011; Kierdorf and Prinz, 2013; Szepesi et al., 2018).

When neurons are damage or endangered, they release what are called “On-signals” which initiate a microglial activation program with protective or detrimental effects (Biber et al., 2007; Li, 2012). Among all the”On” signals, some molecules act as “Help-me/find-me” signals, detected by P2Y purinergic receptors in microglia (Li, 2012). Examples of these alert signals include phosphorylated nucleosides ATP and UTP (Sperlágh and Illes, 2007; Li, 2012), chemokines such as CCL21 and CXCL10 (Rappert et al., 2004), cytokines like IL-1 (Cartier et al., 2005), neuropeptides (Ifuku et al., 2007), neurotransmitters (Färber, Pannasch and Kettenmann, 2005; Liu et al., 2009), cannabinoids (Walter et al., 2003) and morphine (Takayama and Ueda, 2005). In response to these “Help-me/find-me” signals, microglia migrate to the source of these molecules and develop a surveillance function. However, if microglial “On-Receptors”, such as TREM2, are capable to interact with the corresponding ligand on the surface of the damaged neurons, an “Eat-me” signal is triggered, and microglia elicits phagocytosis (Linnartz and Neumann, 2013) (Figure 3).

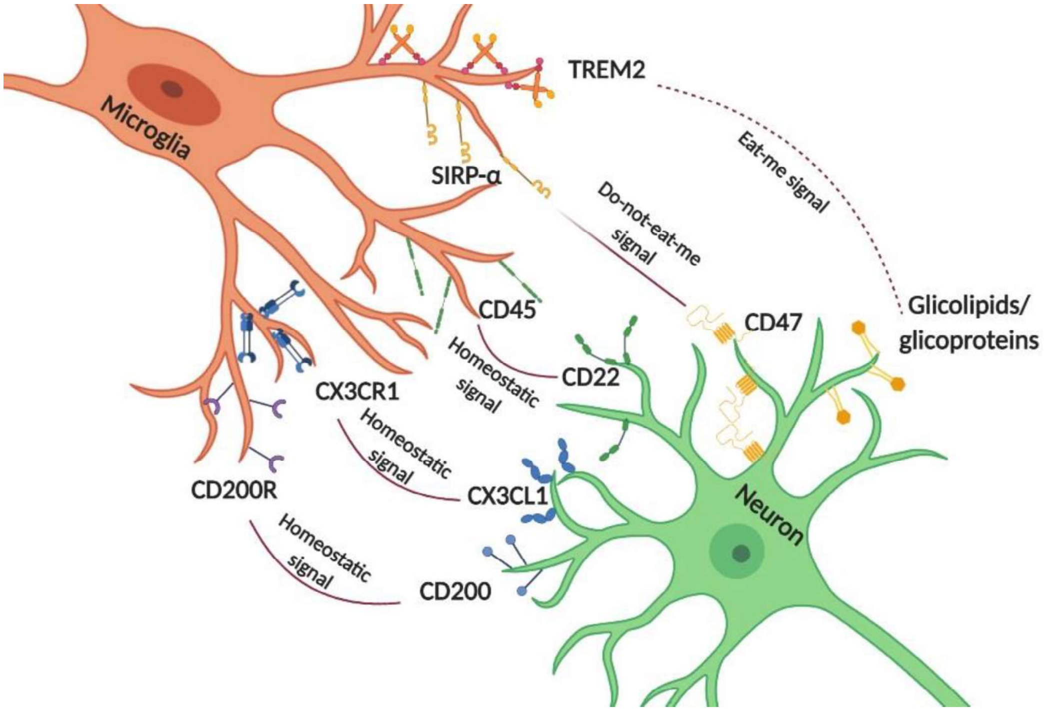
TREM2
Microglia
Eat-me signal
SIRP-α
Do-not-eat-me signal
CD45
CD47
Glicolipids/
glicoproteins
CD22
Homeostatic signal
CX3CR1
Homeostatic signal
CX3CL1
Neuron
CD200R
Homeostatic signal
CD200

Figure 3. "On/Off" signals and their receptors on microglia. Microglia are equipped with a group of surface receptors which trigger signals under homeostatic conditions. Many of these signals are ligands which are released or expressed on the surface of neurons. Inhibitory receptors CD200R, CX3CR1, CD22 and SIRP-α have their ligands on the surface of healthy neurons. A loss of this signal indicates loss of neuronal integrity. Receptors such as TREM2 are essential to mimic neuronal injury and induce phagocytic and anti-inflammatory functions in microglia. The crosstalk between microglia and neurons is also important for the survival of microglia (Created by BioRender).

The dynamics of microglia-neuron communication in the healthy brain has attracted great attention in the field of neurobiology/neuroimmunology during the past decades. Proper function of "On/Off" mechanism has been found to be essential for CNS homeostasis and proper microglial role, since deficiencies on this signalling have been repeatedly observed in several neuroinflammatory conditions, like MS, AD, in the aging brain and in neurodevelopmental disorders, among others. Due to all these findings, all the above-mentioned pairs of "Off" signalling molecules have been proposed as potential tools for treatment of inflammatory and neurodegenerative diseases in the CNS, by regulating microglial activation. Therefore, further studies are needed to understand the exact regulation of this signalling, which will allow to take the next step in therapeutic strategies (Cardona et al., 2006; Wang et al., 2007; Walker et al., 2009; Zhu et al., 2011; Varnum et al., 2015; Chen et al., 2016; Szepesi et al., 2018).

In the following sections we will describe some of the main "Off" signal pairs together with a main "On" signal, –the TREM2 "Eat me" molecule– all of them signals involving direct contact cell-to-cell contact, and in which this work is focused on (Table 1).

OFF SIGNALS	ON SIGNALS
CD200-CD200R	TREM2 ("Eat-me")
CX3CL1-CX3CR1	
CD22-CD45	
CD47-SIRP-α ("Do-not-eat-me")	

Table 1. "On/Off" signals.

2.1 CD200-CD200R

CD200, also known as OX-42, is a 41-47 kDa transmembrane glycoprotein that belongs to the IgSF family, and it is therefore characterized by two IgSF domains, one transmembrane region, and a small cytoplasmatic domain, which do not have intracellular signalling (Biber et al., 2007; Wang et al., 2007; Ngwa and Liu, 2019). CD200 is highly expressed on neurons, but its presence has also been demonstrated on endothelial cells, astrocytes, and oligodendrocytes within CNS (Koning et al., 2009; Shrivastava, Gonzalez and Acarin, 2012; Szepesi et al., 2018; Manich et al., 2019).

CD200R, the corresponding receptor of CD200, is primarily expressed by myeloid lineage cells, being predominant on macrophages and microglia in the brain (Koning et al., 2009; Shrivastava, Gonzalez and Acarin, 2012; Kierdorf and Prinz, 2013). CD200R belongs to the IgSF family as well and is closely structurally related to CD200. However, unlike its ligand, CD200R has signalling motifs in its intracellular domain that, upon triggering, deliver an inhibitory signal (Zhang et al., 2004; Jenmalm et al., 2006; Koning et al., 2009) (Figure 4). This immunomodulatory system, together with CX3CL1-CX3CR1, are the most studied among all the neuron-microglia communication pathways (Szepesi et al., 2018).

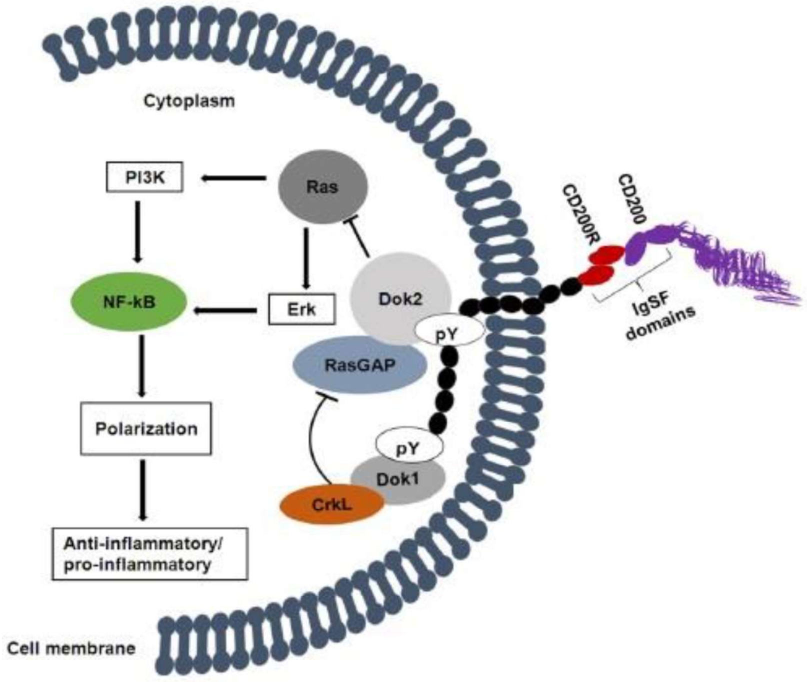

Figure 4. CD200-CD200R structure and intracellular signalling. The primary CD200R mechanism involves activation of Dok2 and RasGAP, leading to the inhibition of Ras activation and suppression of downstream effects on PI3K and Erk, resulting in an increase of multiple anti-inflammatory signals, that occurs due to the inhibition of NF-kB. Activation of RasGAP can be inhibited by the combination of Dok1 and CrkL, leading to activation of NF-κB and the pro-inflammatory signaling pathways pY: Phosphotyrosine (Ngwa and Liu, 2019).

There is growing evidence on CD200/CD200R significance in modulating tissue inflammation in various diseases (Hoek et al., 2000; Wang et al., 2007; Walker et al., 2009). Namely, CD200-deficiency in mice elicited an accelerated and exacerbated microglial and macrophage response after facial nerve axotomy (FNA), enhanced neurodegeneration in a PD model, and induced a faster onset of clinical symptoms in EAE –an experimental animal model of MS– (Hoek et al., 2000; Zhang et al., 2011). Disruption of CD200-CD200R axis, apart from inducing higher microglial activation, enhanced microglial phagocytosis in microglial cultures prepared from CD200-deficient mice (Lyons et al., 2017), stimulated microglial proliferation in toxoplasma encephalitis (Deckert et al., 2006), and triggered increased expression of pro-inflammatory iNOS, TNF-α, IFN-γ and IL-6 in the hippocampus of adult mice (Costello et al., 2011; Denieffe et al., 2013). General histological observation of CNS tissue from CD200-deficient mice revealed a characteristic ramified microglial morphology with spare clusters of microglia located in the spinal cord and basal ganglia (Hoek et al., 2000; Deckert et al., 2006). All those effects are linked to negative effects on neuronal function and impaired long-term potentiation (LTP) in CA1 of hippocampal slices prepared from CD200-/- mice (Costello et al., 2011).

On the contrary, Wld(s) mice (the "slow Wallerian degeneration mice") –a spontaneous mutant with an increase in neuronal CD200 expression–, were protected against different forms of axonal injury, had beneficial effects on experimental autoimmune encephalomyelitis (EAE) symptomatology and decreased microglia/macrophage activation (Chitnis et al., 2007). On top of that, potentiation of CD200-CD200R1 signaling by administrating CD200Fc downregulated the antigen presenting capacity of activated microglia, by decreasing MHC-II expression, and attenuated microglial phagocytosis (Costello et al., 2011; Lyons et al., 2012; Denieffe et al., 2013). In human brain tissue, decreased CD200-CD200R signalling have been observed in several neuroinflammatory conditions, such as AD, PD and MS, which contributed to maintaining chronic inflammation (Koning et al., 2007; Walker et al., 2009; Luo et al., 2010). Overall, this evidence suggests that CD200-CD200R interactions contribute to the immune characteristics of the CNS.

All this evidence indicates that the absence or important decrease of CD200-CD200R activation under inflammatory situations produces an exaggerated response of microglia, a phenomenon called microglial priming, which is characteristic of aging. The main feature of primed microglia is the production of an exacerbated response to a secondary inflammatory stimulus that, in naïve microglia, would result in lower or null microglial activation (Manich et al., 2019). During homeostasis, CD200-CD200R uncoupling may be responsible for microglial disinhibition, promoting, in the end, its priming. Therefore, maintenance of CD200-CD200R signaling during homeostasis protects microglia from priming, and controls microglial pro-inflammatory functions during inflammation.

2.2 CX3CL1-CX3CR1

CX3CL1, also known as fractalkine, is a unique chemokine that is constitutively expressed in neurons (Hulshof et al., 2003; Biber et al., 2007; Szepesi et al., 2018). CX3CL1 is the only member of the CX_3C δ-chemokine subfamily, which has distinct structural features compared to other chemokines, including a CX_3C motif in the N-terminus, a glycosylated mucin-like stalk that binds the chemokine domain to a transmembrane spanning domain, and short intracellular domains (Bazan et al., 1997; Hulshof et al., 2003; Kierdorf and Prinz, 2013) (Figure 5). Even though CX3CL1 is predominantly found on neurons, it has also been described on endothelial cells (Harrison et al., 1998; Nishiyori et al., 1998; Hulshof et al., 2003; Babendreyer et al., 2017). Some studies also claim that astrocytes are capable to express CX3CL1 under physiological and in inflammatory conditions (Pereira et al., 2001; Hughes et al., 2002). CX3CL1 exists in both membrane-bound and soluble secreted form. Its membrane-tethered mucin stalk acts as a cell adhesion molecule, attaching to microglia during an inflammatory reaction. Also, the membrane-bound form can be cleaved by cathepsin S, ADAM-10, and ADAM-17; releasing the soluble form that can serve as a signalling molecule, mediating neural/microglial interaction via its sole receptor CX3CR1 (Chen et al., 2016; Bolós et al., 2018; Pawelec et al., 2020).

CX3CR1, the fractalkine receptor, has been long attributed to be restricted to microglia within the CNS, however, some studies have characterized CX3CR1 on neurons and astrocytes (Nishiyori et al., 1998; Harrison et al., 1998; Jung et al., 2000; Meucci et al., 2000; Hughes et al., 2002; Hulshof et al., 2003). When CX3CL1 binds to its receptor CX3CR1, an activation signalling is triggered in the seven transmembrane domain receptor coupled to G_i and G_z subtypes of G proteins, which is linked to several intracellular second messengers (Figure 5) (Sheridan and Murphy, 2013).

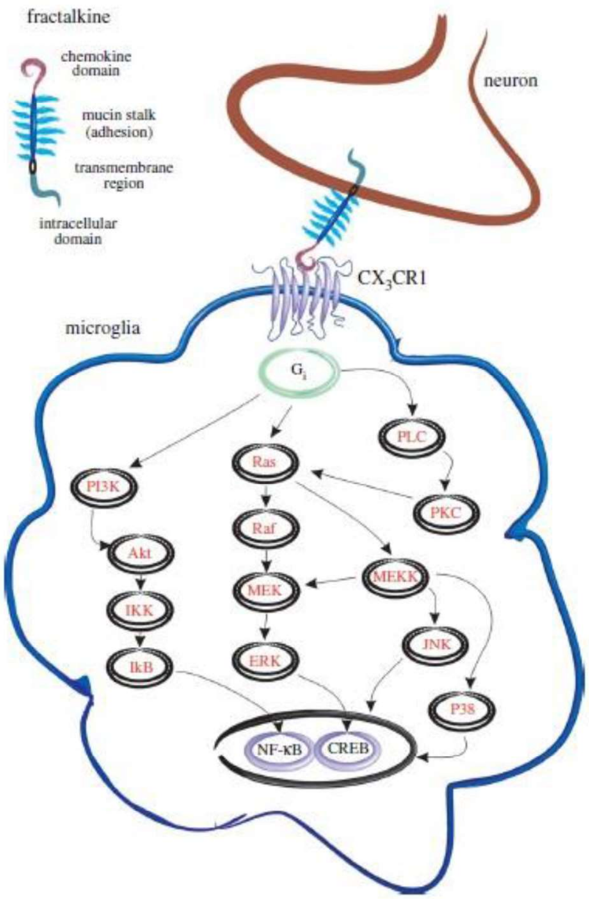
fractalkine
chemokine domain
mucin stalk (adhesion)
transmembrane region
intracellular domain
neuron
CX_3CR1
microglia
G_i
PLC
Ras
PI3K
PKC
Raf
Akt
MEKK
MEK
IKK
JNK
IkB
ERK
P38
NF-κB
CREB

Figure 5. CX3CL1 and CX3CR1 expression and signalling. Fractalkine is a large chemokine molecule consisting of four major functional regions. These include an N-terminal chemokine domain, which can be cleaved by metalloproteinases such as ADAM10, TACE and the lysosomal cysteine protease, cathepsin S. Fractalkine also contains a hydrophobic transmembrane region and intracellular C-terminal domain. Neuronally expressed membrane-bound and soluble cleaved fractalkine can bind to its receptor, CX3CR1, which is G protein-coupled and transduces several well-characterized signaling pathways leading to activation of transcription factors, including NF-κB and CREB. FKN, fractalkine; Gi, heterotrimeric G protein-coupled to Gi protein; PI3K, phosphatidylinositide 3-kinases; Ras, small GTPase; Raf, small GTPase; PLC, phospholipase C; PKC, protein kinase C; Akt, serine/threonine-specific protein kinase; MEK, mitogen-activated protein kinase kinase; MEKK, MAP3kinase; p38, p38 mitogen-activated protein kinase; IkB, inhibitor of kappa B; IKK, inhibitor of kappa B kinase; ERK, extracellular signal-regulated kinases; JNK, c-Jun N-terminal kinase; NFκB, nuclear factor kappa B; CREB, cAMP response element-binding protein (Sheridan and Murphy, 2013).

Notably, some investigations showed a pivotal role for CX3CL1/CX3CR1 signalling in microglial functions under physiological conditions, since it plays a key role in neurogenesis, synaptic pruning and synapse maturation during postnatal development (Paolicelli et al., 2011; Kierdorf and Prinz, 2013). In this way, CX3CR1-deficient animals displayed abnormal synapse formation (Hoshiko et al., 2012), diminished adult neurogenesis (Bachstetter et al., 2011; Bolós et al., 2018), cognitive impairment (Rogers et al., 2011) and marked alterations in emotional behaviours (Bolós et al., 2018).

Neuronal CX3CL1 and microglial CX3CR1 interaction has received considerable attention as an important mediator of inflammatory responses in several neurological disorders (Biber et al., 2007; Kierdorf and Prinz, 2013; Szepesi et al., 2018; Pawelec et al., 2020). *In vitro* experiments revealed that CX3CL1 was a potent chemoattractant for microglia (Nishiyori et al., 1998), and it has been proved that it could serve as an adhesion molecule too (Bazan et al., 1997; Imai et al., 1997). CX3CL1 has also been thought to function as a chemotactic factor to cause the activation and migration of microglial cells during tissue remodelling in the development of MS lesions and in the rat facial nerve model, for instance (Nishiyori et al., 1998; Hulshof et al., 2003). Other studies carried out in FNA model and microglial cell cultures also showed that neuronal-derived CX3CL1 induced microglial proliferation, activation and/or migration at injured brain sites (Harrison et al., 1998; Maciejewski-Lenoir et al., 1999; Boehme et al., 2000; Hatori et al., 2002). Impaired CX3CL1/CX3CR1 signalling in various animal models of CNS diseases, namely cerebral ischemia, ALS and PD, is accompanied by abnormal microglial activation, as demonstrated by enhanced microgliosis and the rapid acute production of pro-inflammatory cytokines, which led to further neurodegeneration and neurotoxicity (Pawelec et al., 2020). For instance, CX3CR1 deficiency worsened neurodegeneration in PD and ALS models, by showing more extensive neuronal cell loss compared to control mice, and increased neuroinflammation, microgliosis and production of pro-inflammatory markers (Cardona et al., 2006; Castro-Sánchez et al., 2018).

2.3 CD22-CD45

CD22 is generally known to be a B-cell-specific member of the IgSF that plays an important role in B-cell maturation and modulation of antigen receptor signalling (Stamenkovic et al., 1991; Tedder et al., 1997; O'Keefe et al., 1999). In addition, CD22 mediates cell-cell interactions with T cells, monocytes, and other B cells (Stamenkovic and Seed, 1990; Stamenkovic et al., 1991). In the CNS tissue, CD22 has also been characterized on neuronal cells (Mott et al., 2004) in two isoforms: a dominant one of ~130kDa, which is similar to the already identified one in the B-cell line, and a second one of ~90kDa that appears to be a secreted form of CD22 by neurons (Boué and Lebien, 1988; Mott et al., 2004).

Currently, there is limited research about CD22 functions and relevance within CNS. Be that as it may, it has been demonstrated that neutralizing CD22 in neuron-microglial co-cultures induces microglial activation, suggesting that CD22 mediates, at least in part, neuronal inhibition of microglial pro-inflammatory cytokines, for instance TNF-α production (Mott et al., 2004).

Novel publications detected CD22 upregulation on aged microglia, and this expression was linked to a negative regulation of excessive microglial phagocytosis. Moreover, CD22 was also enriched in a subpopulation of postnatal microglia (Pluvinage et al., 2019). The authors argued that this increase could be a negative feedback mechanism to restrain excessive phagocytosis in response to overwhelming cellular debris in the developing brain. During aging, this program might be inappropriately re-activated in response to myelin fragmentation and protein aggregation (Pluvinage et al., 2019). Similarly, CD22 was upregulated in the AD brain, in a microglial population correlated with clinicopathological decline (Friedman et al., 2018). Likewise, CD22 levels highly rose in mouse models of ALS, and Niemann-Pick type C, and this pattern was associated to an anti-inflammatory role in the activation of microglia (Cougnoux et al., 2018; Funikov et al., 2018). Hence, targeting CD22 may provide a useful tool in monitoring the response of neuroinflammation to therapeutic interventions (Cougnoux et al., 2018; Funikov et al., 2018; Pluvinage et al., 2019;).

CD45 has been identified as the receptor of CD22 (Stamenkovic et al., 1991; Sgroi and Stamenkovic 1994). The leukocyte common antigen CD45 is a membrane bound PTPase, and is expressed in all nucleated hematopoietic cells, including T and B cells. In the CNS, CD45 is markedly expressed by microglia and macrophages, and is particularly interesting in terms of regulation of microglial function (Tan et al., 2000; Tan, Town and Mullan, 2000; Cosenza-Nashat et al., 2006). Microglial CD45 levels are enhanced following activation of these cells, being involved on microglial cells response in inflammatory conditions (Carson et al., 1998; Tan et al., 2000; Tan, Town and Mullan, 2000). In agreement, increased CD45 levels have been found in AD, graft-versus-host disease, MS and in HIVE too (Licastro et al., 1998; Sedgwick et al., 1998; Johnston et al., 2001; Cosenza et al., 2002; Cosenza-Nashat et al., 2006). In this context, CD45 has been found to inhibit microglial activation in different contexts including murine primary cell cultures co-treated with Aβ and Lipopolysaccharides (LPS) (Tan et al., 2000) and by reducing CD40 pathway which has been correlated with microglial activation (Tan, Town and Mullan, 2000). By the same token, CD45 deficiency in an animal model of AD resulted in accelerated amyloidosis characterized by abundant β-amyloid plaques and increased TNF-α and IL-1β levels, which led to inflammatory microglia, impaired Aβ phagocytosis, and neuronal loss (Zhu et al., 2011).

All these data suggest that microglial CD45 may function to maintain the immunologically characteristic state of the CNS, and to downregulate and control activated microglia during inflammation following injury.

2.4 CD47-SIRP-α

The last pair, belonging to the inhibitory mechanism “Off”signalling, is the so-called CD47-SIRP-α molecules. CD47, also named IAP, is 50 kDa transmembrane IgSF protein found on cells throughout the body (Oldenborg et al., 2000; Koshimizu et al., 2002; Lehrman et al., 2018). It is constituted by a V-type immunoglobulin in its extracellular domain, a five membrane-spanning domain and a short cytoplasmic tail (Koshimizu et al., 2002). Within the CNS, CD47 is ubiquitously expressed in all resident cells, including neurons, astrocytes, myelin, microglia, and macrophages, but is also found on other myeloid cells, fibroblasts, red blood cells, platelets, and endothelial cells (Gitik et al., 2011; Han et al., 2012). Neuronal CD47 triggers a “Do-not-eat-me” signalling by binding to its microglial SIRP-α receptor (also known as CD172a, SHPS-1, p84, gp93 and BIT).

SIRP-α is a member of an immune inhibitory family of receptors (ITIMs) that downregulates innate immune functions in myeloid cells, like microglia and macrophages. Moreover, SIRP-α can also be found on neurons, in which its expression is particularly associated with synapse-rich areas, such as the molecular layer and synaptic glomeruli of the cerebellum, the plexiform layers of the retina, and the hippocampus (Ohnishi et al., 2005; van Beek et al., 2005; Gitik et al., 2011; Zhang et al., 2015) (Figure 6). Signalling through CD47-SIRP-α in neurons is reported to be involved in the regulation of neurite extension and synaptogenesis (Miyashita et al., 2004; Ohnishi et al., 2005).

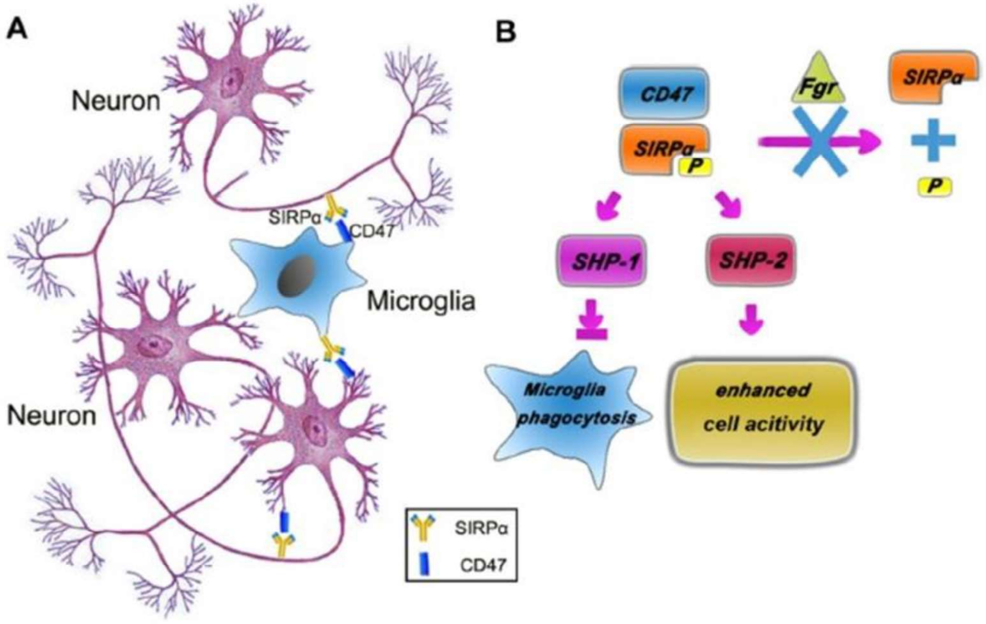

Figure 6. Cell-cell crosstalk through signal regulatory protein SIRP-α-CD47 signaling. (A) Bidirectional signaling between SIRP-α and CD47. SIRP-α and CD47 may be co-expressed on the same cell and their ligation might mediate intercellular signaling in a bidirectional manner. Although SIRP-α-CD47 signaling in microglia has not been thoroughly investigated, the individual roles of CD47 and SIRP-α have been addressed. Both SIRP-α and CD47 participate in the phagocytic functions of microglia. **(B)** SIRP signaling in microglia. The phosphorylation of SIRP-α allows the recruitment and docking of SHP-1 and SHP-2. SHP-1 and SHP-2 perform opposing biological functions. SHP-1 negatively regulates various signaling pathways to inhibit multiple cell functions such as phagocytosis; SHP-2, in contrast, positively regulates signaling events involved in cellular activities such as growth and migration. Fgr, a member of the Src kinase family that can be activated by crosslinking of Fcγ receptor, inhibits the SIRPα dephosphorylation, allowing the recruitment and docking of SHP-1. Fgr therefore inhibits the phagocytic activity of microglia (Zhang et al., 2015).

CD47-SIRP-α interaction requires cell-cell contact since both are cell membrane proteins. This system contributes to the negative regulation of phagocytosis in macrophages and microglia (Ohnishi et al., 2005; Gitik et al., 2011; Zhang et al., 2015). Accordingly, CD47 expression in myelin downregulated its phagocytosis by binding to SIRP-α on macrophages and microglia. In this same study, CD47 deficiency and reduced SIRP-α levels triggered increased myelin phagocytosis in microglial and macrophage cultures (Gitik et al., 2011). Likewise, *in vitro* assays also demonstrated that blocking CD47 enhanced myelin phagocytosis (Han et al., 2012). Another study demonstrated that CD47-SIRP-α was neuroprotective by preventing excess microglia-mediated pruning during brain development, indicating that this mechanism is required for synaptic protection in CNS development (Lehrman et al., 2018).

Concerning neurological disorders, CD47-SIRP-α has been documented to be important in a variety of CNS injuries, including ischemic and haemorrhagic brain injury and spinal cord injury (SCI). Strikingly, absence of CD47 resulted in decreasing infarct volume and ischemic swelling in a mouse model of focal cerebral ischemia, and led to improvements of white matter sparing, decreased inflammation and behavioral recovery from SCI (Jin et al., 2009; Myers et al., 2011). In the same way, CD47-deficient mice were found to be resistant to EAE, but inhibition of CD47 with a monoclonal antibody at the peak of the paralysis deteriorated EAE severity (Han et al., 2012; Gao et al., 2016). All these experiments exemplified the dual and contradictory effects of CD47 during neuroinflammation, which were likely caused by differential expression of CD47 in different cell types, location, and disease phase (Han et al., 2012). In the case of PD, for instance, CD47-SIRP-α interaction has been found to protect dopaminergic neurons against neurotoxicity, thus postulating this axis as a therapeutic strategy for PD (Huang et al., 2017).

Altogether, these results underline the importance of CD47/SIRP-α signalling in neuroinflammation progression. Notwithstanding, better characterization is required to fully understand underlying mechanisms. It would be important to decide whether to block or stimulate this signalling, since it has been demonstrated that CD47/SIRP-α have different effects depending on the disease, progression, and location (Han et al., 2012; Zhang et al., 2015; Gao et al., 2016; Huang et al., 2017).

2.5 TREM2

TREM2, widely considered as “On” molecule, is an IgSF receptor, exclusively expressed by microglia within CNS. It consists of an extracellular domain that includes a single V-type immunoglobulin domain, a short ectodomain, a single transmembrane helix, and a short cytosolic tail that lacks any signal transduction or trafficking motifs (Yeh, Hansen and Sheng, 2017; Zhou, Ulland and Colonna, 2018; Deczkowska, Weiner and Amit, 2020). TREM2 receptor binds to polyanionic molecules such as bacterial LPS, phospholipids, lipoproteins like HDL and LDL, which form complexes with APOE and POJ and apoptotic neurons, and signals through the adaptor protein DAP12, also known as TYROBP (Daws et al., 2003; Atagi et al., 2015; Yeh, Hansen and Sheng, 2017; Zhou, Ulland and Colonna, 2018; Deczkowska, Weiner and Amit, 2020). Upon TREM2-ligand interaction, DAP12 ITAMs get phosphorylated and recruit SYK which initiates protein tyrosine kinase phosphorylation, PI3K activation, efflux of Ca^{2+} and MAPK activation (Peng et al., 2010) (Figure 7).

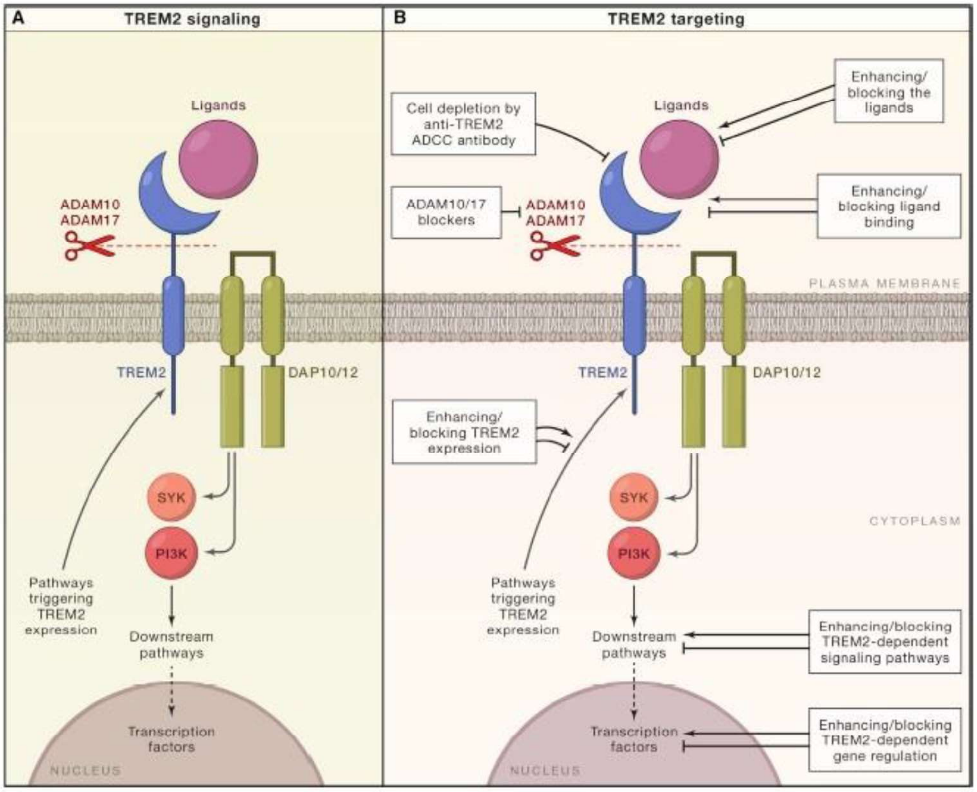
A
TREM2 signaling
Ligands
ADAM10
ADAM17
TREM2
DAP10/12
SYK
PI3K
Pathways triggering TREM2 expression
Downstream pathways
Transcription factors
NUCLEUS
B
TREM2 targeting
Cell depletion by anti-TREM2 ADCC antibody
Ligands
Enhancing/ blocking the ligands
ADAM10/17 blockers
ADAM10
ADAM17
Enhancing/ blocking ligand binding
PLASMA MEMBRANE
TREM2
DAP10/12
Enhancing/ blocking TREM2 expression
SYK
PI3K
CYTOPLASM
Pathways triggering TREM2 expression
Downstream pathways
Enhancing/blocking TREM2-dependent signaling pathways
Transcription factors
Enhancing/blocking TREM2-dependent gene regulation
NUCLEUS

Figure 7. Targeting TREM2 signalling. (A) Upon TREM2 interaction with one of its ligands, the signal is propagated via the adaptor proteins DAP10 and DAP12, resulting in activation of PI3K or Syk, respectively. Cleavage of TREM2 in the stalk region by ADAM10/17 creates sTREM2 and stops the TREM2 signaling cascade. **(B)** Possible approaches to therapeutic targeting of TREM2 and various stages of the signaling cascade (Deczkowska, Weiner and Amit, 2020).

The triggering of kinase cascades by TREM2 activation promotes microglial survival, proliferation, activation, and phagocytosis (Hsieh et al., 2009; Wang et al., 2015; Zhou, Ulland and Colonna, 2018). Hence, TREM2 has been recognized as an “Eat-me” receptor triggered by different ligands that promote phagocytosis of apoptotic neurons in different inflammatory conditions. Lack of TREM2-DAP12 complex has been reported to be a genetic risk factor for neurodegenerative diseases, since it suppresses inflammation and promotes tissue repair (Hsieh et al., 2009; Ulland and Colonna, 2018; Zhou, Ulland and Colonna, 2018). Accordingly, loss-of-function in either TREM2 or DAP12 cause Nasu-Hakola, a rare and fatal neurodegenerative disease (Paloneva et al., 2002). Similarly, blockade of TREM2 with a mAb exacerbated de progression in the EAE animal model, while treatment with intravenously applied TREM2-transduced myeloid precursors reduced inflammation and improved disease progression (Piccio et al., 2007; Takahashi et al., 2007).

Variants and mutations on TREM2 have also been associated with increased risk of PD and frontotemporal dementia, and AD (Jonsson et al., 2013; Rayaprolu et al., 2013; Cady et al., 2014). TREM2 plays a prominent role in driving microgliosis in AD mouse models and patients and is highly expressed on microglial clusters that surround amyloid plaques. These clusters modulate Aβ clearance, thereby reducing neuronal damage (Wang et al., 2015). In the same way, in mouse models of AD lacking TREM2, microglia failed to cluster around Aβ plaques indicating impaired microglial proliferation and survival around plaques, as well as the failure of microglia to migrate towards lesions (Wang et al., 2015; Wang et al., 2016; Yuan et al., 2016). Be that as it may, discrepancies have been arisen about the beneficial or detrimental role of TREM2 in AD outcome. Although TREM2 is necessary to activate microglia for Aβ plaques clearance, some other works have demonstrated that TREM2 deficiency resulted in reduced infiltration of inflammatory myeloid cells and ameliorated AD pathology, and that targeting TREM2 in an AD mouse model at early stages resulted in restored homeostatic microglia associated with Aβ plaque reduction (Jay et al., 2015; Krasemann et al., 2017).

As has been pointed out above, TREM2 has been linked to a recently characterized subset of microglia named DAM or disease-associated microglia, which localize to plaques in AD mouse models and in ALS and EAE too. This novel characterization has allowed to verify that in DAM microglia, microglial homeostatic genes are downregulated, while the expression of several AD-associated activation markers like ApoE, DAP12 and TREM2 is induced, and that TREM2 is necessary for fully activated DAM (Keren-Shaul et al., 2017; Krasemann et al., 2017). DAM microglia together with TREM2 have been shown to be beneficial for several neurodegenerative disorders since they constitute a general program involved in clearance of the protease-resistant misfolded and aggregated proteins than commonly accumulate in neurodegenerative diseases and general aging-induced damage (Keren-Shaul et al., 2017; Krasemann et al., 2017). Hence, diverse therapeutic efforts have focused on stimulating TREM2 function for future treatment of AD and other similar conditions (Keren-Shaul et al., 2017; Zhou, Ulland and Colonna, 2018; Deczkowska, Weiner and Amit, 2020). Nevertheless, blocking TREM2 has also been proposed to be essential to restore homeostatic microglia and treat neurodegenerative diseases (Krasemann et al., 2017). Therefore, further research is needed to fully understand TREM2 mechanism and DAM microglial role in neuroinflammatory processes.

3. CYTOKINES IN THE CNS

The transition from the surveillance mode to various states of activation depends on the triggering stimuli and the local microenvironment. One of the most important regulatory molecules in the local microenvironment are cytokines (Hanisch, 2002; Colton, 2009; Lively and Schlichter, 2018). Cytokines comprise a group of small polypeptides (8-30kDa) possessing tremendous diversity in their potential actions. Most cytokines signal in either an autocrine or paracrine fashion, and modulate local cellular activities including survival, growth, and differentiation. Cytokines are also upregulated in response to disease, injury, and infection, and modulate tissue repair in acute pathologic states. Therefore, they are considered as key regulators of innate and adaptative immune responses (Kim and Joh, 2006; Smith et al., 2012; Werneburg et al., 2017). These peptides have typically been classified according to their biological function in two broad categories (Hanisch, 2002; Smith et al., 2012; Akhmetzyanova et al., 2019; Wang et al., 2015b; Cherry, Olschowka and O'Banion, 2014):

1. Pro-inflammatory cytokines, such as IL-1, TNF-α, IFN-ү, IL-6, IL-12, IL-18 and GM-CSF.
2. Anti-inflammatory cytokines, which include IL-4, IL-10, IL-13 and TGF-β.

Although various types of cells, including tissue infiltrating immune cells, neurons, microglia, and astrocytes have been identified as sources of cytokines in the CNS, microglia appear to be its principal source (Kim and Joh, 2006). Microglia display a full sensory equipment to sense alterations of the surrounding environment and communicate with other cells, based on the exchange of cytokines (Hopkins and Rothwell, 1995; Hanisch, 2002). Traditionally, microglial production of pro-inflammatory cytokines has been linked to a classically activated (pro-inflammatory) phenotype. Despite the crucial role of this phenotype as an initial response following CNS insult, pro-inflammatory cytokines could become neurotoxic and harmful if they last over time. Thus, a special emphasis has been placed on microglial release of pro-inflammatory cytokines in neurodegeneration (Kim and Joh, 2006; Smith et al., 2012; Wang et al., 2015b; Lively and Schlichter, 2018). For instance, several neurological disorders such as AD, PD and ALS, and CNS injuries have shown a widespread inflammatory state with enhanced levels of IL-1β, IL-6, TNF-α, TGF-β, and IL-18 (Sawada, Sekizawa et al., 1998; Hensley et al., 2002; Imamura and Nagatsu, 2006; Swardfager et al., 2010; Akhmetzyanova et al., 2019).

By contrast, the production of anti-inflammatory cytokines has been linked with neuroprotective actions, as they are known to dampen the harmful effects of the pro-inflammatory cytokines and are related with recovery in different CNS injuries. This has been related to the microglial alternative activation phenotype, which promotes tissue remodelling, repair, and neuroprotection (Cherry, Olschowka and O’Banion, 2014; Wang et al., 2015b; Akhmetzyanova et al., 2019). That is why many therapeutic approaches attempted to reverse production of pro-inflammatory cytokines and to increase the presence of anti-inflammatory mediators in the milieu (Rivest, 2011; Laveti et al., 2013; Müller, 2013). All the same, this classification of cytokines in these two categories is a simplistic approach, since cytokines have pleiotropic biological functions depending on the secretory cell, the target cell, the receptor they bind, etc. (Aloisi et al., 1999; Ding et al., 2015). Therefore, multiple factors must be considered before classifying the actions of a specific cytokine such as purely harmful or protective/beneficial. Among the variety of cytokines with proven important effects within the CNS, there are two that have focused the attention of neuroscientists over the years. The first one is the IL-6 cytokine, which is one of the main regulatory mediators of neuroinflammation, and the second one is the IL-10 cytokine, which is considered as a counter-regulatory cytokine involved in the termination of the inflammatory process.

3.1 IL-6 role in CNS and microglial response

IL-6 is a characterized 26 kDa cytokine, originally identified as a B-cell differentiation factor, that induced the maturation of B cells into antibody-producing cells. It was soon realized that IL-6 was also involved in T-cell differentiation factor, hybridoma/plasmacytoma growth factor, and hepatocyte-stimulating factor (Erta, Quintana and Hidalgo, 2012; Smith et al., 2012). IL-6 binds and activates a receptor protein complex comprised of one non-signalling, membrane-associated α subunit (IL-6R), and two gp130 subunits, responsible for signal transduction. Ligand binding of this protein complex results in homodimerization of gp130 and activates multiple signalling mechanisms. Interestingly, a soluble form of IL-6R (sIl-6R) may also be formed by alternative RNA splicing or protease cleavage (Smith et al., 2012; Erta, Quintana and Hidalgo, 2012; Gruol, 2015) (Figure 8).

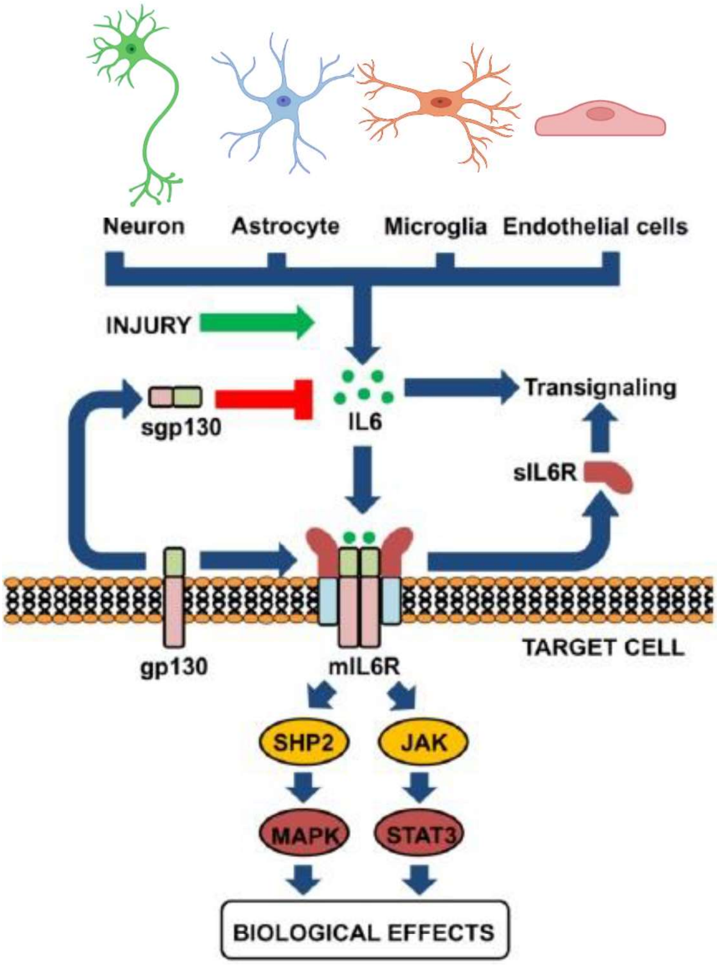
Neuron
Astrocyte
Microglia
Endothelial cells
INJURY
sgp130
IL6
Transignaling
sIL6R
gp130
mIL6R
TARGET CELL
SHP2
JAK
MAPK
STAT3
BIOLOGICAL EFFECTS

Figure 8. IL-6 is produced by different brain cells and may signal in a complex manner. Neurons, astrocytes, microglia, and endothelial cells are the essential sources of IL-6 in the CNS. All of them may produce some amounts of IL-6, but upon proper stimuli such as injury, copious amounts of IL-6 will be secreted. IL-6 can bind to the membrane-bound IL-6 receptor (mIL-6R, expressed in limited cells) or to the soluble form of the receptor (sIL-6R), which is known as trans-signaling; both can properly signal upon interaction with sgp130 protein (expressed ubiquitously). A releasable form of gp130 can also be found in biological fluids, which will exert inhibitory actions on trans-signaling (Erta, Quintana and Hidalgo, 2012).

IL-6 is considered a pleiotropic inflammatory cytokine acting in the initiation and coordination of inflammatory responses and limiting the spread of infectious agents (Hanisch, 2002; Wang et al., 2015b). Within CNS, activated microglia and astrocytes are the main source of IL-6. Neurons can produce IL-6 under some conditions, particularly during CNS disease and injury or strong neuronal activity (Erta, Quintana and Hidalgo, 2012; Gruol, 2015; Wang et al., 2015b). Both neurons and glia express IL-6R and gp130 too (Gruol, 2015; Hampel et al., 2005). IL-6 levels in the brain are typically low under normal conditions but increase significantly in neurons and glial cells in neuroinflammation following CNS infection, injury or in number of CNS diseases (Erta, Quintana and Hidalgo, 2012; Gruol, 2015). It is therefore not surprising that IL-6 expression is altered in AD, MS, PD and Huntington's disease (Bauer et al., 1991; Malmeström et al., 2006; Nagatsu and Sawada, 2007; Björkqvist et al., 2008). In AD, MS and in Huntington's disease, this increase was associated with neuronal damage, and the neutralization of IL-6 led to a reduced disease (Gijbels et al., 1995; Qiu and Gruol, 2003; Björkqvist et al., 2008). In the same way, chronic overproduction of IL-6 achieved in transgenic animals has been linked to neurodegeneration, while IL-6 deficiency or signalling blocking, respectively, improved neuronal survival after optic nerve crush or induced a significant increase in functional recovery and decreased gliosis in SCI (Campbell et al., 1993; Fisher et al., 2001; Mukaino et al., 2010).

In contrast, anti-inflammatory and neuroprotective effects have also been attributed to IL-6, for example in PD, and in Huntington's disease (Müller et al., 1998; Bensadoun et al., 2001). Despite the detrimental role of IL-6 on AD, IL-6 has been also seen to be beneficial at early stages from an AD mouse model (Chakrabarty et al., 2010). Additionally, IL-6 has been reported to be neuroprotective by increasing axonal regeneration in spinal cord-injured rats when administered intrathecally (Cao et al., 2006), after sciatic nerve transection by reducing neuronal loss in intraperitoneally IL-6-treated rats (Ikeda et al., 1996) and in ischemic rats by decreasing the volume lesion after intracerebroventricular IL-6 treatment (Loddick, Turnbull and Rothwell, 1998). Similarly, IL-6-deficient animals displayed higher neuronal death after cryolesion, sciatic nerve axotomy and a reduction in functional recovery in axotomized animals (Murphy et al., 1999; Zhong et al., 1999; Swartz et al., 2001). These finding suggest that IL-6 effects depend on several factors including the time-point and the specific microenvironment where this cytokine is produced or administered in the CNS.

Due to all this, it is not surprising that several therapeutic approaches have proposed the blockade of IL-6 signalling as a treatment option for neuroinflammatory conditions (Erta, Quintana and Hidalgo, 2012; Gruol, 2015; Rothaug, Becker-Pauly and Rose-John, 2016).

3.2 IL-10 role in CNS and microglial response

IL-10, a homodimeric 17 kDa protein, was identified over two decades ago, and is to date the most widely studied anti-inflammatory cytokine (Lobo-Silva et al., 2016; Burmeister and Marriott, 2018). It is already accepted that IL-10 plays a critical role in the balance and prevention of inflammation and is a mediator in many CNS injuries and diseases (Cua et al., 2001; Lobo-Silva et al., 2016; Anderson et al., 2017; Burmeister and Marriott, 2018). Since its initial discovery, IL-10 has been found to be produced by an array of leukocytic cell types, including monocytes and granulocytes, as well as non-immune cells such as epithelial cells and keratinocytes (Lobo-Silva et al., 2016; Burmeister and Marriott, 2018). Within the CNS, IL-10 production has been detected on different cell types as well. Microglial cells are the most investigated innate immune cells in the brain and thus the main studied cytokine producers, including IL-10 (Anderson et al., 2017). Several studies have confirmed microglial IL-10 production and its induction stimulated by the presence of the so-called “alert” signals (Aloisi et al., 1999; Seo, Kim and Lee, 2004; Correa et al., 2010). This suggests that the presence of some molecules in the microenvironment can impact IL-10 production by microglia, thus shaping the outcome of the inflammatory response. In addition to microglia, astrocytes have also shown IL-10 production in response to PAMPs and as a result of Fcγ receptor I stimulation (Speth et al., 2000; Blanco et al., 2005). Meanwhile, the expression of IL-10 receptor has not only been described on microglia and astrocytes, but also on oligodendrocytes and neurons (Mizuno et al., 1994; Gaupp, Cannella and Raine, 2008; Xin et al., 2011).

When binding to its receptor, IL-10 triggers a series of signaling cascades mediated by JAK signal transducer and STAT pathway, particularly by STAT3. Signalling through the IL-10 receptor regulates several steps of the immune response, from decreasing cytokine gene expression to down-regulating the expression of major histocompatibility complex class II (MHC-II) and thus antigen presentation to T-cells. Furthermore, IL-10 has been shown to prevent apoptosis by activating the phosphatidylinositol-4,5-bisphosphate-3-kinase (PI3K)/Akt cascade and enhancing the expression of anti-apoptotic factors as Bcl-2 and Bcl-xl, whilst attenuating that of caspase-3. The processes mediated by IL-10 have important implications at the CNS level (Lobo-Silva et al., 2016) (Figure 9).

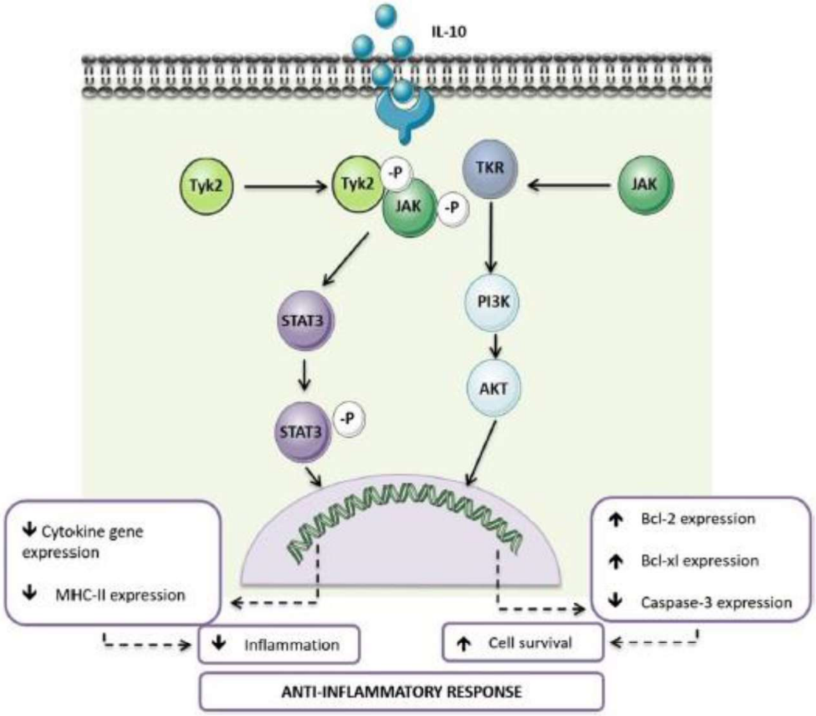
IL-10
Tyk2
Tyk2
-P
JAK
-P
TKR
JAK
STAT3
PI3K
AKT
STAT3
-P
Cytokine gene expression
MHC-II expression
Bcl-2 expression
Bcl-xl expression
Caspase-3 expression
Inflammation
Cell survival
ANTI-INFLAMMATORY RESPONSE

Figure 9. IL-10 cascade signalling. The role of IL-10 receptor signalling in anti-inflammation. Overview of the IL-10R signaling cascade and the main cellular effects triggered by IL-10 (Lobo-Silva et al., 2016).

IL-10 expression is upregulated under pathological conditions, mainly associated with the recovery phase or later time-points after injury (Kennedy et al., 1992; Samoilova, Horton and Chen, 1998; Gonzalez et al., 2009). Thereby IL-10 was shown to be elevated in the injured brain in several neurodegenerative diseases and animal models of disease, including EAE (Kennedy et al., 1992; Samoilova, Horton and Chen, 1998), MS (Hulshof et al., 2002), traumatic brain injury (Kamm et al., 2006), AD (Apelt and Schliebs, 2001) and PD (Rentzos et al., 2009). As a potent anti-inflammatory cytokine, IL-10 is able to inhibit the production of pro-inflammatory cytokines by microglia, thus protecting astrocytes from excessive inflammation and increasing neuronal survival (Balasingam and Yong, 1996; Zhou et al., 2009). Therefore, the increase of IL-10 in various neuroinflammatory conditions have been proposed as a powerful therapeutic target to treat these pathological disorders. Accordingly, intraperitoneal, and intramedullary injection of IL-10 reduced inflammation and improved motor function after SCI in rats (Hellenbrand et al., 2019). Furthermore, increase of IL-10 levels led to symptoms reduction in EAE model and its expression was correlated with the recovery phase in this model (Kennedy et al., 1992; Samoilova, Horton and Chen, 1998; Burkhart et al., 1999). Other observations also revealed IL-10 as therapeutic strategy after traumatic brain injury (TBI) and in ALS and PD diseases, since its induction was linked to an improvement in all these conditions (Joniec-Maciejak et al., 2014; Kwilasz et al., 2015; Gravel et al., 2016; Peruzzaro et al., 2019). In this regard, IL-10 deficiency resulted in exacerbated brain inflammatory response in brain ischemia and noticeable cognitive deficit after LPS administration (Richwine et al., 2009; Pérez-de Puig et al., 2013).

Nevertheless, despite the initially high expectations, the therapeutic success of IL-10 has been conflicting. Taking the case of MS, even the reported benefits of IL-10 administration on EAE models, it has also been observed that depending on the routes of IL-10 administration, its effects varied from decreased, to no effect, to actual increased clinical scores (Kwilasz et al., 2015). In the same way, some authors claimed that IL-10 administration in AD transgenic mice was detrimental since it led to reduced amyloid-β reduced phagocytosis by microglia, and this worsened cognitive decline (Chakrabarty et al., 2015). Conversely, other studies reported that IL-10 overexpression in the hippocampus of AD transgenic mice increased neurogenesis and enhanced cognition (Kiyota et al., 2012). Hence, a deep understanding of the cellular and molecular mechanisms of IL-10 is critical to ensure its effects on preventing neurological disorders instead of exacerbating them.

4. FACIAL NERVE AXOTOMY MODEL

The FNA model is one of the most widely used to study degeneration and regeneration of the CNS *in vivo*. Georg Kreutzberg and co-workers popularised this model at the end of the 20th century, and it has become the best-established model *in vivo* (Kreutzberg, 1986; Kreutzberg, 1996; Moran and Graeber, 2004).

The facial nerve innervates the muscles that control facial expression in man, and thus is of great importance for social interactions. It is the most liable of all cranial nerve damage, and trauma to the facial nerve commonly occurs as a sequel of road traffic-accidents, resulted from intracranial compression from tumour growth, consequential to infectious diseases or due to damage during surgical manipulations (Graeber, Bise and Mehraein, 1993). In rodents, facial nerve controls whisker movement and eye blink (Moran and Graeber, 2004).

This model, which consists in the total transection of the facial nerve, has been extensively characterized, since this system presents numerous benefits. First of all, nerve transection is carried out at the stylomastoid foramen level, fact that implies that there is no direct CNS trauma. Therefore, there is no disruption of the blood-brain barrier, as the lesion is done at peripheral level. Because it is a retrograde model, the injury effects are then analysed on the facial nucleus (FN), which is located on the brainstem and entails groups of FMNs that innervates face muscles in rodents (Semba and Egger, 1986; Streit and Kreutzberg, 1988; Moran and Graeber, 2004). In addition, the surgical procedure is straightforward and of mild severity compared to other models of nerve injury. Researchers further benefit from the analytical strength of an experimental system paired with a contralateral control FN. Lastly, FNA represents several experimental systems in one. Also, facial nerve lesions of varying degrees of severity have been used to examine in detail the quantitative and qualitative differences of FMNs response patterns, and those of their microenvironmental following a range of sublethal and lethal stimuli (Moran and Graeber, 2004) (Figure 10).

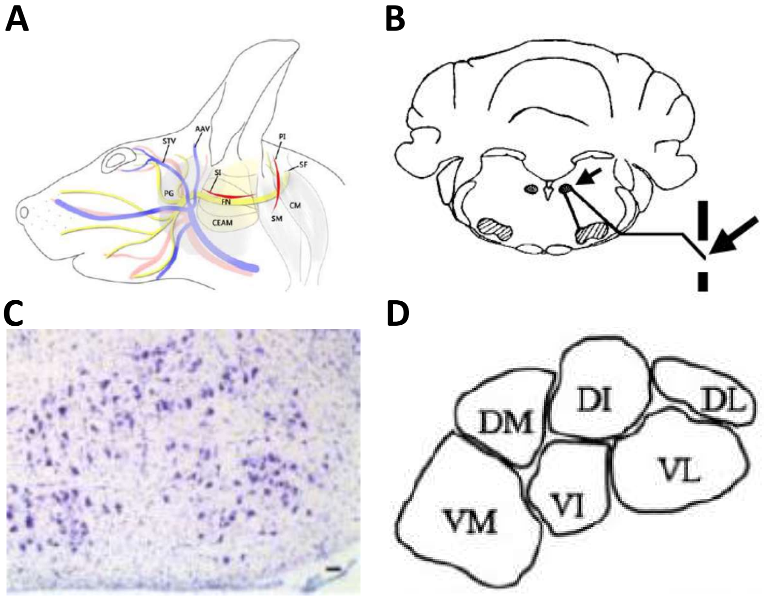

Figure 10. FNA model. (A) Drawing of the topographic anatomy of the facial nerve and the surgical approaches for FNA in mouse. **(B)** Diagram showing the location of the FN on either side of the brainstem (hatched areas). The line indicates the trajectory of the facial nerve from the FMNs. The facial nerve is transected after its exit from the stylomastoid foramen (large arrow). **(C)** Representative FN stained with thionin. **(D)** Template of the facial subnuclei: VM (ventromedial), DM (dorsomedial), VI (ventral intermediate), DI (dorsal intermediate), VL (ventrolateral), DL (dorsolateral) (Moran and Graeber, 2004; Mesnard et al., 2010; Wang et al., 2012; Olmstead et al., 2015).

As previously stated, FNA is a retrograde model, and consequently, all the impacts linked to this injury are triggered on the FN in the brainstem, which involve degeneration and regeneration of FMNs and glial activation. Each nucleus harbours between 3200 and 6500 motoneurons which are organized in 6 subnuclei: dorsolateral, ventrolateral, dorsal intermediate, ventral intermediate, ventromedial, and dorsomedial (Komiyama, Shibata and Suzuki, 1984; Semba and Egger, 1986; Mesnard et al., 2010; Olmstead et al., 2015). These nuclei respond differentially to facial nerve transection. The ultimate aim of these FMNs is to survive injury by reconnecting axotomized axons induced by a regenerative event, that lasts for 2-3 weeks until recovery is achieved. During the process, some neurons will be able to reconnect their inputs, whereas others will fail and undergo cell death.

FNA is characterized by a delayed form of neuronal cell death, with a maximum peak at 14dpi together with the formation of microglial clusters and the higher lymphocyte recruitment, although it has been found that the total number of motor neurons can progressively decrease until 10 weeks after axotomy (Möller et al., 1996; Raivich et al., 1998). Neuronal response depends on the animals used and injury severity. In the adult rat, for instance, most FMNs survive nerve transection, while in mice, the majority of authors have reported around 20-40% of FMNs loss (Ferri, Moore and Bisby, 1998; Moran and Graeber, 2004; Villacampa et al., 2015). Some studies have confirmed that not all the FN subnuclei responds in the same way. While some subnuclei remain unaltered, others undergo significant neuronal death (Mesnard et al., 2010). For instance, whereas the ventrolateral subnucleus results in significant loss, the ventromedial subnucleus maintain full FMNs with the same nerve injury (Moran and Graeber, 2004; Mesnard et al., 2010; Olmstead et al., 2015). The cell death mechanisms involved following axotomy is an area of intensive research.

In parallel with neurodegeneration, a regenerative process of the axotomized axons is also induced in surviving neurons, leading to a partial functional recovery of muscles innervated by the facial nerve after 2-3 weeks of nerve transection, reflecting the establishment of new connections occurring at these time frame. In man, functional recovery following facial nerve trauma remains controversial (Moran and Graeber, 2004). Although the exact mechanisms mediating either neuronal survival and axonal regeneration or neuronal death remain unclear, microglia and lymphocytes are thought to play a role in the maintenance of FMNs viability, and thereby in supporting their ability to regenerate.

4.1 Microglial and astroglial reaction after FNA

Following FNA, microglial cells become activated, proliferate, attach to axotomized FMNs wrapping them, and participate in the so-called phenomenon “synaptic stripping” (Blinzinger and Kreutzberg, 1968; Kreutzberg, 1996). Microglial activation involves the expression of several markers including CR3, MHC-I and MHC-II which allow them to function as antigen-presenting cells, costimulatory molecules such as B7-1, TNF-α, and several cell adhesion molecules like thrombospondin and ICAM-1, an important cell-surface ligand of αMβ2 (CD11b/CD18) and αLβ2 (CD11a/CD18) integrins. In addition, activated microglia express APP and TGF-β which is involved in tissue repair (Kreutzberg, 1996; Raivich et al., 1999). This activation takes place within the first 24 hours after nerve injury, reaching a peak between 7 and 14dpi, and is followed by a burst of proliferative activity, with a peak at days 2 and 3 (Raivich et al., 1994; Kalla et al., 2001). Besides, at these earlier stages is when synaptic stripping takes place as well. Microglia or their processes are placed between the healthy presynaptic and postsynaptic elements to disconnect excitatory inputs to motor neurons allowing axonal regeneration and functional recovery. At later stages of axotomy, those neurons that are not able to regenerate undergo cell death (Blinzinger and Kreutzberg, 1968; Graeber, Bise and Mehraein, 1993; Kreutzberg, 1996). Thereafter, from 14dpi onwards, the number of FMNs wrapped by microglia decrease, supporting the idea that neuronal wrapping and synaptic stripping is a protective phenomenon in this paradigm (Kreutzberg, 1996).

At later stages, from 14-21dpi, microglia are characterised to group in clusters (groups of 4-5 microglial cells tightly grouped and located next to FMNs), with a maximum at 14dpi. Within this time frame is when also a delayed neuronal cell death peak takes place. The presence of microglial clusters at later time-points suggests that this phenomenon is associated with neuronal death (Raivich et al., 1998; Kalla et al., 2001; Petitto et al., 2003) and in some studies, the amount of cluster formation was used as a measure of motor neuron cell death (Petito et al., 2003; Dauer et al., 2011). Notwithstanding, other studies have reported that the increase of these microglial clusters was correlated with higher neuronal survival, pointing out that microglial cluster formation may have another function rather than simple phagocytosis of degenerating neurons (Almolda et al., 2014; Villacampa et al., 2015). Interestingly, these clusters express typical markers of antigen-presenting cells (MHC-I, MHC-II), costimulatory molecules (B7, ICAM1, αXβ2 integrin) and various inflammation-associated cytokines (TNF-α, IL-1β and TGFβ3). As shown in different studies, these clusters attract invading lymphocytes and provide an adhesive substrate for the T-cells, a key component in the function of active antigen presenting cells (Raivich et al., 1998; Kalla et al., 2001), which reinforce other available evidence (as discussed in Section 4.3) on the importance of microglial clusters-lymphocytes crosstalk on neuronal death and phagocytosis processes. Finally, at 28dpi, when the functionality of regenerated FMNs has been recovered, most microglial cells start to adopt a resting ramified morphology (Almolda et al., 2014; Villacampa et al., 2015).

Concomitant with microglial cells proliferation, local astrocytes, which normally express low levels of GFAP, become reactive and undergo hypertrophy as a response to axotomy of FMN reaching their maximum levels of expression 3 weeks after injury (Graeber and Kreutzberg, 1986; Moran and Graeber, 2004). GFAP is synthetised de novo as early as 24 h after axotomy, and following this increase, these reactive astrocytes reorganize their cytoskeleton. The early onset of this transformation suggests an induction of the astroglial response by a signal provided by the lesioned FMN themselves. This increased detected on GFAP synthesis returns to normal levels when neurons become restored, or remains higher if regeneration is impeded, indicating that the time course and extent of GFAP synthesis are strongly influenced by successful or unsuccessful regeneration (Tetzlaff et al., 1988). Additionally, it has been speculated that the transformation of astrocytes also plays an important role for neuronal repair, thus pointing out that both GFAP increase, and astrocyte remodelling are fundamental for neuronal regeneration in FNA paradigm (Graeber and Kreutzberg, 1986; Tetzlaff et al., 1988). In this sense, electron microscopy has revealed that astrocytic cell processes become thin lamellar extensions that begin to take over the perineuronal positions between the second and third week, replacing the spaces that were previously occupied by wrapping microglia. After 3 weeks, these lamellar processes cover virtually all neuronal surfaces and persist if target reinnervation is prevented (Graeber and Kreutzberg, 1988).

The observed long-term deafferentation of the regenerating motoneurons by glial cells is of clinical importance. The delayed astrocyte reaction may serve as a protective role by preventing microglial phagocytosis and may protect vacated post-synaptic sites from being “taken-over” by inappropriate axonal connections. Hence, the changes in astrocytes and microglia observed in the FN represent a high degree of neuroplasticity also seen in other brain regions. In this case, little is still known about the signals that lead to the microglia and astrocytes becoming activated following axotomy, and the final outcome of this activation (Moran and Graeber, 2004).

4.2 Immune cell infiltration after FNA

As discussed previously, FNA model is characterized by lymphocyte infiltration with no disruption of the blood-brain barrier. It is well accepted that T-cells infiltrates in the mouse FN and aggregate around axotomized FMNs in two different waves: one as early as 3dpi and a second one at 14dpi in which the peak of infiltration of these cells occurs in line with the formation of microglial clusters (Raivich et al, 1998; Petitto et al., 2003). This type of T-cells detected to infiltrate as a consequence of the injury in the FNA model were identified as CD4+ T-cells (Serpe et al., 2003) to be thereafter categorized as of the Th2 subtype (Deboy et al., 2006).

It is worth remarking that the second wave of lymphocyte recruitment in FNA model has been linked to microglial clusters capability to act as chemoattractant by changing the adhesion properties of the vascular endothelium which induce lymphocyte infiltration and chemotaxis. These lymphocytes have been seen to continually interact with microglial clusters by the ability of these activated microglia to express MHC-II, which has been described in microglial-lymphocyte crosstalk (Raivich et al., 1998; Byram et al., 2004; Villacampa et al., 2015). These mechanisms, in which microglia act as antigen presenting cells for T-cells, have been demonstrated to be neuroprotective rather neurodegenerative in FNA model (Raivich et al., 1998; Byram et al., 2004). Accordingly, some other studies have also attributed a neuroprotective role to T-cell infiltration in this model, since lack of mature T cells resulted in an increase in neuronal death (Serpe et al., 1999 and 2003; Serpe, Sanders and Jones, 2000). Additionally, $CD4^+$ Th2-like cells have been demonstrated to work collectively together with IL-10 to modulate anti-inflammatory events in the environment surrounding the injured neurons, thus providing neuroprotection to FMNs in FNA model (Xin et al., 2011).

In summary, neuronal cell death can lead to a significant influx of activated T cells, which home on the neuronal debris and the neighbouring phagocytotic microglia located in clusters. It is worth mentioning that the specific subtypes of T-helper lymphocytes infiltrating the parenchyma of the FN and their contribution to the evolution of the lesion are still not well characterized and further research is needed to fully understand the mechanism by which Th2 cells confer neuroprotection to FMNs.

4.3 GFAP-IL6Tg and GFAP-IL10Tg mice after facial nerve axotomy model

Previous published results from our lab using transgenic mice with an overproduction of IL-6 (GFAP-IL6Tg) or IL-10 (GFAP-IL10Tg) in FNA model showed an increase of neuronal death on GFAP-IL6Tg mice and higher neuronal survival on GFAP-IL10Tg in comparison with the corresponding *wild-type* (WT) littermates. All these changes were accompanied by alterations in microglial activation pattern and lymphocyte infiltration (Almolda et al., 2014; Villacampa et al., 2015).

On one hand, IL-6 overproduction led to increased microglial proliferation and activation at earlier time-points, suggesting a more rapid response of microglial cells to axotomy due to IL-6 overproduction. Interestingly, these transgenic animals were also characterized for lower microglial wrapping to FMNs, supporting the idea that synaptic stripping is a protective phenomenon in this paradigm, and that this loss of protection could be involved in the higher FMNs death observed in GFAP-IL6Tg animals. Additionally, GFAP-IL6Tg mice presented lower number of microglial clusters at 14 dpi, at the peak of neuronal death, indicating deficiencies in effective microglial phagocytosis or other roles played by those structures. This fact was coincident with increased infiltration of T-lymphocytes in the FN, a phenomenon that, despite its usually ascribed beneficial effects, it did not protect FMNs in GFAP-IL6Tg, possibly due a shift in T-cell phenotype. Loss of neurons coincided, at later time-points, with downregulated expression of molecules like CD18 and CD11b in GFAP-IL6Tg mice. Altered integrin expression in microglia was hypothesized to be a signal of reduced microglial activation or even may involve a deficient attachment between microglia and lymphocytes, and in the control of the mechanisms of neuronal wrapping and lymphocyte function in this paradigm (Almolda et al., 2014). In general, IL-6 overproduction induced a pro-inflammatory and deficient microglial response, exemplified by lower cluster formation and wrapping, that resulted in increased FMNs death in GFAP-IL6Tg animals after FNA.

On the other hand, IL-10 overproduction did not exert significant effects on microglial activation, proliferation, and morphology after FNA, although an upregulation in the phagocytic CD16/32 receptor and CD18 were found in the early phase of microglial activation. Those effects could be related to increased microglial adhesion to FMNs and earlier phagocytic activity in microglia, which may support FMNs survival.

Interestingly, increased number of microglial clusters were detected in GFAP-IL10Tg at 14 dpi, coinciding with the peak of FMNs death. In these animals, FMNs survival was increased, and therefore, microglial clusters were linked to higher FMNs survival. Changes in microglial cluster formation together with the higher CD16/32 and CD18 staining observed at earlier time-points in GFAP-IL10Tg mice could be related to faster or more effective phagocytosis by microglial cells. In these animals, higher T-lymphocyte infiltration was established in transgenic mice, supporting the idea that, in this paradigm, recruited T-cells play a key role in neuroprotection (Villacampa et al., 2015).

Despite the clear opposite effects of pro-inflammatory IL-6 overproduction or anti-inflammatory IL-10 overproduction in FNA outcome, the specific mechanisms producing microglial changes and its ultimate effects on FMNs survival remain to be clarified.

II. HYPOTHESIS AND OBJECTIVES

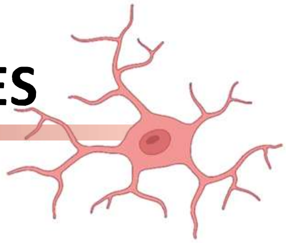

The general hypothesis of this work is that targeted-astrocyte overexpression of either IL-6 or IL-10, which produce a local pro-inflammatory or an anti-inflammatory microenvironment, will induce alterations in the “On/Off” signalling established between microglia and neurons after FNA. These changes will significantly alter the inflammatory response regulating neuronal survival after peripheral axotomy.

The overall objective of this thesis is to characterise the effects of local pro-inflammatory or anti-inflammatory environments in the communication between microglia and neurons through the “On/Off” molecular signalling mechanisms under homeostatic conditions and after peripheral nerve injury.

From this main objective the following specific objectives arise:

1. To establish the expression of the main molecules involved in microglial “Off” receptors, namely CD200R, CX3CR1, CD45 and SIRP-α, and the corresponding neuronal ligands CD200, CX3CL1, CD22 and CD47, in the CNS during homeostatic conditions.
2. To determine if local CNS pro-inflammatory or anti-inflammatory microenvironment induced by chronic overproduction of IL-6 and IL-10 modifiy the microglial “Off” receptors CD200R, CX3CR1, CD45 and SIRP-α or their corresponding ‘Off’ neuronal ligands CD200, CX3CL1, CD22 and CD47 during homeostatic conditions.
3. To characterize the expression of microglial “Off” receptors CD200R, CX3CR1, CD45 and SIRP-α and their corresponding neuronal ligands CD200, CX3CL1, CD22 and CD47 after FNA and their influence in neuronal survival.
4. To determine if local CNS pro-inflammatory or anti-inflammatory microenvironment induced by the overproduction of IL-6 and IL-10 modify microglial “Off” receptors CD200R, CX3CR1, CD45 and SIRP-α and their corresponding neuronal ligands CD200, CX3CL1, CD22 and CD47 after FNA.
5. To explore the expression of the “On” molecule TREM2 in microglia during homeostatic conditions in the FN.
6. To determine if local CNS proinflammatory or anti-inflammatory environment induced by the overexpression of IL-6 and IL-10 exerts any effect on the expression of TREM2 under homeostatic conditions.
7. To characterize the expression of microglial “On” signal TREM2 after FNA.
8. To determine if local CNS proinflammatory or anti-inflammatory microenvironments induced by the overexpression of IL-6 and IL-10 exerts any effect on TREM2 pattern expression after FNA, and its influence in neuronal outcome.

III. METHODOLOGY

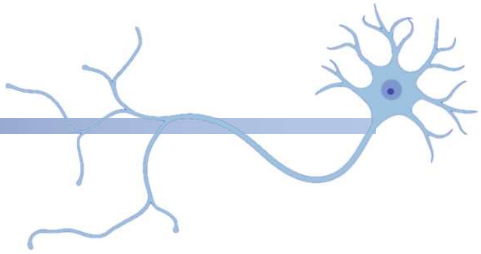

1. MATERIALS AND METHODS

1.1 Animals

For this study, GFAP-IL6Tg and GFAP-IL10Tg animals and the corresponding WT littermates from both sexes of 3-4 months old were used. All mice were maintained with food and water *ad libitum* in a 12-hour light/dark cycle. All experimental animal work was conducted in accordance with Spanish regulations (Ley 32/2007, Real Decreto 1201/2005, Ley 9/2003 and Real Decreto 178/2004) in agreement with European Union directives (86/609/CEE, 91/628/CEE I 92/65/CEE) and was approved by the Ethical Committee of the Autonomous University of Barcelona, Spain. All efforts were aimed to minimize the number of animals used to get reliable scientific data, as well as animal suffering.

1.2 Construction of GFAP-IL6 fusion gene and production of transgenic mice

Construction and characterization of the GFAP-IL6 transgenic mice was previously described (Campbell et al., 1993). In short, an expression vector obtained from the GFAP gene was used to link the expression of IL-6 in astrocytic cells. Once a full-length cDNA for murine IL-6 was obtained, modifications were triggered by replacing the 3' untranslated region with a 196-bp simian virus (SV40) late-region fragment providing a polyadenylyation signal. Afterward, the GFAP fusion genes were injected into fertilized eggs of (C57BL/6J x SJL) F1 hybrid mice. Transgenic offspring were identified by slot-blot analysis of tail DNA with 32P-labeled SV40 late region fragment.

1.3 Construction of GFAP-IL10 fusion gene and production of transgenic mice

The full-length cDNA encoding murine IL-10 was cloned into a construct containing the GFAP promoter and the polyadenylation signal sequence from the hGH gene, as previously described (Campbell et al., 1998; Almolda et al., 2015). The construction of GFAP-IL-10 gene was microinjected into fertilized eggs from SJL/L mice. Then, F1 offspring were backcrossed again with C57/BL6 strain for at least 10 generations to obtain GFAP-IL10Tg mice. This transgenic offspring was identified by PCR using genomic DNA extracted from tail biopsies for the detection of hGH.

1.4. Tissue processing for PCR analysis

DNA was extracted from tail biopsies using the DNA extraction kit (740.952.250, Macherey–Nagel) following the manufacturer's instructions. Briefly, tail samples were incubated for 2 hours at 56ºC in 180 µL T1 buffer and 25 µL proteinase-K. After 5-minute centrifugation at 12,000 rpm (16,128 g), the remaining supernatant was transferred to a new tube, and 200 µL of lysis buffer and 200 µL of 100% ethanol were added and mixed gently. Specific columns provided in the kit were used to separate DNA by centrifuging them at 16,128 g for 3 minutes. After 2 washes and centrifugation rounds (16,128 g for 3 min) with washing buffer, and one additional centrifugation with buffer 5, the DNA was eluted from the column and recovered in a new tube by adding buffer BE and centrifuging at 16,128 g for 2 minutes (Almolda et al., 2015).

1.5 Facial Nerve Axotomy and Experimental Groups

Adult (3-4 months) GFAP-IL6Tg, GFAP-IL10Tg and WT mice were i.p. anesthetized with a solution of xylazine (20mg/kg) and ketamine (80mg/kg) at a dose of 0.01ml/g. The skin behind the right ear was shaved and a little incision was made. The skin and muscles were thoroughly separated so as to expose the facial nerve. The facial nerve was dissected, and then one millimetre of it was rejected at the level of the stylomastoid foramen. After the surgery, the skin was stitched with 5-0 nylon (TC16, Suturas Aragó). Corneal dehydration was prevented by using Lacri-lube® eye ointment. In order to ensure that the facial nerve transection was properly done, the complete whisker paralysis was verified after anaesthesia recovery.

NL and axotomized animals were distributed in different experimental groups and euthanized at 3, 7, 14, 21 and 28dpi to be processed for IHC, flow cytometry and protein analysis.

1.6 5’ Bromodeoxyuridine Injections

To determine microglial proliferation in the FNA model, proliferative cells were labeled with 5’-bromodeoxyuridine (BrdU). BrdU is a synthetic thymidine analog which incorporates into the DNA of dividing cells during the S-phase and can be transferred to daughter cells upon replication. Lesioned WT (n = 4) animals were intraperitoneally injected with BrdU (100 mg/kg, B5002, Sigma-Aldrich, St. Louis) diluted in 0.1 M PBS (pH 7.4) every 24 hours, from the day of the lesion to 14dpi, to be sacrificed afterward.

1.7 Tissue processing for IHC analysis

Animals, deeply anesthetized (dose of 0.015 ml/g of 80 mg/kg ketamine and 20 mg/kg xylazine solution, i.p.), were perfused intracardially for 10 minutes with 4% paraformaldehyde in 0.1 M phosphate buffer (pH 7.4). Brains were immediately removed and post-fixed for 4 hours at 4ºC in the same solution. Subsequently, samples were cryopreserved in a 30% sucrose solution in 0.1 M phosphate buffer for 48 hours at 4ºC, frozen with chilled 2-methylbutane solution (320404, Sigma-Aldrich) and stored at -80ºC. Free-floating coronary sections (30-µm-thick) of the brainstem containing the FN were obtained using a CM5305s Leica cryostat and were stored at -20ºC in Olmos (de Olmos, 1977) antifreeze solution until their use.

1.8 Single IHC staining

Free-floating cryostat sections were processed for the visualization of the following pairs of “Off” and “On” markers expressed in neurons and microglia: CD200-CD200R, CD22-CD45, CX3CL1, SIRP-α-CD47 and TREM2; the proliferation marker pHH3; and the synaptic marker synaptophysin. A minimum of 4 animals were used for each condition. After 10 minutes of endogenous peroxidase blocking with 2% H_2O_2 in 70% methanol, sections were incubated for 1 hour in either blocking buffer solution 1 (BB-1, containing 10% of foetal bovine serum, 0.3% of BSA in 0.05 M TBS (pH 7.4) and 1% Triton X-100 (TBS 1% Triton)), or, in the case of CD200R, CD45 and TREM2, with the blocking buffer solution 2 (BB-2, containing 0.2% gelatin (powder food grade, 104078, Merck) in TBS with 0.5% Triton X-100 (TBS 0.5% Triton)). The appropriate primary antibodies diluted in the same blocking solution were then added overnight at 4ºC followed by 1 hour at RT (Table 2). In the case of TREM2, the incubation was performed for 48 hours at RT. Sections incubated in media without lacking the primary antibody were used as a negative control and spleen sections were used as positive control. After washes with TBS 1% Triton or TBS 0.5% Triton, the corresponding secondary antibodies diluted in their respective blocking solutions were incubated for 1 hour at RT (Table 2). After 1 hour incubation at RT in horseradish streptavidin-peroxidase (Table 2), sections were washed with TB and the staining was visualized by incubating the brain samples with a 0.5 mg/ml DAB solution (D5637-5G; Sigma-Aldrich) for 3 minutes at RT. Sections were then mounted in slides, air dried, dehydrated in graded alcohols, and after xylene treatment, coverslipped with DPX (06522; Sigma-Aldrich).

1.9 Double and triple IHC

Double immunolabeling was carried out to determine the cellular localization of the following “Off” markers CD200, CD45, CD22, CX3CL1 and SIRP-α. In the case of CD200, CD22, CX3CL1 and SIRP-α double immunostainings, free-floating sections were firstly incubated for primary antibodies against CD200, TL (endothelial cells and microglia), GFAP (astrocytes) or SIRP-α, as described above, and then they were detected using a fluorescently labelled secondary antibody (Table 2). After several washes with TBS 1% Triton, sections were incubated for 1 hour at RT in BB-1. Then, the following antibodies were incubated overnight at 4ºC, followed by 1 additional hour at RT: 1) for CD200 staining, GFAP, Iba-1 (microglia), MBP (myelin), NeuN (neurons) and TL were used; 2) for CD22 and CX3CL1 immunostainings, antibodies against those molecules were incubated after TL and GFAP; and 3) for SIRP-α, Iba-1 or TREM2 were used as secondary primary antibodies (Table 2). Subsequently, sections were washed with TBS 1% Triton and incubated for 1 hour at RT with the corresponding secondary fluorescent antibodies diluted in BB-1 (Table 2).

To study CD45 expression in the FN, triple immunolabeling combining CD45, Iba1 and CD3 was carried out. After blocking the endogenous peroxidase for 10 minutes, sections were washed with TBS 0.5% Triton and incubated for 1 hour in BB-2. Thereafter, sections were incubated with CD3 (Table 2) overnight at 4ºC followed by one additional hour at RT. After adding the corresponding fluorescent secondary antibody for 1 hour at RT (Table 2), the CD45 antibody (Table 2) was added overnight at 4ºC plus an additional hour at RT followed by 1 hour incubation with the secondary antibody (Table 2). Lastly, after several washes with TBS 0.5% Triton, a final overnight incubation at 4ºC with Iba1 (Table 2) primary antibody was carried out, followed by an additional hour at RT. An anti-rabbit AlexaFluor 488 (Table 2) was added for 1 hour at RT to visualize the final Iba1 staining.

Furthermore, to characterize the "On" molecule TREM2 expression, double and triple immunolabeling combining antibodies against (1) TREM2, ApoE or pHH3 with (2) either Iba1, CD68, CD16/32, Galectin-3, P2RY12, GFAP or CD11b, and (3) GFAP (Table 2) were performed as described in the preceding paragraphs but using the blocking solution 3 (BB-3), containing 0.2% gelatin in TBS with 0.1% Triton X-100 (TBS 0.1% Triton). In these cases, just as it has been stated before, TREM2 was incubated for 48 hours at RT, while ApoE and pHH3 were incubated overnight at 4ºC plus an additional hour at RT. Besides, TREM2 antibody was simultaneously incubated with an antibody against P2RY12 for 48 hours at RT when combining these two markers. Finally, in double ApoE and Iba1 or GFAP immunostaining, sections were treated for a diminishing fluorescence background (Schnell et al., 2019). Thus, sections were dipped in distilled water, treated with 10 mM $CuSO_4$ in ammonium acetate buffer (50 mM CH_3COONH_4, pH 5.0) for 90 minutes, and rinsed again with distilled water before mounting.

Finally, microglial proliferation was determined by BrdU staining. DNA was denatured by first incubating sections in 0.082 N HCl for 10 minutes at 4ºC and then for 30 minutes in 0.82 N HCl at 37ºC. Sections were subsequently rinsed with borate buffer (pH 8.5) in TBS 0.5% Triton. Afterward, the procedure was forwarded as stated in previous paragraphs using BB-2 and combining BrdU with Iba1 staining (Table 2).

Before being cover slipped with Fluoromount G™ (0100-01, SouthernBiotech), sections were washed with TBS and TB and were nuclei stained with DAPI for 5 min (Table 2).

	Target Antigen	**Host/ Conjugation**	**Dilution**	**Cat Number**	**Manufacturer**
Primary antibodies	ApoE	Goat	1:2500	AB947	EMD Millipore
	BrdU	Rat	1:120	Ab6326	Abcam
	CD3	Hamster	1:500	MCA2690	AbD Serotec
	CD16/32	Rat	1:1000	553142	BD Pharmingen
	CD22	Rabbit	1:200	GTX59644	GeneTex

	CD45	Rat	1:1000	MCA1031	Bio-Rad
	CD47	Rat	1:100	127502	BioLegend
	CD68	Rat	1:1000	MCA1957	AbD Serotec
	CD200	Goat	1:250	AF3355	R&D Systems
	CD200	Rat	1:250	MCA1958	AbD Serotec
	CD200R	Goat	1:300	AF2554	R&D Systems
	CX3CL1	Rabbit	1:500	Ab25088	Abcam
	Galectin-3	Rat	1:500	125402	BioLegend
	GFAP	Mouse	1:6000	63893	Sigma-Aldrich
	Iba1	Rabbit	1:1000	GTX100042	GeneTex
	MBP	rabbit	1:500	A0623	Dako
	NeuN	Mouse	1:200	MAB377B	Merck Millipore
	P2Y12R	Rat	1:50	848001	BioLegend
	pHH3	Rabbit	1:500	06-570	EMD Millipore
	SIRP-α	Rat	1:250	144002	BioLegend
	Synaptophysin	Mouse	1:6000	837103	BioLegend
	TREM2	Sheep	1:400	AF-1729	R&D Systems
Lectin	TL		1:150	L0651	Sigma-Aldrich
Secondary antibodies	Goat	Alexa 488	1:1000	A11055	Invitrogen
	Goat	Alexa 568	1:1000	A11057	Invitrogen
	Hamster	Alexa 568	1:1000	A21112	Invitrogen
	Mouse	Alexa 488	1:1000	A11029	Thermo Fisher
	Mouse	Alexa 555	1:1000	A31570	Invitrogen
	Rabbit	Alexa 488	1:1000	A21206	Invitrogen
	Rabbit	Alexa 555	1:1000	A21428	Invitrogen
	Rabbit	Alexa 568	1:1000	A10042	Invitrogen
	Rat	Alexa 488	1:1000	A11006	Thermo Fisher
	Rat	Alexa 555	1:1000	A21434	Thermo Fisher
	Rat	Alexa 647	1:1000	A21247	Invitrogen
	Sheep	Alexa 488	1:1000	A11015	Invitrogen
	Goat	Biotinylated	1:500	BA-9500	Vector Laboratories
	Mouse	Biotinylated	1:500	E0465	DakoCytomation
	Rabbit	Biotinylated	1:500	BA-1000	Vector Laboratories
	Rat	Biotinylated	1:500	BA-4001	Vector Laboratories
	Sheep	Biotinylated	1:500	BA-6000	Vector Laboratories
Alexa Fluor-488 conjugated Streptavidin			1:1000	S11223	Thermo Fisher
HRP-conjugated Streptavidin			1:500	SA-5004	Vector Laboratories
DAPI			1:10000	D9542	Sigma-Aldrich

Table 2. List of antibodies and reagents used in IHC.

1.10 Densitometric analysis

Densitometric analysis was performed on sections immunolabeled with CD200, CD200R, CD22, CD45, CX3CL1, CD47, SIRP-α, TREM2 and synaptophysin. For each immunostaining, a minimum of 4 WT, GFAP-IL6Tg, and GFAP-IL10Tg animals per time post-lesion were analyzed.

At least three representative sections from the brainstem containing the central part of the FN, from both contralateral and the ipsilateral sides from each animal, were photographed at 10X magnification with a DXM 1200F Nikon digital camera mounted on a Nikon Eclipse 80i brightfield microscope using the software ACT-1 2.20 (Nikon Corporation). The percentage of area covered by the immunolabeling (% Area) as well as the intensity of the immunoreaction (Mean Gray Value Mean) were analysed for each photograph by the AnalySIS® software. Specifically, in TREM2 staining, the threshold was set to quantify only TREM2 cellular staining, excluding the background staining corresponding to soluble TREM2 (sTREM2). Concerning CD200R, CD45 and TREM2, where the staining was absent or extremely low in the contralateral FN, the AI index was used to express the results. This AI index was calculated by multiplying the percentage of the immunolabelled area by the Mean Gray Value Mean (Acarin et al., 1997). Results of the AI index and intensity were expressed in arbitrary units. On the other hand, in CD200, CD22, CX3CL1, CD47, SIRP-α and synaptophysin, the staining was present in both contralateral and ipsilateral FN. Therefore, the gray grade quotient (GGQ) was obtained by dividing the Mean Gray Value Mean on the ipsilateral side by the Mean Gray Value Mean on the contralateral side. The intensity grade (IG) was calculated by multiplying the percentage of the immunolabelled Area (% Area) by the GGQ.

Lastly, the number of pHH3+ cells in the FN were manually counted using a 20X objective. Then, all FN counted were photographed at 10X, and the area of each FN was quantified using ImageJ software (Wayne Rasband, National Institute of Health, Bethesda, MD, USA). PHH3 cell density was calculated from the total pHH3+ cells/FN area for each animal, and results were expressed as pHH3+ cells/mm^2.

1.11 Confocal Microscopy Quantification

Quantification of microglial clusters expressing TREM2 in their ramifications was performed by analyzing the double immunofluorescence for Iba1 and TREM2. A minimum of 4 WT, GFAP-IL6Tg, and GFAP-IL10Tg animals at 14 and 21dpi were used. The number of total microglial clusters in the FN, identified by Iba1+ staining, expressing TREM2 in microglial ramifications were manually counted using a 40X and 63X objective with a Zeiss LSM 700 confocal microscope. Results were expressed in percentage as TREM2 + Iba1+ microglial clusters from the total amount of Iba1+ clusters (% TREM2 + Iba1+ microglial clusters/total Iba1+ clusters).

1.12 Isolation of myelin and fluorescent labeling with pHrodo™ Green STP Ester

Myelin was isolated following the protocol described by Gómez-López et al. (2021) (Article 3 in Annex section). Briefly, six WT animals were dislocated under the effects of anesthesia. Brains were removed quickly and cut into little pieces in a cold 0.32 M sucrose solution prepared in 0.1 M Tris.Cl buffer. After homogenization with a mechanical homogenizer, myelin was separated by using a sucrose gradient in an ultracentrifuge at 105,000 g for 45 minutes at 4ºC (70Ti Rotor, Sorvall). Myelin was isolated from the interphase, and after a hypoosmotic shock using Tris.Cl buffer and 0.32 M sucrose, pelleted myelin was weighted and reconstituted in DPBS at a 100 mg/ml (w/v) suspension (Rolfe et al., 2017).

For myelin fluorescent labeling, conjugation with pHrodo-STP Ester Green® (P35369, Thermo Fisher Scientific), with excitation at 505 nm and emission at 525 nm, was used following the procedure described in Article 3. Briefly, the pHrodo dye was dissolved in 75 ml dimethyl sulfoxide (DMSO, D8418, Sigma–Aldrich), and afterward, 18.5 ml of myelin in a concentration of 15 mg/ml was mixed with 25 ml of pHrodo and resuspended in 206.5 ml of PBS (pH 8.0). After 45 minutes of incubation at RT, with agitation and protected from light, labeled myelin was spun down, resuspended in PBS (pH 7.4), and stored at -80ºC (for further information, see Article 3).

1.13 Flow cytometry

To study the microglia/macrophage/leukocyte population expressing the principal “Off” receptors, NL animals and lesioned animals (7dpi and 14dpi) were analysed using flow cytometry. Anaesthetized animals were intracardially perfused with cold 0.1 M DPBS (pH 7.4, 14190-094; Thermo Fisher Scientific). Then, the brain was removed from the skull and two 0.5-mm-thick coronal slices were obtained from the brainstem using a Mouse Brain Matrix (Zivic Instruments). For each slice, the dorsal inferior half was cut with sterile knives, and tissue containing the contralateral and ipsilateral FN was divided. These FN sections were dissociated hereunder through 160µm and 70µm meshes in order to obtain a cell suspension for each animal. To get a viable number of cells for the FN, a pool of 3 FN was needed for each tube, considered as a n=1. An n=6 per time-point and genotype was used for each experiment. Thereafter, cells were digested for 30 minutes at 37ºC using type IV collagenase (17104-019; Life Technologies) and DNAse I (D5025; Sigma-Aldrich). Subsequently, each cellular suspension was centrifuged at RT for 20 minutes at 600 g in a discontinuous Percoll gradient (17-0891-02; Amersham-Pharmacia) between 1.03 g/ml and 1.08 g/ml. Myelin layer at the top of the tube was removed. Cells in the interphase and the clear upper phase were collected, washed in PBS plus 2% serum and Fc receptors were blocked by incubating for 20 minutes at 4ºC in a solution of purified CD16/32 (Table 3). Then, cells were labelled during 30 minutes at 4ºC with the following surface microglial markers: anti-CD11b-APC-Cy7, anti-CD45-PerCP, anti-CD200R-APC, anti-CX3CR1-PE and anti-SIRPα-FITC (Table 3). Isotype-matched control antibodies were used as negative control and a cell suspension of splenocytes as positive control (Table 3).

Flow cytometry was also performed to analyse the capacity of TREM2+ cells to phagocyte myelin debris labelled with pHrodo™ Green STP Ester. In that case, a myelin phagocytosis assay was performed using this technique by processing NL and axotomized WT animals (21dpi) to isolate microglial cells. Briefly, anesthetized animals were intracardially perfused for 1 minute with 0.1 M DPBS. Flow cytometry protocol was carried out as previously described. After Percoll step, the myelin phagocytosis assay was performed as follows: cells were resuspended in DMEM-F12 medium (ref. 31330-038; Thermo Fisher Scientific) +10% FBS, then 3 µg of pHrodo Green-labeled myelin were added, and samples were incubated at 37ºC for 4 hours. For negative controls, the same procedure was performed without adding myelin, or by resuspending cells in DPBS + 2% FBS and preserving at 4ºC. After myelin incubation, cells were washed two times with DPBS and DPBS + 2% FBS at 310 g for 5 minutes. Then, the protocol was proceeded as stated in the previous paragraph.

Finally, cells were acquired using FACS Canto flow cytometer (Becton Dickinson, San Jose, CA) and results were analysed using the FlowJo software. By selecting CD11b and CD45 positive cells, microglial and macrophage population could be identified in the dot-plots. Subsequently, microglia were identified as $CD11b^{+}/CD45^{low}$ cells and macrophages as $CD11b^{+}/CD45^{high}$ cells. Then, every population was analysed individually for each marker used in each case (For further information, see Article 3).

Target antigen		Format	Dilution	Cat Number	Manufacturer
Fc Blocker	CD16/32	Purified	1:250	553142	BD Biosciences
Primary antibodies	CD11b	APC-Cy7	1:400	557657	BD Biosciences
	CD45	PerCP	1:400	557235	BD Biosciences
	CD200R	Alexa 647	1:50	566345	BD Biosciences
	CX3CR1	PE	1:400	FAB5825P	R&D Systems
	SIRP-α	FITC	1:200	144005	BioLegend
	TREM2	PE	1:400	FAB17291P	R&D Company
Isotype controls	IgG2b κ	APC-Cy7	1:400	552773	BD Biosciences
	IgG2b κ	PerCP	1:400	552991	BD Biosciences
	IgG2a	AF647	1:50	MCA1212	AbD Serotec
	IgG	PE	1:400	403004	BioLegend
	IgG2a κ	FITC	1:200	553929	BD Biosciences

Table 3. List of antibodies used in flow cytometry.

1.14 Tissue processing for protein analysis

Animals used for protein analysis were i.p. anaesthetized and perfused for 1 minute with cold 0.1 M DPBS (pH 7.4). Subsequently, the FN was dissected out as described beforehand in Flow cytometry section, snap frozen individually in liquid nitrogen and stored at -80ºC. Total protein was extracted by solubilization of samples on lysis buffer containing 25mM HEPES, 2% Igepal, 5mM $MgCl_2$, 1.3 mM EDTA, 1 mM EGTA, 0.1 M PMSF and protease (1:100, P8340; Sigma-Aldrich), and phosphatase inhibitor cocktails (1:100, P0044; Sigma-Aldrich) for 2 hours at 4ºC. After solubilization, samples were centrifuged at 6,500 g for 5 minutes at 4ºC and the supernatants collected.

For TREM2, an ELISA was carried out to quantify the soluble fraction of TREM2 (sTREM2). Protein was extracted as explained above. For separating the soluble protein fraction, each protein lysate was ultracentrifuged at 107,000 g for 30 minutes at 4ºC in a Sorvall MTX 150 Series Micro-Ultracentrifuge. After ultracentrifugation, supernatants were collected and concentrated by using microcentrifuge cellulose filter units (MRCPRT010, Merck Millipore).

Total protein concentration was assessed with a commercial Pierce BCA Protein Assay kit (23225; Thermo Fisher Scientific) according to manufacturer's protocol. Protein lysates and soluble fractions were aliquoted and stored at -80ºC until used for protein microarray analysis. The FN of each animal was analysed separately.

1.15 Cytokine analysis

The cytokines IL-6, TNF-α and IL-10 were analysed in GFAP-IL6Tg and WT mice using a Milliplex MAP Mouse High Sensitivity kit (#MHSTCMAG-70K; Merck Millipore) and the cytokines IL-10 and TNF-α were analysed in GFAP-IL10Tg and the corresponding WT littermates at NL, 7 and 21dpi using a Milliplex MAP Mouse Cytokine/Chemokine kit (#MCYTOMAG-70K; Merck Millipore) according to manufacturer's instructions. A minimum of 6 animals were used for each condition. Briefly, 25µL of each FN extracts with a final total protein concentration of 3.0 µg/µL were added to the plates, along with the standards in separate wells, containing 25µL of custom fluorescent beads and 25µL of matrix solution and incubated overnight at 4ºC in a plate-shaker (60 g). After two washes with wash buffer (1x), the plate was incubated with 25µL of detection antibodies for 30 minutes at RT followed by an incubation with 25µL of Streptavidin-Phycoerythrin for 30 minutes at RT in a plate-shaker (60 g). Finally, the plate was washed twice with wash buffer, and 150µL of Drive fluid was added. Luminex MAGPIX device with the xPONENT 4.2 software was used to read the plate. Data were analysed using the Milliplex Analyst 5.1 software and expressed as pg/mL of protein.

1.16 Enzyme-linked adsorbent immunoassay for sTREM2 detection

Quantification of sTREM2 was performed by following the manufacturer's instructions of a Mouse TREM2 ELISA kit (ABIN429539, Antibodies-online). Briefly, standards and the corresponding samples (2.5 mg/ml protein) were incubated in a pre-coated TREM2

ELISA plate for 1 hour at 37ºC. After Detection Reagent A and B incubations for 1 hour and 30 minutes respectively at 37ºC, the Substance Solution was incubated for 10-20 minutes at 37ºC protected from light to start the colorimetric reaction. Finally, the Stop Solution was added to stop the reaction. Results were read at 450 nm in the microplate reader VarioskanTM Lux (ThermoFisher Scientific, Waltham, MA, USA).

1.17 Statistical analysis

Statistics were performed using Graph Pad Prism® software (Graph Pad Software Inc.) and results were expressed as mean ± standard error of the mean (SEM). Two-way ANOVA with Tukey's multiple comparison analysis as a *post-hoc* test was applied to determine statistically significant differences among time-points postinjury, and two-way ANOVA with multiple comparison *post hoc* Sidak's test was used to compare WT with the corresponding transgenic GFAP-IL6Tg or GFAP-IL10Tg. In the case where only WT animals were used, one-way ANOVA with multiple comparison *post hoc* Tukey's test was used. Finally, for sTREM2comparison and flow cytometry analysis, in which only two different conditions were compared, unpaired Student's t-test was used.

IV. RESULTS AND DISCUSSION

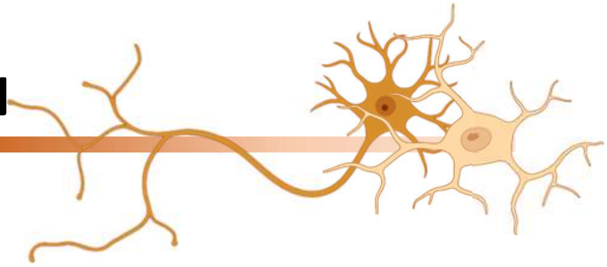

This doctoral thesis is the compendium of the study of the neuron-microglia “On/Off” signaling after FNA and the effects on astrocyte-targeted IL-6 or IL-10 production in this signalling. The “On/Off” signalling has been proposed to be one of the main mechanisms that regulates microglial activation (Biber et al., 2007; Deczkowska, Amit and Schwartz, 2018; Cockram et al., 2021), and recent works have focused their efforts to characterize the role of this signalling on neurodegeneration. Little research has been carried out to date in acute models of degeneration, and concretely in the FNA model. As a classical and well-known model of microglial activation and neuronal degeneration-regeneration, understanding “On/Off” signalling in the FNA model and its regulation in pro-inflammatory and anti-inflammatory contexts may open new therapeutical target strategies to control microglial activation and to prevent neuronal death.

Along this study, two lines of transgenic mice were used: the GFAP-IL6Tg, which was described thirty years ago (Campbell et al., 1993), and the GFAP-IL10Tg generated and described by our laboratory (Almolda et al., 2015). These two transgenic mice overproduce IL-6 and IL-10, respectively, under the astrocytic GFAP promoter. When astrocytes become reactive after injury and increase GFAP expression, so does the production of both cytokines. To achieve our goal, we explored if these two cytokines modified the “On/Off” signaling between microglia and neurons, and if these modifications were causing the changes on neuronal survival and microglial activation pattern after FNA, already described in these mice (Almolda et al., 2014; Villacampa et al., 2015).

In this work, we aimed to study “Off” signaling in membrane-bound neuronal ligands and microglial receptors after FNA (CD200-CD200R, CD22-CD45, CX3CL1-CX3CR1 and CD47-SIRP-α, respectively) and the microglial “On” signal TREM2. As a result of the experimental work conducted, we have written three scientific papers. The results are summarized in the following two papers: **Article 1**, presented as a manuscript to be sent to a scientific journal, which describes the effects of IL-6 and IL-10 on the neuron-microglia “Off” signaling after FNA; and **Article 2**, about the effects of IL-6 and IL-10 on TREM2, which has been already published in “Frontiers in Cellular Neuroscience” journal. In this article, we compared our model with TREM2 expression after another axonal injury model, the perforant pathway transection. We also published a third methodological scientific paper in “Current Protocols” in which we described a method that allow to evaluate the impact of “On/Off” signaling in functional microglial phagocytosis *ex vivo* (**Article 3**).

In the following sections, all the results of this work will be discussed in more detail.

1. NEURONAL-MICROGLIAL “ON/OFF” SIGNALLING EVOLUTION IN FNA MODEL

To our knowledge, no studies have reported how several membrane “On/Off” signals operate in neuroinflammatory situations so far. In this work, we deepen in this complex mechanism to get a collaborative perspective of this signalling, which led us to study neuronal-microglial CX3CL1/CX3CR1, CD22/CD45, CD200/CD200R and CD47/SIRP-α “Off” ligands and receptors, and the “On” microglial molecule TREM2 expression after the well-known acute neuroinflammatory model FNA.

1.1 Neuron-microglia “On/Off” expression in the non-lesioned FN

In the nervous tissue, the ‘Off’ signals are expressed during physiological conditions to maintain microglial in homeostatic state (Cockram et al., 2021). In our work, expression of “Off” ligands and their receptors reinforced a neuron-microglia communication through this signalling in basal conditions since we observed a constitutive expression of all neuronal-microglial “Off” molecules in the FN from WT animals.

Specifically, microglial “Off” receptors CD45, CD200R, CX3CR1 and SIRP-α were detected constitutively in the microglial population using the IHC and flow cytometry techniques (Article 1, Figures 5, 6, 7, 8 and 9), while the “On” receptor TREM2 was only detected intracellularly, (Article 2, Figure 2), in a perinuclear location (Prada et al., 2006). TREM2 has been reported on microglial cells, both *in vitro* and *in vivo*, during development and adulthood under physiological conditions (Schmid et al., 2002; Chertoff et al., 2013). As an “On” receptor, intracellular TREM2 seemed to be inactive, waiting for any input of activation to be exposed to the microglial membrane and develop its function. Nevertheless, intracellular TREM2 have been attributed functions related to microglia survival, according to studies with TREM2-knockout mice (Cantoni et al., 2015; Poliani et al., 2015; Zheng et al., 2017). TREM2 intracellular location, and its lack of activity related to the “On” signalling, contrasts with the constitutive membranal microglial expression of “Off” signals, which as immune checkpoints, hold microglia in a surveillance state.

While CX3CR1 was restricted only to microglial population, in accordance with previous findings (Harrison et al., 1998; Nishiyori et al., 1998; Rogers et al., 2011; Cardona et al., 2006), other cell populations, such as macrophages and lymphocytes, displayed reactivity for other “Off” receptors. Macrophages and highly activated microglia (CD11b/CD45^{high}) expressed CD200R, CD45 and SIRP-α (Article 1, Figures 8 and 9), while CD200R and CD45 were characterized in lymphocytes as well (Suppl. Figure 1), coinciding with previous reports (Adams et al., 1998; Cosenza et al., 2002; Cosenza-Nashat et al., 2006; Koning et al., 2009; Gitik et al., 2011; Lago et al., 2018; Ngwa and Liu, 2019; Sato-Hashimoto et al., 2019). Levels of expression of CD200R, CD45 and SIRP-α in macrophages were higher than in microglia, possibly indicating a need for a tighter “Off” receptor control in those cells. Apart from leukocytes, SIRP-α has also been established to be abundantly on neurons (Adams et al., 1998; Matozaki et al., 2009), as we could also detect by its profuse neuropile expression (Article 1, Figure 5).

In homeostatic conditions, ligands for microglial “Off” receptors CD45, CD200R, CX3CR1 and SIRP-α were detected mainly in neurons. CX3CL1 and CD22 –ligands for CX3CR1 and CD45, respectively– were expressed in FMNs somas (Article 1, Figures 1 and 2), as it had been reported for neurons in the CNS (Harrison et al., 1998; Hatori et al., 2002; Mott et al., 2004; Lyons et al., 2009). CD200, the ligand for CD200R, followed a diffuse pattern throughout the neuropile, being especially strong on neuronal membranes and myelin (Article 1, Figure 3), but not in glial cells, as it had been found in some previous studies (Koning et al., 2009; Shrivastava, Gonzalez and Acarin, 2012; Varnum et al., 2015; Lago et al., 2018). CD47 is an ubiquitous ligand, marker of self, which presented a diffuse pattern in the FN, in the neuropile, which was mostly attributed to neurons (Article 1, Figure 4), although it has also been described on microglia, macrophages, astrocytes, and oligodendrocytes (Koning et al., 2007; Gitik et al., 2011; Han et al., 2012; Zhou et al., 2014; Zhang et al., 2015). In summary, during homeostasis, FMNs expressed constitutively CX3CL1, CD22, CD200 and CD47, and, for the two first cases in an exclusive manner. The fact that CX3CL1 and CD22 were exclusively located in FMNs, and CD200 was located in addition in myelin, but not astrocytes, reinforces the involvement of those signals in the neuron-microglia communication in the FN.

This constitutive expression and interaction between neuronal “Off” ligands and microglial ‘Off’ receptors have been linked to hold microglial cells in a homeostatic state under physiological conditions (Kierdorf and Prinz 2013; Szepesi et al., 2018). In a physiological context like aging, loss of these signals, such as CD200 or CX3CL1, have been reported to increase microglial activation (Jurgens et al., 2012). However, most works studying the loss of those signals have been related to neuroinflammatory or diseased conditions (Tan et al., 2000; Cardona et al., 2006; Wang et al., 2007; Han et al., 2012; Chen et al., 2016; Szepesi et al., 2018), and therefore, the evaluation of the specific contribution of each signal to microglial homeostasis presents several difficulties. Data obtained from SIRP-α, CD200 or CX3CR1 knockout mice (Hoek et al., 2000; Cardona et al., 2006; Sato-Hashimoto et al., 2019) indicate differences in microglial activation responses in basal conditions, ranging from no response, to priming or activation upon the loss of these signals. Concretely, in CD200 knockout mice, microglia presented a priming effect in basal conditions (Hoek et al., 2000; Manich et al., 2019), as exemplified by activated morphology and increase in the expression of CD11b and CD45. In contrast, in CX3CR1 knockout mice, no signs of activation were observed in microglia during homeostatic conditions (Cardona et al., 2006). Interestingly, SIRP-α knockout mice presented signs of activation in microglia located in white matter, according to higher microglia numbers and CD11c and CD68 expression, which were similarly observed in CD47 knockout mice (Sato-Hashimoto et al. 2019).

Despite the fact that in our study the expression of "Off2 signalling supports an important contribution on microglia homeostasis, the relevance of each specific signalling axis in the maintenance of homeostatic conditions needs from a thorough study, in order to clarify the contribution of each to microglial homeostasis.

1.2 Regulation of neuronal-microglial "On/Off" signalling after FNA

In the FNA model, FMNs transection leads to microglial activation in the FN, characterized by increase in microglial cell number (Article 2, Figure 4), changes in morphology and increased expression of CD45, CD11b and other molecules (Raivich et al., 1994; Almolda et al., 2014; Villacampa et al., 2015; Article 1, Figures 6). Microglial activation in this model is characterized by different critical time-points, briefly summarized as follows: at 3dpi microglial proliferation peaks, at 7 dpi microglia reach the peak of microgliosis, at 14-21 dpi, when the FMNs death peaks occurs, microglia form phagocytic clusters next to FMNs, and from 28dpi onwards a repair phase, characterized by decreased microglia activation, takes place. In our work, we found that the time-course of microglial activation after FNA was closely related with the expression of "Off" and "On" receptors and ligands, as well as with microglial phagocytic functions.

1.2.1. Microglia-neuron "Off" signalling protect FMNs during the peak of microgliosis

After FNA, microglia proliferate (Article 2, Figure 4), leading to the peak of microgliosis, at 7dpi, when activated microglia migrate towards injured FMNs and wrap them (Almolda et al., 2014; Villacampa et al., 2015). In our study, we observed an upregulation of the global "Off" receptor levels due to the increase of microglial numbers in microglia population, and also due to its activation in highly activated microglia/macrophages populations (Article 1, Figures 8 and 9). Concretely, microglia (CD11b+/CD45^{low}) showed similar 'Off' receptor expression than basal conditions, with a downregulation of CX3CR1 (Article 1, Figures 8 and 9) that indicated a loss of the homeostatic phenotype (Butovsky et al., 2014). At this time-point, highly activated microglia/macrophages (CD11b+/CD45^{high}) increased in number, and CD45, CD200R and SIRP-α expression was higher than microglia, which suggests the need of a tighter control of activated microglia/macrophages. Activation of microglial cells was also reflected in the increase of intracellular TREM2 expression in most microglia cells that, with few exceptions, was not translocated to the membrane (Article 2, Figure 2; Supplementary Figure 2).

Upregulation of “On” and “Off” receptors in microglia has been observed in several studies in acute and chronic inflammatory conditions. CD45 upregulation is a transversal used marker for microglia and macrophage microglial activation (Sedgwick et al., 1998; Wilcock et al., 2001; Cosenza et al., 2002; Cosenza-Nashat et al., 2006; Herber et al., 2006), and CD200R upregulation has also been reported in acute and chronic inflammatory conditions such as SCI (Lago et al., 2018), EAE (Valente et al., 2017), in Toxoplasma encephalitis (Deckert et al., 2006) and after stroke (Sun et al., 2020). Interestingly, the “On” molecule TREM2 also increased after FNA, being coincident with results from previous general *in vivo* data from chronic (Jay, von Saucken and Landreth, 2017; Sayed et al., 2018) and acute CNS inflammatory injuries (Saber et al., 2017; Scott-Hewitt et al., 2020), as well as in other axonal injury models (Kobayashi et al., 2016; Tay et al., 2018), or as in our observations, in the perforant pathway transection (Manich et al., 2020).

After FNA, we also observed an upregulation of neuronal “Off” ligands at early time-points, since all together, neuronal CX3CL1, CD22 and CD200 -with the exception of CD47, that did not modify its levels–, followed similar expression patterns (Article 1, Figures 1, 2 and 3), coinciding with the peak of microgliosis (Almolda et al., 2014; Villacampa et al., 2015) and maximal expression of their counterpart microglial receptors. The upregulation was produced due to higher expression of “Off” ligands in FMNs. Interestingly, we did neither find “Off” CX3CL1 nor CD200 in astrocytes or endothelial cells, as it had been found in other injuries (Maciejewski-Lenoir et al., 1999; Hatori et al., 2002; Hughes et al., 2002; Koning et al., 2009; Shrivastava, Gonzalez and Acarin, 2012; Cohen et al., 2017), nor aberrant CD22 microglial expression (Cougnoux et al., 2018; Funikov et al., 2018; Pluvinage et al., 2019). Similar to our findings, previous works characterized a first increase at early stages for CX3CL1 in the transient global cerebral ischemia model (Ahn et al., 2019), and few studies also demonstrated an upregulation of CD200 linked to a neuroprotective role towards neurotoxicity in transgenic mouse model of Huntington’s disease and in murine toxoplasma encephalitis (Deckert et al., 2006; Comella Bolla et al., 2019), although most works described a dramatic reduction from both CD200 and CX3CL1 after injury, (Frank et al., 2006; Duan et al., 2008; Lyons et al., 2009; Bachstetter et al., 2011; Valente et al., 2017; Lago et al., 2018) as we also observed at later time-points after FNA. “Off” ligands upregulation occurs during the peak of microgliosis, in which microglia approach to lesioned FMNs, wrapping them –establishing a direct cell-to-cell contact–, and producing the “synaptic stripping” phenomenon (Moran and Graeber, 2004; Kettenmann, Kirchoff and Verkhratsky, 2013). Consequently, upregulation of “Off” neuronal ligands could have chemoattractant and immunoregulatory functions in microglia. Indeed, CX3CL1 could be also released as a soluble form, which acts as a chemoattractant for microglia (Hughes et al., 2002; Carter and Dick, 2004; Zhang et al., 2018). *In vitro* studies, for instance, have attributed adhesion functions to CX3CL1 which may facilitate FMNs microglial wrapping (Lauro et al., 2006). Likewise, soluble CD200 has also been reported to show chemotactic properties, which interestingly are preserved in inflammatory contexts (Carter and Dick, 2004). Taking into account the decrease in CX3CR1 and the loss of chemotactic properties described in inflammatory contexts (Carter and Dick, 2004; Inoue et al., 2021), it is possible that CD200 presents more relevant chemotactic functions in comparison to CX3CL1 after FNA. Also, as commented above, upregulation of "Off" signals could be involved in FMNS wrapping, thus establishing a direct cell-to-cell contact between microglia and neuronal membranes. Former studies in FNA model attributed a protective role of microglia in wrapped FMNs, and in several reports, defective microglia-neuron attachment due to poor integrin expression worsened FMNs survival (Kreutzberg, 1996; Möller et al., 1996; Almolda et al., 2014).

Although "On/Off" microglial receptors have been related to microglial proliferation, in this thesis we did not observe an association of "On/Off" microglial receptors expression with this microglial function. Concretely, after FNA, we and others observed an increase in proliferation at 3dpi, that decreased at 7dpi (Raivich et al., 1994; Almolda et al., 2014; Villacampa et al., 2015; Article 2, Figure 4), while we observed a general upregulation of intracellular TREM2 levels and 'Off' signaling –with the exception of CX3CR1– at 7dpi. TREM2 expression has been tightly related to proliferation based on the results obtained in TREM2KO or DAP12KO mice, and on mice harboring TREM2 dysfunctional variants in acute and chronic CNS injury animal models (Kobayashi et al., 2016; Jay et al. 2017; Cheng-Hathaway et al., 2018; Meilandt et al., 2020). TREM2-related effects on microglia proliferation have been linked to its co-receptor DAP12, since TREM2/DAP12 complex can provide additional signaling to the also downstream colony stimulation factor-1 receptor intracellular signaling pathway, importantly involved in microglia proliferation (Otero et al., 2012; Ulland, Wang and Colonna, 2015). According to our results, we can infer that microglia proliferation leading to microgliosis after FNA is TREM2-independent, as it has also been observed *in vitro* (Noto et al. 2010) and after spinal nerve transection in DAP12KO mice (Guan et al., 2016). On the other hand, microglial proliferation has been usually associated to microglial "Off" receptor downregulation. Concretely, loss of CD200-CD200R has been related to an increase in microglia proliferation in homeostasis (Broderick et al., 2002; Denieffe et al., 2013) and after neuroinflammation, as demonstrated by increased Ki67+ microglia and total microglial population in CD200-deficient mice with toxoplasma encephalitis (Deckert et al., 2006), or decrease in proliferating microglia after recombinant CD200-His administration upon SCI (Lago et al., 2018). Oppositely, in this thesis we observed a slight downregulation of CX3CR1 in microglia during the peak of microgliosis, that we attributed to FNA-induced activation, and loss of homeostasis. Data on CX3CL1-CX3CR1 control on microglia proliferation is scarce, especially after injury. In microglia, administration of CX3CL1 after LPS stimulation *in vitro* did not produce any effect on proliferation (Inoue et al., 2021).

In summary, the increase detected on neuronal "Off" molecules CX3CL1, CD200 and CD22 and the corresponding microglial "Off" ligands CD200R and CD45 –with the exception homeostatic microglial CX3CR1 downregulation– indicates an early attempt to protect FMNs after injury, coinciding with the peak of neuroinflammation and microglial activation. Microglial-neuron "Off" signals, as well as upregulated TREM2, are not involved in early microglia proliferation in this model, but may exert chemotactic and adhesion functions that will facilitate microglia migration to FMNs, and later FMNs wrapping, resulting in FMNs protection.

1.2.2. Disruption of microglia-neuron "Off" signalling and appearance of the "On" signalling promote microglial phagocytosis and regulate FMNs death

At 14dpi, the peak of FMNs death takes place, which reaches 30 to 50% in the adult axotomized FMNs (Möller et al., 1996; Werner et al., 1998; Raivich et al., 2002; Raivich et al., 2003). Concomitantly, microglial cell numbers achieve a steady state or even a slight reduction, due to gradual elimination by programmed cell death (Jones, Kreutzberg and Raivich, 1997; Conde and Streit, 2006), as we also could observe in this thesis and our previous work (Almolda et al., 2014; Villacampa et al., 2015; Article 1, Figure 6). At this stage, microglial "Off" signalling was characterized by the already present downregulation of CX3CR1 in microglia (CD11b+/CD45^{low}), and by the downregulation of SIRP-α in highly activated/macrophages (CD11b+/CD45^{high}). Also, we could observe that microglial clusters or nodules –groups of 4-5 microglial cells formed next to FMNs identified as phagocytic microglia (Raivich et al., 1998; Petitto et al., 2003)– contained high levels of CD45, CD200R and TREM2, and low levels of SIRP-α (Article 1, Figures 6, 7 and 11; Article 2, Figures 2). Those features were preserved in microglial clusters at 21dpi, and indeed TREM2 reached a peak at this timepoint, showing an especially strong expression in those structures (Article 2, Figure 2; Supplementary Figure 2 and 3). Importantly, TREM2 was essentially membrane-bound, and few sTREM2 was released in the lesioned FN parenchyma, as we also quantified by ELISA methods (Article 2, Figure 2). Soluble TREM2 fraction, which can be increased after axonal injury (Manich et al., 2020), is the result of proteolytic TREM2 cleavage by ADAM10 and ADAM17, and this fraction has been related to some opposite effects to membrane bound TREM2 in microglia, such as the pro-inflammatory cytokine production (Zhong et al., 2017 and 2019).

On the other hand, a downregulation of neuronal "Off" signals CD200, CD22 and CX3CL1, reaching even inferior levels than in the NL FN, was observed from 14dpi onwards (Article 1, Figures 1, 2 and 3). As we pointed out before, most works on the "Off" signalling have described a dramatic reduction from both CD200 and CX3CL1 in acute and chronic conditions, including SCI, EAE, aging and AD (Frank et al., 2006; Duan et al., 2008; Lyons et al., 2009; Bachstetter et al., 2011; Valente et al., 2017; Lago et al., 2018). Since in our work CD22 expression and time-course was very akin to CXC3L1, and due to immunoregulatory role of CD22 through CD45 microglia/macrophage inhibitory receptor (Mott et al., 2004), we could suggest that CD22 reflects a similar effect than CX3CL1. Interestingly, FMNs loss could also be related to the presence of "On" neuronal ligands, as we also detected at 14dpi the presence of ApoE+ FMNs (Article 2, Figure 9). ApoE is one of the multiple known ligands for TREM2 and, apart from its constitutive expression in astrocytes (Article 2, Supplementary Figure 2), this molecule has also been observed in the surface of degenerating neurons, such as in the case of apoptotic neurons (Atagi et al., 2015).

Regulation of "On/Off" expression in microglial clusters and degenerating neurons is of special interest due to its association to phagocytosis, although in our work we also observed microglia proliferation in clusters (Article 2, Figure 4). In microglia, the phagocytic role of TREM2 has been extensively studied in acute and chronic neurodegenerative diseases models such as AD or MS (Deming et al., 2018; Karanfilian, Tosto and Malki, 2020), and a TREM2 specificity for phagocytosis of myelin debris and apoptotic neurons has already been suggested based on TREM2 ligands (Gervois and Lambrichts, 2019). The phagocytic role of microglial clusters is also reinforced by the expression of different phagocytic markers, such as CD16/32 and CD68 as we found in our previous and current results (Villacampa et al., 2015; Article 1 Figure 10 and Supplementary Figure 2; Article 2 Figure 6; Supplementary Figure 3). In addition, in this work, we also determined the specific downregulation of microglial SIRP-α, a "Do-not-eat-me" receptor, in some microglial clusters (Article 1, Figure 11). CD47-SIRP-α is an essential "Do-not-eat-me" axis, since interaction of CD47 with its receptor SIRP-α in macrophages and microglia inhibits phagocytosis (Bian et al., 2016; Gitik et al., 2011). For this reason, the downregulation of SIRP-α found in microglial clusters in FNA model could be facilitating FMNs phagocytosis. In accordance to this theory, the effect of SIRP-α has been suggested to be mediated through the control of the cytoskeletal proteins paxillin and cofilin (Gitik et al., 2014), and loss or blockade of either CD47 (Han et al., 2012; Lehrman et al., 2018; Hutter et al., 2019) or SIRP-α (Gitik et al., 2011; Elberg et al., 2019; Sato-Hashimoto et al., 2019; Wang et al., 2019; Ding et al., 2021) results in increased phagocytosis of myelin or synapses.

Amongst the "Eat-me" receptors inhibited by CD47-SIRP-α, CR3 or FcγR-II/III are the ones identified and most studied (Oldenborg, Gresham and Lindberg, 2001; Gitik et al., 2011). In previous work, as well as in this study, we found that CD68 and CD16/32 were expressed in microglial clusters (Article 2, Figure 2; Supplementary Figure 3). Nevertheless, in the last case, the preservation of an intact blood-brain barrier after FNA and lack of IgG infiltration in the FN excludes phagocytosis through IgG opsonization (Villacampa et al., 2015). However, since CD47 activation signals through immunoreceptor tyrosine-based inhibitory motif (ITIM) by reversing Syk signalling, it could be expected that CD47 inhibits other “Eat-me” phagocytic receptors, activated through ITAM and tyrosine kinase Syk, for example, TREM2 (Cockram et al., 2021). Indeed, as we commented above, in this thesis we identified TREM2 expression concentrated in phagocytic microglial clusters after FNA, and since we also observed a downregulation of SIRP-α we may speculate that SIRP-α could control TREM2 phagocytosis through several ligands, as we will discuss later. Other interesting phagocytic receptor include CD11c, which is exclusively located in at 14 dpi in these structures after FNA (Kloss et al., 1999), and its expression has been recently defined to be repressed by SIRP-α in white matter (Sato-Hashimoto et al., 2019). Also, *in vitro* studies suggested a phagocytic complex formed in microglia to phagocyte fibrillar β-amyloid constituted by CD47, CD36 and integrin α6β1, which would overcome classical phagocytic pathways (Bamberger et al., 2003; Koenigsknecht and Landreth, 2004).

Even though this evidence points out to a specific microglial phenotype in clusters related to phagocytosis, the results of this thesis indicate that, apart from microglial cell clusters containing TREM2+ and CD16/32+, CD68+, other clusters being TREM2- and CD16/32+, CD68+ clusters were also found. Indeed, an *ex vivo* myelin phagocytosis assay with microglia isolated from the FN (Article 3) confirmed that, after FNA, TREM2+ microglia phagocyted myelin debris more efficiently compared to TREM2- cells, although TREM2- cells were also phagocyting (Article 2, Figure 13). Some reports indicate that TREM2 is not strictly required for microglia to produce the engulfment of cellular remnants, but it increases the efficient phagocytosis of apoptotic neurons (Hsieh et al., 2009; Cantoni et al., 2015). Overall, this result suggested that, while TREM2+ microglial cells show a specific phagocytic phenotype induced only in a subpopulation of these cells, they do not exclusively retain the ability to perform this function, proving the existence of a TREM2-independent microglial phagocytosis. Therefore, our results suggest that TREM2-mediated phagocytosis and its relevance may be dependent on the microenvironment in which phagocytosis takes place.

The appearance of ApoE in FMNs and the downregulation of neuronal “Off” ligands CD200 and CX3CL1 also indicates a role of the “On/Off” signalling in microglial phagocytosis and death of injured FMNs. In line with this idea, increased phagocytic activity of microglia has been demonstrated for ß-amyloid in CD200KO mice (Varnum et al., 2015; Lyons et al., 2017) and photoreceptors in retina for CX3CR1KO mice (Zabel et al., 2016). On the contrary, in ApoE-KO animals, decreased FMNs death has been reported after FNA (Krasemann et al., 2017). In this work, we found that ApoE was detected in some degenerating FMNs and in microglial clusters (Article 2, Figure 9), as it had been detected into a transcriptomic level in microglia (Tay et al., 2018). ApoE has been suggested to act as an opsonin in apoptotic neurons, enhancing microglial phagocytosis (Atagi et al., 2015), and our results support this idea too. Like ApoE, in this thesis we characterized the expression of Galectin-3, another ligand recently suggested to be involved in TREM2-mediated phagocytosis (Boza-Serrano et al., 2019). Galectin-3 expression was expressed in microglial clusters and in degenerating FMNs as observed for ApoE (Article 2, Figure 10). Galectin-3 has been extensively linked to microglial phagocytosis and clearance (Puigdellívol, Allendorf and Brown, 2020), and its expression has been also described on the surface of neurons after traumatic brain injury, where it has been suggested to act as alarmin (Yip et al., 2017; Boza-Serrano et al., 2019) or an opsonizing molecule in the phagocytosis of desialylated neurons (Puigdellívol, Allendorf and Brown, 2020). In global, ApoE and Galectin-3 expression on degenerating FMNs and in microglia clusters could indicate a role of those molecules as opsonins and ligands for TREM2-mediated phagocytosis in clusters.

Among all “Off” ligands, the neuronal “Do-not-eat-me” CD47 molecule followed a different pattern. After FNA, CD47 levels remained stable in the neuropile of the lesioned FN with a punctual upregulation at 21dpi –after the peak of neuronal death– (Article 1, Figure 4). CD47, has been classified as a “Do-not-eat-me” signal due to the inhibition of phagocytosis through the myeloid SIRP-α receptor, in both homeostatic and inflammatory conditions (Okazawa et al., 2005; Gitik et al., 2011; Gautam and Acharya, 2014; Zhang et al., 2015; Lehrman et al., 2018; Sato-Hashimoto et al., 2019). Very few studies have characterized CD47 progression in neuroinflammatory conditions, and to our knowledge, only after intracerebral haemorrhage a rapid upregulation determined of CD47 levels (Zhou et al., 2014). Strikingly, CD47 was found to be downregulated in MS patients (Koning et al., 2007; Han et al., 2012). In the first case, the reason why was upregulated was uncertain, whereas in MS patients, authors claimed that this decrease was related to an increase of the phagocytic activity from microglia and macrophages, since CD47 has been determined to inhibit microglial and macrophage phagocytosis through the interaction with its receptor SIRP-α (Okazawa et al., 2005; Gitik et al., 2011; Gautam and Acharya, 2014; Zhang et al., 2015; Lehrman et al., 2018; Sato-Hashimoto et al., 2019). Therefore, taking into account the extensively documented role of CD47-SIRP-α on preventing phagocytosis, we could infer that the increase in CD47 prevents the self-engulfment of FMNs. As a result, we could suggest that CD47 upregulation may act as a brake to microglial phagocytosis in the FNA model.

1.2.3 Microglia in clusters show a specific phagocytic phenotype after FNA

Interestingly, we could also stablish a close link between CD200R and CD45 with microglial clusters, at later stages. Microglial clusters are usually defined as accumulations of activated microglial cells. Although, these structures have been commonly associated with neuronal phagocytosis in FNA model (Raivich et al., 1998; Petitto et al., 2003), and this was confirmed with the presence of TREM2 and other

DAM molecules on them (that will be discussed hereunder), and with the phagocytosis assay performed with microglial TREM+ cells, previous work carried out in our lab established that higher number of microglial clusters resulted in increased neuronal survival, pointing out possible other functions of these structures yet to be discovered (Villacampa et al., 2015). The fact that both “Off” receptors were mainly present on microglial clusters strengthens the theory that these nodules should not only used as an indirect way to measure motor neuronal death in this paradigm (Petitto et al. 2003). While it is plausible to suppose that the presence of these molecules on microglial clusters could be involved in keeping their phagocytic function under tight control, they also could play a pivotal role in the interaction between these structure and neurons to have a beneficial effect in the final FMNs fate, for instance.

As we stated on the introduction section, recent single-cell RNA-sequencing analysis in the CNS tissue linked TREM2 with the differentiation of a newly identified specific microglial subtype appearing in mice in neurodegenerative conditions and aging, the so-called DAM or microglia associated to neurodegeneration. These microglia play a key role in chronic neurodegenerative conditions and show a unique transcriptional and functional signature highly differing from homeostatic microglia, characterized by the overexpression of other phagocytic genes, such as ApoE, CD16/32, CD68 and Galectin-3 among others accompanied by a downregulation of microglial homeostatic genes, including P2ry12 (Keren-Shaul et al., 2017; Krasemann et al., 2017; Deczkowska, Amit and Schwartz, 2018; Boza-Serrano et al., 2019).

DAM is regulated by TREM2 expression, and since we established a close relationship between microglial TREM2+ phagocytic clusters and neuronal death, we decided to study other DAM molecules. As we pointed out above, ApoE and Galectin-3, as well as the already mentioned phagocytic molecules CD16/32 and CD68, were positively expressed on microglial clusters at later stages (14-21dpi) after FNA, although membranal TREM2 expression, ApoE and Galectin 3 were not present in all clusters. We also explored the possibility that TREM2+ cells presented a downregulation of the homeostatic microglial receptor P2RY12. Contrary to what was expected, we did not find an overall and homogeneous decrease of P2RY12 levels after FNA, as it had been observed, for example, in the cuprizone-induced demyelination in mice (Klein et al., 2020) or after perforant pathway transection (Manich et al., 2020). Interestingly, different patterns of P2RY12 expression were observed on TREM2+ clusters, including clusters with high P2RY12 levels, which suggested the induction of diverse microglial phenotypes within the TREM2+ microglia subpopulation. The diversity found in microglial P2Y12R expression within clusters recalls results reported in human samples of AD and MS patients (van Wageningen et al., 2019; Walker et al., 2020). Concretely, in these studies, no changes in P2RY12 microglial expression in pre-active and chronic white matter MS lesions, or in gray matter lesions were observed (van Wageningen et al., 2019), as in diffuse Aß plaques in human AD patients (Walker et al., 2020). Similar observations on P2RY12 were also made in experimental models of viral encephalitis (Fekete et al., 2018). From our results, it could be suggested that clusters with high TREM2 expression and preserved levels of P2RY12 could belong to an active microglial state previous to P2RY12 downregulation. Still, the significance of TREM2 microglia with high P2RY12 levels remain to be explored.

Remarkably, after FNA, we did not find microglia without P2RY12 expression, while in other models of AD or in human AD and MS samples TREM2 microglia located in mature Aß plaques of AD mouse models or in active white matter MS lesions, P2RY12 was not expressed (Jay et al., 2017; Krasemann et al., 2017; Wageningen et al., 2019; Walker et al., 2020; van). This observation shows that in axonal injuries, with a reparative process, a microglial DAM phenotype (being P2Y12R-negative) is not fully developed; and may also suggest that P2Y12R-negative microglia could be associated to non-reparative CNS lesions or even deleterious for recovery.

Altogether, the phenotypic characterization of TREM2+ microglia after FNA indicates a clear involvement of this molecule in a subpopulation of phagocytosing microglia, probably aimed at recognizing degenerating neurons that could clear more efficiently these cell remnants. These microglia subpopulation displayed apart from TREM2+ expressions in microglial clusters, CD16/32+, CD68+, Galectin-3+, ApoE+ and P2ry12 variable expression. The presence of other homeostatic molecules apart from P2ry12, like CD200R and CD45, possibly points out the importance of a balance between DAM molecules and homeostatic signals in the phagocytic function of microglial clusters to promote further neuronal regeneration and survival.

1.2.4. “On/Off” signalling in microglia-lymphocyte crosstalk after FNA

In addition to microglia and macrophages, CD45 and CD200R “Off” receptors are present in some subsets of lymphocytes in the FNA model (Barclay, Clark and McCaughan, 1986; Wright et al., 2003; Manich et al., 2019). As stated earlier in previous sections, FNA induces the infiltration of lymphocytes (Raivich et al., 1998) that has been commonly associated with a neuroprotective effect (Serpe, Sanders and Jones, 2000; Jones et al., 2005). Through flow cytometry, we determined an increase on lymphocyte infiltration in WT mice reaching a peak at 14dpi (Annex, Suppl. Figure 1), coinciding with previous reports (Almolda et al., 2014; Villacampa et al., 2015). Regulation of lymphocyte infiltration through CD200-CD200R has been suggested based on the expression of CD200 in endothelial cells from brain capillaries (Ko et al., 2009; Denieffe et al., 2013), as we also found in our study, at 14dpi (Supplementary Figure 1). Despite CD200 has been suggested to play a role in lymphocyte adhesion (Ko et al., 2009), lack of CD200 expression does not seem to impede brain infiltration. The involvement of CD200-CD200R axis in lymphocyte infiltration has been studied in models of autoimmune diseases, such as EAE or experimental autoimmune uveitis

(Hoek et al., 2000; Broderick et al., 2002; Banerjee and Dick, 2004; Chitnis et al., 2007; Copland et al., 2007; Meuth et al., 2008). In these studies, either lack of expression of CD200 or blockade of CD200R led to increased lymphocyte infiltration. On the contrary, CD200 upregulation or administration of CD200Fc reduced monocyte infiltration. In our study we observed a progressive decrease of CD200R expression from NL to 14dpi (Supplementary Figure 1), which is coincident with increased lymphocyte infiltration, in accordance with previous studies. Indeed, some works suggested that, instead of a direct effect, the involvement of CD200-CD200R in lymphocyte infiltration is dependent on the degree of microglial activation, enhanced upon loss of CD200-CD200R interaction, and the increase of released chemokines produced by microglia, such as CCL-5, CXCL-10 or CCL-2 (Denieffe et al., 2013). Taking into account the time-course of CD200-CD200R expression we describe in our work (Article 1, Figures 3 and 7), the involvement of chemokine release over CD200-CD200R axis regulation of T-cell infiltration seems more plausible.

1.2.5. "On/Off" signalling may affect FMNs repair in the FNA model

After FNA, some FMNs die, but others are able to regenerate, establishing new functional connections. Since "On/Off" signalling is involved in microglia-neuron communication, and the role of microglial cells greatly influence FNA outcome, we can expect an involvement of this signalling in FMNs regeneration.

The upregulation of neuron-microglia "Off" signals have been usually associated with increased repair and reduced cell damage. For instance, CD200 upregulation in transgenic Wlds animals produced reduced axonal after lesion and lower demyelination after EAE (Chitnis et al., 2007). However, in our works, CD200, CX3CL1 and CD22 were importantly downregulated from 14dpi onwards, excluding any effect of those "Off" signalling axis in FMNs regeneration. On the contrary, CD47 upregulated its levels in the lesioned FN at 21dpi, and therefore, this "Off" signal could be involved in this process. In the nervous tissue, CD47-SIRP-α is an "Off" signal involved in neuron-microglia communication, but it also plays an important role in the communication between neurons, since the SIRP-α receptor is also expressed in neurons (Adams et al., 1998). To our knowledge, upregulation of CD47 in nervous tissue has been involved in several physiological and pathological situations: in human iPSCs obtained from patients with brain overgrowth condition, associated to autism and schizophrenia (Li et al., 2021), which could be explained by microglial SIRP-α-mediated inhibition of phagocytosis, regulating synapse pruning (Lehrman et al., 2019; Li et al., 2021), in neuronal differentiation in cell cultures (Miyashita et al., 2004; Ohnishi et al., 2005; Murata et al., 2006; Hsieh et al., 2015), or in processes of memory formation, according to increases in CD47 mRNA observed in rats (Huang et al., 1998). A key role in CD47-SIRP-α axis has been demonstrated in synapse maturation (Toth et al., 2013), and lack of CD47 in knockout mice impaired granular neuron cell differentiation in the cerebellum during postnatal development, which resulted in behavioural abnormalities (Hsieh et al., 2015). Some authors hypothesized, based on some of these results, that neuronal CD47-SIRP-α axis is involved in developmental network formation in the hippocampus and other brain areas, and during adulthood in processes of memory formation (Matozaki et al., 2009). Because in our case CD47 upregulation occurs at 21dpi, and since the reestablishment of functional connections of FMNs occur from 14dpi onwards (Makwana et al., 2010), we can suggest that the also existing neuron-to-neuron CD47-SIRP-α signalling plays a role in FMNs regeneration.

Microglial "On" TREM2 has been qualified to play a role in CNS reparation due to the qualified as "anti-inflammatory" TREM2-mediated phagocytosis, since it results in the production of anti-inflammatory cytokines (Takahashi et al., 2007; Hsieh et al., 2009). Cuprizone studies showed that the absence of TREM2 expression in microglia increases axonal injury and impairs repair (Cantoni et al., 2015; Poliani et al., 2015), and this injury can be rescued with TREM2 activating antibodies (Cignarella et al., 2020). In our study, FNA inflammation is downregulated around the peak of TREM2 expression, which indicates a reparatory role for this receptor. The reparatory effect could be the result of the efficient TREM2-mediated phagocytosis accompanied by the secretion of anti-inflammatory cytokines, that could facilitate FMNs clearance and neuronal regeneration. Indeed, quantification of cytokine expression after FNA (Article 1, Supplementary Figure 1) pointed out to elevated levels of IL-10, an anti-inflammatory cytokine, coinciding with the peak of TREM2 expression and the reparatory phase of FMNs.

2. EFFECTS OF CHRONIC IL-6 AND IL-10 OVERPRODUCTION IN NEURONAL-MICROGLIAL "ON/OFF" SIGNALLING AFTER FNA

2.1 Chronic IL-6, but not IL-10 overproduction alters microglial "On/Off" signalling in homeostasis and after FNA

Chronic overproduction of IL-6 or IL-10 results in diverse levels of microglia activation in different brain areas of the CNS, as it has been widely reported in several works from our group and others (Campbell et al., 1993; Almolda et al., 2015; Recasens et al., 2019; Sánchez-Molina et al., 2021). Concretely, astrocyte-targeted production of IL-6 induced an enhanced microglial reactivity and primed phenotype in basal conditions, which was especially observed in areas such as the hippocampus, cortex, cerebellum or several white matter areas. In the case of GFAP-IL10Tg, activation of microglia was mainly observed in the hippocampus, according to changes in morphology, cell number and expression of Iba1 (Almolda et al., 2015; Recasens et al., 2019; Sánchez-Molina et al., 2021).

In the NL FN, previous work indicated divergent effects produced by the chronic overproduction of those cytokines: while in GFAP-IL6Tg mice microglia presented higher activation and cell number, in GFAP-IL10Tg, at first glance, we did not observe obvious microglial alterations (Almolda et al., 2014; Villacampa et al., 2015). Results obtained in this thesis supported previous work, since alterations in microglial activation in basal conditions were also reflected in the expression of “Off” and “On” receptors. Concretely, in GFAP-IL6Tg mice we found significantly higher microglial cells and highly activated microglia/macrophages, as well as increased microglial reactivity, according to increased basal levels of CD45, and downregulation of SIRP-α and CX3CR1 levels (Article 1, Figures 5, 6 and 8). Those results suggested that chronic IL-6 overproduction was triggering an abnormal microglial activation in basal conditions and producing a loss of the homeostatic phenotype (Butovsky et al., 2014). Indeed, loss of CX3CR1 and SIRP-α were observed in microglia from WT mice upon its activation after FNA, as discussed in previous sections. Downregulation of CX3CR1 and SIRP-α receptors also supported the microglial primed phenotype described in other brain areas of GFAP-IL6Tg. In contrast, chronic IL-10 overproduction did not alter neither cell number nor activation of microglial cells, and similarly, “Off” receptors and TREM2 showed similar levels compared to WT under physiological conditions, indicating a lack of effects of the overproduction of this cytokines (Article 1, Figures 5, 6, 7 and 9; Article 2, Figure 14). These results were not in accordance with previous reported alterations of CD200R expression in the hippocampus of GFAP-IL10Tg in physiological conditions, however, this could be explained by the enhanced microglial activation in the hippocampal area of GFAP-IL10Tg (Recasens et al., 2019; Sánchez-Molina et al., 2021)

After FNA, a similar pattern of alterations in the microglial phenotype was observed in GFAP-IL6Tg and GFAP-IL10Tg. Specifically, chronic overproduction of IL-10 did not significantly affect expression of both of “On” and “Off” receptors in these cells compared to WT (Article 1, Figures 5, 6, 7 and 9 and Article 2, Figure 14). A downregulation of microglia activation could be observed in the peak of microgliosis due to the lower increase in microglia number observed in these animals (Article 1, Figure 9). This effect may be produced by reduced microglia proliferation during microgliosis after FNA, as we had already observed in other injury models using GFAP-IL10Tg (Recasens et al., 2019; Shanaki, 2020). On the contrary, chronic IL-6 overproduction resulted in higher number of microglial cells and highly activated microglia/macrophages (Article 1, Figure 8). In addition, in microglia we observed increased expression of CD45, and lower expression of CX3CR1 and SIRP-α after FNA at early time-points (7 and 14dpi), as we had already in basal conditions (Article 1, Figures 5, 6 and 8). Indeed, when CD45 upregulation was referenced to basal conditions, a lower fold increase was observed in GFAP-IL6Tg in comparison to WT mice (Article 1, Figures 6). Overall, these alterations indicated that chronic IL-6 overproduction induced a specific microglial phenotype that produced altered and deficient microglial response after FNA. Alterations in the “On” and “Off” signalling could be related to previous modifications in the microglial response observed in these animals (Almolda et al., 2014). Concretely, in GFAP-IL6Tg we had previously reported a lower microglial wrapping of FMNs and cluster formation (Almolda et al., 2014), which may be influenced by decreased chemotaxis or altered adhesion functions caused by lower CX3CR1 microglial expression, since CX3CL1-CX3CR1 axis is involved in those functions (Hughes et al., 2002; Carter and Dick, 2004, Lauro et al., 2006). Although less explored, SIRP-α has also been involved in the chemotaxis and control of monocytes and macrophages, and lack of SIRP-α has been related to delayed transmigration and chemotaxis *in vitro* and in an *in vivo* model of peritonitis (de Vries et al., 2002; Álvarez-Zarate et al., 2015). In consequence, both the downregulation of CX3CR1 and SIRP-α could be involved in a decrease of the chemotactic abilities of activated microglia and its adhesion functions. As a result, these alterations may cause lower FMNs microglial wrapping, which may result in reduced FMNs neuroprotection. In addition, apart from its early alterations, that may cause a lower FMNs protection, chronic IL-6 overproduction may result in modification of the phagocytic abilities of microglia. During basal conditions and after FNA, microglia presented a sustained downregulation of SIRP-α, a receptor that has been mainly involved in the inhibition of phagocytosis in microglia and macrophages during aging and neuroinflammatory situations (Wang et al., 2019). This downregulation, that after FNA in WT and GFAP-IL10Tg is only observed at 14dpi (Article 1, Figure 9), is maintained in GFAP-IL6Tg. The study of the microglial phenotype in GFAP-IL6Tg after FNA showed that CD16/32 expression was importantly increased at 14dpi in comparison to WT mice (Almolda et al., 2014). Our results suggest that microglia presented an increased functional capacity through higher myelin phagocytosis, as we had previously observed in basal conditions in adult GFAP-IL6Tg mice (Sánchez-Molina et al., 2021). These results contrast with the lower TREM2 levels reported in GFAP-IL6Tg at 21 dpi, during the peak of expression of this receptor in WT mice after FNA (Article 2, Figure 14). The significant reduction detected in GFAP-IL6Tg mice could be explained by the lower microglial cluster formation rather than a direct effect of this cytokine overproduction on TREM2 signaling. This interpretation is reinforced by the fact that most microglia clusters expressed TREM2 in microglial ramifications, and the percentage of TREM2+ clusters found in GFAP-IL6Tg was similar to the one reported in WT mice (Article 2, Figure 2). Thus, our results suggest that chronic IL-6 overproduction downregulates TREM2 expression due to changes in the microglial activation pattern, which affect cluster formation, and may not be a direct effect of IL-6 on TREM2 levels. A similar effect on the microglial phenotype was reported in GFAP-IL6Tg cuprizone demyelinated mice, in which a reduction of TREM2 levels accompanied by an important decrease in the phagocytosis of degenerated myelin was during the peak of demyelination (Petkovic et al., 2016). Strikingly, we could expect that, matching with the phagocytic microglial phenotype found in GFAP-IL6Tg, TREM2 should be enhanced in these mice, verifying an increase of microglial phagocytosis at later stages. However, into a functional level, a decrease in TREM2 levels in GFAP-IL6Tg may result in the phagocytosis of degenerating FMNs through other receptors, that would not affect the ability to engulf but to efficiently phagocyte degenerated FMNs (Hsieh et al., 2009; Cantoni et al., 2015), as we had already observed for TREM2+ microglia in the myelin phagocytic assay (Article 2, Figure 13). On the other hand, TREM2 deficiency in GFAP-IL6Tg could not only impair an efficient removal of degenerating FMNs, but the digestion of cell remnants phagocyted by microglia (Nugent et al., 2020). The result of a lower TREM2-mediated phagocytosis in microglia from GFAP-IL6Tg mice, as well as the alteration of the "Off" signalling along the FNA time-course may have consequences not only in FMNs survival, increasing the FMNs death rate (Almolda et al., 2014), but also in microglia and FMNs repair. Indeed, TREM2-mediated phagocytosis is known to produce the secretion of anti-inflammatory cytokines (Takahashi et al., 2007; Hsieh et al., 2009), but since TREM2 levels were downregulated in GFAP-IL6Tg, low levels of anti-inflammatory cytokines –resulting in a highly pro-inflammatory environment– and worsened FMNs repair may be expected. In agreement, in our work we found lower levels of IL-10 at 21 dpi (Article 1, Suppl. Figure 1), and microglia at 28 dpi showed increased levels of CD68 expression and lower levels of the "Off" receptor CD200R (Article 1, Figures 7 and 10).

Overall, the results obtained in this thesis indicate that chronic overproduction of pro-inflammatory IL-6 significantly modifies "On" and "Off" microglial receptor signalling in basal and neuroinflammatory conditions, while chronic overproduction of IL-10 does not alter the microglial expression of any of those receptors. Specifically, chronic overproduction of IL-6 results in a highly activated, phagocytic, and unresponsive microglial phenotype characterized by a lowered expression of the Off receptors SIRP-α and CX3CR1 and increased expression of CD45, in addition to a deficient induction of TREM2 expression after FNA. Alterations described in microglia may facilitate the increase in FMNs death observed in GFAP-IL6Tg after FNA in comparison to WT mice (Almolda et al., 2014). By contrast, it appears that IL-10 overproduction did not alter neither "Off" nor "On" TREM2 receptors in a significant way under physiological conditions and after FNA. These findings suggest that the inhibitory "Off" signalling present on microglial membranes are not enhanced by IL-10 overproduction, thus triggering the higher neuronal survival found on GFAP-IL10Tg mice (Villacampa et al., 2015). Be that as it may, GFAP-IL10Tg presented lower number of microglial cells at the peak of microgliosis in all "Off" markers, suggesting that IL-10 overproduction slows down microglial microgliosis and activation, inducing a dampened microglia inflammatory reaction.

2.2 Chronic IL-6 and IL-10 overproduction only modifies neuronal "Off" CD47 ligand, but no other neuronal "Off" signals were altered after FNA

When comparing CD200, CX3CL1 and CD22 levels characterized in WT animals with those detected in GFAP-IL6Tg and GFAP-IL10Tg, we could conclude that neither IL-6 nor IL-10 overproduction exerted a significant impact on the pattern evolution of these "Off" signals (Article 1, Figures 1, 2, 3). These results suggest that the previous changes found on neuronal survival and microglial activation in these animals are not related by a direct effect of these cytokines on these neuronal signals (Almolda et al., 2014: Villacampa et al., 2015). Only, GFAP-IL6Tg mice displayed a tendency to show lower CD22 levels at early time-points, specifically at 3dpi, compared to WT ones (Article 1, Figure 1), which according to the latter development of CD22 expression did not seem to have a relevant effect. Those effects may be surprising since, for example, IL-10 has been suggested to increase CD200 expression in several works (Mecha et al., 2013; Hernangómez et al., 2016), although this effect has not been unequivocally demonstrated. For instance, previous data in the hippocampus of GFAP-IL10Tg, did not result in increased expression of CD200 (Recasens, 2021), thus proving that IL-10 may not have a direct effect in CD200 expression.

On the contrary, in this study we found alterations in CD47 expression in both GFAP-IL6Tg and GFAP-IL10Tg compared to WT mice. CD47-SIRP-α axis has been mainly identified as a "Do-not-eat-me" signal, since avoidance of phagocytosis has been well-characterized in several physiologic contexts, such as removal of old erythrocytes by macrophages or migrating hematopoietic stem cells (Oldenborg, Gresham and Lindberg, 2001; Jaiswal et al., 2009), or in pathological situations, as a protective mechanism to avoid the immune system (Jaiswal et al., 2009; Kojima et al., 2016; Cham et al., 2020). As it had been previously highlighted, WT animals underwent an upregulation of CD47 at 21dpi, possibly due to the reestablishment of FMNs synapses, as discussed in previous sections. As a result, upregulated CD47 interacts with microglial SIRP-α, and constrains phagocytosis. Interestingly, CD47 upregulation started earlier in GFAP-IL10Tg, a tendency at 7dpi that with significantly increased levels at 14dpi (Article 1, Figure 4), inhibiting before microglial phagocytosis, during the peak of FMNs death. Otherwise, in GFAP-IL6Tg mice, CD47 levels remained like basal levels in all conditions, and since, as previously discussed, microglial SIRP-α is downregulated in basal conditions and after FNA, the loss of CD47-SIRP-α signalling would facilitate FMNs phagocytosis by microglia (Article 1, Figures 4 and 8). In global, these results could explain higher FMNs survival encountered in GFAP-IL10Tg (Villacampa et al., 2015) and lower survival of FMNs in GFAP-IL6Tg (Almolda et al., 2014).

In the FN of WT and GFAP-IL10Tg animals, IL-10R is located in FMNs in both GFAP-IL10Tg and WT animals (Villacampa et al., 2015). Taking into account that microglia does not express IL-10R, any effect produced in this cell type should be mediated by other cells. On the contrary, effects exerted by IL-10 in microglia-neuron communication may be produced directly to FMNs. Bian et al. (2016) identified key pathways in the inhibition of macrophage phagocytosis by CD47, which was potentiated by IL-10. However, this scenario does not apply in our case since, as commented above, IL-10R is expressed in FMNs but not microglia in this model. Since IL-10R is expressed in FMNs, IL-10 could directly increase CD47 upregulation in FMNs as a result of synapse formation and FMNs regeneration. Indeed, IL-10 has been proven *in vitro* to increase neurite outgrowth and synapse formation in neurons (Lim et al., 2013; Chen et al., 2016b), processes that have been both related to the upregulation of CD47 in those cells (Miyashita et al., 2004; Murata et al., 2006, Hsieh et al., 2015), and which can be potentiated with CD47 overexpression in neuronal cells *in vitro* (Hsieh et al., 2015). Our observations support these effects with several evidence: IL-10 expression in mice after FNA explains the earlier upregulation of CD47 observed in GFAP-IL10Tg due to its chronic overproduction, but also the upregulation of CD47 in lesioned FMNs of WT mice at 21dpi –or its absence in GFAP-IL6Tg–, according to the expression profile of IL-10 in both mouse lines (Article 1, Supplementary Figure 1). Our results suggest that a sustained overproduction of IL-10 promotes neurite outgrowth and synapse formation in FMNs, consequently upregulating CD47 in those cells. In order to provide more evidence on this effect, in this thesis we determined synaptophysin levels in both GFAP-IL10Tg and WT mice. Our results showed a tendency to form new synaptic contacts, according to the increase in synaptophysin levels at 21dpi, in GFAP-IL10Tg (Article 1, Figure 12). Consequently, IL-10-derived effects resulting in CD47 upregulation in FMNs could modulate microglial phagocytic activity. Also, lack of upregulation of CD47 in GFAP-IL6Tg mice suggest a deficient reestablishment of functional synapses in these animals.

These findings match with results obtained using the phagocytic markers CD16/32 and CD68 in all mouse lines after FNA (Villacampa, 2016). While GFAP-IL10Tg showed earlier upregulation of CD47, these animals also displayed lower levels of phagocytic CD16/32 (Villacampa et al., 2015) and CD68 at late time-points, confirming that when neuronal death peak takes place, these transgenic mice presented lower phagocytosis activity than WT mice. On the other hand, GFAP-IL6Tg mice showed higher CD16/32 and CD68 at later stages corroborating that apart from a lack of an upregulation of the inhibitory CD47 molecule, these animals also displayed higher levels of these phagocytic markers.

The relation of lesion outcomes with the inhibition of the phagocytic activity modulated through interaction of CD47 with its receptor SIRP-α in macrophages show contradictory effects. Loss or blockade of either CD47 (Han et al., 2012; Lehrman et al., 2018; Hutter et al., 2019) or SIRP-α (Sato-Hashimoto et al., 2019; Wang et al., 2019; Ding et al., 2021) resulted in increased phagocytosis of myelin or synapses, as exemplified in several experimental models. For instance, in mouse models of Wallerian axonal degeneration or in cuprizone-induced demyelination, loss of SIRP-α improved recovery (Elberg et al., 2019; Sato-Hashimoto et al., 2019); on the contrary, worsening was observed in neurodegeneration mouse models of Parkinson's and Alzheimer's mouse model, due to accelerated neuronal loss or decreased synaptic density (Wang et al., 2019; Ding et al., 2021) or in EAE, where clinical score was aggravated (Han et al., 2012). Oppositely, induced upregulation of CD47 in a model of retinitis pigmentosa increased retinal cone survival (Wang et al., 2021). Despite the effects of CD47-SIRP-α axis in phagocytosis are clear, with different outcomes depending on this function, establishing whether CD47 exerts a beneficial or detrimental role during inflammatory conditions is still a subject of controversy, since this axis participates in multiple functions. For instance, blockade of CD47 has been seen to reduce brain infarct in ischemic brain (Jin et al., 2009) and improve functional recovery in SCI model (Myers et al., 2011). Similarly, in chronic conditions such as in EAE model, CD47 deficient mice showed resistance to EAE development as well (Han et al., 2012; Gao et al., 2016). Nevertheless, blocking CD47 with a monoclonal antibody at the peak of disease worsened EAE (Han et al., 2012). These experiments exemplify the dual and contradictory effects of CD47 during initiation and progression of neuroinflammation. While it is true that targeting CD47 has been revealed to be a therapeutic approach for cancer treatment (Majeti et al., 2009; Zhang et al., 2016; Hutter et al., 2019), in CNS, further studies are needed since both blocking or replenishing CD47 may be an option depending on CD47 cell type expression, location, and kind and phase stage disease (Han et al., 2012; Zhang et al., 2015).

In our case, it appears that the upregulation of CD47 in WT and GFAP-IL10Tg animals may reduce neuronal phagocytosis and microglial activation, resulting in higher neuronal survival in these animals compared to GFAP-IL6Tg (Almolda et al., 2014; Villacampa et al., 2015). The fact that the increase of CD47 levels started earlier in GFAP-IL10Tg could indicate higher microglial regulation and increased improvement of neuronal survival. Taking into account the results obtained in this thesis, we could suggest that CD47-SIRP-α axis modulate FMNs survival after FNA, pointing out this signalling axis as a candidate for assaying therapeutical strategies to promote neuron survival in inflammatory contexts.

2.3 IL-6 overproduction modifies "Off" signalling present in lymphocytes while IL-10 overproduction does not interfere on it

In previous work from our group, we determined that chronic IL-6 overproduction induced an increase on lymphocyte infiltration being more significant at the peak, at 14dpi (Almolda et al., 2014). T-lymphocyte infiltration was higher in GFAP-IL6Tg than in GFAP-IL10Tg, where an increase in T-cell infiltration in comparison to WT mice was observed as well (Villacampa et al., 2015). When analyzing CD45 and CD200R levels, we determined that chronic IL-6 overproduction caused higher CD45 levels and decreased CD200R in basal conditions, and also lower CD200R in the peak of T-cell infiltration compared to WT, while chronic IL-10 overproduction exerted no effect

(Supplementary Figure 1). In line with these results, percentage of CD200R+ cells in GFAP-IL6Tg were significantly lower compared to WT at this later time-point. As we discussed in section 1.2.4, blockade or loss of CD200R-CD200 had been related to an increase in lymphocyte infiltration (Hoek et al., 2000; Broderick et al., 2002; Copland et al., 2007). Accordingly, in GFAP-IL6Tg, the decrease of CD200R expression in T-lymphocyte at 14dpi is associated to an increased infiltration in the brain parenchyma, as we observed in this study and had already been reported (Almolda et al., 2014; Supplementary Figure 1). Apart from the role on T-cell infiltration, the possible involvement of CD200-CD200R in T-cell function and differentiation has also been studied in experimental models of neuroinflammation. Concretely, CD200 expression has been reported in Th2 activated lymphocytes (Wright et al., 2003), and CD200R activation has been reported to control Th1 autoreactive lymphocytes (Penberthy and Tsunoda, 2009). However, increase in CD200 expression or stimulation of CD200R1 in the EAE did not cause any change in neither T-lymphocyte cell subset percentages, nor cytokine production (Chitnis et al., 2007; Liu et al., 2010). In our study we did not determine the specific T-cell phenotype infiltrating in GFAP-IL6Tg, although other studies performed in perforant pathway transection model in GFAP-IL6Tg also found increased T-cell infiltration without T-cell differentiation, resulting in a tolerogenic response (Recasens et al., 2021). In view of these results and results reported by previous literature, determination of CD200R levels in T-cell and its role in infiltration seem to be more linked to the microenvironment produced by chronic IL-6 overproduction in parenchymal microglia than its direct effect on T-cells.

As summarized in Figure 11, altogether our work suggests that, in the case of FNA, the increase detected on neuronal “Off” ligands CX3CL1, CD200 and CD22 attempts to protect FMNs after injury at early stages, coinciding with the peak of neuroinflammation. Later, a downregulation of the “Off signals” was observed, coinciding with neuronal loss and degeneration and the increase of the microglial ‘On’ receptor TREM2. Upregulation of the ‘Off’ ligand CD47 was detected at later time-points, during early FMN regeneration. Neuronal regulation of the ‘Off’ signals, together with the regulation of ‘Off’ receptors in microglia will first protect and then allow phagocytosis of FMN. Therefore, in this study we identified specific neuronal mechanisms by which FMNs regulate microglia activation at early and later stages, due to a direct cell-to-cell contact.

In conclusion, we elaborated the following figure that represents de overall findings detected in the “On/Off” signaling in the FNA model and the effects triggered by the pro-inflammatory and anti-inflammatory cytokines IL-6 and IL-10 on it:

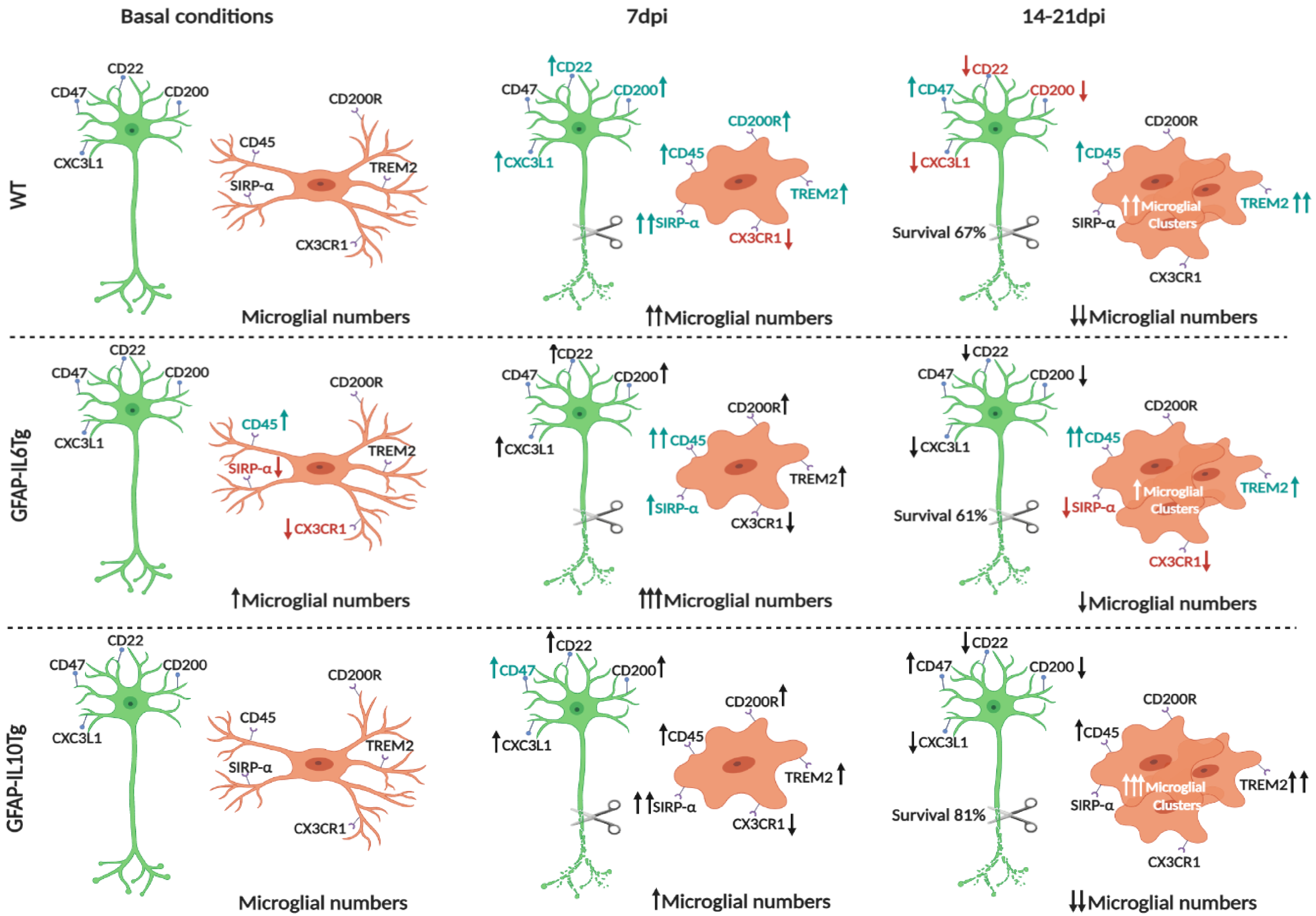
Basal conditions
7dpi
14-21dpi
WT
CD22
CD47
CD200
CXC3L1
CD200R
CD45
TREM2
SIRP-α
CX3CR1
Microglial numbers
↑CD22
CD47
CD200↑
↑CXC3L1
CD200R↑
↑CD45
TREM2↑
↑↑SIRP-α
CX3CR1↓
↑↑Microglial numbers
↓CD22
↑CD47
CD200 ↓
↓CXC3L1
CD200R
↑CD45
↑↑Microglial Clusters
TREM2 ↑↑
SIRP-α
Survival 67%
CX3CR1
↓↓Microglial numbers
GFAP-IL6Tg
CD22
CD47
CD200
CXC3L1
CD200R
CD45↑
TREM2
SIRP-α↓
↓CX3CR1
↑Microglial numbers
↑CD22
CD47
CD200↑
↑CXC3L1
CD200R↑
↑↑CD45
TREM2↑
↑SIRP-α
CX3CR1↓
↑↑↑Microglial numbers
↓CD22
CD47
CD200 ↓
↓CXC3L1
CD200R
↑↑CD45
↑Microglial Clusters
TREM2↑
↓SIRP-α
Survival 61%
CX3CR1↓
↓Microglial numbers
GFAP-IL10Tg
CD22
CD47
CD200
CXC3L1
CD200R
CD45
TREM2
SIRP-α
CX3CR1
Microglial numbers
↑CD22
↑CD47
CD200↑
↑CXC3L1
CD200R↑
↑CD45
TREM2 ↑
↑↑SIRP-α
CX3CR1↓
↑Microglial numbers
↓CD22
↑CD47
CD200 ↓
↓CXC3L1
CD200R
↑CD45
↑↑↑Microglial Clusters
TREM2↑↑
SIRP-α
Survival 81%
CX3CR1
↓↓Microglial numbers

Figure 11. "On/Off" and "Eat-me/Do-not-eat-me" signaling evolution after FNA. Schematic representation of the main changes on "Off" and "On" signals in both neurons and microglia in FNA paradigm. Additionally, a summary of the main differences is represented between WT, GFAP-IL6Tg and GFAP-IL10Tg mice lines regarding this mechanism. Differences are expressed as followed: increased levels are indicated with green color whereas decreased levels are indicated with red color. Differences in WT animals are represented versus the previous time-point whereas differences in transgenic mice are indicated in comparison to WT animals in the same conditions (Created by BioRender).

V. CONCLUSIONS

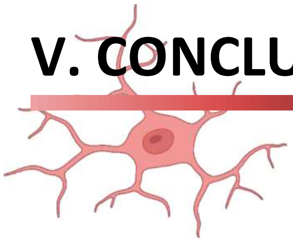

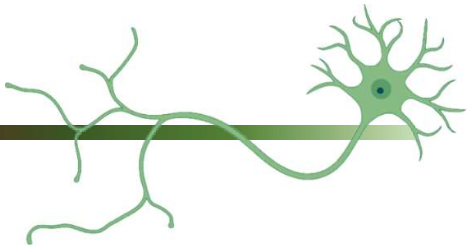

The results generated during this study indicate that chronic IL-6 overproduction clearly modified microglial “On” and “Off” signalling, and that this could be related to worsened short-term survival after FNA. On the other hand, IL-10 overproduction did not exert a significant impact in “On” and “Off” signalling except for CD47 neuronal ligand, a key inhibitory molecule of microglial phagocytosis, which could be fundamental for an improvement of the neuronal fate.

In more detail, the following specific conclusions were reached:

1. Under physiological conditions, all “Off” neuronal ligands CD200, CX3CL1, CD22 and CD47 and the corresponding microglial receptors CD200R, CX3CR1, CD45 and SIRP-α are constitutively expressed in the FN.
2. The “On” TREM2 molecule is constitutively expressed on microglia in the FN, displaying an inactive perinuclear location.
3. Under physiological conditions, chronic IL-6 overproduction induces a primed microglial phenotype showing an upregulation of CD45 and a downregulation of CX3CR1 and SIRP-α.
4. Chronic IL-10 overproduction does not affect microglial “Off” signalling in homeostatic conditions.
5. Neither IL-6 nor IL-10 exert any effect on TREM2 expression in basal conditions.
6. Neuronal “Off” ligands CD200, CX3CL1, CD22 and CD47 are not modified by either IL-6 or IL-10.
7. After FNA, microglial “Off” CD45, CD200R and SIRP-α levels of expression are increased coinciding with microglial activation.
8. Microglial “Off” CX3CR1 is progressively downregulated after injury, reaching its minimum levels at the neuronal death peak.
9. After injury, TREM2 “On” microglial receptor is translocated to the membrane surface and is mainly upregulated in microglial clusters, reaching its peak at later stages, when neuronal death takes place.
10. Through an *ex vivo* assay, microglial TREM+ positive cells have demonstrated to phagocyte in a more efficient manner compared to TREM2- ones.
11. There are different microglial clusters subtypes, identified by diverse pattern expression of TREM2 and other molecules including ApoE, Galectin-3, CD16/32, CD68 and P2ry12.
12. After FNA, neuronal CD200, CX3CL1 and CD22 “Off” signals are upregulated at early time-points reaching the maximum expression levels at the peak of microgliosis, followed by a downregulation concomitant with neuronal death.
13. After injury, CD47 is upregulated at later stages in the FN when neurons undergo a death cell process.
14. Chronic IL-6 overproduction induces an altered microglial response by enhancing CD45 levels together with the downregulation of CX3CR1, SIRP-α and CD200R at later stages.

15. Chronic IL-6 overproduction downregulates TREM2 microglial expression at later stages.
16. Chronic IL-10 overproduction does not affect either microglial “Off” receptor (CD200R, CX3CR1, CD45 and SIRP-α) or TREM2 expressions after FNA.
17. The expression of the “On” molecule TREM2 is not directly related to the different neuronal survival rates found in both transgenics mouse lines after FNA.
18. Neither IL-6 nor IL-10 chronic overproduction exerts a direct impact on the expression of neuronal “Off” CD200, CX3CL1 and CD22 ligands.
19. Chronic IL-10 overproduction upregulates CD47 at earlier stages, which is linked to synapse reestablishment.
20. Chronic IL-6 overproduction does not upregulate CD47 and keep its levels as in basal conditions.
21. Alterations in CD47 levels are correlated to the different survival rates determined in all mouse lines.
22. In the three mouse lines studied, microglial cells located in clusters express high levels of microglial “Off” CD45, CD200R and variable levels of SIRP-α.

VI. BIBLIOGRAPHY

Adams S, van der Laan LJ, Vernon-Wilson E, Renardel de Lavalette C, Döpp EA, Dijkstra CD, Simmons DL, van den Berg TK. Signal-regulatory protein is selectively expressed by myeloid and neuronal cells J Immunol. (1998) 161(4):1853-9

Ahn JH, Kim DW, Park JH, Lee TK, Lee HA, Won MH, Lee CH. Expression changes of CX3CL1 and CX3CR1 proteins in the hippocampal CA1 field of the gerbil following transient global cerebral ischemia. Int J Mol Med. (2019) 44(3):939-948

Akhmetzyanova E, Kletenkov K, Mukhamedshina Y, Rizvanov A. Different Approaches to Modulation of Microglia Phenotypes After Spinal Cord Injury. Front Syst Neurosci. (2019) 13:37. doi: 10.3389/fnsys.2019.00037

Alliot F, Godin I, Pessac B. Microglia derive from progenitors, originating from the yolk sac, and which proliferate in the brain. Brain Res Dev Brain Res. (1999) 117(2):145-52. doi: 10.1016/s0165-3806(99)00113-3

Almolda B, de Labra C, Barrera I, Gruart A, Delgado-Garcia JM, Villacampa N, Vilella A, Hofer MJ, Hidalgo J, Campbell IL, González B, Castellano B. Alterations in microglial phenotype and hippocampal neuronal function in transgenic mice with astrocyte-targeted production of interleukin-10. Brain Behav Immun. (2015) 45:80-97. doi: 10.1016/j.bbi.2014.10.015

Almolda B, Villacampa N, Manders P, Hidalgo J, Campbell IL, González B, Castellano B. Effects of astrocyte-targeted production of interleukin-6 in the mouse on the host response to nerve injury. Glia. (2014) 62(7):1142-61. doi: 10.1002/glia.22668

Aloisi F, De Simone R, Columba-Cabezas S, Levi G. Opposite effects of interferon-gamma and prostaglandin E2 on tumor necrosis factor and interleukin-10 production in microglia: a regulatory loop controlling microglia pro- and anti-inflammatory activities. J Neurosci Res. (1999) 56(6):571-80. doi: 10.1002/(SICI)1097-4547(19990615)56:6<571::AID-JNR3>3.0.CO;2-P

Alvarez-Zarate J, Matlung HL, Matozaki T, Kuijpers TW, Maridonneau-Parini I, van den Berg TK. Regulation of Phagocyte Migration by Signal Regulatory Protein-Alpha Signaling. PLoS One. (2015) 10(6):e0127178. doi: 10.1371/journal.pone.0127178

Anderson WD, Greenhalgh AD, Takwale A, David S, Vadigepalli R. Novel Influences of IL-10 on CNS Inflammation Revealed by Integrated Analyses of Cytokine Networks and Microglial Morphology. Front Cell Neurosci. (2017) 11:233. doi: 10.3389/fncel.2017.00233

Apelt J, Schliebs R. Beta-amyloid-induced glial expression of both pro- and anti-inflammatory cytokines in cerebral cortex of aged transgenic Tg2576 mice with Alzheimer plaque pathology. Brain Res. (2001) 894(1):21-30. doi: 10.1016/s0006-8993(00)03176-0

Askew K, Li K, Olmos-Alonso A, Garcia-Moreno F, Liang Y, Richardson P, Tipton T, Chapman MA, Riecken K, Beccari S, Sierra A, Molnár Z, Cragg MS, Garaschuk O, Perry VH, Gomez-Nicola D. Coupled Proliferation and Apoptosis Maintain the Rapid Turnover of Microglia in the Adult Brain. Cell Rep. (2017) 18(2):391-405. doi: 10.1016/j.celrep.2016.12.041

Atagi Y, Liu CC, Painter MM, Chen XF, Verbeeck C, Zheng H, Li X, Rademakers R, Kang SS, Xu H, Younkin S, Das P, Fryer JD, Bu G. Apolipoprotein E Is a Ligand for Triggering Receptor Expressed on Myeloid Cells 2 (TREM2). J Biol Chem. (2015) 290(43):26043-50. doi: 10.1074/jbc.M115.679043

Babendreyer A, Molls L, Dreymueller D, Uhlig S, Ludwig A Shear Stress Counteracts Endothelial CX3CL1 Induction and Monocytic Cell Adhesion. Mediators Inflamm (2017) 2017:1515389. doi: 10.1155/2017/1515389

Bachstetter AD, Morganti JM, Jernberg J, Schlunk A, Mitchell SH, Brewster KW, Hudson CE, Cole MJ, Harrison JK, Bickford PC, Gemma C. Fractalkine and CX3CR1 regulate hippocampal neurogenesis in adult and aged rats. Neurobiol Aging. (2011) 32(11):2030-44. doi: 10.1016/j.neurobiolaging.2009.11.022

Balasingam V, Yong VW. Attenuation of astroglial reactivity by interleukin-10. J Neurosci. (1996) 16(9):2945-55. doi: 10.1523/JNEUROSCI.16-09-02945.1996

Bamberger ME, Harris ME, McDonald DR, Husemann J, Landreth GE. A cell surface receptor complex for fibrillar beta-amyloid mediates microglial activation. J Neurosci. (2003) 23(7):2665-74. doi: 10.1523/JNEUROSCI.23-07-02665.2003

Banerjee D, Dick AD. Blocking CD200-CD200 receptor axis augments NOS-2 expression and aggravates experimental autoimmune uveoretinitis in Lewis rats. Ocul Immunol Inflamm. (2004) 12(2):115-25. doi: 10.1080/09273940490895326

Barclay AN, Clark MJ, McCaughan GW. Neuronal/lymphoid membrane glycoprotein MRC OX-2 is a member of the immunoglobulin superfamily with a light-chain-like structure. Biochem Soc Symp. (1986) 51:149-57

Bauer J, Strauss S, Schreiter-Gasser U, Ganter U, Schlegel P, Witt I, Yolk B, Berger M. Interleukin-6 and alpha-2-macroglobulin indicate an acute-phase state in Alzheimer's disease cortices. FEBS Lett. (1991) 285(1):111-4. doi: 10.1016/0014-5793(91)80737-n

Bazan JF, Bacon KB, Hardiman G, Wang W, Soo K, Rossi D, Greaves DR, Zlotnik A, Schall TJ. A new class of membrane-bound chemokine with a CX3C motif. Nature. (1997) 385(6617):640-4. doi: 10.1038/385640a0

Béchade C, Cantaut-Belarif Y, Bessis A. Microglial control of neuronal activity. Front Cell Neurosci. (2013) 7:32. doi: 10.3389/fncel.2013.00032

Bennett FC, Bennett ML, Yaqoob F, Mulinyawe SB, Grant GA, Hayden Gephart M, Plowey ED, Barres BA. A Combination of Ontogeny and CNS Environment Establishes Microglial Identity. Neuron. (2018) 98(6):1170-1183.e8. doi: 10.1016/j.neuron.2018.05.014

Bensadoun JC, de Almeida LP, Dréano M, Aebischer P, Déglon N. Neuroprotective effect of interleukin-6 and IL6/IL6R chimera in the quinolinic acid rat model of Huntington's syndrome. Eur J Neurosci. (2001)

Bessis A, Béchade C, Bernard D, Roumier A. Microglial control of neuronal death and synaptic properties. Glia. (2007) 55(3):233-8. doi: 10.1002/glia.20459

Bian Z, Shi L, Guo YL, Lv Z, Tang C, Niu S, Tremblay A, Venkataramani M, Culpepper C, Li L, Zhou Z, Mansour A, Zhang Y, Gewirtz A, Kidder K, Zen K, Liu Y. Cd47-Sirpα interaction and IL-10 constrain inflammation-induced macrophage phagocytosis of healthy self-cells. Proc Natl Acad Sci U S A. (2016) 113(37):E5434-43. doi: 10.1073/pnas.1521069113

Bianchi ME. DAMPs, PAMPs and alarmins: all we need to know about danger. J Leukoc Biol. (2007) 81(1):1-5. doi: 10.1189/jlb.0306164

Biber K, Neumann H, Inoue K, Boddeke HW. Neuronal 'On' and 'Off' signals control microglia. Trends Neurosci. (2007) 30(11):596-602. doi: 10.1016/j.tins.2007.08.007

Björkqvist M, Wild EJ, Thiele J, Silvestroni A, Andre R, Lahiri N, Raibon E, Lee RV, Benn CL, Soulet D, Magnusson A, Woodman B, Landles C, Pouladi MA, Hayden MR, Khalili-Shirazi A, Lowdell MW, Brundin P, Bates GP, Leavitt BR, Möller T, Tabrizi SJ. A novel pathogenic pathway of immune activation detectable before clinical onset in Huntington's disease. J Exp Med. (2008) 205(8):1869-77. doi: 10.1084/jem.20080178

Blanco AM, Vallés SL, Pascual M, Guerri C. Involvement of TLR4/type I IL-1 receptor signaling in the induction of inflammatory mediators and cell death induced by ethanol in cultured astrocytes. J Immunol (2005) 175(10):6893-9. doi: 10.4049/jimmunol.175.10.6893

Blinzinger K, Kreutzberg G. Displacement of synaptic terminals from regenerating motoneurons by microglial cells. Z Zellforsch Mikrosk Anat. (1968) 85(2):145-57. doi: 10.1007/BF00325030

Boche D, Gordon MN. Diversity of transcriptomic microglial phenotypes in aging and Alzheimer's disease. Alzheimers Dement. (2021) doi:10.1002/alz.12389

Boehme SA, Lio FM, Maciejewski-Lenoir D, Bacon KB, Conlon PJ. The chemokine fractalkine inhibits Fas-mediated cell death of brain microglia. J Immunol. (2000) 65(1):397-403. doi: 10.4049/jimmunol.165.1.397

Bolós M, Perea JR, Terreros-Roncal J, Pallas-Bazarra N, Jurado-Arjona J, Ávila J, Llorens-Martín M. Absence of microglial CX3CR1 impairs the synaptic integration of adult-born hippocampal granule neurons. Brain Behav Immun. (2018) 68:76-89. doi: 10.1016/j.bbi.2017.10.002

Boué DR, Lebien TW. Structural characterization of the human B lymphocyte-restricted differentiation antigen CD22. Comparison with CD21 (complement receptor type 2/Epstein-Barr virus receptor). J Immunol. (1988) 140(1):192-9

Boza-Serrano A, Ruiz R, Sanchez-Varo R, García-Revilla J, Yang Y, Jimenez-Ferrer I, Paulus A, Wennström M, Vilalta A, Allendorf D, Davila JC, Stegmayr J, Jiménez S, Roca-Ceballos MA, Navarro-Garrido V, Swanberg M, Hsieh CL, Real LM, Englund E, Linse S, Leffler H, Nilsson UJ, Brown GC, Gutierrez A, Vitorica J, Venero JL, Deierborg T. Galectin-3, a novel endogenous TREM2 ligand, detrimentally regulates inflammatory response in Alzheimer's disease. Acta Neuropathol. (2019) 138(2):251-273. doi: 10.1007/s00401-019-02013-z

Brioschi S, Zhou Y, Colonna M. Brain Parenchymal and Extraparenchymal Macrophages in Development, Homeostasis, and Disease. J Immunol. (2020) 204(2):294-305. doi: 10.4049/jimmunol.1900821

Broderick C, Hoek RM, Forrester JV, Liversidge J, Sedgwick JD, Dick AD. Constitutive retinal CD200 expression regulates resident microglia and activation state of inflammatory cells during experimental autoimmune uveoretinitis. Am J Pathol. (2002) 161(5):1669-77. doi: 10.1016/S0002-9440(10)64444-6.

Burkhart C, Liu GY, Anderton SM, Metzler B, Wraith DC. Peptide-induced T cell regulation of experimental autoimmune encephalomyelitis: a role for IL-10. Int Immunol. (1999) 11(10):1625-34. doi: 10.1093/intimm/11.10.1625

Burmeister AR, Marriott I. The Interleukin-10 Family of Cytokines and Their Role in the CNS. Front Cell Neurosci. (2018) 12:458. doi: 10.3389/fncel.2018.00458

Butovsky O, Jedrychowski MP, Moore CS, Cialic R, Lanser AJ, Gabriely G, Koeglsperger T, Dake B, Wu PM, Doykan CE, Fanek Z, Liu L, Chen Z, Rothstein JD, Ransohoff RM, Gygi SP, Antel JP, Weiner HL. Identification of a unique TGF-β-dependent molecular and functional signature in microglia. Nat Neurosci. (2014) 17(1):131-43. doi: 10.1038/nn.3599

Butovsky O, Weiner HL. Microglial signatures and their role in health and disease. Nat Rev Neurosci. (2018) 19(10):622-635. doi: 10.1038/s41583-018-0057-5

Byram SC, Carson MJ, DeBoy CA, Serpe CJ, Sanders VM, Jones KJ CD4-positive T cell-mediated neuroprotection requires dual compartment antigen presentation. J Neurosci. (2004) 24(18):4333-9. doi: 10.1523/JNEUROSCI.5276-03.2004

Cady J, Koval ED, Benitez BA, Zaidman C, Jockel-Balsarotti J, Allred P, Baloh RH, Ravits J, Simpson E, Appel SH, Pestronk A, Goate AM, Miller TM, Cruchaga C, Harms MB. TREM2 variant p.R47H as a risk factor for sporadic amyotrophic lateral sclerosis. JAMA Neurol. (2014) 71(4):449-53. doi: 10.1001/jamaneurol.2013.6237

Campbell IL, Abraham CR, Masliah E, Kemper P, Inglis JD, Oldstone MB, Mucke L. Neurologic disease induced in transgenic mice by cerebral overexpression of interleukin 6. Proc Natl Acad Sci U S A. (1993) 90(21):10061-5. doi: 10.1073/pnas.90.21.10061

Cantoni C, Bollman B, Licastro D, Xie M, Mikesell R, Schmidt R, Yuede CM, Galimberti D, Olivecrona G, Klein RS, Cross AH, Otero K, Piccio L. TREM2 regulates microglial cell activation in response to demyelination in vivo. Acta Neuropathol. (2015) 129(3):429-47. doi: 10.1007/s00401-015-1388-1

Cao Z, Gao Y, Bryson JB, Hou J, Chaudhry N, Siddiq M, Martinez J, Spencer T, Carmel J, Hart RB, Filbin MT. The cytokine interleukin-6 is sufficient but not necessary to mimic the peripheral conditioning lesion effect on axonal growth. J Neurosci. (2006) 26(20):5565-73. doi: 10.1523/JNEUROSCI.0815-06.2006

Cardona AE, Pioro EP, Sasse ME, Kostenko V, Cardona SM, Dijkstra IM, Huang D, Kidd G, Dombrowski S, Dutta R, Lee JC, Cook DN, Jung S, Lira SA, Littman DR, Ransohoff RM. Control of microglial neurotoxicity by the fractalkine receptor. Nat Neurosci. (2006) 9(7):917-24. doi: 10.1038/nn1715

Carniglia L, Ramírez D, Durand D, Saba J, Turati J, Caruso C, Scimonelli TN, Lasaga M. Neuropeptides and Microglial Activation in Inflammation, Pain, and Neurodegenerative Diseases. Mediators Inflamm. (2017) 2017:5048616. doi: 10.1155/2017/5048616

Carson MJ, Reilly CR, Sutcliffe JG, Lo D. Mature microglia resemble immature antigen-presenting cells. Glia. (1998) 22(1):72-85. doi: 10.1002/(sici)1098-1136(199801)22:1<72::aid-glia7>3.0.co;2-a

Carter DA, Dick AD. CD200 maintains microglial potential to migrate in adult human retinal explant model. Curr Eye Res. (2004) 28(6):427-36. doi: 10.1080/02713680490503778

Cartier L, Hartley O, Dubois-Dauphin M, Krause K-H. Chemokine receptors in the central nervous system: role in brain inflammation and neurodegenerative diseases. Brain Res Brain Res Rev. (2005) 48(1):16-42. doi: 10.1016/j.brainresrev.2004.07.021

Casali BT, Reed-Geaghan EG. Microglial Function and Regulation during Development, Homeostasis and Alzheimer's Disease. Cells. (2021) 10(4):957. doi: 10.3390/cells10040957

Castro-Sánchez S, García-Yagüe ÁJ, López-Royo T, Casarejos M, Lanciego JL, Lastres-Becker I. Cx3cr1-deficiency exacerbates alpha-synuclein-A53T induced neuroinflammation and neurodegeneration in a mouse model of Parkinson's disease. Glia. (2018) 66(8):1752-1762. doi: 10.1002/glia.23338

Chakrabarty P, Jansen-West K, Beccard A, Ceballos-Diaz C, Levites Y, Verbeeck C, Zubair AC, Dickson D, Golde TE, Das P. Massive gliosis induced by interleukin-6 suppresses Abeta deposition in vivo: evidence against inflammation as a driving force for amyloid deposition. FASEB J. (2010) 24(2):548-59. doi: 10.1096/fj.09-141754

Chakrabarty P, Li A, Ceballos-Diaz C, Eddy JA, Funk CC, Moore B, DiNunno N, Rosario AW, Cruz PE, Verbeeck C, Sacino A, Nix S, Janus C, Price ND, Das P, Golde TE. IL-10 alters immunoproteostasis in APP mice, increasing plaque burden and worsening cognitive behavior. Neuron (2015) 85(3):519-33. doi: 10.1016/j.neuron.2014.11.020

Cham LB, Adomati T, Li F, Ali M, Lang KS. CD47 as a Potential Target to Therapy for Infectious Diseases. Antibodies (Basel). (2020) 9(3):44. doi: 10.3390/antib9030044

Checchin D, Sennlaub F, Levavasseur E, Leduc M, Chemtob S. Potential role of microglia in retinal blood vessel formation. Invest Ophthalmol Vis Sci. (2006) 47(8):3595-602. doi: 10.1167/iovs.05-1522

Chen H, Lin W, Zhang Y, Lin L, Chen J, Zeng Y, Zheng M, Zhuang Z, Du H, Chen R, Liu N. IL-10 Promotes Neurite Outgrowth and Synapse Formation in Cultured Cortical Neurons after the Oxygen-Glucose Deprivation via JAK1/STAT3 Pathway. Sci Rep. (2016b) 6:30459. doi: 10.1038/srep30459

Chen Z, Trapp BD. Microglia and neuroprotection. J Neurochem. (2016) 136 Suppl 1:10-7. doi: 10.1111/jnc.13062

Chen P, Zhao W, Guo Y, Xu J, Yin M. CX3CL1/CX3CR1 in Alzheimer's Disease: A Target for Neuroprotection. Biomed Res Int. (2016) 2016:8090918. doi: 10.1155/2016/8090918

Cheng-Hathaway PJ, Reed-Geaghan EG, Jay TR, Casali BT, Bemiller SM, Puntambekar SS, von Saucken VE, Williams RY, Karlo JC, Moutinho M, Xu G, Ransohoff RM, Lamb BT, Landreth GE. The Trem2 R47H variant confers loss-of-function-like phenotypes in Alzheimer’s disease. Mol Neurodegener. (2018) 13(1):29. doi: 10.1186/s13024-018-0262-8

Cherry JD, Olschowka JA, O'Banion MK.. Neuroinflammation and M2 microglia: the good, the bad, and the inflamed. J Neuroinflammation. (2014) 11:98. doi: 10.1186/1742-2094-11-98

Chertoff M, Shrivastava K, Gonzalez B, Acarin L, Giménez-Llort L. Differential modulation of TREM2 protein during postnatal brain development in mice. PLoS One. (2013) 8(8):e72083. doi: 10.1371/journal.pone.0072083

Chitnis T, Imitola J, Wang Y, Elyaman W, Chawla P, Sharuk M, Raddassi K, Bronson RT, Khoury SJ. Elevated neuronal expression of CD200 protects Wlds mice from inflammation mediated neurodegeneration. Am J Pathol. (2007) 170(5):1695-712. doi: 10.2353/ajpath.2007.060677

Christoforidou E, Joilin G, Hafezparast M. Potential of activated microglia as a source of dysregulated extracellular microRNAs contributing to neurodegeneration in amyotrophic lateral sclerosis. J Neuroinflammation. (2020) 17(1):135. doi: 10.1186/s12974-020-01822-4

Cignarella F, Filipello F, Bollman B, Cantoni C, Locca A, Mikesell R, Manis M, Ibrahim A, Deng L, Benitez BA, Cruchaga C, Licastro D, Mihindukulasuriya K, Harari O, Buckland M, Holtzman DM, Rosenthal A, Schwabe T, Tassi I, Piccio L. TREM2 activation on microglia promotes myelin debris clearance and remyelination in a model of multiple sclerosis. Acta Neuropathol. (2020);140(4):513-534. doi: 10.1007/s00401-020-02193-z

Cockram TOJ, Dundee JM, Popescu AS, Brown GC. The Phagocytic Code Regulating Phagocytosis of Mammalian Cells. Front Immunol. (2021) 12:629979. doi: 10.3389/fimmu.2021.629979

Cohen M, Ben-Yehuda H, Porat Z, Raposo C, Gordon S, Schwartz M. Newly Formed Endothelial Cells Regulate Myeloid Cell Activity Following Spinal Cord Injury via Expression of CD200 Ligand. J Neurosci. (2017) 37(4):972-985. doi: 10.1523/JNEUROSCI.2199-16.2016

Colonna M, Butovsky O. Microglia Function in the Central Nervous System During Health and Neurodegeneration. Annu Rev Immunol. (2017) 35:441-468. doi: 10.1146/annurev-immunol-051116-052358

Colton CA. Heterogeneity of microglial activation in the innate immune response in the brain. J Neuroimmune Pharmacol. (2009) 4(4):399-418. doi: 10.1007/s11481-009-9164-4

Comella Bolla A, Valente T, Miguez A, Brito V, Gines S, Solà C, Straccia M, Canals JM. CD200 is up-regulated in R6/1 transgenic mouse model of Huntington's disease. PLoS One. (2019) 14(12): e0224901

Conde JR, Streit WJ. Effect of aging on the microglial response to peripheral nerve injury. Neurobiol Aging. (2006) 27(10):1451-61. doi: 10.1016/j.neurobiolaging.2005.07.012

Copland D, Calder CJ, Raveney BJE, Nicholson LB, Phillips J, Cherwinski H, Jenmalm M, Sedgwick JD, Dick AD. Monoclonal antibody-mediated CD200 receptor signaling suppresses macrophage activation and tissue damage in experimental autoimmune uveoretinitis. Am J Pathol. (2007) 171(2):580-8. doi: 10.2353/ajpath.2007.070272.

Correa F, Hernangómez M, Mestre L, Loría F, Spagnolo A, Docagne F, Di Marzo V, Guaza C. Anandamide enhances IL-10 production in activated microglia by targeting CB(2) receptors: roles of ERK1/2, JNK, and NF-kappaB. Glia. (2010) 58(2):135-47. doi: 10.1002/glia.20907

Cosenza-Nashat MA, Kim MO, Zhao ML, Suh HS, Lee SC. CD45 isoform expression in microglia and inflammatory cells in HIV-1 encephalitis. Brain Pathol. (2006) 16(4):256-65. doi: 10.1111/j.1750-3639.2006.00027.x

Cosenza MA, Zhao ML, Si Q, Lee SC. Human brain parenchymal microglia express CD14 and CD45 and are productively infected by HIV-1 in HIV-1 encephalitis. Brain Pathol. (2002) 12(4):442-55. doi: 10.1111/j.1750-3639.2002.tb00461.x

Costello DA, Lyons A, Denieffe S, Browne TC, Cox FF, Lynch MA. Long term potentiation is impaired in membrane glycoprotein CD200-deficient mice: a role for Toll-like receptor activation. J Biol Chem. (2011) 286(40):34722-32. doi: 10.1074/jbc.M111.280826.

Cougnoux A, Drummond RA, Collar AL, Iben JR, Salman A, Westgarth H, Wassif CA, Cawley NX, Farhat NY, Ozato K, Lionakis MS, Porter FD. Microglia activation in Niemann-Pick disease, type C1 is amendable to therapeutic intervention. Hum Mol Genet. (2018) 27(12):2076-2089. doi: 10.1093/hmg/ddy112

Crotti A, Ransohoff RM. Microglial Physiology and Pathophysiology: Insights from Genome-wide Transcriptional Profiling. Immunity. (2016) 44(3):505-515. doi: 10.1016/j.immuni.2016.02.013

Cua DJ, Hutchins B, LaFace DM, Stohlman SA, Coffman RL. Central nervous system expression of IL-10 inhibits autoimmune encephalomyelitis. J Immunol. (2001) 166(1):602-8. doi: 10.4049/jimmunol.166.1.602

Cunningham CL, Martínez-Cerdeño V, Noctor SC. Microglia Regulate the Number of Neural Precursor Cells in the Developing Cerebral Cortex. J Neurosci. (2013) 33(10):4216-33. doi: 10.1523/JNEUROSCI.3441-12.2013

Dauer DJ, Huang Z, Ha GK, Kim J, Khosrowzadeh D, Petitto JM. Age and facial nerve axotomy-induced T cell trafficking: relation to microglial and motor neuron status. Brain Behav Immun. (2011) 25(1):77-82. doi: 10.1016/j.bbi.2010.08.005

Davalos D, Grutzendler J, Yang G, Kim JV, Zuo Y, Jung S, Littman DR, Dustin ML, Gan WB. ATP mediates rapid microglial response to local brain injury in vivo. Nat Neurosci. (2005) 8(6):752-8. doi: 10.1038/nn1472

Daws MR, Sullam PM, Niemi EC, Chen TT, Tchao NK, Seaman WE. Pattern recognition by TREM-2: binding of anionic ligands. J Immunol. (2003) 171(2):594-9. doi: 10.4049/jimmunol.171.2.594

de Groot CJ, Huppes W, Sminia T, Kraal G, Dijkstra CD. Determination of the origin and nature of brain macrophages and microglial cells in mouse central nervous system, using non-radioactive in situ hybridization and immunoperoxidase techniques. Glia. (1992) 6(4):301-9. doi: 10.1002/glia.440060408

de Haas AH, Boddeke HW, Biber K. Region-specific expression of immunoregulatory proteins on microglia in the healthy CNS. Glia. (2008) 56(8):888-94. doi: 10.1002/glia.20663.

de Vries HE, Hendriks JJ, Honing H, De Lavalette CR, van der Pol SM, Hooijberg E, Dijkstra CD, van den Berg TK. Signal-regulatory protein alpha-CD47 interactions are required for the transmigration of monocytes across cerebral endothelium. J Immunol. (2002) 168(11):5832-9. doi: 10.4049/jimmunol.168.11.5832

Deboy CA, Xin J, Byram SC, Serpe CJ, Sanders VM, Jones KJ. Immune-mediated neuroprotection of axotomized mouse facial motoneurons is dependent on the IL-4/STAT6 signaling pathway in CD4(+) T cells. Exp Neurol. (2006) 201(1):212-24. doi: 10.1016/j.expneurol.2006.04.028

Deckert M, Sedgwick JD, Fischer E, Schlüter D. Regulation of microglial cell responses in murine Toxoplasma encephalitis by CD200/CD200 receptor interaction. Acta Neuropathol. (2006) 111(6):548-58

Deczkowska A, Amit I, Schwartz M. Microglial immune checkpoint mechanisms. Nat Neurosci. (2018) 21(6):779-786. doi: 10.1038/s41593-018-0145-x

Deczkowska A, Keren-Shaul H, Weiner A, Colonna M, Schwartz M, Amit I. Disease-Associated Microglia: A Universal Immune Sensor of Neurodegeneration. Cell. (2018) 173(5):1073-1081. doi: 10.1016/j.cell.2018.05.003

Deczkowska A, Weiner A, Amit I. The Physiology, Pathology, and Potential Therapeutic Applications of the TREM2 Signaling Pathway. Cell. (2020) 181(6):1207-1217. doi: 10.1016/j.cell.2020.05.003

Deming Y, Li Z, Benitez BA, Cruchaga C. Triggering receptor expressed on myeloid cells 2 (TREM2): a potential therapeutic target for Alzheimer disease? Expert Opin Ther Targets. (2018) 22(7):587-598. doi: 10.1080/14728222.2018.1486823

Denieffe S, Kelly RJ, McDonald C, Lyons A, Lynch MA. Classical activation of microglia in CD200-deficient mice is a consequence of blood brain barrier permeability and infiltration of peripheral cells. Brain Behav Immun. (2013) 34:86-97. doi: 10.1016/j.bbi.2013.07.174

Dheen ST, Kaur C, Ling EA. Microglial activation and its implications in the brain diseases. Curr Med Chem. (2007) 14(11):1189-97. doi: 10.2174/092986707780597961

Ding X, Wang J, Huang M, Chen Z, Liu J, Zhang Q, Zhang C, Xiang Y, Zen K, Li L. Loss of microglial SIRPα promotes synaptic pruning in preclinical models of neurodegeneration. Nat Commun. (2021) 12(1):2030. doi: 10.1038/s41467-021-22301-1

Ding X, Yan Y, Li X, Li K, Ciric B, Yang J, Zhang Y, Wu S, Xu H, Chen W, Lovett-Racke AE, Zhang GX, Rostami A. Silencing IFN-γ binding/signaling in astrocytes versus microglia leads to opposite effects on central nervous system autoimmunity. J Immunol. (2015) 194(9):4251-64. doi: 10.4049/jimmunol.1303321

Duan RS, Yang X, Chen ZG, Lu MO, Morris C, Winblad B, Zhu J. Decreased fractalkine and increased IP-10 expression in aged brain of APP(swe) transgenic mice. Neurochem Res. (2008) 33(6):1085-9. doi: 10.1007/s11064-007-9554-z

Elberg G, Liraz-Zaltsman S, Reichert F, Matozaki T, Tal M, Rotshenker S. Deletion of SIRPα (signal regulatory protein-α) promotes phagocytic clearance of myelin debris in Wallerian degeneration, axon regeneration, and recovery from nerve injury. J Neuroinflammation. (2019) 16(1):277. doi: 10.1186/s12974-019-1679-x

Erblich B, Zhu L, Etgen AM, Dobrenis K, Pollard JW. Absence of colony stimulation factor-1 receptor results in loss of microglia, disrupted brain development and olfactory deficits. PLoS One. (2011) 6(10):e26317. doi: 10.1371/journal.pone.0026317

Erta M, Quintana A, Hidalgo J. Interleukin-6, a major cytokine in the central nervous system. Int J Biol Sci. (2012) 8(9):1254-66. doi: 10.7150/ijbs.4679

Färber K, Pannasch U, Kettenmann H. Dopamine and noradrenaline control distinct functions in rodent microglial cells. Mol Cell Neurosci. (2005) 29(1):128-38. doi: 10.1016/j.mcn.2005.01.003

Fedoroff S, Zhai R, Novak JP. Microglia and astroglia have a common progenitor cell. J Neurosci Res. (1997) 50(3):477-86. doi: 10.1002/(SICI)1097-4547(19971101)50:3<477::AID-JNR14>3.0.CO;2-3

Fekete R, Cserép C, Lénárt N, Tóth K, Orsolits B, Martinecz B, Méhes E, Szabó B, Németh V, Gönci B, Sperlágh B, Boldogkői Z, Kittel Á, Baranyi M, Ferenczi S, Kovács K, Szalay G, Rózsa B, Webb C, Kovacs GG, Hortobágyi T, West BL, Környei Z, Dénes Á. Microglia control the spread of neurotropic virus infection via P2Y12 signalling and recruit monocytes through P2Y12-independent mechanisms. Acta Neuropathol. 2018 Sep;136(3):461-482. doi: 10.1007/s00401-018-1885-0

Ferri CC, Moore FA, Bisby MA. Effects of facial nerve injury on mouse motoneurons lacking the p75 low-affinity neurotrophin receptor. J Neurobiol. (1998) 34(1):1-9

Fisher J, Mizrahi T, Schori H, Yoles E, Levkovitch-Verbin H, Haggiag S, Revel M, Schwartz M. Increased post-traumatic survival of neurons in IL-6-knockout mice on a background of EAE susceptibility. J Neuroimmunol. (2001)

Frade JM, Barde YA. Microglia-derived nerve growth factor causes cell death in the developing retina. Neuron. (1998) 20(1):35-41. doi: 10.1016/s0896-6273(00)80432-8

Frank MG, Barrientos RM, Biedenkapp JC, Rudy JW, Watkins LR, Maier SF. mRNA Up-Regulation of MHC II and Pivotal Pro-Inflammatory Genes in Normal Brain Aging. Neurobiol Aging. (2006) 27(5):717-22

Friedman BA, Srinivasan K, Ayalon G, Meilandt WJ, Lin H, Huntley MA, Cao Y, Lee SH, Haddick PCG, Ngu H, Modrusan Z, Larson JL, Kaminker JS, van der Brug MP, Hansen DV. Diverse Brain Myeloid Expression Profiles Reveal Distinct Microglial Activation States and Aspects of Alzheimer's Disease Not Evident in Mouse Models. Cell Rep. (2018) 22(3):832-847. doi: 10.1016/j.celrep.2017.12.066

Funikov SY, Rezvykh AP, Mazin PV, Morozov AV, Maltsev AV, Chicheva MM, Vikhareva EA, Evgen'ev MB, Ustyugov AA. FUS(1-359) transgenic mice as a model of ALS: pathophysiological and molecular aspects of the proteinopathy. Neurogenetics. (2018) 19(3):189-204. doi: 10.1007/s10048-018-0553-9

Gao HM, Liu B, Zhang W, Hong JS. Novel anti-inflammatory therapy for Parkinson's disease. Trends Pharmacol Sci. (2003) 24(8):395-401. doi: 10.1016/S0165-6147(03)00176-7

Gao HM, Zhou H, Zhang F, Wilson BC, Kam W, Hong JS. HMGB1 acts on microglia Mac1 to mediate chronic neuroinflammation that drives progressive neurodegeneration. J Neurosci. (2011) 31(3):1081-92. doi: 10.1523/JNEUROSCI.3732-10.2011

Gao Q, Zhang Y, Han C, Hu X, Zhang H, Xu X, Tian J, Liu Y, Ding Y, Liu J, Wang C, Guo Z, Yang Y, Cao X. Blockade of CD47 ameliorates autoimmune inflammation in CNS by suppressing IL-1-triggered infiltration of pathogenic Th17 cells. J Autoimmun. (2016) 69:74-85. doi: 10.1016/j.jaut.2016.03.002

Gaupp S, Cannella B, Raine CS. Amelioration of experimental autoimmune encephalomyelitis in IL-4Ralpha-/- mice implicates compensatory up-regulation of Th2-type cytokines. Am J Pathol. (2008) 173(1):119-29. doi: 10.2353/ajpath.2008.071156

Gautam PK, Acharya A. Suppressed expression of homotypic multinucleation, extracellular domains of CD172α (SIRP-α) and CD47 (IAP) receptors in TAMs upregulated by Hsp70-peptide complex in Dalton's lymphoma. Scand J Immunol. (2014) 80(1):22-35. doi: 10.1111/sji.12180

Gautier EL, Shay T, Miller J, Greter M, Jakubzick C, Ivanov S, Helft J, Chow A, Elpek KG, Gordonov S, Mazloom AR, Ma'ayan A, Chua WJ, Hansen TH, Turley SJ, Merad M, Randolph GJ; Immunological Genome Consortium. Gene-expression profiles and transcriptional regulatory pathways that underlie the identity and diversity of mouse tissue macrophages. Nat Immunol. (2012) 13(11):1118-28. doi: 10.1038/ni.2419

Gemma C, Bachstetter AD. The role of microglia in adult hippocampal neurogenesis. Front Cell Neurosci. (2013) 7:229. doi: 10.3389/fncel.2013.00229

Gervois P, Lambrichts I. The emerging role of triggering receptor expressed on myeloid cells 2 as a target for immunomodulation in ischemic stroke. Front Immunol. (2019) 10:1668. doi: 10.3389/fimmu.2019.01668

Gijbels K, Brocke S, Abrams JS, Steinman L. Administration of neutralizing antibodies to interleukin-6 (IL-6) reduces experimental autoimmune encephalomyelitis and is associated with elevated levels of IL-6 bioactivity in central nervous system and circulation. Mol Med. (1995) 1(7):795-805

Ginhoux F, Greter M, Leboeuf M, Nandi S, See P, Gokhan S, Mehler MF, Conway SJ, Ng LG, Stanley ER, Samokhvalov IM, Merad M. Fate mapping analysis reveals that adult microglia derive from primitive macrophages. Science. (2010) 330(6005):841-5. doi: 10.1126/science.1194637

Ginhoux F, Lim S, Hoeffel G, Low D, Huber T. Origin and differentiation of microglia. Front Cell Neurosci. (2013) 7:45. doi: 10.3389/fncel.2013.00045

Ginhoux F, Prinz M. Origin of microglia: current concepts and past controversies. Cold Spring Harb Perspect Biol. (2015) 7(8):a020537. doi: 10.1101/cshperspect.a020537

Gitik M, Kleinhaus R, Hadas S, Reichert F, Rotshenker S. Phagocytic receptors activate and immune inhibitory receptor SIRPα inhibits phagocytosis through paxillin and cofilin. Front Cell Neurosci. (2014) 8:104. doi: 10.3389/fncel.2014.00104

Gitik M, Liraz-Zaltsman S, Oldenborg PA, Reichert F, Rotshenker S. Myelin down-regulates myelin phagocytosis by microglia and macrophages through interactions between CD47 on myelin and SIRPα (signal regulatory protein-α) on phagocytes. J Neuroinflammation. (2011) 8:24. doi: 10.1186/1742-2094-8-24

Gonzalez P, Burgaya F, Acarin L, Peluffo H, Castellano B, Gonzalez B. Interleukin-10 and interleukin-10 receptor-I are upregulated in glial cells after an excitotoxic injury to the postnatal rat brain. J Neuropathol Exp Neurol. (2009) 68(4):391-403. doi: 10.1097/NEN.0b013e31819dca30

Graeber MB, Bise K, Mehraein P. Synaptic stripping in the human facial nucleus. Acta Neuropathol. (1993) 86(2):179-81. doi: 10.1007/BF00334886

Graeber MB, Kreutzberg GW. Astrocytes increase in glial fibrillary acidic protein during retrograde changes of facial motor neurons. J Neurocytol. (1986) 15(3):363-73. doi: 10.1007/BF01611438

Graeber MB, Kreutzberg GW. Delayed astrocyte reaction following facial nerve axotomy. J Neurocytol. (1988) 17(2):209-20. doi: 10.1007/BF01674208.

Gravel M, Béland LC, Soucy G, Abdelhamid E, Rahimian R, Gravel C, Kriz J. IL-10 Controls Early Microglial Phenotypes and Disease Onset in ALS Caused by Misfolded Superoxide Dismutase 1. J Neurosci. (2016) 36(3):1031-48. doi: 10.1523/JNEUROSCI.0854-15.2016

Gruol DL. IL-6 regulation of synaptic function in the CNS. Neuropharmacology. (2015) 96(Pt A):42-54. doi: 10.1016/j.neuropharm.2014.10.023

Guan Z, Kuhn JA, Wang X, Colquitt B, Solorzano C, Vaman S, Guan AK, Evans-Reinsch Z, Braz J, Devor M, Abboud-Werner SL, Lanier LL, Lomvardas S, Basbaum AI. Injured sensory neuron-derived CSF1 induces microglial proliferation and DAP12-dependent pain. Nat. Neurosci. (2016) 19(1):94-101. doi: 10.1038/nn.4189

Hagemeyer N, Hanft KM, Akriditou MA, Unger N, Park ES, Stanley ER, Staszewski O, Dimou L, Prinz M. Microglia contribute to normal myelinogenesis and to oligodendrocyte progenitor maintenance during adulthood. Acta Neuropathol. (2017) 134(3):441-458. doi: 10.1007/s00401-017-1747-1

Hampel H, Haslinger A, Scheloske M, Padberg F, Fischer P, Unger J, Teipel SJ, Neumann M, Rosenberg C, Oshida R, Hulette C, Pongratz D, Ewers M, Kretzschmar HA, Möller HJ. Pattern of interleukin-6 receptor complex immunoreactivity between cortical regions of rapid autopsy normal and Alzheimer's disease brain. Eur Arch Psychiatry Clin Neurosci. (2005) 255(4):269-78. doi: 10.1007/s00406-004-0558-2

Han MH, Lundgren DH, Jaiswal S, Chao M, Graham KL, Garris CS, Axtell RC, Ho PP, Lock CB, Woodard JI, Brownell SE, Zoudilova M, Hunt JF, Baranzini SE, Butcher EC, Raine CS, Sobel RA, Han DK, Weissman I, Steinman L. Janus-like opposing roles of CD47 in autoimmune brain inflammation in humans and mice. J Exp Med. (2012) 209(7):1325-34. doi: 10.1084/jem.20101974

Hanisch UK. Microglia as a source and target of cytokines. Glia. (2002) 40(2):140-55. doi: 10.1002/glia.10161

Hanisch UK, Kettenmann H. Microglia: active sensor and versatile effector cells in the normal and pathologic brain. Nat Neurosci. (2007) 10(11):1387-94. doi: 10.1038/nn1997

Harrison JK, Jiang Y, Chen S, Xia Y, Maciejewski D, McNamara RK, Streit WJ, Salafranca MN, Adhikari S, Thompson DA, Botti P, Bacon KB, Feng L. Role for neuronally derived fractalkine in mediating interactions between neurons and CX3CR1-expressing microglia. Proc Natl Acad Sci U S A. (1998) 95(18):10896-901. doi: 10.1073/pnas.95.18.10896

Hashimoto D, Chow A, Noizat C, Teo P, Beasley MB, Leboeuf M, Becker CD, See P, Price J, Lucas D, Greter M, Mortha A, Boyer SW, Forsberg EC, Tanaka M, van Rooijen N, García-Sastre A, Stanley ER, Ginhoux F, Frenette PS, Merad M. Tissue-resident macrophages self-maintain locally throughout adult life with minimal contribution from circulating monocytes. Immunity. (2013) 38(4):792-804. doi: 10.1016/j.immuni.2013.04.004

Hatori K, Nagai A, Heisel R, Ryu JK, Kim SU. Fractalkine and fractalkine receptors in human neurons and glial cells. J Neurosci Res. (2002) 69(3):418-26. doi: 10.1002/jnr.10304

Hellenbrand DJ, Reichl KA, Travis BJ, Filipp ME, Khalil AS, Pulito DJ, Gavigan AV, Maginot ER, Arnold MT, Adler AG, Murphy WL, Hanna AS. Sustained interleukin-10 delivery reduces inflammation and improves motor function after spinal cord injury. J Neuroinflammation. (2019) 16(1):93. doi: 10.1186/s12974-019-1479-3

Hensley K, Floyd RA, Gordon B, Mou S, Pye QN, Stewart C, West M, Williamson K. Temporal patterns of cytokine and apoptosis-related gene expression in spinal cords of the G93A-SOD1 mouse model of amyotrophic lateral sclerosis. J Neurochem. (2002) 82(2):365-74. doi: 10.1046/j.1471-4159.2002.00968.x

Herber DL, Maloney JL, Roth LM, Freeman MJ, Morgan D, Gordon MN. Diverse microglial responses after intrahippocampal administration of lipopolysaccharide. Glia. (2006) 53(4):382-91. doi: 10.1002/glia.20272

Hernangómez M, Klusáková I, Joukal M, Hradilová-Svíženská I, Guaza C, Dubový P. CD200R1 agonist attenuates glial activation, inflammatory reactions, and hypersensitivity immediately after its intrathecal application in a rat neuropathic pain model. J Neuroinflammation. (2016) 13:43. doi: 10.1186/s12974-016-0508-8. PMID: 26891688; PMCID: PMC4759712.

Hickman SE, Kingery ND, Ohsumi TK, Borowsky ML, Wang LC, Means TK, El Khoury J. The microglial sensome revealed by direct RNA sequencing. Nat Neurosci. (2013) 16(12):1896-905. doi: 10.1038/nn.3554

Hoek RM, Ruuls SR, Murphy CA, Wright GJ, Goddard R, Zurawski SM, Blom B, Homola ME, Streit WJ, Brown MH, Barclay AN, Sedgwick JD. Down-regulation of the macrophage lineage through interaction with OX2 (CD200). Science. (2000) 290(5497):1768-71. doi: 10.1126/science.290.5497.1768

Hong S, Dissing-Olesen L, Stevens B. New insights on the role of microglia in synaptic pruning in health and disease. Curr Opin Neurobiol. (2016) 36:128-34. doi: 10.1016/j.conb.2015.12.004

Hopkins SJ, Rothwell NJ. Cytokines and the nervous system. I: Expression and recognition. Trends Neurosci. (1995) 18(2):83-8

Hoshiko M, Arnoux I, Avignone E, Yamamoto N, Audinat E. Deficiency of the microglial receptor CX3CR1 impairs postnatal functional development of thalamocortical synapses in the barrel cortex. J Neurosci. (2012) 32(43):15106-11. doi: 10.1523/JNEUROSCI.1167-12.2012

Hsieh CL, Koike M, Spusta SC, Niemi EC, Yenari M, Nakamura MC, Seaman WE. A role for TREM2 ligands in the phagocytosis of apoptotic neuronal cells by microglia. J Neurochem. (2009) 109(4):1144-56. doi: 10.1111/j.1471-4159.2009.06042.x

Hsieh CP, Chang WT, Lee YC, Huang AM. Deficits in cerebellar granule cell development and social interactions in CD47 knockout mice. Dev Neurobiol. (2015) 75(5):463-84. doi: 10.1002/dneu.22236

Hu X, Leak RK, Shi Y, Suenaga J, Gao Y, Zheng P, Chen J. Microglial and macrophage polarization—new prospects for brain repair. Nat Rev Neurol. (2015) 11(1):56-64. doi: 10.1038/nrneurol.2014.207

Huang Y, Liu Z, Cao BB, Qiu YH, Peng YP. Treg Cells Protect Dopaminergic Neurons against MPP+ Neurotoxicity via CD47-SIRPA Interaction. Cell Physiol Biochem. (2017) 41(3):1240-1254. doi: 10.1159/000464388

Huang AM, Wang HL, Tang YP, Lee EH. Expression of integrin-associated protein gene associated with memory formation in rats. J Neurosci. (1998) 18(11):4305-13. doi: 10.1523/JNEUROSCI.18-11-04305.1998

Hughes PM, Botham MS, Frentzel S, Mir A, Perry VH. Expression of fractalkine (CX3CL1) and its receptor, CX3CR1, during acute and chronic inflammation in the rodent CNS. Glia. (2002) 37(4):314-27

Hulshof S, van Haastert ES, Kuipers HF, van den Elsen PJ, De Groot CJ, van der Valk P, Ravid R, Biber K. CX3CL1 and CX3CR1 expression in human brain tissue: noninflammatory control versus multiple sclerosis. J Neuropathol Exp Neurol. (2003) 62(9):899-907. doi: 10.1093/jnen/62.9.899

Hulshof S, Montagne L, De Groot CJ, Van Der Valk P. Cellular localization and expression patterns of interleukin-10, interleukin-4, and their receptors in multiple sclerosis lesions. Glia. (2002) 38(1):24-35. doi: 10.1002/glia.10050

Hume DA, Perry VH, Gordon S. Immunohistochemical localization of a macrophage-specific antigen in developing mouse retina: phagocytosis of dying neurons and differentiation of microglial cells to form a regular array in the plexiform layers. J Cell Biol. (1983) 97(1):253-7. doi: 10.1083/jcb.97.1.253

Husemann J, Loike JD, Anankov R, Febbraio M, Silverstein SC. Scavenger receptors in neurobiology and neuropathology: their role on microglia and other cells of the nervous system. Glia. (2002) 40(2):195-205. doi: 10.1002/glia.10148

Hutter G, Theruvath J, Graef CM, Zhang M, Schoen MK, Manz EM, Bennett ML, Olson A, Azad TD, Sinha R, Chan C, Assad Kahn S, Gholamin S, Wilson C, Grant G, He J, Weissman IL, Mitra SS, Cheshier SH. Microglia are effector cells of CD47-SIRPα antiphagocytic axis disruption against glioblastoma. Proc Natl Acad Sci U S A. (2019) 116(3):997-1006. doi: 10.1073/pnas.1721434116

Ifuku M, Färber K, Okuno Y, Yamakawa Y, Miyamoto T, Nolte C, Merrino VF, Kita S, Iwamoto T, Komuro I, Wang B, Cheung G, Ishikawa E, Ooboshi H, Bader M, Wada K, Kettenmann H, Noda M. Bradykinin-induced microglial migration mediated by B1-bradykinin receptors depends on Ca2+ influx via reverse-mode activity of the Na+/Ca2+ exchanger. J Neurosci. (2007) 27(48):13065-73. doi: 10.1523/JNEUROSCI.3467-07.2007

Ikeda K, Iwasaki Y, Shiojima T, Kinoshita M. Neuroprotective effect of various cytokines on developing spinal motoneurons following axotomy. J Neurol Sci. (1996) 135(2):109-13. doi: 10.1016/0022-510x(95)00263-2

Imai T, Hieshima K, Haskell C, Baba M, Nagira M, Nishimura M, Kakizaki M, Takagi S, Nomiyama H, Schall TJ, Yoshie O. Identification and molecular characterization of fractalkine receptor CX3CR1, which mediates both leukocyte migration and adhesion. Cell. (1997) 91(4):521-30. doi: 10.1016/s0092-8674(00)80438-9

Inoue K, Morimoto H, Ohgidani M, Ueki T. Modulation of inflammatory responses by fractalkine signaling in microglia. PLoS One. (2021) 16(5):e0252118. doi: 10.1371/journal.pone.0252118

Iosif RE, Ekdahl CT, Ahlenius H, Pronk CJ, Bonde S, Kokaia Z, Jacobsen SE, Lindvall O. Tumor necrosis factor receptor 1 is a negative regulator of progenitor proliferation in adult hippocampal neurogenesis. J Neurosci. (2006) 26(38):9703-12. doi: 10.1523/JNEUROSCI.2723-06.2006

Jaiswal S, Jamieson CH, Pang WW, Park CY, Chao MP, Majeti R, Traver D, van Rooijen N, Weissman IL. CD47 is upregulated on circulating hematopoietic stem cells and leukemia cells to avoid phagocytosis. Cell. (2009) 138(2):271-85. doi: 10.1016/j.cell.2009.05.046

Jay TR, Hirsch AM, Broihier ML, Miller CM, Neilson LE, Ransohoff RM, Lamb BT, Landreth GE. Disease progression-dependent effects of TREM2 deficiency in a mouse model of Alzheimer’s disease. J. Neurosci. (2017) 37(3):637-647. doi: 10.1523/JNEUROSCI.2110-16.2016

Jay TR, Miller CM, Cheng PJ, Graham LC, Bemiller S, Broihier ML, Xu G, Margevicius D, Karlo JC, Sousa GL, Cotleur AC, Butovsky O, Bekris L, Staugaitis SM, Leverenz JB, Pimplikar SW, Landreth GE, Howell GR, Ransohoff RM, Lamb BT. TREM2 deficiency eliminates TREM2+ inflammatory macrophages and ameliorates pathology in Alzheimer's disease mouse models. J Exp Med. (2015) 212(3):287-95. doi: 10.1084/jem.20142322

Jay TR, von Saucken VE, Landreth GE. TREM2 in neurodegenerative diseases. Mol Neurodegener. (2017) 12(1):56. doi: 10.1186/s13024-017-0197-5

Jenmalm MC, Cherwinski H, Bowman EP, Phillips JH, Sedgwick JD. Regulation of myeloid cell function through the CD200 receptor. J Immunol. (2006) 176(1):191-9. doi: 10.4049/jimmunol.176.1.191

Jin G, Tsuji K, Xing C, Yang YG, Wang X, Lo EH. CD47 gene knockout protects against transient focal cerebral ischemia in mice. Exp Neurol. (2009) 217(1):165-70. doi: 10.1016/j.expneurol.2009.02.004

Johnston JB, Silva C, Gonzalez G, Holden J, Warren KG, Metz LM, Power C. Diminished adenosine A1 receptor expression on macrophages in brain and blood of patients with multiple sclerosis. Ann Neurol. (2001) 49(5):650-8

Jones LL, Kreutzberg GW, Raivich G. Regulation of CD44 in the Regenerating Mouse Facial Motor Nucleus. Eur J Neurosci. (1997) 9(9):1854-63. doi: 10.1111/j.1460-9568.1997.tb00752.x

Jones KJ, Serpe CJ, Byram SC, Deboy CA, Sanders VM. Role of the immune system in the maintenance of mouse facial motoneuron viability after nerve injury. Brain Behav Immun. (2005) 19(1):12-9. doi: 10.1016/j.bbi.2004.05.004

Joniec-Maciejak I, Ciesielska A, Wawer A, Sznejder-Pachołek A, Schwenkgrub J, Cudna A, Hadaczek P, Bankiewicz KS, Członkowska A, Członkowski A. The influence of AAV2-mediated gene transfer of human IL-10 on neurodegeneration and immune response in a murine model of Parkinson's disease. Pharmacol Rep. (2014) 66(4):660-9. doi: 10.1016/j.pharep.2014.03.008

Jonsson T, Stefansson H, Steinberg S, Jonsdottir I, Jonsson PV, Snaedal J, Bjornsson S, Huttenlocher J, Levey AI, Lah JJ, Rujescu D, Hampel H, Giegling I, Andreassen OA, Engedal K, Ulstein I, Djurovic S, Ibrahim-Verbaas C, Hofman A, Ikram MA, van Duijn CM, Thorsteinsdottir U, Kong A, Stefansson K. Variant of TREM2 associated with the risk of Alzheimer's disease. N Engl J Med. (2013) 368(2):107-16. doi: 10.1056/NEJMoa1211103

Jordan CA, Watkins BA, Kufta C, Dubois-Dalcq M. Infection of brain microglial cells by human immunodeficiency virus type 1 is CD4 dependent. J Virol. (1991) 65(2):736-42. doi: 10.1128/JVI.65.2.736-742.1991

Ju F, Ran Y, Zhu L, Cheng X, Gao H, Xi X, Yang Z, Zhang S. Increased BBB Permeability Enhances Activation of Microglia and Exacerbates Loss of Dendritic Spines After Transient Global Cerebral Ischemia. Front Cell Neurosci. (2018) 12:236. doi: 10.3389/fncel.2018.00236

Jung S, Aliberti J, Graemmel P, Sunshine MJ, Kreutzberg GW, Sher A, Littman DR. Analysis of fractalkine receptor CX(3)CR1 function by targeted deletion and green fluorescent protein reporter gene insertion. Mol Cell Biol. (2000)

Jurgens HA, Johnson RW. Environmental enrichment attenuates hippocampal neuroinflammation and improves cognitive function during influenza infection. Brain Behav Immun. (2012) 26(6):1006-16. doi: 10.1016/j.bbi.2012.05.015

Kalla R, Liu Z, Xu S, Koppius A, Imai Y, Kloss CU, Kohsaka S, Gschwendtner A, Möller JC, Werner A, Raivich G. Microglia and the early phase of immune surveillance in the axotomized facial motor nucleus: impaired microglial activation and lymphocyte recruitment but no effect on neuronal survival or axonal regeneration in macrophage-colony stimulating factor-deficient mice. J Comp Neurol. (2001) 436(2):182-201

Kamm K, Vanderkolk W, Lawrence C, Jonker M, Davis AT. The effect of traumatic brain injury upon the concentration and expression of interleukin-1beta and interleukin-10 in the rat. J Trauma. (2006) 60(1):152-7. doi: 10.1097/01.ta.0000196345.81169.a1

Karanfilian L, Tosto MG, Malki K. The role of TREM2 in Alzheimer’s disease; evidence from transgenic mouse models. Neurobiol Aging. (2020) 86:39-53. doi: 10.1016/j.neurobiolaging.2019.09.004

Kaur C, Ling EA, Wong WC. Origin and fate of neural macrophages in a stab wound of the brain of the young rat. J Anat. (1987) 154:215-27

Kennedy MK, Torrance DS, Picha KS, Mohler KM. Analysis of cytokine mRNA expression in the central nervous system of mice with experimental autoimmune encephalomyelitis reveals that IL-10 mRNA expression correlates with recovery. J Immunol. (1992) 149(7):2496-505

Keren-Shaul H, Spinrad A, Weiner A, Matcovitch-Natan O, Dvir-Szternfeld R, Ulland TK, David E, Baruch K, Lara-Astaiso D, Toth B, Itzkovitz S, Colonna M, Schwartz M, Amit I. A Unique Microglia Type Associated with Restricting Development of Alzheimer's Disease. Cell. (2017) 169(7):1276-1290.e17. doi: 10.1016/j.cell.2017.05.018

Kettenmann H, Hanisch UK, Noda M, Verkhratsky A. Physiology of microglia. Physiol Rev (2011) 91(2): 461-553. doi: 10.1152/physrev.00011.2010

Kettenmann H, Kirchhoff F, Verkhratsky A. Microglia: new roles for the synaptic stripper. Neuron. (2013) 77(1):10-8. doi: 10.1016/j.neuron.2012.12.023

Kierdorf K, Erny D, Goldmann T, Sander V, Schulz C, Perdiguero EG, Wieghofer P, Heinrich A, Riemke P, Hölscher C, Müller DN, Luckow B, Brocker T, Debowski K, Fritz G, Opdenakker G, Diefenbach A, Biber K, Heikenwalder M, Geissmann F, Rosenbauer F, Prinz M. Microglia emerge from erythromyeloid precursors via Pu.1- and Irf8-dependent pathways. Nat Neurosci. (2013) 16(3):273-80. doi: 10.1038/nn.3318

Kierdorf K, Prinz M. Factors regulating microglia activation. Front Cell Neurosci (2013) 7:44. doi: 10.3389/fncel.2013.00044.

Kierdorf K, Prinz M. Microglia in steady state. J Clin Invest. (2017) 127(9):3201-3209. doi: 10.1172/JCI90602

Kim YS, Joh TH. Microglia, major player in the brain inflammation: their roles in the pathogenesis of Parkinson's disease. Exp Mol Med. (2006) 38(4):333-47. doi: 10.1038/emm.2006.40

Kiyota T, Ingraham KL, Swan RJ, Jacobsen MT, Andrews SJ, Ikezu T. AAV serotype 2/1-mediated gene delivery of anti-inflammatory interleukin-10 enhances neurogenesis and cognitive function in APP+PS1 mice. Gene Ther. (2012) 19(7):724-33. doi: 10.1038/gt.2011.126

Kloss CU, Werner A, Klein MA, Shen J, Menuz K, Probst JC, Kreutzberg GW, Raivich G. Integrin family of cell adhesion molecules in the injured brain: regulation and cellular localization in the normal and regenerating mouse facial motor nucleus. J Comp Neurol. (1999) 411(1):162-78. doi: 10.1002/(sici)1096-9861(19990816)411:1<162::aid-cne12>3.0.co;2-w. PMID: 10404114

Ko YC, Chien HF, Jiang-Shieh YF, Chang CY, Pai MH, Huang JP, Chen HM, Wu CH. Endothelial CD200 is heterogeneously distributed, regulated and involved in immune cell-endothelium interactions. J Anat. (2009) 214(1):183-95. doi: 10.1111/j.1469-7580.2008.00986.x

Kobayashi M, Konishi H, Sayo A, Takai T, Kiyama H. TREM2/DAP12 signal elicits proinflammatory response in microglia and exacerbates neuropathic pain. J Neurosci. (2016) 36(43):11138-11150. doi: 10.1523/JNEUROSCI.1238-16.2016

Koenigsknecht J, Landreth G. Microglial phagocytosis of fibrillar beta-amyloid through a beta1 integrin-dependent mechanism. J Neurosci. (2004) 24(44):9838-46. doi: 10.1523/JNEUROSCI.2557-04.2004

Kojima Y, Volkmer JP, McKenna K, Civelek M, Lusis AJ, Miller CL, Direnzo D, Nanda V, Ye J, Connolly AJ, Schadt EE, Quertermous T, Betancur P, Maegdefessel L, Matic LP, Hedin U, Weissman IL, Leeper NJ. CD47-blocking antibodies restore phagocytosis and prevent atherosclerosis. Nature. (2016) 536(7614):86-90. doi: 10.1038/nature18935

Komiyama M, Shibata H, Suzuki T. Somatotopic representation of facial muscles within the facial nucleus of the mouse. A study using the retrograde horseradish peroxidase and cell degeneration techniques. Brain Behav Evol. (1984) 24(2-3):144-51. doi: 10.1159/000121312

Koning N, Bö L, Hoek RM, Huitinga I. Downregulation of macrophage inhibitory molecules in multiple sclerosis lesions. Ann Neurol. (2007) 62(5):504-14. doi: 10.1002/ana.21220

Koning N, Swaab DF, Hoek RM, Huitinga I. Distribution of the immune inhibitory molecules CD200 and CD200R in the normal central nervous system and multiple sclerosis lesions suggests neuron-glia and glia-glia interactions. J Neuropathol Exp Neurol. (2009) 68(2):159-67. doi: 10.1097/NEN.0b013e3181964113

Koo JW, Duman RS. IL-1beta is an essential mediator of the antineurogenic and anhedonic effects of stress. Proc Natl Acad Sci U S A. (2008) 105(2):751-6. doi: 10.1073/pnas.0708092105

Koshimizu H, Araki T, Takai S, Yokomaku D, Ishikawa Y, Kubota M, Sano S, Hatanaka H, Yamada M. Expression of CD47/integrin-associated protein induces death of cultured cerebral cortical neurons. J Neurochem. (2002) 82(2):249-57. doi: 10.1046/j.1471-4159.2002.00965.x

Kotter MR, Li WW, Zhao C, Franklin RJ. Myelin impairs CNS remyelination by inhibiting oligodendrocyte precursor cell differentiation. J Neurosci. (2006) 26(1):328-32. doi: 10.1523/JNEUROSCI.2615-05.2006

Krasemann S, Madore C, Cialic R, Baufeld C, Calcagno N, El Fatimy R, Beckers L, O'Loughlin E, Xu Y, Fanek Z, Greco DJ, Smith ST, Tweet G, Humulock Z, Zrzavy T, Conde-Sanroman P, Gacias M, Weng Z, Chen H, Tjon E, Mazaheri F, Hartmann K, Madi A, Ulrich JD, Glatzel M, Worthmann A, Heeren J, Budnik B, Lemere C, Ikezu T, Heppner FL, Litvak V, Holtzman DM, Lassmann H, Weiner HL, Ochando J, Haass C, Butovsky O. The TREM2-APOE Pathway Drives the Transcriptional Phenotype of Dysfunctional Microglia in Neurodegenerative Diseases. Immunity (2017) 47(3):566-581.e9. doi: 10.1016/j.immuni.2017.08.008

Kreutberg GW. Neurobiology of regeneration and degeneration. The Facial Nerve. Thieme, New York, 1986, pp. 75–83

Kreutzberg GW. Microglia: a sensor for pathological events in the CNS. Trens Neurosci. (1996) 19(8):312-8. doi: 10.1016/0166-2236(96)10049-7

Kubota Y, Takubo K, Shimizu T, Ohno H, Kishi K, Shibuya M, Saya H, Suda T. M-CSF inhibition selectively targets pathological angiogenesis and lymphangiogenesis. J Exp Med. (2009) 206(5):1089-102. doi: 10.1084/jem.20081605

Kwilasz AJ, Grace PM, Serbedzija P, Maier SF, Watkins LR. The therapeutic potential of interleukin-10 in neuroimmune diseases. Neuropharmacology. (2015) 96(Pt A):55-69. doi: 10.1016/j.neuropharm.2014.10.020

Lago N, Pannunzio B, Amo-Aparicio J, López-Vales R, Peluffo H. CD200 Modulates Spinal Cord Injury Neuroinflammation and Outcome Through CD200R1. Brain Behav Immun. (2018) 73:416-426

Lauro C, Catalano M, Trettel F, Mainiero F, Ciotti MT, Eusebi F, Limatola C. The chemokine CX3CL1 reduces migration and increases adhesion of neurons with mechanisms dependent on the beta1 integrin subunit. J Immunol. (2006) 177(11):7599-606. doi: 10.4049/jimmunol.177.11.7599

Laveti D, Kumar M, Hemalatha R, Sistla R, Naidu VG, Talla V, Verma V, Kaur N, Nagpal R. Anti-inflammatory treatments for chronic diseases: a review. Inflamm Allergy Drug Targets. (2013) 12(5):349-61. doi: 10.2174/18715281113129990053

Lawson LJ, Perry VH, Gordon S. Turnover of resident microglia in the normal adult mouse brain. Neuroscience (1992) 48(2):405-15. doi: 10.1016/0306-4522(92)90500-2

Lee E, Eo JC, Lee C, Yu JW. Distinct Features of Brain-Resident Macrophages: Microglia and Non-Parenchymal Brain Macrophages. Mol Cells. (2021) 44(5):281-291. doi: 10.14348/molcells.2021.0060

Lehnardt S. Innate immunity and neuroinflammation in the CNS: the role of microglia in Toll-like receptor-mediated neuronal injury. Glia. (2010) 58(3):253-63. doi: 10.1002/glia.20928

Lehrman EK, Wilton DK, Litvina EY, Welsh CA, Chang ST, Frouin A, Walker AJ, Heller MD, Umemori H, Chen C, Stevens B. CD47 Protects Synapses from Excess Microglia-Mediated Pruning during Development. Neuron. (2018) 100(1):120-134.e6. doi: 10.1016/j.neuron.2018.09.017

Lenz KM, Nelson LH. Microglia and Beyond: Innate Immune Cells As Regulators of Brain Development and Behavioral Function. Front Immunol. (2018) 9:698. doi: 10.3389/fimmu.2018.00698

Li G, Keenan A, Daskiran M, Mathews M, Nuamah I, Orman C, Joshi K, Singh A, Godet A, Pungor K, Gopal S. Relapse and Treatment Adherence in Patients with Schizophrenia Switching from Paliperidone Palmitate Once-Monthly to Three-Monthly Formulation: A Retrospective Health Claims Database Analysis. Patient Prefer Adherence. (2021) 15:2239-2248. doi: 10.2147/PPA.S322880

Li Q, Cheng Z, Zhou L, Darmanis S, Neff NF, Okamoto J, Gulati G, Bennett ML, Sun LO, Clarke LE, Marschallinger J, Yu G, Quake SR, Wyss-Coray T, Barres BA. Developmental Heterogeneity of Microglia and Brain Myeloid Cells Revealed by Deep Single-Cell RNA Sequencing. Neuron. (2019) 101(2):207-223.e10. doi: 10.1016/j.neuron.2018.12.006

Li Q, Barres BA. Microglia and macrophages in brain homeostasis and disease. Nat Rev Immunol. (2018) 18(4):225-242. doi: 10.1038/nri.2017.125

Li W. Eat-me signals: keys to molecular phagocyte biology and "appetite" control. J Cell Physiol. (2012) 227(4):1291-7. doi: 10.1002/jcp.22815

Licastro F, Mallory M, Hansen LA, Masliah E. Increased levels of alpha-1-antichymotrypsin in brains of patients with Alzheimer's disease correlate with activated astrocytes and are affected by APOE 4 genotype. J Neuroimmunol. (1998) 88(1-2):105-10. doi: 10.1016/s0165-5728(98)00096-4

Lim SH, Park E, You B, Jung Y, Park AR, Park SG, Lee JR. Neuronal synapse formation induced by microglia and interleukin 10. PLoS One. (2013) 8(11):e81218. doi: 10.1371/journal.pone.0081218

Ling EA. Monocytic origin of ramified microglia in the corpus callosum in postnatal rat. Neuropathol Appl Neurobiol. (1994) 20(2):182-3

Linnartz B, Neumann H. Microglial activatory (immunoreceptor tyrosine-based activation motif)- and inhibitory (immunoreceptor tyrosine-based inhibition motif)-signaling receptors for recognition of the neuronal glycocalyx. Glia. (2013) 61(1):37-46. doi: 10.1002/glia.22359

Liu GJ, Nagarajah R, Banati RB, Bennett MR. Glutamate induces directed chemotaxis of microglia. Eur J Neurosci. (2009) 29(6):1108-18. doi: 10.1111/j.1460-9568.2009.06659.x

Lively S, Schlichter LC. Microglia Responses to Pro-inflammatory Stimuli (LPS, IFNγ+TNFα) and Reprogramming by Resolving Cytokines (IL-4, IL-10). Front Cell Neurosci. (2018) 12:215. doi: 10.3389/fncel.2018.00215

Lobo-Silva D, Carriche GM, Castro AG, Roque S, Saraiva M. Balancing the immune response in the brain: IL-10 and its regulation. J Neuroinflammation. (2016) 13(1):297. doi: 10.1186/s12974-016-0763-8

Loddick SA, Turnbull AV, Rothwell NJ. Cerebral interleukin-6 is neuroprotective during permanent focal cerebral ischemia in the rat. J Cereb Blood Flow Metab. (1998) 18(2):176-9. doi: 10.1097/00004647-199802000-00008

Lull ME, Block ML. Microglial activation and chronic neurodegeneration. Neurotherapeutics. (2010) 7(4):354-65. doi: 10.1016/j.nurt.2010.05.014

Lund H, Pieber M, Parsa R, Han J, Grommisch D, Ewing E, Kular L, Needhamsen M, Espinosa A, Nilsson E, Överby AK, Butovsky O, Jagodic M, Zhang XM, Harris RA. Competitive repopulation of an empty microglial niche yields functionally distinct subsets of microglia-like cells. Nat Commun. (2018) 9(1):4845. doi: 10.1038/s41467-018-07295-7

Luo XG, Zhang JJ, Zhang CD, Liu R, Zheng L, Wang XJ, Chen SD, Ding JQ. Altered regulation of CD200 receptor in monocyte-derived macrophages from individuals with Parkinson's disease. Neurochem Res. (2010) 35(4):540-7. doi: 10.1007/s11064-009-0094-6

Lyons A, Downer EJ, Costello DA, Murphy N, Lynch MA. Dok2 mediates the CD200Fc attenuation of Aβ-induced changes in glia. J Neuroinflammation. (2012) 9:107. doi: 10.1186/1742-2094-9-107

Lyons A, Lynch AM, Downer EJ, Hanley R, O'Sullivan JB, Smith A, Lynch MA. Fractalkine-induced activation of the phosphatidylinositol-3 kinase pathway attenuates microglial activation in vivo and in vitro. J Neurochem. (2009) 110(5):1547-56. doi: 10.1111/j.1471-4159.2009.06253.x

Lyons A, Minogue AM, Jones RS, Fitzpatrick O, Noonan J, Campbell VA, Lynch MA. Analysis of the Impact of CD200 on Phagocytosis. Mol Neurobiol. (2017) 54(7):5730-5739. doi: 10.1007/s12035-016-0223-6

Maciejewski-Lenoir D, Chen S, Feng L, Maki R, Bacon KB. Characterization of fractalkine in rat brain cells: migratory and activation signals for CX3CR-1-expressing microglia. J Immunol. (1999) 163(3):1628-35

Majeti R, Chao MP, Alizadeh AA, Pang WW, Jaiswal S, Gibbs KD Jr, van Rooijen N, Weissman IL. CD47 is an adverse prognostic factor and therapeutic antibody target on human acute myeloid leukemia stem cells. Cell. (2009) 138(2):286-99. doi: 10.1016/j.cell.2009.05.045

Makwana M, Werner A, Acosta-Saltos A, Gonitel R, Pararajasingam A, Ruff C, Rumajogee P, Cuthill D, Galiano M, Bohatschek M, Wallace AS, Anderson PN, Mayer U, Behrens A, Raivich G. Peripheral facial nerve axotomy in mice causes sprouting of motor axons into perineuronal central white matter: time course and molecular characterization. J Comp Neurol. (2010) 518(5):699-721. doi: 10.1002/cne.22240

Mallat M, Chamak B. Brain macrophages: neurotoxic or neurotrophic effector cells? J Leukoc Biol. (1994) 56(3):416-22. doi: 10.1002/jlb.56.3.416

Malm TM, Jay TR, Landreth GE. The evolving biology of microglia in Alzheimer's disease. Neurotherapeutics. (2015) 12(1):81-93. doi: 10.1007/s13311-014-0316-8

Malmeström C, Andersson BA, Haghighi S, Lycke J. IL-6 and CCL2 levels in CSF are associated with the clinical course of MS: implications for their possible immunopathogenic roles. J Neuroimmunol. (2006) 175(1-2):176-82. doi: 10.1016/j.jneuroim.2006.03.004

Manich G, Gómez-López AR, Almolda B, Villacampa N, Recasens M, Shrivastava K, González B, Castellano B. Differential Roles of TREM2+ Microglia in Anterograde and Retrograde Axonal Injury Models. Front Cell Neurosci. (2020) 14:567404. doi: 10.3389/fncel.2020.567404

Manich G, Recasens M, Valente T, Almolda B, González B, Castellano B. Role of the CD200-CD200R Axis During Homeostasis and Neuroinflammation. Neuroscience. (2019) 405:118-136. doi: 10.1016/j.neuroscience.2018.10.030

Marín-Teva JL, Cuadros MA, Martín-Oliva D, Navascués J. Microglia and neuronal cell death. Neuron Glia Biol. (2011) 7(1):25-40. doi: 10.1017/S1740925X12000014

Marín-Teva JL, Dusart I, Colin C, Gervais A, van Rooijen N, Mallat M. Microglia promote the death of developing Purkinje cells. Neuron. (2004) 41(4):535-47. doi: 10.1016/s0896-6273(04)00069-8

Martinez FO, Gordon S. The M1 and M2 paradigm of macrophage activation: time for reassessment. F1000Prime Rep. (2014) 6:13. doi: 10.12703/P6-13

Matcovitch-Natan O, Winter DR, Giladi A, Vargas Aguilar S, Spinrad A, Sarrazin S, Ben-Yehuda H, David E, Zelada González F, Perrin P, Keren-Shaul H, Gury M, Lara-Astaiso D, Thaiss CA, Cohen M, Bahar Halpern K, Baruch K, Deczkowska A, Lorenzo-Vivas E, Itzkovitz S, Elinav E, Sieweke MH, Schwartz M, Amit I. Microglia development follows a stepwise program to regulate brain homeostasis. Science. (2016) 353(6301):aad8670. doi: 10.1126/science.aad8670

Matozaki T, Murata Y, Okazawa H, Ohnishi H. Functions and molecular mechanisms of the CD47-SIRPalpha signalling pathway. Trends Cell Biol. (2009) 19(2):72-80. doi: 10.1016/j.tcb.2008.12.001

Matzinger P. Friendly and dangerous signals: is the tissue in control?. Nat Immunol. (2007) 8(1):11-3. doi: 10.1038/ni0107-11

McGeer PL, McGeer EG. Inflammatory processes in amyotrophic lateral sclerosis. Muscle Nerve. (2002) 26(4):459-70. doi: 10.1002/mus.10191

Mecca C, Giambanco I, Donato R, Arcuri C. Microglia and Aging: The Role of the TREM2-DAP12 and CX3CL1-CX3CR1 Axes. Int J Mol Sci. (2018) 19(1):318. doi: 10.3390/ijms19010318

Mecha M, Carrillo-Salinas FJ, Mestre L, Feliú A, Guaza C. Viral models of multiple sclerosis: neurodegeneration and demyelination in mice infected with Theiler's virus. Prog Neurobiol. (2013) 101-102:46-64. doi: 10.1016/j.pneurobio.2012.11.003

Meilandt WJ, Ngu H, Gogineni A, Lalehzadeh G, Lee SH, Srinivasan K, Imperio J, Wu T, Weber M, Kruse AJ, Stark KL, Chan P, Kwong M, Modrusan Z, Friedman BA, Elstrott J, Foreman O, Easton A, Sheng M, Hansen DV. Trem2 deletion reduces late-stage amyloid plaque accumulation, elevates the Aβ42:Aβ40 ratio, and exacerbates axonal dystrophy and dendritic spine loss in the PS2APP Alzheimer's mouse model. J Neurosci. (2020) 40(9):1956-1974. doi: 10.1523/JNEUROSCI.1871-19.2019

Menassa DA, Gomez-Nicola D. Microglial Dynamics During Human Brain Development. Front Immunol. (2018) 9:1014. doi: 10.3389/fimmu.2018.01014

Mesnard NA, Alexander TD, Sanders VM, Jones KJ. Use of laser microdissection in the investigation of facial motoneuron and neuropil molecular phenotypes after peripheral axotomy. Exp Neurol. (2010) 225(1):94-103. doi: 10.1016/j.expneurol.2010.05.019

Meucci O, Fatatis A, Simen AA, Miller RJ. Expression of CX3CR1 chemokine receptors on neurons and their role in neuronal survival. Proc Natl Acad Sci U S A. (2000) 97(14):8075-80. doi: 10.1073/pnas.090017497

Meuth SG, Simon OJ, Grimm A, Melzer N, Herrmann AM, Spitzer P, Landgraf P, Wiendl H. CNS inflammation and neuronal degeneration is aggravated by impaired CD200-CD200R-mediated macrophage silencing. J Neuroimmunol. (2008) 194(1-2):62-9. doi: 10.1016/j.jneuroim.2007.11.013.

Mildner A, Schmidt H, Nitsche M, Merkler D, Hanisch UK, Mack M, Heikenwalder M, Brück W, Priller J, Prinz M. Microglia in the adult brain arise from Ly-6ChiCCR2+ monocytes only under defined host conditions. Nat Neurosci. (2007) 10(12):1544-53. doi: 10.1038/nn2015

Minagar A, Shapshak P, Fujimura R, Ownby R, Heyes M, Eisdorfer C. The role of macrophage/microglia and astrocytes in the pathogenesis of three neurologic disorders: HIV-associated dementia, Alzheimer disease, and multiple sclerosis. J Neurol Sci. (2002) 202(1-2):13-23. doi: 10.1016/s0022-510x(02)00207-1

Ming GL, Song H. Adult neurogenesis in the mammalian brain: significant answers and significant questions. Neuron. (2011) 70(4):687-702. doi: 10.1016/j.neuron.2011.05.001

Miron VE. Microglia-driven regulation of oligodendrocyte lineage cells, myelination, and remyelination. J Leukoc Biol. (2017) 101(5):1103-1108. doi: 10.1189/jlb.3RI1116-494R

Miron VE, Boyd A, Zhao JW, Yuen TJ, Ruckh JM, Shadrach JL, van Wijngaarden P, Wagers AJ, Williams A, Franklin RJM, Ffrench-Constant C. M2 microglia and macrophages drive oligodendrocyte differentiation during CNS remyelination. Nat Neurosci. (2013) 16(9):1211-1218. doi: 10.1038/nn.3469

Miyamoto A, Wake H, Ishikawa AW, Eto K, Shibata K, Murakoshi H, Koizumi S, Moorhouse AJ, Yoshimura Y, Nabekura J. Microglia contact induces synapse formation in developing somatosensory cortex. Nat Commun. (2016) 7:12540. doi: 10.1038/ncomms12540

Miyashita M, Ohnishi H, Okazawa H, Tomonaga H, Hayashi A, Fujimoto TT, Furuya N, Matozaki T. Promotion of neurite and filopodium formation by CD47: roles of integrins, Rac, and Cdc42. Mol Biol Cell. (2004) 15(8):3950-63. doi: 10.1091/mbc.e04-01-0019

Mizuno T, Sawada M, Marunouchi T, Suzumura A. Production of interleukin-10 by mouse glial cells in culture. Biochem Biophys Res Commun. (1994) 205(3):1907-15. doi: 10.1006/bbrc.1994.2893

Möller JC, Klein MA, Haas S, Jones LL, Kreutzberg GW, Raivich G. Regulation of thrombospondin in the regenerating mouse facial motor nucleus. Glia. (1996) 17(2):121-32. doi: 10.1002/(SICI)1098-1136(199606)17:2<121::AID-GLIA4>3.0.CO;2-5.PMID: 8776579

Monje ML, Toda H, Palmer TD. Inflammatory blockade restores adult hippocampal neurogénesis. Science. (2003) 302(5651):1760-5. doi: 10.1126/science.1088417

Moran LB, Graeber MB. The facial nerve axotomy model. Brain Res Brain Res Rev. (2004) 44(2-3):154-78. doi: 10.1016/j.brainresrev.2003.11.004.

Mosser CA, Baptista S, Arnoux I, Audinat E. Microglia in CNS development: Shaping the brain for the future. Prog Neurobiol. (2017) 149-150:1-20. doi: 10.1016/j.pneurobio.2017.01.002

Mott RT, Ait-Ghezala G, Town T, Mori T, Vendrame M, Zeng J, Ehrhart J, Mullan M, Tan J. Neuronal expression of CD22: novel mechanism for inhibiting microglial proinflammatory cytokine production. Glia. (2004) 46(4):369-79. doi: 10.1002/glia.20009

Mukaino M, Nakamura M, Yamada O, Okada S, Morikawa S, Renault-Mihara F, Iwanami A, Ikegami T, Ohsugi Y, Tsuji O, Katoh H, Matsuzaki Y, Toyama Y, Liu M, Okano H. Anti-IL-6-receptor antibody promotes repair of spinal cord injury by inducing microglia-dominant inflammation. Exp Neurol. (2010) 224(2):403-14. doi: 10.1016/j.expneurol.2010.04.020

Müller N. The role of anti-inflammatory treatment in psychiatric disorders. Psychiatr Danub. (2013) 25(3):292-8

Müller T, Blum-Degen D, Przuntek H, Kuhn W. Interleukin-6 levels in cerebrospinal fluid inversely correlate to severity of Parkinson's disease. Acta Neurol Scand. (1998) 98(2):142-4. doi: 10.1111/j.1600-0404.1998.tb01736.x

Murabe Y, Sano Y. Morphological studies on neuroglia. VII. Distribution of "brain macrophages" in brains of neonatal and adult rats, as determined by means of immunohistochemistry. Cell Tissue Res. (1983) 229(1):85-95. doi: 10.1007/BF00217882

Murata T, Ohnishi H, Okazawa H, Murata Y, Kusakari S, Hayashi Y, Miyashita M, Itoh H, Oldenborg PA, Furuya N, Matozaki T. CD47 promotes neuronal development through Src- and FRG/Vav2-mediated activation of Rac and Cdc42. J Neurosci. (2006) 26(48):12397-407. doi: 10.1523/JNEUROSCI.3981-06.2006

Murphy PG, Borthwick LS, Johnston RS, Kuchel G, Richardson PM. Nature of the retrograde signal from injured nerves that induces interleukin-6 mRNA in neurons. J Neurosci. (1999) 19(10):3791-800. doi: 10.1523/JNEUROSCI.19-10-03791.1999

Myers SA, DeVries WH, Andres KR, Gruenthal MJ, Benton RL, Hoying JB, Hagg T, Whittemore SR. CD47 knockout mice exhibit improved recovery from spinal cord injury. Neurobiol Dis. (2011) 42(1):21-34. doi: 10.1016/j.nbd.2010.12.010

Nagatsu T, Sawada M. Biochemistry of postmortem brains in Parkinson's disease: historical overview and future prospects. J Neural Transm Suppl. (2007) (72):113-20. doi: 10.1007/978-3-211-73574-9_14

Nakajima K, Kohsaka S. Microglia: activation and their significance in the central nervous system. J Biochem. (2001) 130(2):169-75. doi: 10.1093/oxfordjournals.jbchem.a002969

Nakamura Y. Regulating factors for microglial activation. Biol Pharm Bull. (2002) 25(8):945-53. doi: 10.1248/bpb.25.945

Napoli I, Neumann H. Microglial clearance function in health and disease. Neuroscience. (2009) 158(3):1030-8. doi: 10.1016/j.neuroscience.2008.06.046

Neher JJ, Neniskyte U, Zhao JW, Bal-Price A, Tolkovsky AM, Brown GC. Inhibition of microglial phagocytosis is sufficient to prevent inflammatory neuronal death. J Immunol. (2011) 186(8):4973-83. doi: 10.4049/jimmunol.1003600

Ngwa C, Liu F. CD200-CD200R signaling and diseases: a potential therapeutic target? Int J Physiol Pathophysiol Pharmacol. (2019) 11(6):297-309

Nimmerjahn A, Kirchhoff F, Helmchen F. Resting microglial cells are highly dynamic surveillants of brain parenchyma in vivo. Science. (2005) 308(5726):1314-8. doi: 10.1126/science.1110647

Nishiyori A, Minami M, Ohtani Y, Takami S, Yamamoto J, Kawaguchi N, Kume T, Akaike A, Satoh M. Localization of fractalkine and CX3CR1 mRNAs in rat brain: does fractalkine play a role in signaling from neuron to microglia?. FEBS Lett. (1998) 429(2):167-72. doi: 10.1016/s0014-5793(98)00583-3

Nolte C, Möller T, Walter T, Kettenmann H. Complement 5a controls motility of murine microglial cells in vitro via activation of an inhibitory G-protein and the rearrangement of the actin cytoskeleton. Neuroscience. (1996) 73(4):1091-107. doi: 10.1016/0306-4522(96)00106-6

Noto D, Takahashi K, Miyake S, Yamada M. In vitro differentiation of lineage-negative bone marrow cells into microglia-like cells. Eur. J. Neurosci. (2010) 31(7):1155-63. doi: 10.1111/j.1460-9568.2010.07152.x

Nugent AA, Lin K, van Lengerich B, Lianoglou S, Przybyla L, Davis SS, Llapashtica C, Wang J, Kim DJ, Xia D, Lucas A, Baskaran S, Haddick PCG, Lenser M, Earr TK, Shi J, Dugas JC, Andreone BJ, Logan T, Solanoy HO, Chen H, Srivastava A, Poda SB, Sanchez PE, Watts RJ, Sandmann T, Astarita G, Lewcock JW, Monroe KM, Di Paolo G. TREM2 Regulates Microglial Cholesterol Metabolism upon Chronic Phagocytic Challenge. Neuron. (2020) 105(5):837-854.e9. doi: 10.1016/j.neuron.2019.12.007

Obst J, Simon E, Mancuso R, Gomez-Nicola D. The Role of Microglia in Prion Diseases: A Paradigm of Functional Diversity. Front Aging Neurosci. (2017) 9:207. doi: 10.3389/fnagi.2017.00207

Ohnishi H, Kaneko Y, Okazawa H, Miyashita M, Sato R, Hayashi A, Tada K, Nagata S, Takahashi M, Matozaki T. Differential localization of Src homology 2 domain-containing protein tyrosine phosphatase substrate-1 and CD47 and its molecular mechanisms in cultured hippocampal neurons. J Neurosci. (2005) 25(10):2702-11. doi: 10.1523/JNEUROSCI.5173-04.2005

Okazawa H, Motegi S, Ohyama N, Ohnishi H, Tomizawa T, Kaneko Y, Oldenborg PA, Ishikawa O, Matozaki T. Negative regulation of phagocytosis in macrophages by the CD47-SHPS-1 system. J Immunol. (2005) 174(4):2004-11. doi: 10.4049/jimmunol.174.4.2004

O'Keefe TL, Williams GT, Batista FD, Neuberger MS. Deficiency in CD22, a B cell-specific inhibitory receptor, is sufficient to predispose to development of high affinity autoantibodies. J Exp Med. (1999) 189(8):1307-13. doi: 10.1084/jem.189.8.1307

Oldenborg PA, Gresham HD, Lindberg FP. CD47-signal regulatory protein alpha (SIRPalpha) regulates Fcgamma and complement receptor-mediated phagocytosis. J Exp Med. (2001) 193(7):855-62. doi: 10.1084/jem.193.7.855

Oldenborg PA, Zheleznyak A, Fang YF, Lagenaur CF, Gresham HD, Lindberg FP. Role of CD47 as a marker of self on red blood cells. Science. (2000) 288(5473):2051-4. doi: 10.1126/science.288.5473.2051

Olmstead DN, Mesnard-Hoaglin NA, Batka RJ, Haulcomb MM, Miller WM, Jones KJ. Facial nerve axotomy in mice: a model to study motoneuron response to injury. J Vis Exp. (2015) (96):e52382. doi: 10.3791/52382

Otero K, Shinohara M, Zhao H, Cella M, Gilfillan S, Colucci A, Faccio R, Ross FP, Teitelbaum SL, Takayanagi H, Colonna M. TREM2 and β-catenin regulate bone homeostasis by controlling the rate of osteoclastogenesis. J Immunol. (2012) 188(6):2612-21. doi: 10.4049/jimmunol.1102836

Paloneva J, Manninen T, Christman G, Hovanes K, Mandelin J, Adolfsson R, Bianchin M, Bird T, Miranda R, Salmaggi A, Tranebjaerg L, Konttinen Y, Peltonen L. Mutations in two genes encoding different subunits of a receptor signaling complex result in an identical disease phenotype. Am J Hum Genet. (2002) 71(3):656-62. doi: 10.1086/342259

Paolicelli RC, Bolasco G, Pagani F, Maggi L, Scianni M, Panzanelli P, Giustetto M, Ferreira TA, Guiducci E, Dumas L, Ragozzino D, Gross CT. Synaptic pruning by microglia is necessary for normal brain development. Science. (2011) 333(6048):1456-8. doi: 10.1126/science.1202529

Parkhurst CN, Yang G, Ninan I, Savas JN, Yates JR 3rd, Lafaille JJ, Hempstead BL, Littman DR, Gan WB. Microglia promote learning-dependent synapse formation through brain-derived neurotrophic factor. Cell. (2013) 155(7):1596-609. doi: 10.1016/j.cell.2013.11.030

Pawelec P, Ziemka-Nalecz M, Sypecka J, Zalewska T. The Impact of the CX3CL1/CX3CR1 Axis in Neurological Disorders. Cells. (2020) 9(10):2277. doi: 10.3390/cells9102277

Penberthy WT, Tsunoda I. The importance of NAD in multiple sclerosis. Curr Pharm Des. (2009) 15(1):64-99. doi: 10.2174/138161209787185751

Peng Q, Malhotra S, Torchia JA, Kerr WG, Coggeshall KM, Humphrey MB. TREM2- and DAP12-dependent activation of PI3K requires DAP10 and is inhibited by SHIP1. Sci Signal. (2010) 3(122):ra38. doi: 10.1126/scisignal.2000500

Penzes P, Cahill ME, Jones KA, VanLeeuwen JE, Woolfrey KM. Dendritic spine pathology in neuropsychiatric disorders. Nat Neurosci. (2011) 14(3):285-93. doi: 10.1038/nn.2741

Pereira CF, Middel J, Jansen G, Verhoef J, Nottet HS. Enhanced expression of fractalkine in HIV-1 associated dementia. J Neuroimmunol. (2001) 115(1-2):168-75. doi: 10.1016/s0165-5728(01)00262-4

Pérez-de Puig I, Miró F, Salas-Perdomo A, Bonfill-Teixidor E, Ferrer-Ferrer M, Márquez-Kisinousky L, Planas AM. IL-10 deficiency exacerbates the brain inflammatory response to permanent ischemia without preventing resolution of the lesion. J Cereb Blood Flow Metab. (2013) 33(12):1955-66. doi: 10.1038/jcbfm.2013.155

Perry VH, Cunningham C, Boche D. Atypical inflammation in the central nervous system in prion disease. Curr Opin Neurol. (2002) 15(3):349-54. doi: 10.1097/00019052-200206000-00020

Perry VH, Hume DA, Gordon S. Immunohistochemical localization of macrophages and microglia in the adult and developing mouse brain. Neuroscience. (1985) 15(2):313-26. doi: 10.1016/0306-4522(85)90215-5

Peruzzaro ST, Andrews MMM, Al-Gharaibeh A, Pupiec O, Resk M, Story D, Maiti P, Rossignol J, Dunbar GL. Transplantation of mesenchymal stem cells genetically engineered to overexpress interleukin-10 promotes alternative inflammatory response in rat model of traumatic brain injury. J Neuroinflammation. (2019) 16(1):2. doi: 10.1186/s12974-018-1383-2

Petitto JM, Huang Z, Lo J, Streit WJ. IL-2 gene knockout affects T lymphocyte trafficking and the microglial response to regenerating facial motor neurons. J Neuroimmunol. (2003) 134(1-2):95-103. doi: 10.1016/s0165-5728(02)00422-8

Petković F, Campbell IL, Gonzalez B, Castellano B. Astrocyte-targeted production of interleukin-6 reduces astroglial and microglial activation in the cuprizone demyelination model: Implications for myelin clearance and oligodendrocyte maturation. Glia. (2016) 64(12):2104-2119. doi: 10.1002/glia.23043.

Piccio L, Buonsanti C, Mariani M, Cella M, Gilfillan S, Cross AH, Colonna M, Panina-Bordignon P. Blockade of TREM-2 exacerbates experimental autoimmune encephalomyelitis. Eur J Immunol. (2007) 37(5):1290-301. doi: 10.1002/eji.200636837

Pluvinage JV, Haney MS, Smith BAH, Sun J, Iram T, Bonanno L, Li L, Lee DP, Morgens DW, Yang AC, Shuken SR, Gate D, Scott M, Khatri P, Luo J, Bertozzi CR, Bassik MC, Wyss-Coray T. CD22 blockade restores homeostatic microglial phagocytosis in ageing brains. Nature. (2019) 568(7751):187-192. doi: 10.1038/s41586-019-1088-4

Poliani PL, Wang Y, Fontana E, Robinette ML, Yamanishi Y, Gilfillan S, Colonna M. TREM2 sustains microglial expansion during aging and response to demyelination. J. Clin Invest. (2015) 125(5):2161-70. doi: 10.1172/JCI77983

Prada I, Ongania GN, Buonsanti C, Panina-Bordignon P, Meldolesi J. Triggering receptor expressed in myeloid cells 2 (TREM2) trafficking in microglial cells: continuous shuttling to and from the plasma membrane regulated by cell stimulation. Neuroscience. (2006) 140(4):1139-48. doi: 10.1016/j.neuroscience.2006.03.058

Prinz M, Mildner A. Microglia in the CNS: immigrants from another world. Glia. (2011) 59(2):177-87. doi: 10.1002/glia.21104

Prinz M, Priller J. Microglia and brain macrophages in the molecular age: from origin to neuropsychiatric disease. Nat Rev Neurosci. (2014) 15(5):300-12. doi: 10.1038/nrn3722

Puigdellívol M, Allendorf DH, Brown GC. (2020). Sialylation and Galectin-3 in microglia-mediated neuroinflammation and neurodegeneration. Front Cell Neurosci. (2020) 14:162. doi: 10.3389/fncel.2020.00162.

Qiu Z, Gruol DL. Interleukin-6, beta-amyloid peptide and NMDA interactions in rat cortical neurons. J Neuroimmunol. (2003) 139(1-2):51-7. doi: 10.1016/s0165-5728(03)00158-9

Ramírez G, Toro R, Döbeli H, von Bernhardi R. Protection of rat primary hippocampal cultures from A beta cytotoxicity by pro-inflammatory molecules is mediated by astrocytes. Neurobiol Dis. (2005) 19(1-2):243-54. doi: 10.1016/j.nbd.2005.01.007

Raivich G, Bohatschek M, Kloss CU, Werner A, Jones LL, Kreutzberg GW. Neuroglial activation repertoire in the injured brain: graded response, molecular mechanisms and cues to physiological function. Brain Res Brain Res Rev. (1999) 30(1):77-105. doi: 10.1016/s0165-0173(99)00007-7

Raivich G, Bohatschek M, Werner A, Jones LL, Galiano M, Kloss CU, Zhu XZ, Pfeffer K, Liu ZQ. Lymphocyte infiltration in the injured brain: role of proinflammatory cytokines. J Neurosci Res. (2003) 72(6):726-33. doi: 10.1002/jnr.10621

Raivich G, Jones LL, Kloss CU, Werner A, Neumann H, Kreutzberg GW. Immune surveillance in the injured nervous system: T-lymphocytes invade the axotomized mouse facial motor nucleus and aggregate around sites of neuronal degeneration. J Neurosci. (1998) 18(15):5804-16. doi: 10.1523/JNEUROSCI.18-15-05804.1998

Raivich G, Liu ZQ, Kloss CU, Labow M, Bluethmann H, Bohatschek M. Cytotoxic potential of proinflammatory cytokines: combined deletion of TNF receptors TNFR1 and TNFR2 prevents motoneuron cell death after facial axotomy in adult mouse. Exp Neurol. (2002) 178(2):186-93. doi: 10.1006/exnr.2002.8024

Raivich G, Moreno-Flores MT, Möller JC, Kreutzberg GW. Inhibition of posttraumatic microglial proliferation in a genetic model of macrophage colony-stimulating factor deficiency in the mouse. Eur J Neurosci. (1994) 6(10):1615-8. doi: 10.1111/j.1460-9568.1994.tb00552.x

Ramesh G, MacLean AG, Philipp MT. Cytokines and chemokines at the crossroads of neuroinflammation, neurodegeneration, and neuropathic pain. Mediators Inflamm. (2013) 2013:480739. doi: 10.1155/2013/480739

Ransohoff RM. A polarizing question: do M1 and M2 microglia exist? Nat Neurosci. (2016) 9(8):987-91. doi: 10.1038/nn.4338

Rappert A, Bechmann I, Pivneva T, Mahlo J, Biber K, Nolte C, Kovac AD, Gerard C, Boddeke HW, Nitsch R, Kettenmann H. CXCR3-dependent microglial recruitment is essential for dendrite loss after brain lesion. J Neurosci. (2004) 24(39):8500-9. doi: 10.1523/JNEUROSCI.2451-04.2004

Rayaprolu S, Mullen B, Baker M, Lynch T, Finger E, Seeley WW, Hatanpaa KJ, Lomen-Hoerth C, Kertesz A, Bigio EH, Lippa C, Josephs KA, Knopman DS, White CL 3rd, Caselli R, Mackenzie IR, Miller BL, Boczarska-Jedynak M, Opala G, Krygowska-Wajs A, Barcikowska M, Younkin SG, Petersen RC, Ertekin-Taner N, Uitti RJ, Meschia JF, Boylan KB, Boeve BF, Graff-Radford NR, Wszolek ZK, Dickson DW, Rademakers R, Ross OA. TREM2 in neurodegeneration: evidence for association of the p.R47H variant with frontotemporal dementia and Parkinson's disease. Mol Neurodegener. (2013) 8:19. doi: 10.1186/1750-1326-8-19

Recasens M. Chronic Overproduction of IL-6 and IL-10 modulates the Microglial Response after Anterograde Degeneration. (2021) [PhD Thesis] Universitat Autònoma de Barcelona

Recasens M, Almolda B, Pérez-Clausell J, Campbell IL, González B, Castellano B. Chronic exposure to IL-6 induces a desensitized phenotype of the microglia. J Neuroinflammation. (2021) 18(1):31. doi: 10.1186/s12974-020-02063-1

Recasens M, Shrivastava K, Almolda B, González B, Castellano B. Astrocyte-targeted IL-10 production decreases proliferation and induces a downregulation of activated microglia/macrophages after PPT. Glia. (2019) 67(4):741-758. doi: 10.1002/glia.23573

Rentzos M, Nikolaou C, Andreadou E, Paraskevas GP, Rombos A, Zoga M, Tsoutsou A, Boufidou F, Kapaki E, Vassilopoulos D. Circulating interleukin-10 and interleukin-12 in Parkinson's disease. Acta Neurol Scand. (2009) 119(5):332-7. doi: 10.1111/j.1600-0404.2008.01103.x

Rezaie P, Male D. Mesoglia & microglia--a historical review of the concept of mononuclear phagocytes within the central nervous system. J Hist Neurosci. (2002) 11(4):325-74. doi: 10.1076/jhin.11.4.325.8531

Richwine AF, Sparkman NL, Dilger RN, Buchanan JB, Johnson RW. Cognitive deficits in interleukin-10-deficient mice after peripheral injection of lipopolysaccharide. Brain Behav Immun. (2009) 23(6):794-802. doi: 10.1016/j.bbi.2009.02.020

Rigato C, Buckinx R, Le-Corronc H, Rigo JM, Legendre P. Pattern of invasion of the embryonic mouse spinal cord by microglial cells at the time of the onset of functional neuronal networks. Glia. (2011) 59(4):675-95. doi: 10.1002/glia.21140

Rivest S. The promise of anti-inflammatory therapies for CNS injuries and diseases. Expert Rev Neurother. (2011) 11(6):783-6. doi: 10.1586/ern.11.64

Rogers JT, Morganti JM, Bachstetter AD, Hudson CE, Peters MM, Grimmig BA, Weeber EJ, Bickford PC, Gemma C. CX3CR1 deficiency leads to impairment of hippocampal cognitive function and synaptic plasticity. J Neurosci. (2011) 31(45):16241-50. doi: 10.1523/JNEUROSCI.3667-11.2011

Rothaug M, Becker-Pauly C, Rose-John S. The role of interleukin-6 signaling in nervous tissue. Biochim Biophys Acta. (2016) 1863(6 Pt A):1218-27. doi: 10.1016/j.bbamcr.2016.03.01

Rymo SF, Gerhardt H, Wolfhagen Sand F, Lang R, Uv A, Betsholtz C. A two-way communication between microglial cells and angiogenic sprouts regulates angiogenesis in aortic ring cultures. PLoS One. (2011) 6(1):e15846. doi: 10.1371/journal.pone.0015846

Saber M, Kokiko-Cochran O, Puntambekar SS, Lathia JD, Lamb BT. Triggering receptor expressed on myeloid cells 2 deficiency alters acute macrophage distribution and improves recovery after traumatic brain injury. J Neurotrauma. (2017) 34(2):423-435. doi: 10.1089/neu.2016.4401

Saijo K, Glass CK. Microglial cell origin and phenotypes in health and disease. Nat Rev Immunol. (2011) 11(11):775-87. doi: 10.1038/nri3086

Salter MW, Beggs S. Sublime microglia: expanding roles for the guardians of the CNS. Cell. (2014) 158(1):15-24. doi: 10.1016/j.cell.2014.06.008

Salter MW, Stevens B. Microglia emerge as central players in brain disease. Nat Med. (2017) 23(9):1018-1027. doi: 10.1038/nm.4397

Samoilova EB, Horton JL, Chen Y. Acceleration of experimental autoimmune encephalomyelitis in interleukin-10-deficient mice: roles of interleukin-10 in disease progression and recovery. Cell Immunol. (1998) 188(2):118-24. doi: 10.1006/cimm.1998.1365

Sanchez-Molina P, Almolda B, Benseny-Cases N, González B, Perálvarez-Marín A, Castellano B. Specific microglial phagocytic phenotype and decrease of lipid oxidation in white matter areas during aging: Implications of different microenvironments. Neurobiol Aging. (2021) 105:280-295. doi: 10.1016/j.neurobiolaging.2021.03.015

Sapp E, Kegel KB, Aronin N, Hashikawa T, Uchiyama Y, Tohyama K, Bhide PG, Vonsattel JP, DiFiglia M. Early and progressive accumulation of reactive microglia in the Huntington disease brain. J Neuropathol Exp Neurol. (2001) 60(2):161-72. doi: 10.1093/jnen/60.2.161

Sato-Hashimoto M, Nozu T, Toriba R, Horikoshi A, Akaike M, Kawamoto K, Hirose A, Hayashi Y, Nagai H, Shimizu W, Saiki A, Ishikawa T, Elhanbly R, Kotani T, Murata Y, Saito Y, Naruse M, Shibasaki K, Oldenborg PA, Jung S, Matozaki T, Fukazawa Y, Ohnishi H. Microglial SIRPα regulates the emergence of CD11c$^+$ microglia and demyelination damage in white matter. Elife (2019) 8:e42025.doi: 10.7554/eLife.42025

Sawada M, Imamura K, Nagatsu T. Role of cytokines in inflammatory process in Parkinson's disease. J Neural Transm Suppl. (2006) (70):373-81. doi: 10.1007/978-3-211-45295-0_57

Sayed FA, Telpoukhovskaia M, Kodama L, Li Y, Zhou Y, Le D, Hauduc A, Ludwig C, Gao F, Clelland C, Zhan L, Cooper YA, Davalos D, Akassoglou K, Coppola G, Gan L. Differential effects of partial and complete loss of TREM2 on microglial injury response and tauopathy. Proc Natl Acad Sci U S A (2018) 115(40):10172-10177. doi: 10.1073/pnas.1811411115

Schafer DP, Lehrman EK, Kautzman AG, Koyama R, Mardinly AR, Yamasaki R, Ransohoff RM, Greenberg ME, Barres BA, Stevens B. Microglia sculpt postnatal neural circuits in an activity and complement-dependent manner. Neuron. (2012) 74(4):691-705. doi: 10.1016/j.neuron.2012.03.026

Schilling T, Stock C, Schwab A, Eder C. Functional importance of Ca2+-activated K+ channels for lysophosphatidic acid-induced microglial migration. Eur J Neurosci. (2004) 19(6):1469-74. doi: 10.1111/j.1460-9568.2004.03265.x

Schlachetzki JC, Hüll M. Microglial activation in Alzheimer's disease. Curr Alzheimer Res. (2009) 6(6):554-63. doi: 10.2174/156720509790147179

Schmid CD, Sautkulis LN, Danielson PE, Cooper J, Hasel KW, Hilbush BS, Sutcliffe JG, Carson MJ. Heterogeneous expression of the triggering receptor expressed on myeloid cells-2 on adult murine microglia. J. Neurochem. (2002) 83(6):1309-20. doi: 10.1046/j.1471-4159.2002.01243.x

Schwab A. Ion channels and transporters on the move. News Physiol Sci. (2001) 16:29-33. doi: 10.1152/physiologyonline.2001.16.1.29

Schwartz M. Macrophages and microglia in central nervous system injury: are they helpful or harmful? J Cereb Blood Flow Metab. (2003) 23(4):385-94. doi: 10.1097/01.WCB.0000061881.75234.5E

Scott-Hewitt N, Perrucci F, Morini R, Erreni M, Mahoney M, Witkowska A, Carey A, Faggiani E, Schuetz LT, Mason S, Tamborini M, Bizzotto M, Passoni L, Filipello F, Jahn R, Stevens B, Matteoli M. Local externalization of phosphatidylserine mediates developmental synaptic pruning by microglia. EMBO J. (2020) 39(16):e105380. doi: 10.15252/embj.2020105380.

Sedel F, Béchade C, Vyas S, Triller A. Macrophage-derived tumor necrosis factor alpha, an early developmental signal for motoneuron death. J Neurosci. (2004) 24(9):2236-46. doi: 10.1523/JNEUROSCI.4464-03.2004

Sedgwick JD, Ford AL, Foulcher E, Airriess R. Central nervous system microglial cell activation and proliferation follows direct interaction with tissue-infiltrating T cell blasts. J Immunol. (1998) 160(11):5320-30

Sekizawa T, Openshaw H, Ohbo K, Sugamura K, Itoyama Y, Niland JC. Cerebrospinal fluid interleukin 6 in amyotrophic lateral sclerosis: immunological parameter and comparison with inflammatory and non-inflammatory central nervous system diseases. J Neurol Sci. (1998) 154(2):194-9. doi: 10.1016/s0022-510x(97)00228-1

Sellner S, Paricio-Montesinos R, Spieß A, Masuch A, Erny D, Harsan LA, Elverfeldt DV, Schwabenland M, Biber K, Staszewski O, Lira S, Jung S, Prinz M, Blank T. Microglial CX3CR1 promotes adult neurogenesis by inhibiting Sirt 1/p65 signaling independent of CX3CL1. Acta Neuropathol Commun. (2016) 4(1):102. doi: 10.1186/s40478-016-0374-8

Semba K, Egger MD. The facial "motor" nerve of the rat: control of vibrissal movement and examination of motor and sensory components. J Comp Neurol. (1986) 247(2):144-58. doi: 10.1002/cne.902470203

Seo DR, Kim KY, Lee YB. Interleukin-10 expression in lipopolysaccharide-activated microglia is mediated by extracellular ATP in an autocrine fashion. Neuroreport. (2004) 15(7):1157-61. doi: 10.1097/00001756-200405190-00015

Serpe CJ, Coers S, Sanders VM, Jones KJ. CD4+ T, but not CD8+ or B, lymphocytes mediate facial motoneuron survival after facial nerve transection. Brain Behav Immun. (2003) 17(5):393-402. doi: 10.1016/s0889-1591(03)00028-x

Serpe CJ, Kohm AP, Huppenbauer CB, Sanders VM, Jones KJ. Exacerbation of facial motoneuron loss after facial nerve transection in severe combined immunodeficient (scid) mice. J Neurosci. (1999) 19(11):RC7. doi: 10.1523/JNEUROSCI.19-11-j0004.1999

Serpe CJ, Sanders VM, Jones KJ. Kinetics of facial motoneuron loss following facial nerve transection in severe combined immunodeficient mice. J Neurosci Res. (2000) 62(2):273-8. doi: 10.1002/1097-4547(20001015)62:2<273::AID-JNR11>3.0.CO;2-C

Sgroi D, Stamenkovic I. The B-cell adhesion molecule CD22 is cross-species reactive and recognizes distinct sialoglycoproteins on different functional T-cell sub-populations. Scand J Immunol. (1994) 39(5):433-8. doi: 10.1111/j.1365-3083.1994.tb03397.x

Shanaki M. Astrocyte-targeted production of IL-10 reduces the neuroinflammatory response associated to TBI and improves neurodegeneration (2020) [PhD Thesis]. Universitat Autònoma de Barcelona

Sheridan GK, Murphy KJ. Neuron-glia crosstalk in health and disease: fractalkine and CX3CR1 take centre stage Open Biol. (2013) 3(12):130181. doi: 10.1098/rsob.130181

Shigemoto-Mogami Y, Hoshikawa K, Goldman JE, Sekino Y, Sato K. Microglia enhance neurogenesis and oligodendrogenesis in the early postnatal subventricular zone. J Neurosci. (2014) 34(6):2231-43. doi: 10.1523/JNEUROSCI.1619-13.2014

Shrivastava K, Gonzalez P, Acarin L. The immune inhibitory complex CD200/CD200R is developmentally regulated in the mouse brain. J Comp Neurol. (2012) 520(12):2657-75. doi: 10.1002/cne.23062

Smith JA, Das A, Ray SK, Banik NL. Role of pro-inflammatory cytokines released from microglia in neurodegenerative diseases. Brain Res Bull. (2012) 87(1):10-20. doi: 10.1016/j.brainresbull.2011.10.004

Sperlágh B, Illes P. Purinergic modulation of microglial cell activation. Purinergic Signal. (2007) 3(1-2):117-27. doi: 10.1007/s11302-006-9043-x

Speth C, Dierich MP, Sopper S. HIV-infection of the central nervous system: the tightrope walk of innate immunity. Mol Immunol. (2005) 42(2):213-28. doi: 10.1016/j.molimm.2004.06.018

Speth C, Joebstl B, Barcova M, Dierich MP. HIV-1 envelope protein gp41 modulates expression of interleukin-10 and chemokine receptors on monocytes, astrocytes and neurones. AIDS. (2000) 14(6):629-36. doi: 10.1097/00002030-200004140-00001

Stamenkovic I, Seed B. The B-cell antigen CD22 mediates monocyte and erythrocyte adhesion. Nature. (1990) 345(6270):74-7. doi: 10.1038/345074a0

Stamenkovic I, Sgroi D, Aruffo A, SY MS, Anderson T. The B lymphocyte adhesion molecule CD22 interacts with leukocyte common antigen CD45RO on T cells and alpha 2-6 sialyltransferase, CD75, on B cells. Cell (1991). 66(6):1133-44. doi: 10.1016/0092-8674(91)90036-x

Stevens B, Allen NJ, Vazquez LE, Howell GR, Christopherson KS, Nouri N, Micheva KD, Mehalow AK, Huberman AD, Stafford B, Sher A, Litke AM, Lambris JD, Smith SJ, John SW, Barres BA. The classical complement cascade mediates CNS synapse elimination. Cell. (2007) 131(6):1164-78. doi: 10.1016/j.cell.2007.10.036

Stratoulias V, Venero JL, Tremblay MÈ, Joseph B. Microglial subtypes: diversity within the microglial community. EMBO J. (2019) 38(17):e101997. doi: 10.15252/embj.2019101997

Streit WJ, Kreutzberg GW. Response of endogenous glial cells to motor neuron degeneration induced by toxic ricin. J Comp Neurol. (1988) 268(2):248-63. doi: 10.1002/cne.902680209

Sun H, He X, Tao X, Hou T, Chen M, He M, Liao H. The CD200/CD200R signalling pathway contributes to spontaneous functional recovery by enhancing synaptic plasticity after stroke. J Neuroinflammation. (2020) 17(1):171. doi: 10.1186/s12974-020-01845-x

Swardfager W, Lanctôt K, Rothenburg L, Wong A, Cappell J, Herrmann N. A meta-analysis of cytokines in Alzheimer's disease. Biol Psychiatry. (2010) 68(10):930-41. doi: 10.1016/j.biopsych.2010.06.012

Swartz KR, Liu F, Sewell D, Schochet T, Campbell I, Sandor M, Fabry Z. Interleukin-6 promotes post-traumatic healing in the central nervous system. Brain Res. (2001) 896(1-2):86-95. doi: 10.1016/s0006-8993(01)02013-3

Szepesi Z, Manouchehrian O, Bachiller S, Deierborg T. Bidirectional Microglia-Neuron Communication in Health and Disease. Front Cell Neurosci. (2018) 12:323. doi: 10.3389/fncel.2018.00323

Takahashi K, Prinz M, Stagi M, Chechneva O, Neumann H. TREM2-transduced myeloid precursors mediate nervous tissue debris clearance and facilitate recovery in an animal model of multiple sclerosis. PLoS med. (2007) 4(4):e124. doi: 10.1371/journal.pmed.0040124

Takayama N, Ueda H. Morphine-induced chemotaxis and brain-derived neurotrophic factor expression in microglia. J Neurosci. (2005) 25(2):430-5. doi: 10.1523/JNEUROSCI.3170-04.2005

Tan J, Town T, Mori T, Wu Y, Saxe M, Crawford F, Mullan M. CD45 opposes beta-amyloid peptide-induced microglial activation via inhibition of p44/42 mitogen-activated protein kinase. J Neurosci. (2000) 20(20):7587-94. doi: 10.1523/JNEUROSCI.20-20-07587.2000

Tan J, Town T, Mullan M. CD45 inhibits CD40L-induced microglial activation via negative regulation of the Src/p44/42 MAPK pathway. J Biol Chem. (2000) 275(47):37224-31. doi: 10.1074/jbc.M002006200

Tan YL, Yuan Y, Tian L. Microglial regional heterogeneity and its role in the brain. Mol Psychiatry. (2020) 25(2):351-367. doi: 10.1038/s41380-019-0609-8

Tay TL, Sagar, Dautzenberg J, Grün D, Prinz M. Unique microglia recovery population revealed by single-cell RNAseq following neurodegeneration. Acta Neuropathol Commun. (2018) 6(1):87. doi: 10.1186/s40478-018-0584-3

Tay TL, Savage JC, Hui CW, Bisht K, Tremblay MÈ. Microglia across the lifespan: from origin to function in brain development, plasticity and cognition. J Physiol. (2017) 595(6):1929-1945. doi: 10.1113/JP272134

Tedder TF, Tuscano J, Sato S, Kehrl JH. CD22, a B lymphocyte-specific adhesion molecule that regulates antigen receptor signaling. Annu Rev Immunol. (1997) 15:481-504. doi: 10.1146/annurev.immunol.15.1.481

Tetzlaff W, Graeber MB, Bisby MA, Kreutzberg GW. Increased glial fibrillary acidic protein synthesis in astrocytes during retrograde reaction of the rat facial nucleus. Glia. (1988) 1(1):90-5. doi: 10.1002/glia.440010110

Toth AB, Terauchi A, Zhang LY, Johnson-Venkatesh EM, Larsen DJ, Sutton MA, Umemori H. Synapse maturation by activity-dependent ectodomain shedding of SIRPα. Nat Neurosci. (2013) 16(10):1417-25. doi: 10.1038/nn.3516

Ueno M, Fujita Y, Tanaka T, Nakamura Y, Kikuta J, Ishii M, Yamashita T. Layer V cortical neurons require microglial support for survival during postnatal development. Nat Neurosci. (2013) 16(5):543-51. doi: 10.1038/nn.3358

Ulland TK, Colonna M. TREM2 - a key player in microglial biology and Alzheimer disease. Nat Rev Neurol. (2018) 14(11):667-675. doi: 10.1038/s41582-018-0072-1

Ulland TK, Wang Y, Colonna M. Regulation of microglial survival and proliferation in health and diseases. Semin Immunol. (2015) 27(6):410-5. doi: 10.1016/j.smim.2016.03.011

Valente T, Serratosa J, Perpiñá U, Saura J, Solà C. Alterations in CD200-CD200R1 System during EAE Already Manifest at Presymptomatic Stages. Front Cell Neurosci. (2017) 11:129. doi: 10.3389/fncel.2017.00129

van Beek EM, Cochrane F, Barclay AN, van der Berg TK. Signal regulatory proteins in the immune system. J Immunol. (2005) 175(12):7781-7. doi: 10.4049/jimmunol.175.12.7781

van Wageningen TA, Vlaar E, Kooij G, Jongenelen CAM, Geurts JJG, van Dam AM. Regulation of microglial TMEM119 and P2RY12 immunoreactivity in multiple sclerosis white and grey matter lesions is dependent on their inflammatory environment. Acta Neuropathol Commun. (2019) 7(1):206. doi: 10.1186/s40478-019-0850-z.

Varnum MM, Kiyota T, Ingraham KL, Ikezu S, Ikezu T. The anti-inflammatory glycoprotein, CD200, restores neurogenesis and enhances amyloid phagocytosis in a mouse model of Alzheimer's disease. Neurobiol Aging. (2015) 36(11):2995-3007. doi: 10.1016/j.neurobiolaging.2015.07.027

Villacampa N. Effects of astrocyte-targeted production of IL-6 and IL-10 after facial nerve axotomy in the adult mouse. (2016) [PhD Thesis] Universitat Autònoma de Barcelona

Villacampa N, Almolda B, Vilella A, Campbell IL, González B, Castellano B. Astrocyte-targeted production of IL-10 induces changes in microglial reactivity and reduces motor neuron death after facial nerve axotomy. Glia. (2015) 63(7):1166-84. doi: 10.1002/glia.22807

von Bernhardi R. Glial cell dysregulation: a new perspective on Alzheimer disease. Neurotox Res. (2007) 12(4):215-32. doi: 10.1007/BF03033906

Wake H, Fields RD. Physiological Function of Microglia. Neuron Glia Biol. (2011) 7(1):1-3. doi: 10.1017/S1740925X12000166

Walker DG, Dalsing-Hernandez JE, Campbell NA, Lue LF. Decreased expression of CD200 and CD200 receptor in Alzheimer's disease: a potential mechanism leading to chronic inflammation. Exp Neurol. (2009) 215(1):5-19. doi: 10.1016/j.expneurol.2008.09.003

Walker DG, Tang TM, Mendsaikhan A, Tooyama I, Serrano GE, Sue LI, Beach TG, Lue LF. Patterns of Expression of Purinergic Receptor P2RY12, a Putative Marker for Non-Activated Microglia, in Aged and Alzheimer's Disease Brains. Int J Mol Sci. 2020 Jan 20;21(2):678. doi: 10.3390/ijms21020678

Walter L, Franklin A, Witting A, Wade C, Xie Y, Kunos G, Mackie K, Stella N. Nonpsychotropic cannabinoid receptors regulate microglial cell migration. J Neurosci. (2003) 23(4):1398-405. doi: 10.1523/JNEUROSCI.23-04-01398.2003

Wang Y, Cella M, Mallinson K, Ulrich JD, Young KL, Robinette ML, Gilfillan S, Krishnan GM, Sudhakar S, Zinselmeyer BH, Holtzman DM, Cirrito JR, Colonna M. TREM2 lipid sensing sustains the microglial response in an Alzheimer's disease model. Cell. (2015) 160(6):1061-71. doi: 10.1016/j.cell.2015.01.049

Wang J, Ding X, Wu X, Liu J, Zhou R, Wei P, Zhang Q, Zhang C, Zen K, Li L. SIRPα deficiency accelerates the pathologic process in models of Parkinson disease. Glia. (2019) 67(12):2343-2359. doi: 10.1002/glia.23689

Wang H, Fang F, Yi J, Xiang Z, Sun M, Jiang H. Establishment and assessment of the perinatal mouse facial nerve axotomy model via a subauricular incision approach. Exp Biol Med (Maywood). (2012) 237(11):1249-55. doi: 10.1258/ebm.2012.012134

Wang H, Newton G, Wu L, Lin LL, Miracco AS, Natesan S, Luscinskas FW. CD47 antibody blockade suppresses microglia-dependent phagocytosis and monocyte transition to macrophages, impairing recovery in EAE. JCI Insight. (2021) 6(21):e148719. doi: 10.1172/jci.insight.148719

Wang WY, Tan MS, Yu JT, Tan L. Role of pro-inflammatory cytokines released from microglia in Alzheimer's disease. Ann Transl Med. (2015b) 3(10):136. doi: 10.3978/j.issn.2305-5839.2015.03.49

Wang Y, Ulland TK, Ulrich JD, Song W, Tzaferis JA, Hole JT, Yuan P, Mahan TE, Shi Y, Gilfillan S, Cella M, Grutzendler J, DeMattos RB, Cirrito JR, Holtzman DM, Colonna M. TREM2-mediated early microglial response limits diffusion and toxicity of amyloid plaques. J Exp Med. (2016) 213(5):667-75. doi: 10.1084/jem.20151948

Wang XJ, Ye M, Zhang YH, Chen SD. CD200-CD200R regulation of microglia activation in the pathogenesis of Parkinson's disease. J Neuroimmune Pharmacol. (2007) 2(3):259-64. doi: 10.1007/s11481-007-9075-1

Werneburg S, Feinberg PA, Johnson KM, Schafer DP. A microglia-cytokine axis to modulate synaptic connectivity and function. Curr Opin Neurobiol. (2017) 47:138-145. doi: 10.1016/j.conb.2017.10.002

Werner A, Kloss CU, Walter J, Kreutzberg GW, Raivich G. Intercellular adhesion molecule-1 (ICAM-1) in the mouse facial motor nucleus after axonal injury and during regeneration. J Neurocytol. (1998) 27(4):219-32

Wilcock DM, Gordon MN, Ugen KE, Gottschall PE, DiCarlo G, Dickey C, Boyett KW, Jantzen PT, Connor KE, Melachrino J, Hardy J, Morgan D. Number of A*β* Inoculations in APP+PS1 Transgenic Mice Influences Antibody Titers, Microglial Activation, and Congophilic Plaque Levels. DNA Cell Biol. (2001) 20(11):731-6. doi: 10.1089/10445490152717596

Wlodarczyk A, Holtman IR, Krueger M, Yogev N, Bruttger J, Khorooshi R, Benmamar-Badel A, de Boer-Bergsma JJ, Martin NA, Karram K, Kramer I, Boddeke EW, Waisman A, Eggen BJ, Owens T. A novel microglial subset plays a key role in myelinogenesis in developing brain. EMBO J. (2017) 36(22):3292-3308. doi: 10.15252/embj.201696056

Wolf SA, Boddeke HW, Kettenmann H. Microglia in Physiology and Disease. Annu Rev Physiol. (2017) 79:619-643. doi: 10.1146/annurev-physiol-022516-034406

Wright GJ, Cherwinski H, Foster-Cuevas M, Brooke G, Puklavec MJ, Bigler M, Song Y, Jenmalm M, Gorman D, McClanahan T, Liu MR, Brown MH, Sedgwick JD, Phillips JH, Barclay AN. Characterization of the CD200 receptor family in mice and humans and their interactions with CD200. J Immunol. (2003) 171(6):3034-46. doi: 10.4049/jimmunol.171.6.3034

Wu R, Li X, Xu P, Huang L, Cheng J, Huang X, Jiang J, Wu LJ, Tang Y. TREM2 protects against cerebral ischemia/reperfusion injury. Mol Brain. (2017) 10(1):20. doi: 10.1186/s13041-017-0296-9

Xin J, Wainwright DA, Mesnard NA, Serpe CJ, Sanders VM, Jones KJ. IL-10 within the CNS is necessary for CD4+ T cells to mediate neuroprotection. Brain Behav Immun. (2011) 25(5):820-9. doi: 10.1016/j.bbi.2010.08.004

Xu Y, Jin MZ, Yang ZY, Jin WL. Microglia in neurodegenerative diseases. Neural Regen Res. (2021) 16(2):270-280. doi: 10.4103/1673-5374.290881

Yamasaki R, Lu H, Butovsky O, Ohno N, Rietsch AM, Cialic R, Wu PM, Doykan CE, Lin J, Cotleur AC, Kidd G, Zorlu MM, Sun N, Hu W, Liu L, Lee JC, Taylor SE, Uehlein L, Dixon D, Gu J, Floruta CM, Zhu M, Charo IF, Weiner HL, Ransohoff RM. Differential roles of microglia and monocytes in the inflamed central nervous system. J Exp Med. (2014) 211(8):1533-49. doi: 10.1084/jem.20132477

Yeh FL, Hansen DV, Sheng M. TREM2, Microglia, and Neurodegenerative Diseases. Trends Mol Med. (2017) 23(6):512-533. doi: 10.1016/j.molmed.2017.03.008

Yip PK, Carrillo-Jimenez A, King P, Vilalta A, Nomura K, Chau CC, Egerton AM, Liu ZH, Shetty AJ, Tremoleda JL, Davies M, Deierborg T, Priestley JV, Brown GC, Michael-Titus AT, Venero JL, Burguillos MA. Galectin-3 released in response to traumatic brain injury acts as an alarmin orchestrating brain immune response and promoting neurodegeneration. Sci Rep. (2017) 7:41689. doi: 10.1038/srep41689

Yuan P, Condello C, Keene CD, Wang Y, Bird TD, Paul SM, Luo W, Colonna M, Baddeley D, Grutzendler J. TREM2 Haplodeficiency in Mice and Humans Impairs the Microglia Barrier Function Leading to Decreased Amyloid Compaction and Severe Axonal Dystrophy. Neuron. (2016) 90(4):724-39. doi: 10.1016/j.neuron.2016.05.003

Zabel MK, Zhao L, Zhang Y, Gonzalez SR, Ma W, Wang X, Fariss RN, Wong WT. Microglial phagocytosis and activation underlying photoreceptor degeneration is regulated by CX3CL1-CX3CR1 signaling in a mouse model of retinitis pigmentosa. Glia. (2016) 64(9):1479-91. doi: 10.1002/glia.23016

Zhang S. Microglial activation after ischaemic stroke. Stroke Vasc Neurol. (2019) 4(2):71-74. doi: 10.1136/svn-2018-000196

Zhang S, Cherwinski H, Sedgwick JD, Phillips JH. Molecular mechanisms of CD200 inhibition of mast cell activation. J Immunol. (2004) 173(11):6786-93. doi: 10.4049/jimmunol.173.11.6786

Zhan L, Krabbe G, Du F, Jones I, Reichert MC, Telpoukhovskaia M, Kodama L, Wang C, Cho SH, Sayed F, Li Y, Le D, Zhou Y, Shen Y, West B, Gan L. Proximal recolonization by self-renewing microglia re-establishes microglial homeostasis in the adult mouse brain. PLoS Biol. (2019) 17(2):e3000134. doi: 10.1371/journal.pbio.3000134

Zhang H, Li F, Yang Y, Chen J, Hu X. SIRP/CD47 signaling in neurological disorders. Brain Res. (2015) 1623:74-80. doi: 10.1016/j.brainres.2015.03.012

Zhang M, Hutter G, Kahn SA, Azad TD, Gholamin S, Xu CY, Liu J, Achrol AS, Richard C, Sommerkamp P, Schoen MK, McCracken MN, Majeti R, Weissman I, Mitra SS, Cheshier SH. Anti-CD47 Treatment Stimulates Phagocytosis of Glioblastoma by M1 and M2 Polarized

Macrophages and Promotes M1 Polarized Macrophages In Vivo. PLoS One. (2016) 11(4):e0153550. doi: 10.1371/journal.pone.0153550

Zhang S, Wang XJ, Tian LP, Pan J, Lu GQ, Zhang YJ, Ding JQ, Chen SD. CD200-CD200R dysfunction exacerbates microglial activation and dopaminergic neurodegeneration in a rat model of Parkinson's disease. J Neuroinflammation. (2011) 8:154. doi: 10.1186/1742-2094-8-154

Zhang Y, Zhao L, Wang X, Ma W, Lazere A, Qian HH, Zhang J, Abu-Asab M, Fariss RN, Roger JE, Wong WT. Repopulating retinal microglia restore endogenous organization and function under CX3CL1-CX3CR1 regulation. Sci Adv. (2018) 4(3):eaap8492. doi: 10.1126/sciadv.aap8492

Zheng H, Jia L, Liu CC, Rong Z, Zhong L, Yang L, Chen XF, Fryer JD, Wang X, Zhang YW, Xu H, Bu G. TREM2 promotes microglial survival by activating Wnt/β-catenin pathway. J. Neurosci. (2017) 37(7):1772-1784. doi: 10.1523/JNEUROSCI.2459-16.2017

Zhong L, Chen XF, Wang T, Wang Z, Liao C, Wang Z, Huang R, Wang D, Li X, Wu L, Jia L, Zheng H, Painter M, Atagi Y, Liu CC, Zhang YW, Fryer JD, Xu H, Bu G. Soluble TREM2 induces inflammatory responses and enhances microglial survival. J Exp Med. (2017) 214(3):597-607. doi: 10.1084/jem.20160844

Zhong J, Dietzel ID, Wahle P, Kopf M, Heumann R. Sensory impairments and delayed regeneration of sensory axons in interleukin-6-deficient mice. J Neurosci. (1999) 19(11):4305-13. doi: 10.1523/JNEUROSCI.19-11-04305.1999

Zhong L, Xu Y, Zhuo R, Wang T, Wang K, Huang R, Wang D, Gao Y, Zhu Y, Sheng X, Chen K, Wang N, Zhu L, Can D, Marten Y, Shinohara M, Liu CC, Du D, Sun H, Wen L, Xu H, Bu G, Chen XF. Soluble TREM2 ameliorates pathological phenotypes by modulating microglial functions in an Alzheimer’s disease model. Nat Commun. (2019) 10(1):1365. doi: 10.1038/s41467-019-09118-9

Zhou Z, Peng X, Insolera R, Fink DJ, Mata M. IL-10 promotes neuronal survival following spinal cord injury. Exp Neurol. (2009) 220(1):183-90. doi: 10.1016/j.expneurol.2009.08.018

Zhou Y, Ulland TK, Colonna M. TREM2-Dependent Effects on Microglia in Alzheimer's Disease. Front Aging Neurosci. (2018) 10:202. doi: 10.3389/fnagi.2018.00202

Zhou X, Xie Q, Xi G, Keep RF, Hua Y. Brain CD47 expression in a swine model of intracerebral hemorrhage. Brain Res. (2014) 1574:70-6. doi: 10.1016/j.brainres.2014.06.003

Zhu Y, Hou H, Rezai-Zadeh K, Giunta B, Ruscin A, Gemma C, Jin J, Dragicevic N, Bradshaw P, Rasool S, Glabe CG, Ehrhart J, Bickford P, Mori T, Obregon D, Town T, Tan J. CD45 deficiency drives amyloid-β peptide oligomers and neuronal loss in Alzheimer's disease mice. J Neurosci. (2011) 31(4):1355-65. doi: 10.1523/JNEUROSCI.3268-10.2011

VII. ANNEXES

ANNEX 1

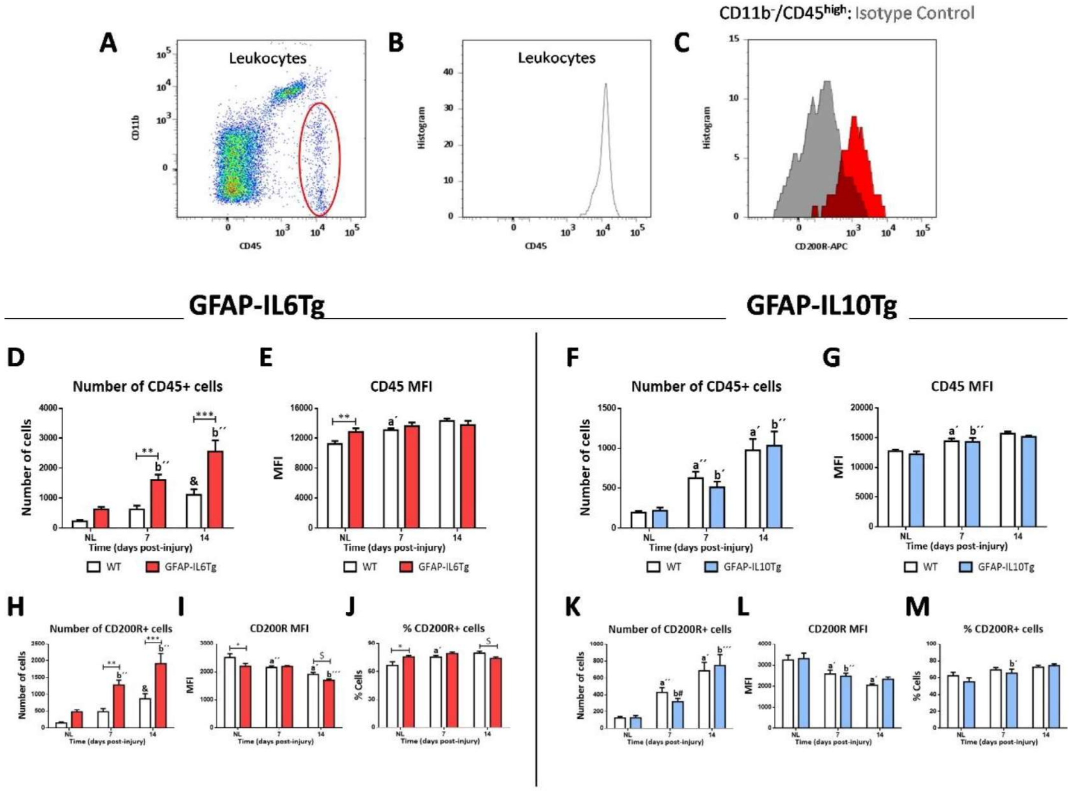

Supplementary Figure 1. Flow cytometry analysis of leukocyte "Off" population. (A) Representative dot-plot of CD11b/CD45 expression in cells obtained from a pool of 3 NL WT FN. The population surrounded by a red circle is what was considered as leukocytes. **(B)** Representative histogram showing leukocyte population identified as CD11b$^-$/CD45$^+$. **(C)** Representative histogram-plot showing the expression of CD200R in the leukocyte population compared to the corresponding isotype control. **(D-E)** Histograms showing the total number of leukocyte cells expressing CD45 (D) and CD45 MFI (E) in basal conditions and at 7 and 14dpi in both WT and GFAP-IL6Tg mice. **(H-I)** Histograms showing the total number (H), MFI (I) and percentage of leukocytes cells (J) expressing CD200R in basal conditions and at 7 and 14dpi from WT and GFAP-IL6Tg. **(F-G)** Histograms showing the total number of leukocyte cells expressing CD45 (F) and CD45 MFI (G) in basal conditions and at 7 and 14dpi in both WT and GFAP-IL10Tg mice. **(K-M)** Histograms showing the total number (K), MFI (L) and percentage (M) of leukocytes cells expressing CD200R in basal conditions and at 7 and 14dpi from WT and GFAP-IL10Tg. Data are represented as ± SEM. Significances are represented as: WT vs. GFAP-IL6Tg (***p≤0.001; **p≤0.01; *p≤0.05, $p≤0.1); in WT animals, a (´´p≤0.01; ´p≤0.05): indicates differences vs. the previous time-point, and & (p≤0.05): indicates significance vs. NL ; in GFAP-IL6Tg or GFAP-IL10Tg animals, b (´´´p≤0.001; ´´p≤0.01; ´p≤0.05; #p≤0.1): indicates significance vs. the previous time-point.

ANNEX 2

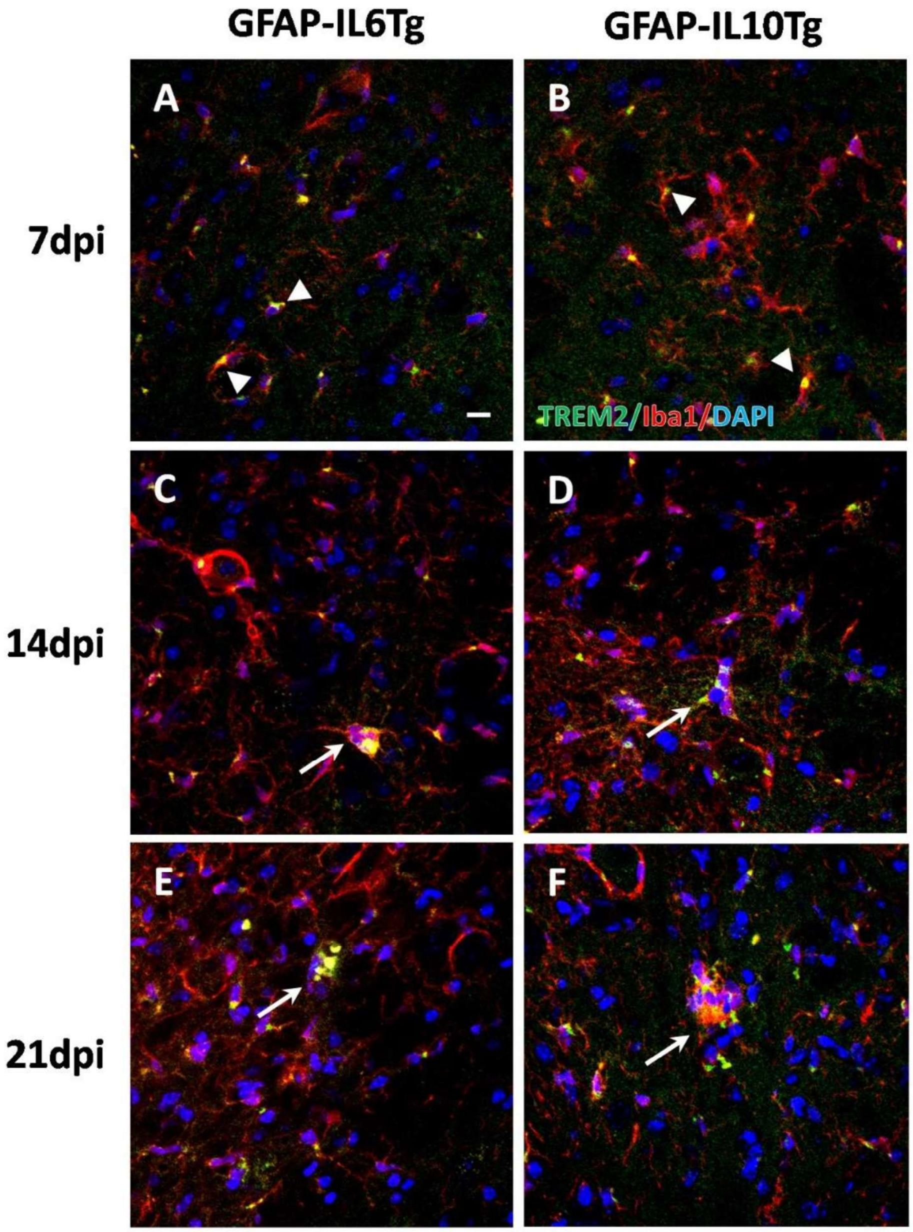
GFAP-IL6Tg
GFAP-IL10Tg
7dpi
14dpi
21dpi
A
B
C
D
E
F
TREM2/Iba1/DAPI

Supplementary Figure 2. Temporal pattern expression of TREM2 in GFAP-IL6Tg and GFAP-IL10Tg mice after FNA. (A-F) Double immunohistochemistry showing microglial cells positive for TREM2 (green) and Iba1 (red). Note that at 7dpi, TREM2 is confined to areas around the nucleus of some Iba1+ cells (arrowheads in A and B), whereas at 14 and 21dpi, the expression was detected in microglial prolongations and in some microglial clusters (white arrows in C-F). Scale bar (A–F) = 10 µm

ANNEX 3

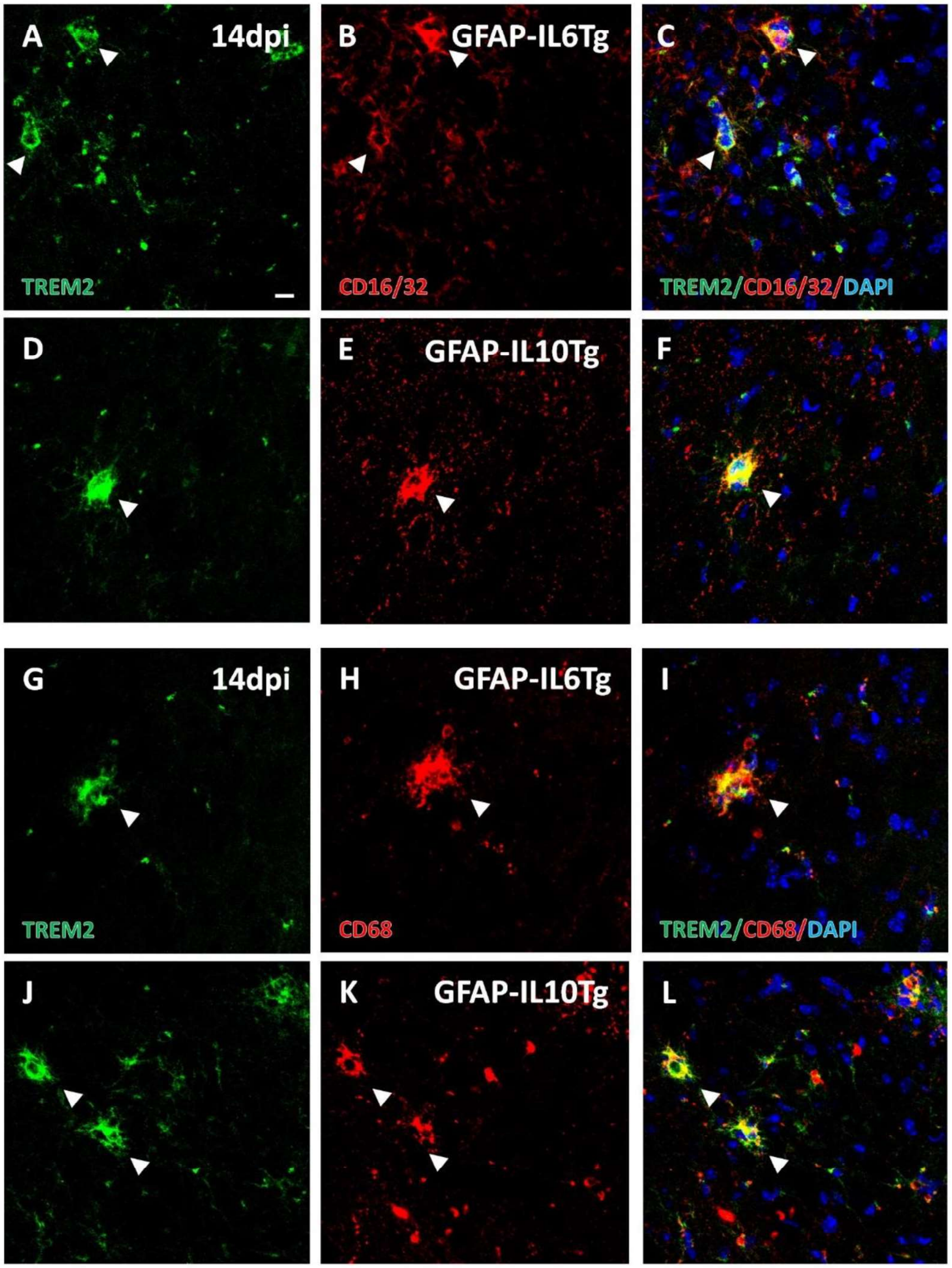
A
14dpi
TREM2
B
GFAP-IL6Tg
CD16/32
C
TREM2/CD16/32/DAPI
D
E
GFAP-IL10Tg
F
G
14dpi
TREM2
H
GFAP-IL6Tg
CD68
I
TREM2/CD68/DAPI
J
K
GFAP-IL10Tg
L

Supplementary Figure 3. Analysis of CD16/32 and CD68 expression in TREM2+ microglial cells in GFAP-IL6Tg and GFAP-IL10Tg mice after FNA. (A–F) Representative double-immunolabeled images combining TREM2 (green) and CD16/32 (red) in the ipsilateral FN at 14dpi from both GFAP-IL6Tg (A-C) and GFAP-IL10Tg (D-F) mice. Note that microglial clusters presented staining for both markers (white arrowheads). **(G–L)** Representative double-immunolabeled images combining TREM2 (green) and CD68 (red) in ipsilateral FN of lesioned animals at 14dpi in GFAP-IL6Tg (G-I) and GFAP-IL10Tg animals (J–L). Note that, similarly to CD16/32, CD68+ microglial clusters col-localized with TREM2 (arrowheads in G–L). Scale bar (A–L) = 10 µm.

ANNEX 4: ARTICLE 1

ALTERATIONS IN MICROGLIAL SIRP-α AND CD47 SIGNALLING MODIFY NEURONAL SURVIVAL AFTER PERIPHERAL NERVE INJURY

ALTERATIONS IN MICROGLIAL SIRP-α AND CD47 SIGNALLING MODIFY NEURONAL SURVIVAL AFTER PERIPHERAL NERVE INJURY

Manuscript in preparation

ABSTRACT (337w)

Microglial activation is controlled by the ‘On’/‘Off’ signalling, which consist in signalling pairs of neuronal ligands and microglial receptors. Expression of ‘Off’ signals maintain microglia in a homeostatic state, but their downregulation, or *de novo* expression of ‘On’ signals, triggers its activation. Previous results from our group showed that, after a facial nerve axotomy (FNA), transgenic mice with chronic overexpression of either interleukin (IL)-6 or IL-10 (GFAP-IL6Tg and GFAP-IL10Tg) showed reduced or increased neuronal survival, respectively, compared to wild-type (WT) mice. Changes in neuronal survival correlated with altered microglial activation phenotype, including differences in microglial phagocytic cluster formation. In this work, we aimed to determine if possible alterations in microglia-neuron ‘Off’ signalling after FNA, produced by the chronic overexpression of IL-6 or IL-10, defined differences in facial motor neuron (FMN) survival. For this purpose, we used non-lesioned (NL) and axotomized GFAP-IL6Tg, GFAP-IL10Tg and WT mice at different time-points, and we studied the expression of neuronal ligands CD200, CX3CL1, CD47 and CD22 and microglial ‘Off’ receptors CD200R, CX3CR1, SIRP-α and CD45. Our study found that, after FNA, “Off” signalling –with the exception of CD47– was first upregulated in both neurons and microglia during microgliosis, and then was downregulated in neurons during phagocytosis and FMN death. Chronic overproduction of pro-inflammatory IL-6 inhibited the upregulation of CD47 in the FN and promoted a more phagocytic and unresponsive microglial phenotype, with altered SIRP-α, CX3CR1 and CD45 expression, all consistent with increased FMN death. Overproduction of anti-inflammatory IL-10 slowed down microglial activation without modifying microglial ‘Off’ receptors, but induced CD47 upregulation in the FN at earlier time-points –related to the new formation of synaptic contacts–, which could inhibit phagocytosis through microglial SIRP-α. Our work demonstrates that “Off” signalling attempted to cooperatively protect FMNs, and highlights the decisive role of CD47-SIRPα axis in the control of FMN death through microglial phagocytosis. Also, we identified how IL-10 protected FMN through CD47-SIRPα effects in both FMNs and microglia. This work points out to CD47-SIRPα as a potential therapeutic axis for neuronal protection in neuroinflammation.

1. INTRODUCTION

Microglia, known as the main resident immune cells of the CNS, play an important role in CNS homeostasis and in the neuroinflammatory response (Kettenmann et al., 2011; Perry and Teeling, 2013). In the healthy brain, microglia are continually surveying the parenchyma looking for disturbances of the homeostasis, and when they detect any, they change their phenotype through a process called “microglial activation” (Kettenmann et al., 2011). This shift in microglial immune function is controlled by two classes of signals: the “Off” and the “On” signals. In the healthy CNS, microglial “Off” inhibitory receptors interact with their corresponding neuronal ligands, which helps to display a deactivated microglia phenotype and trigger a homeostatic signal (Elward and Gasque, 2003; Grimsley and Ravichandran, 2003). Some of the proposed inhibitory microglial ‘Off’ receptors include CD200R, CD45, CX3CL1 and SIRP-α, and their corresponding neuronal ligands are CD200, CD22, CX3CR1 and CD47, respectively (Biber et al., 2007; Hanisch and Kettenmann, 2007; Deczkowska et al., 2018). Loss of interaction in “Off” signalling lead to microglial activation (Biber et al., 2007; Deczkowska et al., 2018). Alterations or deficiencies on the “Off” signalling have been described in acute and chronic injuries (Hoek et al., 2000; Szepesi et al., 2018; Ahn et al, 2019), and have also been strongly associated with exacerbated microglial response in several neurodegenerative conditions, such as Alzheimer’s disease (AD), Parkinson’s disease (PD) or multiple sclerosis (MS), among others (Tan et al., 2000; Cardona et al., 2006; Wang et al., 2007; Han et al., 2012; Chen et al., 2016a; Szepesi et al., 2018). For this reason, new therapeutic strategies are focusing on this signalling as a potential candidate for treating neuroinflammation in degenerative disorders.

Despite microglial activation is importantly controlled by the neuron-microglia “On” and “Off” signalling, the inflammatory response is locally modulated by several molecules. One of the most important regulatory molecules are cytokines, a group of small polypeptides (8-30kDa) with diverse range of functions (Hanisch, 2002; Colton, 2009; Lively and Schlichter, 2018). Depending on their biological activity, cytokines can be classified in pro-inflammatory, such as the regulatory interleukin (IL)-6 (Erta et al., 2012), or anti-inflammatory, like the counterregulatory cytokine IL-10 (Burmeister and Marriott, 2018). The effect of cytokines in the “Off” signalling is barely known, and few examples on the cytokine effect on the “Off” signal expression have been reported to date. For instance, the role of the anti-inflammatory IL-4 in the upregulation of CD200 is well established (Lyons et al., 2009; Varnum et al., 2015), or the effect of IL-1ß or IL-10 through CX3CR1-CX3CL1 signalling (Rogers et al., 2011; Sánchez-Molina et al., 2022) have been reported to exert functions in hippocampal memory and learning, as well as neurogenesis. Still, no data are available on the effect of pro- or anti-inflammatory environments in CD47-SIRPα, or CD22-CD45 ‘Off’ pairs after a lesion.

Previous work from our lab showed that, after FNA, transgenic mice overproducing IL-6 (GFAP-IL6Tg) or IL-10 (GFAP-IL10Tg) displayed changes in microglial activation pattern, which correlated with higher or lower neuronal death, respectively, compared to WT littermates (Almolda et al., 2014; Villacampa et al., 2015). Phenotype alterations in GFAP-IL6Tg included lower microglial wrapping and number of microglial clusters, –phagocytic structures formed next to FMN (Raivich et al., 1998, Petitto et al., 2003)– and higher microglial activation (Almolda et al., 2014). Oppositely, in GFAP-IL10Tg mice, microglial cluster number increased, fact that was linked to a possible beneficial role in injury reparation (Villacampa et al., 2015).

Based in our previous observations, in this work, we hypothesized that IL-6 or IL-10 overproduction could be affecting microglia-neuron communication through the alteration of the 'Off' signalling after FNA, and that changes in this signalling may explain differences in neuronal outcome and microglial activation. To test our hypothesis, we studied the expression of the neuron-microglia 'Off' signalling pairs CD200-CD200R, CD47-SIRP-α, CD22-CD45 after FNA in WT mice, GFAP-IL6Tg and GFAP-IL10Tg, and we determined alterations produced by the overexpression of both IL-6 and IL-10 in the 'Off' signalling, as well as its relation to the FMN outcome. The study of this signalling provides a first picture on the time-course of various 'Off' signals in the FNA model and deepens in the role of microglia-neuron communication after an acute reparative injury in pro- and anti-inflammatory contexts.

2. MATERIALS AND METHODS

2.1. Animals

For this study, GFAP-IL6Tg and GFAP-IL10Tg animals and the corresponding wild-type (WT) littermates from both sexes of 3-4 months old were used. All mice were maintained with food and water *ad libitum* in a 12-h light/dark cycle. All experimental work animal work was conducted in accordance with Spanish regulations (Ley 32/2007, Real Decreto 1201/2005, Ley 9/2003 and Real Decreto 178/2004) in agreement with European Union directives (86/609/CEE, 91/628/CEE I 92/65/CEE) and was approved by the Ethical Committee of the Autonomous University of Barcelona, Spain. All efforts were aimed to minimize the number of animals used to get reliable scientific data, as well as animal suffering.

2.2. Facial Nerve Axotomy and Experimental Groups

113 GFAP-IL6Tg, 113 GFAP-IL10Tg and 221 WT mice were intraperitoneally (i.p) anesthetized with a solution of xylazine (20mg/kg) and ketamine (80mg/kg) at a dose of 0.01ml/g. The skin behind the right ear was shaved and a little incision was made. The skin and muscles were thoroughly separated so as to expose the facial nerve. The facial nerve was dissected and then one millimetre of it was rejected at the level of the

stylomastoid foramen. After the surgery, the skin was stitched with 5-0 nylon. Corneal dehydration was prevented by using Lacri-tube eye ointment. In order to ensure that the facial nerve transection was properly done, the complete whisker paralysis was verified after anaesthesia recovery.

Non-lesioned (NL) and axotomized animals were distributed in different experimental groups and euthanized at 3, 7, 14, 21 and 28 days post-injury (dpi) and processed for immunohistochemistry (IHC), flow cytometry and protein analysis.

2.3. Tissue processing for IHC analysis

Animals, deeply anesthetized at a dose of 0.015ml/g, were perfused intracardially for 10 minutes with 4% paraformaldehyde in 0.1 M phosphate buffer (pH 7.4). Brains were immediately removed and post-fixed for 4 h at 4ºC with the same solution. Subsequently, samples were cryopreserved in a 30% sucrose solution in 0.1 M phosphate buffer for 48 h at 4ºC, frozen with 2-methylbutane solution (Sigma-Aldrich, St. Louis) and stored at -80ºC. Free-floating coronary sections (30 µm) of the brainstem containing the facial nucleus (FN) were obtained using a CM5305s Leica cryostat and were stored at -20ºC in Olmos antifreeze solution until their use.

2.4. Single IHC staining

Free-floating cryostat sections were processed for the visualization of the following pairs of “Do-not-eat-me” markers expressed in neurons and microglia CD200-CD200R, CD22-CD45, CX3CL1, SIRP-α and CD47, the phagocytic molecules CD16/32 and CD68, and the synaptic marker synaptophysin. A minimum n of 4 animals were used for each condition. After 10 minutes of endogenous peroxidase blocking with 2% H_2O_2 in 70% methanol, sections were incubated for 1 h in either blocking buffer solution 1 (BB-1), containing 10% of foetal bovine serum, 0.3% of bovine serum albumin (BSA) in 0.05 M Tris-buffered saline (TBS), pH 7.4 and 1% Triton X-100 (TBS-1%T) or in the case of CD200R and CD45 with the blocking buffer solution 2 (BB-2), containing 0.2% gelatin (powder food grade, 104078, Merck) in TBS with 0.5% Triton X-100 (TBS-0.5%T). The corresponding primary antibodies diluted in the same blocking solution were then added overnight at 4ºC followed by 1 h at room temperature (RT): goat anti-CD200, goat anti-CD200R, rabbit anti-CD22, rat anti-CD45, rabbit anti-CX3CL1, rat anti-CD47, rat anti-SIRP-α, mouse anti-synaptophysin, rat anti-CD16/32 and rat anti-CD68 (Table 1). Sections incubated in media without lacking the primary antibody were used as a negative control and spleen sections were used as positive control. After washes with TBS-1%T or TBS-0.5%T, the following secondary antibodies diluted in the corresponding blocking solution were incubated for 1 h at RT: biotinylated anti-goat IgG, biotinylated anti-rabbit IgG, biotinylated anti-rat IgG and biotinylated anti-mouse IgM (Table 1). After 1 h at RT in horseradish streptavidin-peroxidase (Table 1), the staining was visualized by incubating the brain samples with DAB (D5637-5G; Sigma-Aldrich) for 3 minutes at RT. Sections were air dried, if appropriate counterstained with toluidine blue, dehydrated in graded alcohols, and after xylene treatment, coverslipped with DPX.

2.5. Double and triple IHC

Double immunolabeling was carried out to determine the cellular localization of the "Off" markers SIRP-α, CD200, CD45, CD22 and CX3CL1 and CD68. Free-floating sections were firstly processed for rat anti-CD200, rat anti-SIRP-α or rat anti-CD68 as described above, but using as a secondary antibody an anti-rat Alexa-Fluor 488, to label SIRP-α, anti-rat Alexa-Fluor 555 conjugated, to label CD68, or either one or the other for rat anti-CD200, depending on the labelling (Table 1). After several washes with TBS-1%T, sections were incubated for 1 h at RT in BB-1. Then, sections were incubated with rabbit anti-Iba1, mouse anti-GFAP, rabbit anti-MBP, NeuN biotinylated or Tomato Lectin (TL) biotinylated (Table 1) overnight at 4ºC, followed by 1 additional h at RT. Subsequently, sections were washed with TBS-1%T and incubated for 1 h at RT with anti-mouse Alexa-Fluor 555, anti-rabbit Alexa-Fluor 555 or Streptavidin Alexa-Fluor 488 secondary antibodies diluted in BB-1.

For both CD22 and CX3CL1, double immunolabelling was performed together with TL and GFAP, respectively. After blocking the tissue for 1 h at RT with BB-1, free-floating sections were firstly incubated with an anti-TL biotinylated or an anti-GFAP antibodies (Table 1) overnight at 4ºC plus 1 h at RT. Following several washes with TBS-1%T and 1-h incubation with Streptavidin Alexa-Fluor 488 or anti-mouse Alexa-Fluor 488 (Table 1), either anti-CD22 or anti-CX3CL1 antibodies (Table 1) were added in a final dilution of 1/200 for 48 h at RT. Sections were washed with TBS-1%T and incubated for 1 h with an anti-rabbit Alexa 555 secondary antibody (Table 1) for 1 h at RT.

Finally, to study CD45 expression in the FN and SIRP-α location in TREM2+ clusters, triple and double immunolabellings were performed combining CD45, Iba1 and CD3 or TREM2 and Iba1, respectively. After blocking the endogenous peroxidase for 10 minutes, sections were washed with TBS-0.5%T and incubated for 1 h in the blocking buffer solution-2 (BB-2). Thereafter, sections were incubated with anti-CD3 overnight at 4ºC followed by one additional h at RT or anti-TREM2 for 48h at RT (Table 1). After 1-h incubation at RT with an anti-hamster Alexa-Fluor 555 secondary antibody or Alexa-Fluor 488 anti-sheep secondary antibody (Table 1), the rat anti-CD45 or rat anti-SIRP-α antibody (Table 1) was added overnight at 4ºC plus an additional h at RT. Then, an anti-rat Alexa-Fluor 647 or anti-rat AlexaFluor 594 (Table 1) was incubated for 1 h at RT. Lastly, after several washes with TBS-0.5%T, a final overnight incubation at 4ºC with rabbit anti-Iba1 (Table 1) primary antibody was carried out for the triple immunolabelling followed by an additional h at RT. An anti-rabbit Alexa 488 (Table 1) was added for 1 h at RT to visualize the final Iba1 staining.

Before being cover slipped with Fluoromount G™ (0100-01, SouthernBiotech), sections were washed with TBS, TBS and TB and were nuclei stained with 4,9,6-diamidino-2-phenylindole (DAPI) for 5 min (Table 1). Col-localization was analysed with a Zeiss LSM 700 confocal microscope.

2.6. Densitometric analysis

Densitometric analysis was performed on sections immunolabeled with CD200, CD200R, CD22, CD45, CX3CL1, CD47, SIRP-α, synaptophysin, CD16/32 and CD68 and CD47. At least three representative sections from the brain stem containing the central part of the FN from both contralateral and the ipsilateral sides from each animal were photographed at 10X magnification with a DXM 1200F Nikon digital camera mounted on a Nikon Eclipse 80i brightfield microscope using the software ACT-1 2.20 (Nikon Corporation). The percentage of area (A) occupied by the staining as well as the intensity of the immunoreaction (Mean Gray Value Mean) were analysed for each photographed by the AnalySIS® software. For each marker, the AI index was calculated by multiplying the percentage of the immunolabelled area by the Mean Gray Value Mean as described in Acarin et al. (1997). In the case of CD200, CD22, CX3CL1, CD47 SIRP-α, synaptophysin and CD68, the staining was present in both contralateral and ipsilateral FN. Therefore, the gray grade quotient (GGQ) was obtained by dividing the Mean Gray Value Mean on the ipsilateral side by the Mean Gray Value Mean on the contralateral side. The intensity grade (IG) was calculated by multiplying the percentage of the immunolabelled area by the GGQ. On the other hand, in CD45, CD200R and CD16/32 where the staining was absent or extremely low in the contralateral FN, the AI index was used to express the results.

2.7. Flow cytometry

To study the microglia/macrophage/leukocyte population expressing the principal “Do-not-eat-me” receptors, NL animals and lesioned animals (7dpi and 14dpi) were analysed using flow cytometry. Anaesthetized animals were intracardially perfused with 0.1M phosphate buffer solution (PBS). Then, the brain was removed from the skull and two 0.5-mm-thick coronal slices were obtained from the brain trunk using a Mouse Brain Matrix (Zivic Instruments). For each slice, the dorsal inferior half was cut with sterile knives, and tissue containing the contralateral and ipsilateral FN was divided. These FN sections were dissociated hereunder through 160µm and 70µm meshes in order to obtain a cell suspension for each animal. To get a viable number of cells for the FN, a pool of 3 FN was needed for each tube, considered as a n=1. A n=6 per time-point and genotype was used for each experiment. Thereafter, cells were digested for 30 minutes at 37ºC using type IV collagenase (17104-019; Life Technologies) and DNAse I (D5025; Sigma-Aldrich). Subsequently, each cellular suspension was centrifuged at RT for 20min at 2400rpm in a discontinuous Percoll gradient (17-0891-02; Amersham-Pharmacia) between 1.112 g/ml and 1.08 g/ml. Myelin layer at the top of the tube was removed. Cells in the interphase and the clear upper phase were collected, washed in PBS plus 2% serum and Fc receptors were blocked by incubating for 20 minutes at 4ºC in a solution of purified CD16/32 (Table 2). Then, cells were labelled during 30 minutes at 4ºC with the following surface microglial markers: anti-CD11b-APC-Cy7, anti-CD45-PerCP, anti-CD200R-APC, anti-CX3CR1-PE and anti-SIRPα-FITC (Table 2). Isotype-matched control antibodies were used as negative control and a cell suspension of splenocytes as positive control. Finally, cells were acquired using FACS Canto flow cytometer (Becton Dickinson, San Jose, CA) and results were analysed using the FlowJo software.

2.8. Tissue processing for protein analysis

Animals used for protein analysis were i.p anaesthetized and perfused for 1 min with cold 0.1 M PBS (pH 7.4). Subsequently, the FN was dissected out as previously described in Flow cytometry section, snap frozen individually in liquid nitrogen and stored at -80ºC. Total protein was extracted by solubilization of samples on lysis buffer containing 25mM HEPES, 2% Igepal, 5mM $MgCl_2$, 1.3 mM EDTA, 1 mM EGTA, 0.1 M PMSF and protease (1:100, P8340; Sigma-Aldrich), and phosphatase inhibitor cocktails (1:100, P0044; Sigma-Aldrich) for 2 h at 4ºC. After solubilization, samples were centrifuged at 13000 rpms for 5 min at 4ºC and the supernatants collected. Total protein concentration was assessed with a commercial Pierce BCA Protein Assay kit (23225; ThermoFisher Scientific) according to manufacturer's protocol. Protein lysates were aliquot and stored at -80ºC until used for protein microarray analysis. The FN of each animal was analysed separately.

2.9. Cytokine analysis

The cytokines IL-6, TNF-α and IL-10 were analysed in GFAP-IL6Tg and WT mice using a Milliplex MAP Mouse High Sensitivity kit (#MHSTCMAG-70K; Merck Millipore) and the cytokines IL-10 and TNF-α were analysed in GFAP-IL10Tg and the corresponding WT littermates at NL, 7 and 21dpi using a Milliplex MAP Mouse Cytokine/Chemokine kit (#MCYTOMAG-70K; Merck Millipore) according to manufacturer's instructions. A minimum N of 6 animals were used for each condition. Briefly, 25µL of each FN extracts with a final total protein concentration of 3.0 µg/µL were added to the plates, along with the standards in separate wells, containing 25µL of custom fluorescent beads and 25µL of matrix solution, and incubated overnight at 4ºC in a plate-shaker (750rpm). After two washes with wash buffer (1x), the plate was incubated with 25µL of detection antibodies for 30 min at RT followed by an incubation with 25µL of

Streptavidin-Phycoerythrin for 30 min at RT in a plate-shaker (750rpm). Finally, the plate was washed twice with wash buffer and 150µL of Drive fluid was added. Luminex MAGPIX device with the xPONENT 4.2 software was used to read the plate. Data were analysed using the Milliplex Analyst 5.1 software and expressed as pg/mL of protein.

2.10. Statistical analysis

Statistics were performed using Graph Pad Prism® software (Graph Pad Software Inc.) and results were expressed as mean ± standard error of the mean (SEM). Two-way ANOVA with Tukey's multiple comparison analysis as a *post-hoc* test was applied to determine statistically significant differences among time-points postinjury, and two-way ANOVA with multiple comparison *post hoc* Sidak's test was used to compare WT with the corresponding transgenic GFAP-IL6Tg or GFAP-IL10Tg mice.

3. RESULTS

3.1 Chronic overproduction of IL-6 or IL-10 modify CD47 expression, but not other neuronal 'Off' ligands, after FNA compared to WT

Determination of either IL-6 or IL-10 cytokine levels was performed, respectively, in the NL and lesioned FN of the transgenic GFAP-IL6Tg and GFAP-IL10Tg, at 7 and 21 dpi (Suppl. Figure 1A and D). Our results indicated that GFAP-IL6Tg contained higher IL-6 levels at all timepoints when compared to WT mice (Suppl. Figure 1A). Similarly, GFAP-IL10Tg showed increased levels of IL-10 in basal conditions and at 7 dpi, but IL-10 levels were not significantly increased in the ipsilateral FN at 21 dpi compared to WT (Suppl. Figure 1D). These results showed that both transgenes were effectively generating a pro- or anti-inflammatory CNS microenvironment due to the chronic overproduction of IL-6 and IL-10, in both basal conditions and after injury.

In the NL FN of WT, GFAP-IL6Tg and GFAP-IL10Tg mice, CD22 expression was mainly restricted to FMN somas (Figure 1A-C, M-O), and this cellular expression pattern was maintained along all time-points. After FNA, neuronal CD22 levels were upregulated until 7dpi in WT, GFAP-IL6Tg and GFAP-IL10Tg mice (Figure 1D-F, V, W), due to increased expression of CD22 in FMN somas and projections (Figure 1P-R). Afterward, CD22 expression levels decreased progressively until 28dpi, reaching even inferior levels than its respective NL FN (Figure 1G-I, V, W). Detailed observation showed that, at 7dpi, CD22 was not expressed in microglia in neither WT, GFAP-IL6Tg nor GFAP-IL10Tg (Figure 1S-U).

CX3CL1 showed a similar expression pattern than CD22 in all mouse lines. In the NL FN of WT, GFAP-IL6Tg and GFAP-IL10Tg mice, CX3CL1 was expressed exclusively in FMN somas (Figure 2A-C, J-L). After FNA, CX3CL1 levels were upregulated at 7dpi, due to a specific increase in FMNs (Figure 2D-F, M-O, S, T), but not due to *de novo* expression in astrocytes in all WT, GFAP-IL6Tg and GFAP-IL10Tg mice (Figure 2P-R). Later, CX3CL1 levels were progressively downregulated until 28dpi in all mouse lines (Figure 2G-I. S, T).

CD200 presented a diffuse pattern of staining in the neuropile of the NL FN of WT, GFAP-IL6Tg and GFAP-IL10Tg mice (Figure 3A-C). Only spaces occupied by neuronal bodies showed lack of staining, and CD200 was strongly present in the boundaries of the outer limits of FMNs (Figure 3J-L). After FNA, CD200 increased progressively in the neuropile, and reached a peak of expression at 7dpi in all mouse lines (Figure 3D-F, V, W). According to double immunohistochemical stainings, this increase was not due to *de novo* CD200 expression in glial cells, such as oligodendrocytes or wrapping microglia (Figure 3M-U). Then, at 14dpi, CD200 was downregulated, coinciding with the peak of neuronal death. Interestingly, at this time-point, some capillary blood vessels expressed CD200 (Figure 3S-U). At later time-points, CD200 reached similar levels to the NL FN of WT, GFAP-IL6Tg and GFAP-IL10Tg (Figure 3V, W).

CD47 maintained a diffuse expression pattern in the neuropile of the NL FN of WT mice, similar to CD200 expression (Figure 4A). After FNA, CD47 levels of the lesioned FN were maintained as in the NL FN, and only a significant increase of CD47 levels was observed at 21dpi (Figure 4D, G, J, K). CD47 was the only “Off” ligand that displayed expression differences in both transgenic mouse lines compared to WT mice. Specifically, in GFAP-IL6Tg, CD47 expression levels remained unchanged after the lesion, and therefore, CD47 was not increased in the ipsilateral FN at 21 dpi, like we detected in WT mice (Figure 4E, H, J). On the other hand, GFAP-IL10Tg showed increased CD47 levels in the lesioned FN, starting at 7 dpi and being significantly higher at 14 and 21 dpi compared to previous timepoints, and therefore, at 14 dpi, CD47 levels were significantly increased in GFAP-IL10Tg compared to WT mice (Figure 4F, I, K).

In the brain, CD47 counterreceptor SIRP-α is detected in microglia –as well as other myeloid and hematopoietic cells–, and neurons (Adams et al., 1998). To explore whether effects observed in CD47 were also affecting neuronal SIRP-α, we determined SIRP-α expression in the NL and lesioned FN of WT, GFAP-IL6Tg and GFAP-IL10Tg mice. SIRP-α showed strong immunohistochemical staining covering all the neuropile of the NL FN of WT, GFAP-IL6Tg and GFAP-IL10Tg, with the exception of the FMN bodies (Figure 5A-C, I-K). After FNA, SIRP-α showed a similar distribution in the lesioned FN of all mouse lines (Figure 5D-F, L-N). Occasionally, a stronger expression of SIRP-α could be observed surrounding lesioned FMN somas at 14 dpi (Figure 5L-N), corresponding to wrapping microglia (Figure 5O-Q). Despite these slight changes, SIRP-α levels remained invariable throughout all the FNA time-course in all WT, GFAP-IL6Tg and GFAP-IL10Tg mice (Figure 5G, H).

3.2 Microglial 'Off' receptors in GFAP-IL6Tg, GFAP-IL10Tg and WT mice in basal conditions and after FNA

Analysis of microglial 'Off' receptors CD45 and CD200R along the FNA time-course showed alterations in microglial reactivity in GFAP-IL6Tg and GFAP-IL10Tg compared to WT mice. Briefly, in WT mice, CD45 staining showed low levels of expression in microglia of the NL FN (Figure 6A, V, X). After injury, microglia increased in number and upregulated CD45 expression until 7dpi (Figure 6D, G, V, X). At this time-point, microglial cells surrounded FMN bodies (arrowheads in Figure 6G-I) in the so-called microglial wrapping, and next, at 14dpi, formed newly microglial clusters, in close contact with FMN (black arrowheads in Figure 6J) and infiltrated T lymphocytes (empty arrowheads in Figure 6J, white arrowheads in P). Later, at 21 and 28dpi, CD45 levels and microglial cluster number decreased progressively (Figure 6V, X).

In the NL FN of GFAP-IL10Tg, CD45 expression was similar to the NL FN of WT mice (Figure 6A, C, X). After FNA, GFAP-IL10Tg mice showed a specific reduction of CD45 levels at 7dpi, in the peak of microgliosis, and also tended to express lower levels at later time-points (Figure 6I, X). On the contrary, GFAP-IL6Tg animals showed major differences in CD45 expression in both NL and lesioned FN. Concretely, GFAP-IL6Tg contained higher microglia numbers and increased CD45 expression in microglia of the NL FN, which resulted in higher CD45 levels compared to WT (Figure 7A, B, V). After FNA, at 3 and 14dpi, CD45 levels were increased in the FN of GFAP-IL6Tg compared to WT littermates (Figure 7E, K, V). Since GFAP-IL6Tg presented significantly higher CD45 levels under homeostatic conditions when compared to WT, we represented the dynamics of microglial activation in GFAP-IL6Tg and WT along FNA lesion calculating CD45 fold changes in reference to the respective NL FN (Figure 7W). This histogram revealed that, although GFAP-IL6Tg presented higher CD45 in basal conditions and after injury, CD45 upregulation in reference to the NL FN was less pronounced in GFAP-IL6Tg than WT in every single time-point after FNA.

Determination of CD200R demonstrated a barely detectable expression in microglia in NL FN from WT, and occasional expression on ameboid cells, compatible with meningeal and perivascular macrophages (empty arrowheads, Figure 7A). After FNA, microglial CD200R increased rapidly in the whole FN at 7dpi (Figure 7D, V, W) and was subsequently downregulated from 14 to 28dpi (Figure 7G,V, W), concentrating its expression in microglial clusters and spherical cells identified as lymphocytes (arrows and black arrowheads in Figure 7G-L, M-U). Despite similar CD200R cellular expression and dynamics were found in GFAP-IL10Tg and GFAP-IL6Tg mouse lines compared to WT, we detected lower levels of CD200R at 28dpi in GFAP-IL6Tg animals (Figure 7V).

Until now, in our study we had identified critical time-points for microglia-neuron 'Off' signalling at 7 and 14 dpi, corresponding, respectively, to the peak of microgliosis and

‘Off’ ligand/receptor expression, and to the peak of FMN death and microglia cluster formation. To deepen in the expression of microglial “Off” receptors in microglia/macrophage populations after FNA, we analysed them by flow cytometry in NL and at 7 and 14dpi.

Two different populations were distinguished based on CD11b and CD45 expression: microglia was identified as CD11b$^+$/CD45^{low}, while macrophages and highly activated microglia were CD11b$^+$/CD45^{high} (Figure 8A and 9A). Both populations were split using the CD45 histogram, and for each ‘Off’ receptor, the number of cells, mean fluorescence intensity (MFI) and percentage of cells were obtained.

In a first glance, we observed that most microglia expressed “Off” receptors CX3CR1, CD200R and SIRP-α (above 80-90%) in all WT, GFAP-IL6Tg and GFAP-IL10Tg mice, while macrophage/highly activated microglial population, that showed similar expression rates, did not express CX3CR1 in either genotype. In general, CD11b$^+$/CD45^{high} showed higher levels of expression for all markers compared to microglia in all mouse lines, as reflected in higher MFI values (Figures 8 and 9).

3.2.1. Chronic overexpression of IL-6 alters microglial ‘Off’ receptors CD45, CX3CR1 and SIRP-α, inducing a more activated and phagocytic microglial phenotype

In the NL FN of GFAP-IL6Tg mice, microglial cells were more numerous than in WT (Figure 8E, I, O, U). Expression of ‘Off’ receptors in microglia of the NL GFAP-IL6Tg was altered, since higher CD45 and lower CX3CR1 and SIRP-α levels were found compared to WT (Figure 8F, P, V, Q). Highly activated microglia/ macrophages in NL GFAP-IL6Tg showed significantly increased cell number and CD45 levels compared to WT, without modifications in CD200R and SIRP-α levels (Figure 8G, H, L, M, R, S). In global, these results suggest that chronic IL-6 overproduction increased microglia activation in the NL FN by altering ‘Off’ receptor expression.

In the lesioned FN of WT mice, both microglia population and highly activated microglia/macrophage populations increased in cell numbers until 7dpi and then, at 14dpi, remained stable (Figure 8E, G). Changes in microglia cell numbers were similarly observed for CX3CR1, CD200R and SIRP-α (Figure 8I, O, U). In microglia from lesioned WT mice, only CX3CR1 levels and cell percentage of expression followed a modest downregulation at 7dpi (Figure 8V, W), and no alterations were found in neither levels nor percentage of expression of CD45, CD200R and SIRP-α (Figure 8J, K, P, Q). Highly activated microglia/macrophage population showed a downregulation of SIRP-α levels and percentage of expression at 14 dpi, coinciding with the peak of FMN death and microglial phagocytic cluster formation, and no differences were observed for CD200R (Figure 8L-T).

In lesioned GFAP-IL6Tg, an increase in cell numbers were also detected for microglia at 7dpi and 14dpi, while highly activated microglia/macrophages, at this timepoint remained stable. Cell numbers were always higher for both populations compared to WT (Figure 8E, G), and differences between genotypes were preserved for CX3CR1, CD200R and SIRP-α cell numbers (Figure 8I, O, U, L, R). Modifications observed in microglia during basal conditions in GFAP-IL6Tg were also observed after FNA, meaning that higher CD45, and lower SIRP-α and CX3CR1 levels were found in microglia, and lower percentage of SIRP-α-positive microglia cells was also identified (Figure 8F, P, Q, V, W). In highly activated microglial/macrophage population from lesioned GFAP-IL6Tg, SIRP-α expression was downregulated earlier than WT, at 7 dpi, and decreased SIRP-α levels were maintained at 14 dpi (Figure 8S, T). CD200R did not show differences in neither levels nor percentages of cell expression in both genotypes (Figure 8M, N).

In summary, it could be said that chronic IL-6 overproduction results in a primed or activated microglia phenotype in basal conditions and after lesion, altering the expression of the 'Off' receptors CD45 and SIRP-α in both microglia/ macrophages, and CX3CR1 in microglia. Downregulation of SIRP-α in microglia/macrophages, suggests an earlier phagocytic microglial phenotype, anticipating the decrease in microglial SIRP-α observed in lesioned WT during the peak of maximal FMN death.

3.2.2. Chronic overexpression of IL-10 slows down microglia activation in the axotomized FN

Analysis of the NL FN of GFAP-IL10Tg showed no differences in both microglia and highly activated microglia/macrophages compared to WT littermates in neither cell number nor percentages or levels of cell expression of CD45, CX3CR1, CD200R or SIRP-α (Figure 9E-W).

After FNA, microglia in GFAP-IL10Tg mice increased later than WT mice, since at 7dpi microglial numbers were lower, or tended to be lower in all receptors analysed (Figure 9E, I, O, U), suggesting a delayed microgliosis. CD45, CD200R and SIRP-α levels or percentages of cell expression were not modified in microglia from lesioned FN of both WT and GFAP-IL10Tg (Figure 9F, J, K, P, Q). At 7dpi, GFAP-IL10Tg showed, like in WT mice, a modest microglial CX3CR1 decrease in both levels and cell percentage of expression, that remained later, at 14dpi (Figure 9V, W). Highly activated microglia/macrophages population in GFAP-IL10Tg showed no differences in cell numbers compared to WT, thus increasing at 7dpi, and remaining stable later, at 14dpi (Figure 9G). At 7dpi, in the peak of microgliosis, CD200R was downregulated in GFAP-IL10Tg compared to WT (Figure 9M). Later, at 14 dpi, highly activated microglia and macrophages showed increased CD45 levels and slight decreased the percentage of

SIRP-α-positive cells in both WT and GFAP-IL10Tg when compared to the previous time-point (Figure 9H, T).

In summary, chronic IL-10 overproduction slowed down microgliosis, but did not importantly modify 'Off' receptors in microglia, since only a reduction of CD200R expression in highly activated microglia/macrophages was detected in GFAP-IL10Tg animals compared to WT.

3.3. Chronic overexpression of IL-6 or IL-10 alters the phagocytic capacity in non-lesioned and axotomized animals

Since our work identified main differences in the 'Do-not-eat-me' signalling CD47-SIRP-α in both transgenic animals, we studied the microglial phagocytic capacity in these mice through the expression of lysosomal CD68. Previous work from our group identified CD68 time-course expression after FNA in WT (Manich et al., 2020). In the NL FN, CD68 was located in microglia perinuclearly (Figure 10A-C, M), and expressed at low levels in all WT, GFAP-IL6Tg and GFAP-IL10Tg mice. After injury, CD68 was also expressed throughout the cell body (black arrows in Figure 10N-T) and CD68 was concentrated in microglial clusters at 14, 21 and 28dpi (black arrows in Figure 10G-L). After FNA, CD68 levels in the FN of WT mice increased rapidly at 3 and 7dpi, remained elevated until 21dpi, and decreased at 28dpi (Figure 10D-M). GFAP-IL6Tg mice displayed lower CD68 staining at 3dpi and higher CD68 expression at 28dpi compared to WT. On the contrary, a significant decrease on CD68 levels were detected at 14dpi in GFAP-IL10Tg, while CD68 levels were upregulated at 21dpi in these animals.

3.4. SIRP-α is expressed in microglial cells forming phagocytic clusters

In order to determine whether CD47-SIRP-α was specifically involved in the regulation of FMN phagocytosis after FNA, we closely examined SIRP-α expression in microglia clusters. Our results showed that SIRP-α was found in activated microglia and microglial clusters showing a variable expression. Concretely, some microglial clusters contained highly intense expression of SIRP-α, while other clusters did not specifically upregulate SIRP-α expression in all WT, GFAP-IL6Tg and GFAP-IL10Tg (Figure 11A-C). Taking into account the heterogeneous distribution of SIRP-α, we explored whether SIRP-α upregulation was specifically produced in clusters expressing the phagocytic microglial 'On' receptor TREM2. Our results showed that SIRP-α was intensely upregulated in microglia clusters showing an elevated expression of TREM2 (Figure 11D-F).

3.5. IL-10 upregulates CD47 and the formation of synaptic contacts in the FN after FNA

In our work we identified an upregulation in CD47 expression in the lesioned FN at 21dpi, that started earlier, at 14 dpi, in GFAP-IL10Tg. In neurons, CD47 upregulation has been related to neurite outgrowth and synapse formation (Miyashita et al., 2004; Murata et al., 2006, Hsieh et al., 2015). To prove whether CD47 upregulation was related to the reestablishment of synapses, we detected synaptophysin in NL and lesioned GFAP-IL10Tg and WT mice (Figure 12). Our results showed that the NL FN of WT and GFAP-IL10Tg presented similar levels of synaptophysin (Figure 12A, D, G). After FNA, a loss of synapses was identified in both WT and GFAP-IL10Tg at 14 dpi, since synaptophysin levels tended to decrease (Figure 12B, E, G). At 21 dpi, levels of synaptophysin showed a trend to increase in lesioned GFAP-IL10Tg and, despite no significant differences were observed, levels of synaptophysin in GFAP-IL10Tg tended to be higher than WT mice (Figure 12C, F, G).

DISCUSSION

In the present study, we aimed to study "Off" signalling in membrane-bound neuronal ligands and microglial receptors after FNA. In addition, we explored if either pro-inflammatory IL-6 or anti-inflammatory IL-10 cytokine overproduction showed alterations in membrane "Off" signalling that could explain previous differences related to FMN survival (Almolda et al., 2014; Villacampa et al., 2015). In the following lines we will discuss our main findings in relation to the current literature.

1) Neuron-microglia 'Off' signalling is regulated after peripheral nerve injury

1.1. Neuron-microglia 'Off' signals in homeostatic conditions

In our work, expression of 'Off' ligands and receptors support the neuron-microglia communication in basal conditions. Concretely, in the NL FN of WT, we detected neuronal expression of CX3CL1 and CD22, as it had been reported (Harrison et al., 1998; Mott et al., 2004), and CD200 in the neuronal membrane and neuropile, but not astrocytes, as found in other studies (Shrivastava et al., 2012; Varnum et al., 2015; Lago et al., 2018; Manich et al., 2019). CD47 diffuse neuropile staining coincided with previous data determining its widespread expression in CNS cell types (Koning et al., 2007; Gitik et al., 2011; Zhou et al., 2014). On the other hand, microglia/macrophages expressed CD200R, CD45 and SIRP-α in basal conditions, while CX3CR1 was only detected in microglia but not macrophages, as already reported (Cosenza-Nashat el al., 2006; Chitnis et al., 2007; Koning et al., 2009; Gitik et al., 2011; Lago et al., 2018; Harrison et al., 1998; Nishiyori et al., 1998; Cardona et al., 2006). In global, our results support the interaction between microglia and neurons through CD200-CD200R, CX3CL1-CX3CR1 and CD47-SIRP-α as a signal of homeostasis, and outlines the role of neuron signalling in the preservation of an homeostatic microglial phenotype in basal conditions. In spite of this, the relevance of each signal remains to be clarified, since data obtained from SIRP-α, CD200 or CX3CR1 knockout mice (Hoek et al., 2000;

Cardona et al., 2006; Sato-Hashimoto et al., 2019) indicate different microglial activation responses during basal conditions, ranging from no response, to priming or activation upon loss of these signals.

1.2. Neuron-microglia 'Off' signals after peripheral nerve injury

In this study, we found a first increase of the number of CD200R, CX3CR1, CD45 and SIRP-α-positive microglia, during microgliosis, coinciding with the upregulation of the neuronal expression of CX3CL1, CD22 and CD200 –with the exception of CD47–. An early increase in "Off" ligands after injury has been linked to the control of microglial activation in several acute and chronic inflammatory models, resulting in neuroprotective effects (Lago et al., 2018; Valente et al., 2017; Duan et al., 2008; Comella et al., 2019; Ahn at al., 2019; Funikov et al., 2018). In the case of FNA, upregulation of neuronal 'Off' ligands could have chemoattractant and immunoregulatory functions in microglia, since microglia approaches and wraps lesioned FMN during the peak of microgliosis, producing a neuroprotective effect (Möller et al., 1996; Almolda et al., 2014). Indeed, CX3CL1, also released as a soluble form, acts as a chemokine for microglia (Hughes et al., 2002; Carter and Dick, 2004), and *in vitro* studies suggest adhesion functions for this molecule (Lauro et al., 2006). Also, soluble CD200 has been reported to show chemotactic properties, which are preserved in inflammatory contexts (Carter and Dick, 2004), and CD200 showed immunoregulatory functions, since CD200 knockout mice after FNA displayed accelerated microglia activation (Hoek et al., 2000).

After FNA, from 14 dpi onwards, downregulation of neuronal CD200, CX3CL1 and CD22 'Off' signals could be explained by both neuronal loss, peaking at 14 dpi, and degeneration of living FMNs (Möller et al., 1996; Raivich et al., 1999 and 2002). Lower expression of neuronal 'Off' signals observed at later timepoints may increase FMN phagocytosis by activated microglia, as it had been observed for higher microglial phagocytosis of ß-amyloid in CD200 knockout mice (Varnum et al., 2015; Lyons et al., 2007). At 14 dpi, during the peak of FMN death, elevated levels of CD200R, CD45 and variable expression of SIRP-α were observed in phagocytic microglia clusters –i.e., groups of 4-5 microglial cells tightly grouped and located next to FMN (Möller et al., 1996; Raivich et al., 1998; Petitto et al., 2003; Villacampa et al., 2015; Manich et al., 2020)–. Our results suggest that 'Off' receptor expression tightly control microglia activation along the inflammatory response, and regulate phagocytic functions after FNA, especially in microglia forming clusters.

CD47 was the only neuronal 'Off' signal that followed a different pattern since, after FNA, its levels remained stable in the FN, with a punctual upregulation at 21dpi –after the peak of neuronal death–. CD47, has been classified as a 'Do-not-eat-me' signal due to the inhibition of phagocytosis through the myeloid SIRP-α receptor, in both homeostatic and inflammatory conditions (Okazawa H et al., 2005; Gitik et al., 2011; Gautam and Acharya, 2014; Zhang et al., 2015; Lehrman et al., 2018; Sato-Hashimoto et al., 2019). In most neuroinflammatory conditions, such as in MS, CD47 is downregulated, increasing the phagocytic activity of microglia and macrophages (Koning et al., 2007). Because CD47-SIRP-α holds a key role on preventing phagocytosis, we could infer that CD47 upregulation prevents the self-engulfment of FMNs. Indeed, CD47 upregulation could mediate some effects through the also existing neuron-to-neuron CD47-SIRP-α signalling (Matozaki et al., 2009). Upregulation of CD47 in nervous tissue has been reported in processes of neuronal differentiation *in vitro* and *in vivo* (Miyashita et al., 2004; Ohnishi et al., 2005; Murata et al., 2006; Hsieh et al., 2015), or memory formation in rats, according to increases in CD47 mRNA (Huang et al., 1998). These results led to the hypothesis that neuronal CD47-SIRP-α axis is involved in developmental network formation, and in processes of memory formation during adulthood (Matozaki et al., 2009). Indeed, a key role in CD47-SIRP-α neuronal axis has been demonstrated in synapse maturation (Toth et al., 2013). In our case, CD47 upregulation could reflect the re-establishment of neuronal synapses in regenerating FMN, which occur from 14 dpi onwards (Makwana et al., 2010), and may act as a brake to microglial phagocytosis in the FNA model.

In this study we identify specific neuronal mechanisms by which FMN attempt self-protection and regulate microglia activation at early stages. Uncoupling of neuron-microglia 'Off' signalling at later timepoints triggers FMN phagocytosis and death. Exclusive neuron-microglia communication is reinforced by the fact that we neither detect CX3CL1 or CD200 upregulation in astrocytes, as found in some studies (Hughes et al., 2002; Koning et al., 2009), nor CD22 aberrant microglia expression, as it had also been reported (Funikov et al., 2018; Cougnoux et al., 2018; Pluvinage et al., 2019).

2) Chronic overproduction of pro-inflammatory IL-6 alters 'Off' receptors inducing a primed and phagocytic microglial phenotype in basal conditions and after FNA

Chronic overproduction of IL-6 altered microglial 'Off' signalling in both basal conditions and after FNA, and presented a phenotype characterised by increased CD45 expression, decreased SIRP-α and CX3CR1. Those alterations reflect the loss of the homeostatic microglial phenotype, as CX3CR1, a key gene of the microglial signature (Butovsky et al., 2014), was downregulated. Our results support the primed microglial phenotype observed in other CNS areas of GFAP-IL6Tg in basal conditions, such as hippocampus, cortex or several white matter areas (Recasens et al., 2021; Sánchez-Molina et al., 2021).

After FNA, GFAP-IL6Tg microglia maintained alterations in 'Off' receptor expression, such as the lower fold increase in CD45, which could explain the altered and defficient response after FNA (Almolda et al., 2014). Alterations in of CX3CR1 and SIRP-α receptors may be impairing microglial chemotaxis and wrapping of FMN in GFAP-IL6Tg. Lower microglial CX3CR1 could decrease chemotaxis (Hughes et al., 2002; Carter and Dick, 2004) and adhesion produced by CX3CL1 (Lauro et al., 2006). Downregulation of SIRP-α could also be related to deffective chemotaxis, since lack of SIRP-α has been related to delayed transmigration of monocytes *in vitro* and lower chemotactic and migration of macrophages *in vitro* and in an experimental model of peritonitis (Álvarez-Zarate et al., 2015; de Vries et al., 2002). Primed microglia in GFAP-IL6Tg showed also a phagocytic phenotype, characterised by increased CD16/32 expression and lower SIRP-α expression. Downregulation of SIRP-α in aging and neurodegeneration increased phagocytosis in neuroinflammatory contexts (Wang et al, 2019), as we observed in previous work in GFAP-IL6Tg, where microglia showed increased functional phagocytosis capacity in basal conditions through a myelin phagocytosis assay (Sánchez-Molina et al., 2021). The increase of the phagocytic phenotype and the lack of CD47 upregulation at 21 dpi in GFAP-IL6Tg suggests higher phagocytosis of lesioned FMN that could explain the lower FMN survival observed in GFAP-IL6Tg (Almolda et al., 2014).

3) Chronic overproduction of anti-inflammatory IL-10 promotes FMN regeneration and prevents microglial phagocytosis of FMN through CD47 upregulation

In our previous work, GFAP-IL10Tg animals showed increased FMN survival after FNA that correlated with decreased microglial activation (Villacampa et al., 2015). Our results indicate that chronic IL-10 overproduction did not significantly alter 'Off' receptors in microglia during basal conditions and after FNA, since only lower microglia number at 7dpi and a modest CD200R downregulation in CD11b+/CD45^{high} was detected in those animals. However, in this study, GFAP-IL10Tg showed an earlier upregulation of CD47 in the lesioned FN, suggesting an involvement of CD47-SIRP-α "Do-not-eat-me" signalling in FMN death differences. In our previous work we identified IL-10R in FMN in both GFAP-IL10Tg and WT animals (Villacampa et al., 2015), and therefore any effect of IL-10 exerted in microglia should be mediated, at least, through FMN.

Because IL-10R is expressed in FMN, IL-10 could directly upregulate CD47 in FMN as a result of synapse formation and FMN regeneration. Indeed, IL-10 has proved to increase neurite outgrowth and synapse formation *in vitro* (Lim et al., 2013; Chen et al., 2016b), processes both related to the CD47 upregulation in those cells (Miyashita et al., 2004; Murata et al., 2006, Hsieh et al., 2015). In support of this hypotheses, in our work we identify in GFAP-IL10Tg an increase in synapse formation –detected through synaptophysin–, at 21 dpi compared to WT mice. Other observations that link IL-10 expression in lesioned mice and CD47 upregulation are the relation between sustained IL-10 levels and CD47 upregulation: 1) in GFAP-IL10Tg, chronic overproduction of IL-10 results in CD47 upregulation in the FN at 14 dpi; 2) in WT, IL-10 increase observed at 7 dpi and maintained at 21 dpi precedes CD47 upregulation at 21 dpi; and 3) IL-10 levels in GFAP-IL6Tg, which are elevated at 7 dpi but significantly decreased at 21 dpi, result in absence of CD47 upregulation (Suppl. Figure 1). While our results support positive effects in FMN due to chronic IL-10 overproduction, lack of IL-10, in IL10 knockout mice, result in increased FMN death compared to WT, an effect that could not be rescued by IL-10 peripheral administration (Xin et al., 2011). Our results suggest that chronic overproduction of IL-10 promotes neurite outgrowth and synapse formation in FMN, upregulating CD47 in those cells. As a consequence, and as it will be discussed in the following section, IL-10-derived upregulation of CD47 could inhibit microglial phagocytic activity by interacting with SIRP-α.

4) CD47-SIRP-α regulates microglial phagocytosis and FMN survival after FNA

CD47-SIRP-α is recognised as an essential ‘Do-not-eat-me’ axis, due to its widely proved effects on phagocytosis. Interaction of CD47 with its receptor SIRP-α in macrophages inhibits phagocytosis (Bian et al., 2016), and loss or blockade of either CD47 (Han et al., 2012; Hutter et al., 2019; Lehrman et al., 2018) or SIRP-α (Sato-Hashimoto et al., 2019; Wang et al., 2019; Ding et al., 2021) results in increased phagocytosis of myelin or synapses. Outcomes of CD47-SIRP-α loss are contradictory: in mouse models of Wallerian axonal degeneration or in cuprizone-induced demyelination, loss of SIRP-α improved recovery (Elberg et al., 2019; Sato-Hashimoto et al., 2019); on the contrary, worsening was observed in neurodegeneration mouse models of Parkinson’s and Alzheimer’s mouse model, due to a accelerated neuronal loss or decreased synaptic density (Wang et al., 2019; Ding et al., 2021), or in EAE, where clinical score was aggravated (Han et al., 2012). Oppositely, induced upregulation of CD47 in a model of retinitis pigmentosa increased retinal cone survival (Wang et al., 2021).

In our study we found that WT animals upregulated CD47 at 21dpi as a result of restablishment of synapses in FMN, as discussed above, which consequently, constrains microglial phagocytosis through SIRP-α inhibition. Interestingly, CD47 upregulation started earlier in GFAP-IL10Tg animals, inhibiting before microglial phagocytosis, during the peak of FMN death. On the other hand, in GFAP-IL6Tg mice, CD47 was not upregulated, and since, in those animals, microglial SIRP-α is downregulated in basal conditions and after FNA, loss of CD47-SIRP-α signalling would facilitate FMN phagocytosis by microglia. While the upregulation of SIRP-α expression in some microglial phagocytic clusters is surprising, it may indicate a specific and tight control of microglial phagocytosis in these structures. In global, these results could explain higher FMN survival encountered in GFAP-IL10Tg (Villacampa et al., 2015) and lower survival of FMNs in GFAP-IL6Tg (Almolda et al., 2014).

Inhibition of FMN phagocytosis through CD47-SIRP-α signalling is also reflected in the phenotype of phagocytic microglia and its phagocytic capacity. While CD47 was upregulated in GFAP-IL10Tg, at 14 dpi, microglia displayed lower phagocytic CD16/32 (Villacampa et al., 2015) and CD68 at late time-points. On the contrary, microglia in GFAP-IL6Tg mice expressed higher CD16/32 (Suppl. Figure 2) and CD68 levels at later stages, consistent with enhanced microglial phagocytic phenotype in basal conditions and after FNA. In global, CD47-SIRP-α interaction inhibits phagocytosis through several 'eat-me' receptors, including CR3 or FcγR-II/III, amongst the ones identified and most studied (Oldenberg et al., 2001; Gitik et al., 2011). However, since CD47 activation signals through immunoreceptor tyrosine-based inhibitory motif (ITIM) by reversing Syk signalling, it could be expected that CD47 inhibits other 'eat-me' phagocytic receptors, activated through ITAM and tyrosine kinase Syk, for example, TREM2 (Cokram et al., 2021). Our results showing an intense expression of TREM2 and SIRP-α in microglia clusters supports this hypothesis. In our previous work we identified TREM2 expression after FNA, which was concentrated in phagocytic microglial clusters, in WT and transgenic animals, however differences were only observed in GFAP-IL6Tg, suggesting that this receptor did not explain changes in FMN death rates (Manich et al., 2020). Also, we showed that CD11b/CD18 expression and CD16/32 (Suppl. Figure 2) were altered in GFAP-IL6Tg (Almolda et al., 2014), but the preservation of an intact blood-brain barrier after FNA and lack of IgG infiltration in the FN excludes phagocytosis through IgG opsonization (Villacampa et al., 2015; Manich et al., 2020). Another interesting phagocytic receptor candidates that may be involved microglial cluster phagocytosis are CD11c, which is exclusively located in the microglial clusters at 14 dpi (Kloss et al., 1999), and its expression has been recently defined to be repressed by SIRP-α in white matter (Sato-Hashimoto et al., 2019). Also*, in vitro* studies suggested a phagocytic complex formed in microglia to phagocyte fibrillar β-amyloid constituted by CD47, CD36 and integrin α6β1, which would overcome classical phagocytic pathways (Bamberger et al., 2003; Koenigsknecht and Landreth, 2004). In the FNA model, neither the process of FMN cell death –which is not apoptotic and had been proposed to be through 'aposklesis' (Graeber and Moran, 2002)– nor the 'eat-me' signal or receptor/s involved have been unequivocally clarified, and therefore, further studies are needed to understand how FMNs are dying and phagocyted, and how CD47-SIRP-α inhibit microglial phagocytosis in lesioned FMNs.

CONCLUSIONS

Our study found that the expression of "Off" signalling was constitutively expressed in both neurons and microglia in basal conditions and after FNA. Firstly, both neurons and microglia upregulated 'Off' signals in a coordinated manner, during the microglial wrapping of FMNs occurring in microgliosis, thus protecting FMNs. Then, loss of neuronal 'Off' signals showed a dyscoordinated pattern, subsequently producing loss of FMN through phagocytosis and death. Chronic overproduction of pro-inflammatory IL-6 resulted in a phagocytic and primed microglial phenotype accompanied by alterations in Off receptors SIRP-α, CX3CR1 and CD45, consistent with the increased FMN death associated to the deleterious microglial response. Contrarily, overproduction of anti-inflammatory IL-10 slowed down microglial activation and the phagocytic phenotype without modifying microglial 'Off' receptors, but promoted the upregulation of CD47 in the FN at early time-points, increasing synaptic formation and protecting FMNs from phagocytosis through microglial SIRP-α. Overall, our work demonstrates that, while "Off" signalling attempt to cooperatively protect FMN, CD47-SIRPα axis has a decisive role in controlling FMN death through microglial phagocytosis, and points out to CD47-SIRPα as a potential therapeutic axis for neuronal protection in acute neuroinflammatory injuries.

FIGURES

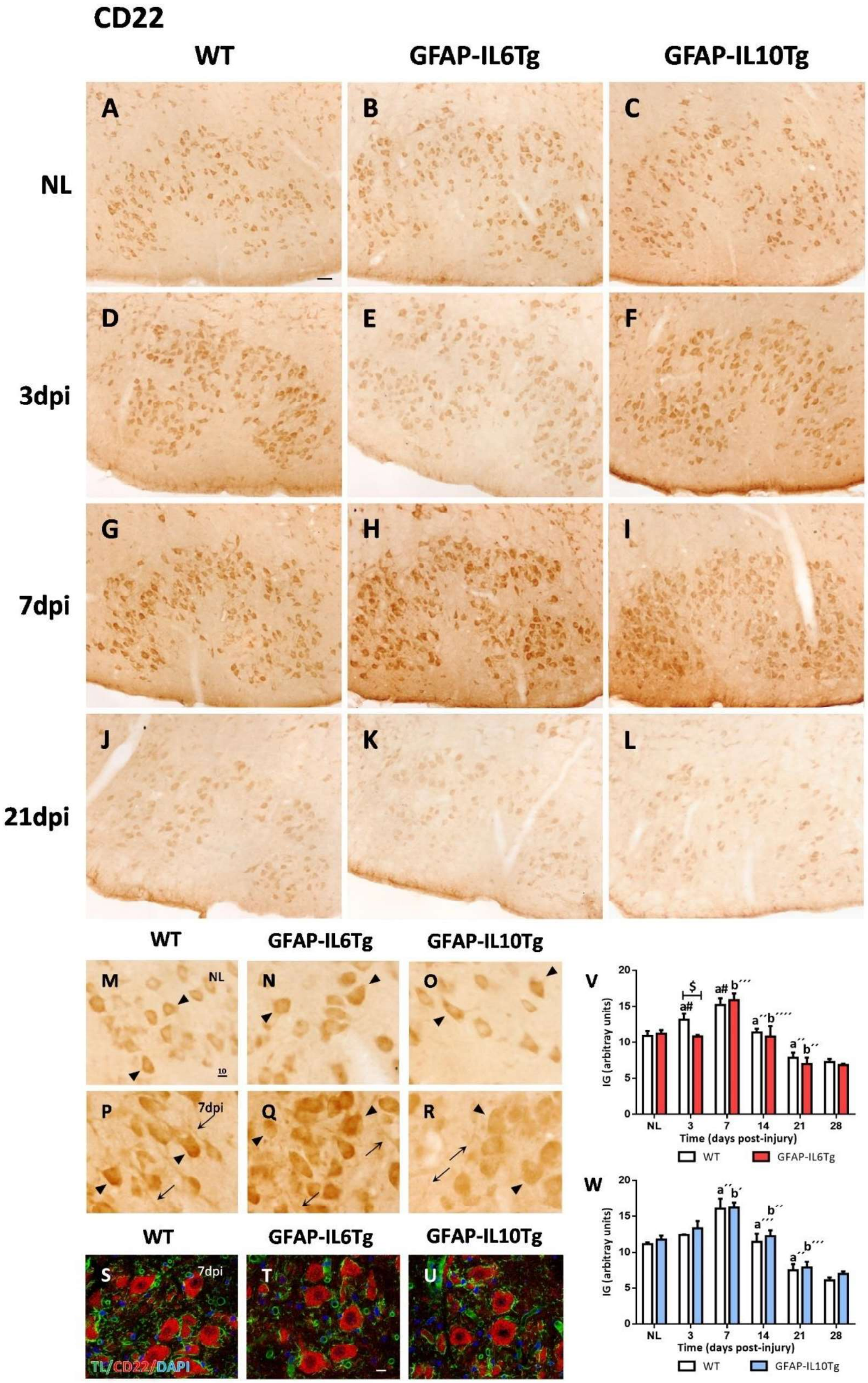
CD22
WT
GFAP-IL6Tg
GFAP-IL10Tg
A
B
C
NL
D
E
F
3dpi
G
H
I
7dpi
J
K
L
21dpi
WT
GFAP-IL6Tg
GFAP-IL10Tg
M
NL
10
N
O
P
7dpi
Q
R
WT
GFAP-IL6Tg
GFAP-IL10Tg
S
7dpi
T
U
TL/CD22/DAPI
V
20
15
10
5
0
IG (arbitray units)
$
a#
a#
b´´´
a´´
b´´´´
a´´
b´´
NL
3
7
14
21
28
Time (days post-injury)
WT
GFAP-IL6Tg
W
20
15
10
5
0
IG (arbitray units)
a´´
b´
a´´´
b´´
a´´
b´´´
NL
3
7
14
21
28
Time (days post-injury)
WT
GFAP-IL10Tg

Figure 1. Temporal expression pattern of CD22 after FNA in GFAP-IL6Tg, GFAP-IL10Tg and WT mice. (A-L) Representative images of CD22 immunohistochemistry in the NL (A-C) and ipsilateral FN at 3 (D-F), 7 (G-I) and 21dpi (J-L) from WT, GFAP-IL6Tg and GFAP-IL10Tg animals. Note that, in every single time-point, CD22 is restricted to neuronal somas. **(M-R)** Magnifications showing how CD22 was localized on neuronal somas (black arrowheads) in NL FN and at 7dpi. At 7dpi, CD22 staining increased due to the spread of CD22 into neuronal prolongations (black arrows). **(S-U)** Double immunolabelling combining CD22 (red) with TL (green) counterstained with DAPI (blue) confirmed that microglia did not express CD22 at 7dpi in any mouse line. **(V-W)** Histograms showing the quantification of CD22 intensity grade (IG) from 3 to 28dpi after FNA lesion in GFAP-IL6Tg, GFAP-IL10Tg and their corresponding WT littermates. Note that all mouse lines showed a significant increase of CD22 at early time-points, reaching a peak at 7dpi followed by a progressive downregulation till 28dpi (differences are represented comparing to the previous time-point in WT a# $p \leq 0.1$; a´´$p \leq 0.01$; a´´´$p \leq 0.001$, and transgenic mice b´$p \leq 0.05$; b´´$p \leq 0.01$; b´´´$p \leq 0.001$; b´´´´$p \leq 0.0001$). GFAP-IL6Tg mice presented lower CD22 levels at 3dpi (\$$p \leq 0.1$). Data are represented as ± SEM. Scale bar (A-L): 50 µm, (M-U): 10 µm.

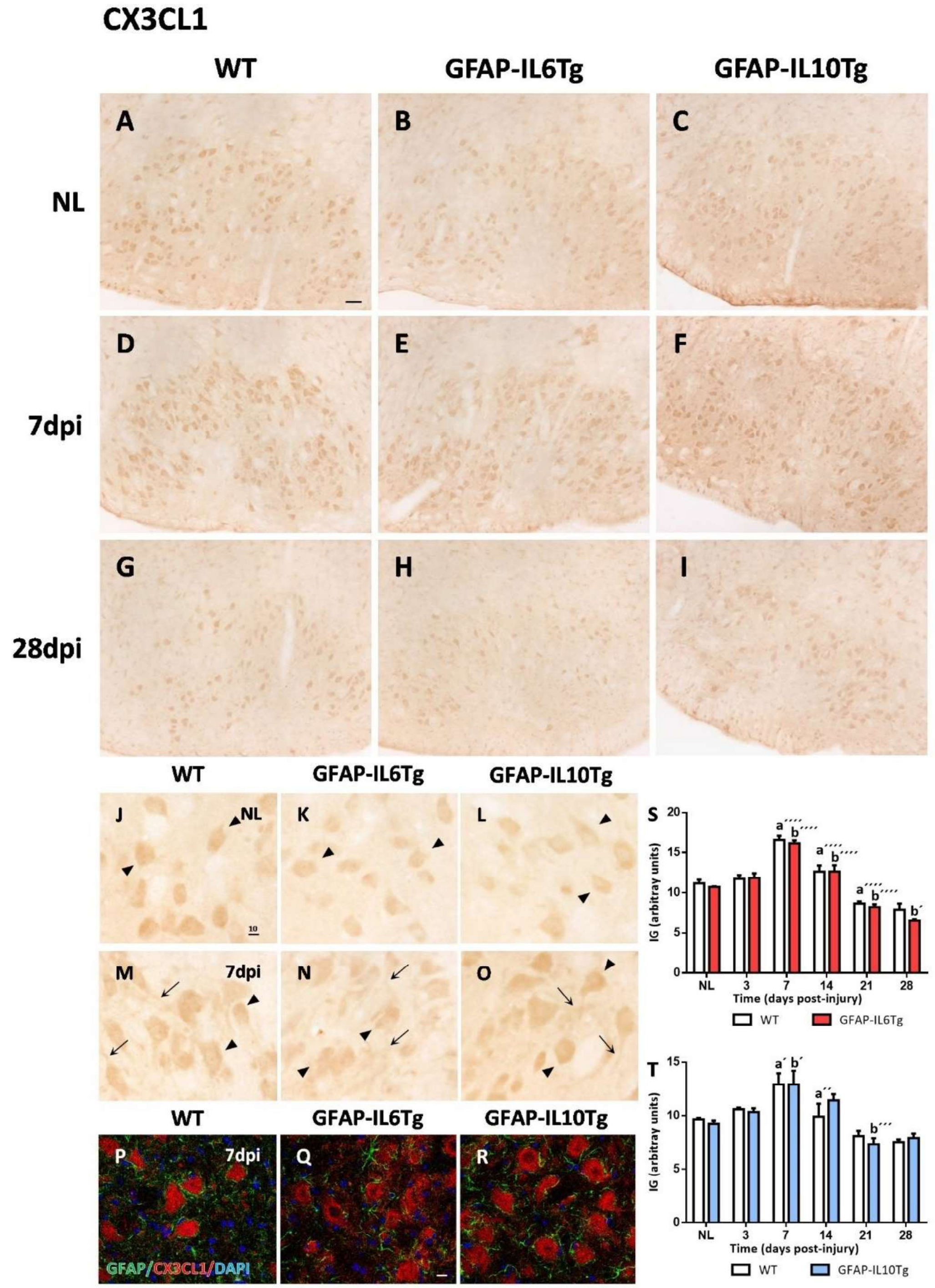
CX3CL1
WT
GFAP-IL6Tg
GFAP-IL10Tg
NL
7dpi
28dpi
A
B
C
D
E
F
G
H
I
J
K
L
M
N
O
P
Q
R
10
GFAP/CX3CL1/DAPI
S
IG (arbitray units)
Time (days post-injury)
NL
3
7
14
21
28
0
5
10
15
20
a´´´´
b´´´´
a´´´´
b´´´´
a´´´´
b´´´´
b´
WT
GFAP-IL6Tg
T
a´
b´
a´´
b´´´
GFAP-IL10Tg

Figure 2. Temporal expression pattern of CX3CL1 after FNA in GFAP-IL6Tg, GFAP-IL10Tg and WT mice. (A-I) Representative images of CX3CL1 immunohistochemistry in NL (A-C) and axotomized FN at 7 (D-F) and 28dpi (G-I) from all WT, GFAP-IL6Tg and GFAP-IL10Tg animals. **(J-O)** Magnification images from WT, GFAP-IL6Tg and GFAP-IL10Tg mice showing that CX3CL1 was restricted to neuronal somas (black arrowheads) in NL FN and the later increase of CX3CL1 at 7dpi was due to its spread to neuronal

prolongations (black arrows). **(P-R)** Double immunolabelling combining CX3CL1 (red) with GFAP (green) and counterstained with DAPI (blue) at 7dpi confirmed that astrocytes did not express CX3CL1 in any condition. **(S-T)** Histograms showing the quantification of CX3CL1 IG time course along the lesion in GFAP-IL6Tg, GFAP-IL10Tg and their corresponding WT. Differences assessed comparing to the previous time-point in WT (a´$p \leq 0.05$; a´´$p \leq 0.01$; a´´´´$p \leq 0.0001$) and transgenic mice (b´$p \leq 0.05$; a´´´$p \leq 0.001$; b´´´´$p \leq 0.0001$) showed that, there was a significant increase of CX3CL1 at 7dpi, followed by a downregulation at 14 and 21dpi. No differences were detected between genotypes. Data are represented as ± SEM. Scale bar (A-I): 50 µm, (J-R): 10 µm.

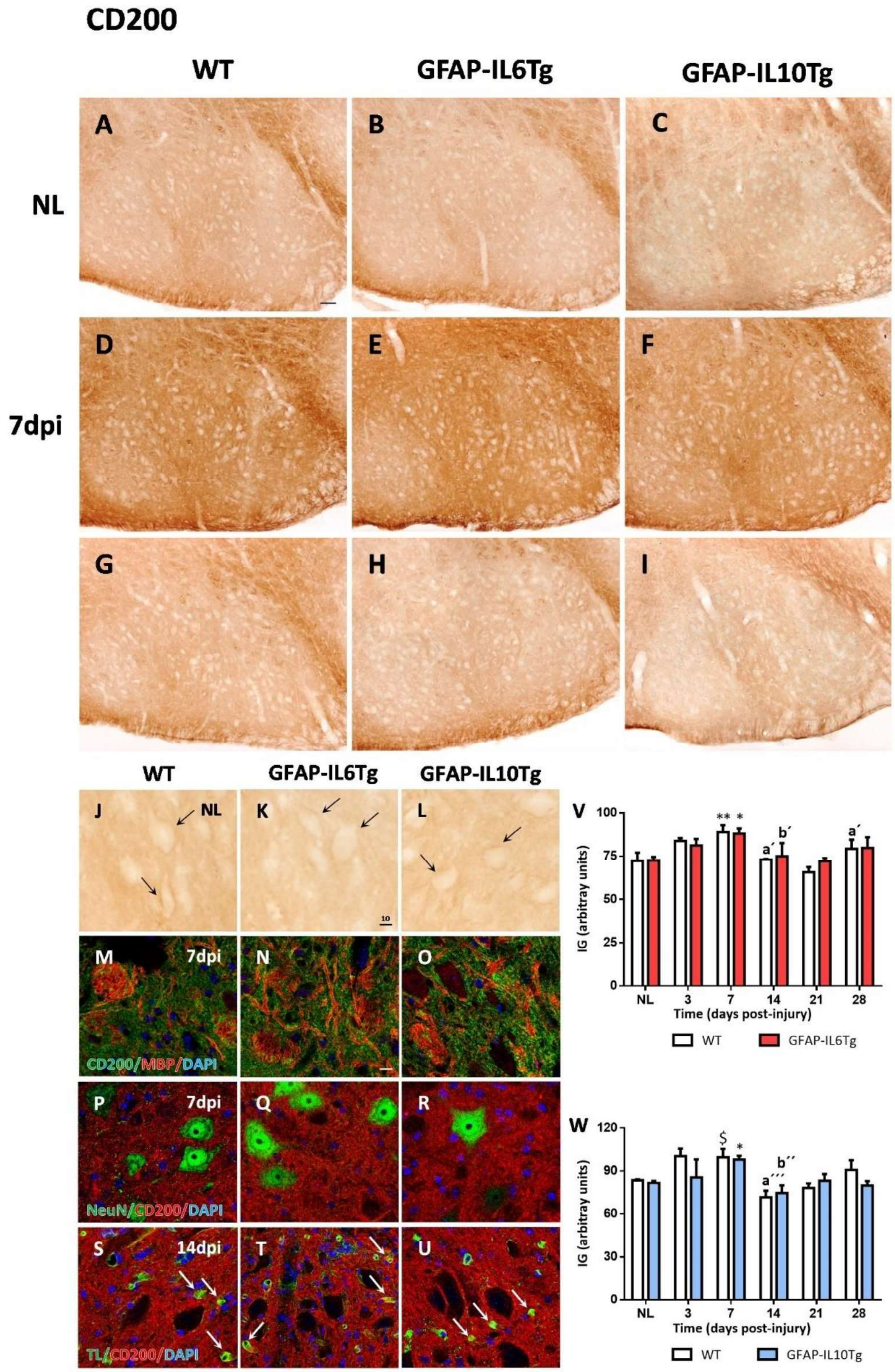
CD200
WT
GFAP-IL6Tg
GFAP-IL10Tg
NL
7dpi
A
B
C
D
E
F
G
H
I
WT
GFAP-IL6Tg
GFAP-IL10Tg
J
NL
K
L
10
M
7dpi
N
O
CD200/MBP/DAPI
P
7dpi
Q
R
NeuN/CD200/DAPI
S
14dpi
T
U
TL/CD200/DAPI
V
100
75
50
25
0
IG (arbitray units)
** *
a´
b´
a´
NL
3
7
14
21
28
Time (days post-injury)
WT
GFAP-IL6Tg
W
120
90
60
30
0
IG (arbitray units)
$
*
a´´´
b´´
NL
3
7
14
21
28
Time (days post-injury)
WT
GFAP-IL10Tg

Figure 3. Temporal pattern expression of CD200 after FNA in GFAP-IL6Tg, GFAP-IL10Tg and WT mice. (A-I) Representative images of CD200 immunohistochemistry in the NL (A-C) and the ipsilateral FN at 7 (D-F) and 14dpi (G-I) from WT, GFAP-IL6Tg and

GFAP-IL10Tg mice. Note that CD200 showed a diffuse pattern along all the FN. **(J-L)** Magnification images in NL showed CD200 distribution in the neuropile and strong expression on neuronal cell membrane (black arrows) in all mouse lines. **(M-U)** Double immunolabelling of CD200 (green in M-O and red in P-U) with MBP (red in M-O) and NeuN (green in P-R) at 7dpi indicated that, no expression of CD200 was found in oligodendrocytes or neurons. However, at 14dpi, TL (green in S-U) showed col-localization with CD200 in some blood vessels (white arrows S-U) in all animal lines. **(V-W)** Histograms of CD200 IG time course after FNA in GFAP-IL6Tg, GFAP-IL10Tg animals and the corresponding WT showed that, there was a significant increase of CD200 at early time-points, followed by a downregulation at 14 and 21dpi (a´$p \leq 0.05$; a´´´$p \leq 0.001$ compared to previous time-point in WT, b´$p \leq 0.05$; b´´$p \leq 0.01$ compared to previous time-point in transgenic mice, \$$p \leq 0.1$; *$p \leq 0.05$; **$p \leq 0.01$ compared to NL in all mouse lines). No differences were detected between genotypes at any time-point. Data are represented as ± SEM. Scale bar (A-I): 50 µm, (J-U): 10 µm.

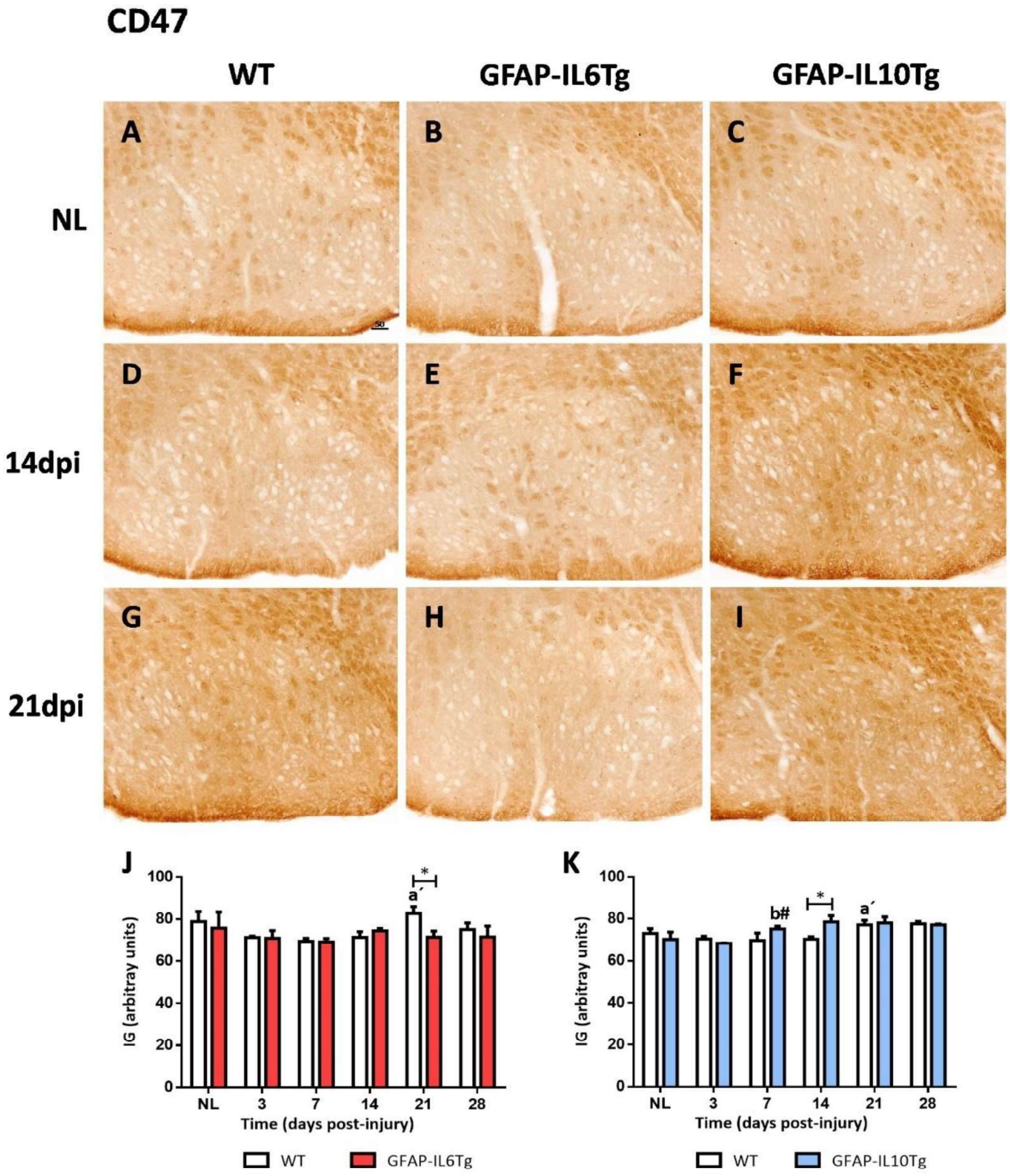
CD47
WT
GFAP-IL6Tg
GFAP-IL10Tg
NL
14dpi
21dpi
A
B
C
D
E
F
G
H
I
50
J
K
IG (arbitray units)
100
80
60
40
20
0
NL
3
7
14
21
28
Time (days post-injury)
a´
*
b#
WT
GFAP-IL6Tg
GFAP-IL10Tg

Figure 4. Temporal expression pattern of CD47 after FNA in GFAP-IL6Tg, GFAP-IL10Tg and WT mice. (A-I) Representative images showing single CD47 staining in the NL (A-C) and lesioned FN at 14 and 21dpi (D-I) from WT, GFAP-IL6Tg and GFAP-IL10Tg mice. Note that CD47 showed a diffuse pattern of expression covering the neuropile along all the FN**. (J-K)** Histograms showing CD47 time course, expressed as IG along all the lesion in all mouse lines. Note that at 21dpi, WT showed a significant increase on CD47 staining (´$p \leq 0.05$ compared to the previous time-point), whereas GFAP-IL6Tg remained unaltered and GFAP-IL10Tg increased their CD47 levels at 7dpi (#$p \leq 0.1$ compared to the previous time-point). While GFAP-IL6Tg displayed downregulated CD47 compared to WT littermates at 21dpi (*$p \leq 0.05$), GFAP-IL10Tg had higher CD47 levels at 14dpi (*$p \leq 0.05$). Data are represented as ± SEM. Scale bar (A-I): 50 µm.

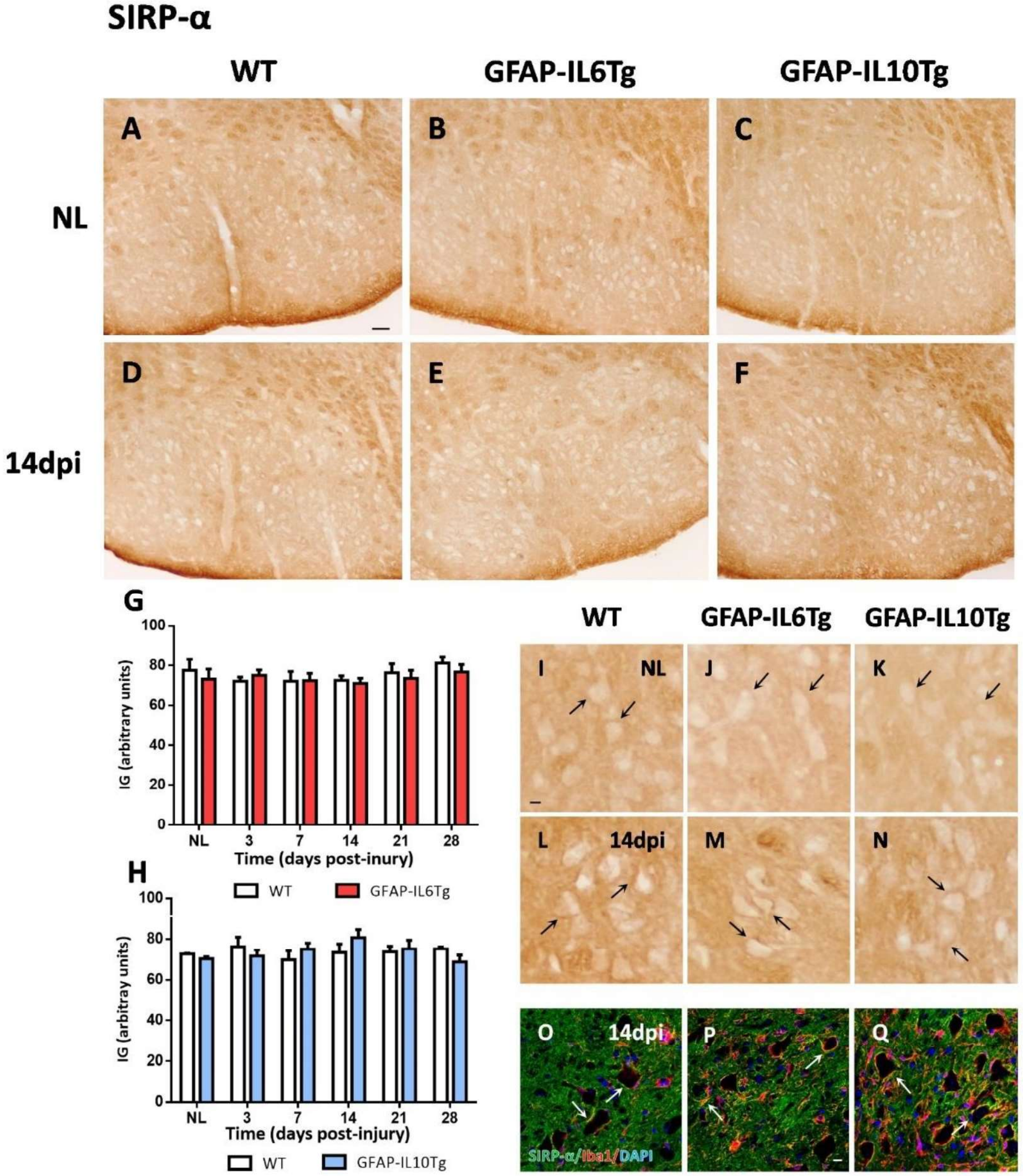
SIRP-α
WT
GFAP-IL6Tg
GFAP-IL10Tg
A
B
C
NL
D
E
F
14dpi
G
IG (arbitrary units)
100
80
60
40
20
0
NL
3
7
14
21
28
Time (days post-inury)
WT
GFAP-IL6Tg
H
IG (arbitray units)
100
80
60
40
20
0
NL
3
7
14
21
28
Time (days post-injury)
WT
GFAP-IL10Tg
WT
GFAP-IL6Tg
GFAP-IL10Tg
I
NL
J
K
L
14dpi
M
N
O
14dpi
P
Q
SIRP-α/Iba1/DAPI

Figure 5. Temporal expression pattern of SIRP-α after FNA in GFAP-IL6Tg, GFAP-IL10Tg and WT mice. (A-F) Representative images showing single SIRP-α staining in the NL (A-C) and lesioned FN at 14 dpi (D-F) from WT, GFAP-IL6Tg and GFAP-IL10Tg mice. Note that SIRP-α showed a diffuse pattern of expression covering the neuropile along all the FN**. (G-H)** Histograms showing SIRP-α time course, expressed as IG along all the lesion in all mouse lines. Note that no differences were detected between time-points and genotypes. Data are represented as ± SEM. **(I-N)** Magnification images in NL (I-K) and lesioned FN at 14 and 21dpi (L-N) showed SIRP-α distribution in the neuropile and noticeable stronger expression on neuronal cell membrane (black arrows) in all mouse lines. **(O-Q)** Double immunolabelling of SIRP-α (green) with Iba-1 (red) showed that microglia wrapping FMNs showed SIRP-α-expression (arrows). Scale bar (A-F): 50 µm, (I-N): 10 µm; (O-Q)= 10 µm.

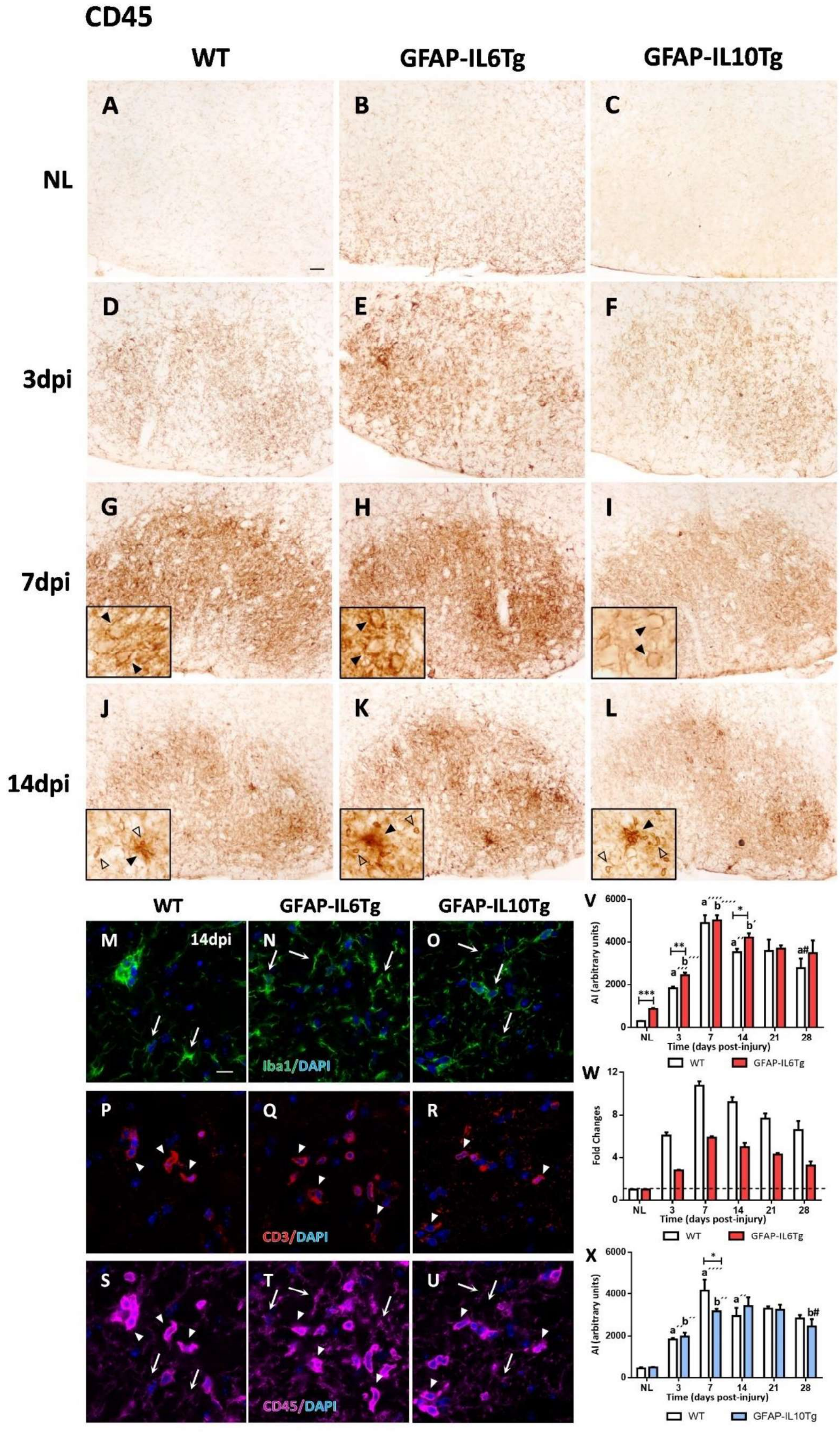
CD45
WT
GFAP-IL6Tg
GFAP-IL10Tg
NL
3dpi
7dpi
14dpi
A
B
C
D
E
F
G
H
I
J
K
L
WT
GFAP-IL6Tg
GFAP-IL10Tg
M
14dpi
N
O
Iba1/DAPI
P
Q
R
CD3/DAPI
S
T
U
CD45/DAPI
V
AI (arbitrary units)
6000
4000
2000
0
***
**
*
a´´´
b´´´
a´´´´
b´´´´
a´´
b´
a#
NL
3
7
14
21
28
Time (days post-injury)
WT
GFAP-IL6Tg
W
Fold Changes
12
8
4
0
NL
3
7
14
21
28
Time (days post-injury)
WT
GFAP-IL6Tg
X
AI (arbitrary units)
6000
4000
2000
0
*
a´´
b´´
a´´´´
b´´
a´´
b#
NL
3
7
14
21
28
Time (days post-injury)
WT
GFAP-IL10Tg

Figure 6. Temporal expression pattern of CD45 after FNA in GFAP-IL6Tg, GFAP-IL10Tg and WT mice. (A-L) Representative images of CD45 immunohistochemistry in NL (A-C) and lesioned FN at 3 (D-F), 7 (G-I) and 14dpi (J-L) from WT, GFAP-IL6Tg and GFAP-IL10Tg mice. Note that, at 7dpi some microglial cells surround neuronal bodies (black arrowheads in magnified images G-I), while at 14, 21 and 28dpi microglial clusters (black arrowheads in magnified images J-L) and lymphocytes (empty arrowheads in magnified images J-L) are easily identifiable. **(M-U)** Triple immunolabelling combining Iba1 (green in M-O) with CD3 (red in P-R) and CD45 (purple in S-U) at 14dpi counterstained with DAPI (blue) in WT, GFAP-IL6Tg and GFAP-IL10Tg, confirmed the infiltration of T-lymphocytes (white arrowheads) near to highly CD45-positive microglia, also forming clusters (white arrows). **(V, X)** Histograms showing the time course of CD45 staining, expressed as AI (Area x Intensity) from GFAP-IL6Tg and GFAP-IL10Tg mice with their corresponding WT. Note that in all mouse lines, there was a significant increase of CD45 staining at 3 and 7dpi followed by a downregulation until 28dpi. Differences were determined in comparison with the previous time-point in WT (a# $p \leq 0.1$; a´´$p \leq 0.01$; a´´´$p \leq 0.001$; a´´´´$p \leq 0.0001$) and in transgenic mice line (b# $p \leq 0.1$; b´´$p \leq 0.01$; b´´´ $p \leq 0.001$; b´´´´ $p \leq 0.001$). Differences between transgenic and WT levels (*$p \leq 0.05$; **$p \leq 0.01$; ***$p \leq 0.001$) were represented in the graphs as well. GFAP-IL6Tg animals showed higher CD45 levels in basal conditions and at 3 and 14dpi, whereas GFAP-IL10Tg presented lower CD45 at 7dpi. Data are represented as ± SEM. **(W)** Histogram showing the fold changes increase of CD45 expression in comparison to the corresponding NL animals from both WT and GFAP-IL6Tg mice. Remarkably, transgenic animals showed lower fold increase than WT ones. Scale bar (A-L): 50 µm, (M-U): 10 µm.

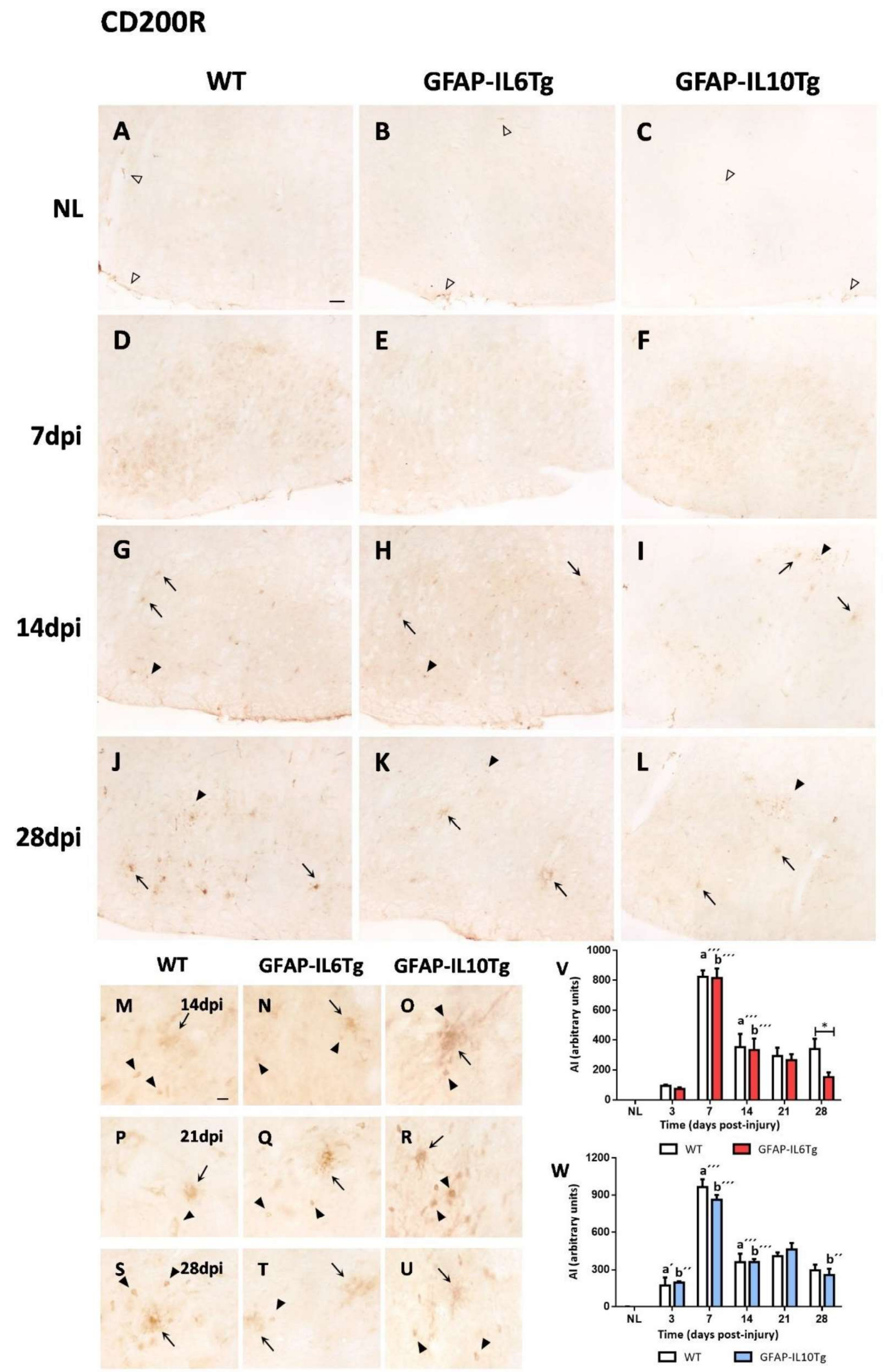
CD200R
WT
GFAP-IL6Tg
GFAP-IL10Tg
NL
7dpi
14dpi
28dpi
A
B
C
D
E
F
G
H
I
J
K
L
WT
GFAP-IL6Tg
GFAP-IL10Tg
M
14dpi
N
O
P
21dpi
Q
R
S
28dpi
T
U
V
AI (arbitrary units)
1000
800
600
400
200
0
NL
3
7
14
21
28
Time (days post-injury)
a´´´
b´´´
*
WT
GFAP-IL6Tg
W
AI (arbitrary units)
1200
900
600
300
0
a´
b´´
Time (days post-injury)
WT
GFAP-IL10Tg

Figure 7. Temporal expression pattern of CD200R after FNA in GFAP-IL6Tg, GFAP-IL10Tg and WT mice. (A-L) Representative images of single CD200R staining in the NL

(A-C) and lesioned FN at 7, 14 and 28dpi (D-L) from WT, GFAP-IL6Tg and GFAP-IL10Tg mice. Note that, in basal conditions, only peripheral and perivascular macrophages could be detected to express CD200R in all genotypes (empty arrowheads in A-C). After lesion, at 7dpi, CD200R diffuse expression covered all the FN (D-F), and at later time-points (14 to 28dpi), CD200R staining was mainly restricted to microglial clusters (black arrows in G-L) and spherical cells that could be considered as lymphocytes (black arrowheads in G-L). **(M-U)** Magnification of CD200R at 14 (M-O), 21 (P-R) and 28dpi (S-U) clearly showed that CD200R was mostly present on microglial clusters (black arrows) and lymphocytes (black arrowheads) in all mouse lines. **(V-W)** Histograms showing CD200R time course, expressed as AI. Note that, at early time-points WT, GFAP-IL6Tg and GFAP-IL10Tg animals showed an increase of CD200R, being significant at 7dpi, followed by a significant decrease at 14, 21 and 28dpi (a´$p \leq 0.05$; a´´´$p \leq 0.001$ compared to previous time-point in WT, b´´$p \leq 0.01$; b´´´$p \leq 0.001$ compared to previous time-point in transgenic animals). At 28dpi, GFAP-IL6Tg displayed lower CD200R levels compared to WT littermates (*$p \leq 0.05$). Data are represented as ± SEM. Scale bar (A-L): 50 µm, (M-U): 10 µm.

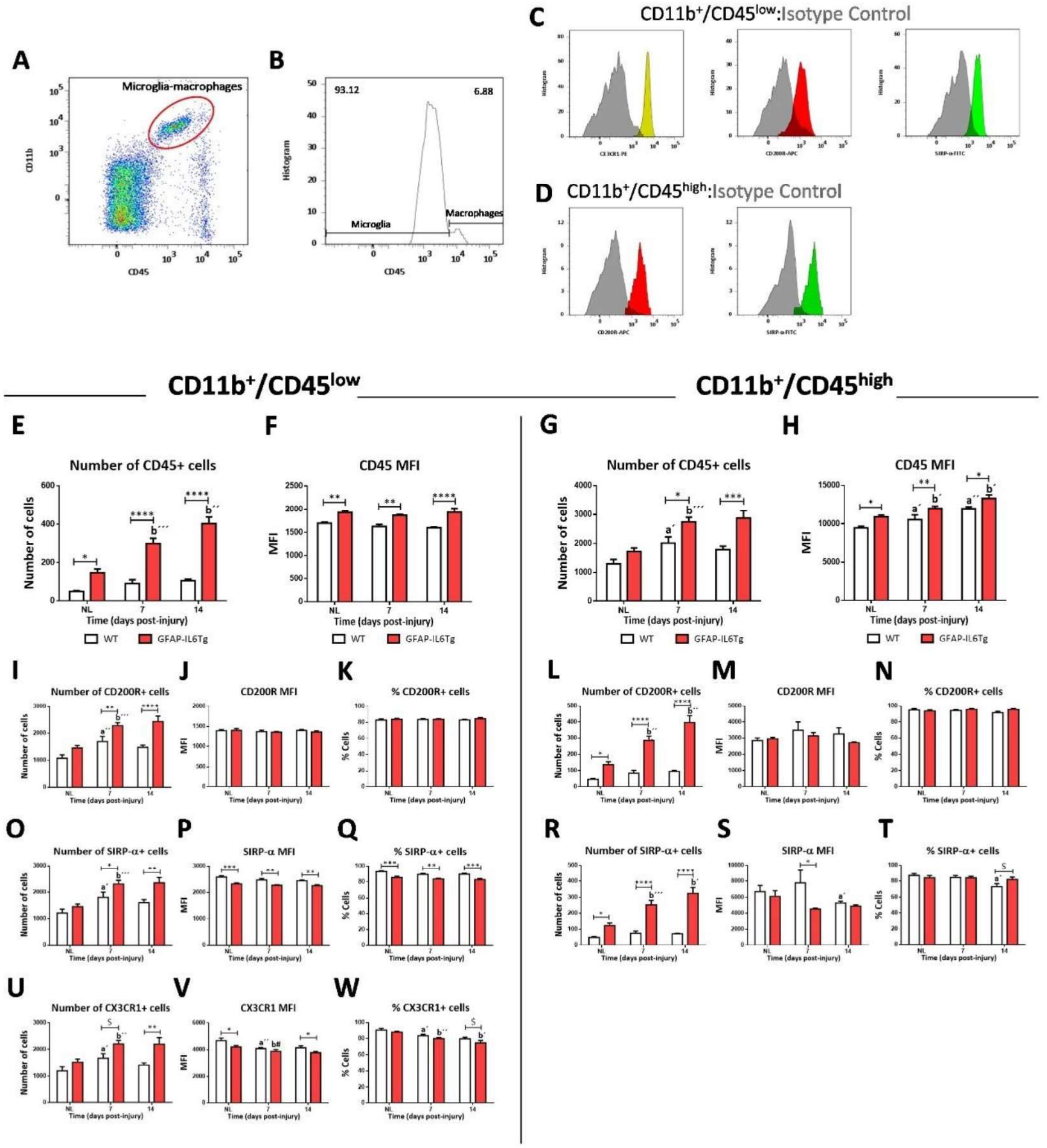

Figure 8. Flow cytometry analysis of "Off" receptors CD200R, SIRP-α and CX3CR1 expression in microglial (CD11b$^+$/CD45^{low}) and macrophage/highly activated microglial (CD11b$^+$/CD45^{high}) populations after FNA in GFAP-IL6Tg mice and the corresponding WT littermates. (A) Representative dot-plot of CD11b/CD45 expression in cells obtained from NL FN. The population surrounded by a red circle was considered microglia/macrophages. (**B**) Representative histogram showing microglial/macrophage population. From the two peaks detected, it was possible to define two different populations: CD11b$^+$/CD45^{low} considered as microglia and CD11b$^+$/CD45^{high} considered as macrophages/highly activated microglia. **(C-D)** Representative histogram-plot showing the expression of CX3CR1, CD200R and SIRP-α in the population of microglia (C) and macrophages/highly activated microglia (D) in comparison to the corresponding isotype control. **(E-H)** Histograms showing the total number of cells and mean fluorescent intensity (MFI) of CD45 in microglial (E-F) and

macrophage/highly activated microglial (G-H) populations in basal conditions and at 7 and 14dpi in both WT and GFAP-IL6Tg mice. **(I-K, O-Q, U-W)** Histograms showing the total number of cells in microglial populations, MFI, and percentage of cells expressing CD200R (I-K), SIRP-α (O-Q) and CX3CR1 (U-W) in basal conditions and at 7 and 14dpi from both genotypes. **(L-N, R-T)** Histograms showing the total number of macrophages and highly activated microglial cells, MFI, and percentage of cells expressing CD200R (L-N) and SIRP-α (R-T) in basal conditions and at 7 and 14dpi from both genotypes. Differences between time-points were assessed in comparison to the previous time-point in WT (a´$p\leq0.05$; a ´´$p\leq0.01$) and in GFAP-IL6Tg animals, (b#$p\leq0.1$; b´$p\leq0.05$; b´´$p\leq0.01$; b´´´$p\leq0.001$). Significant differences between genotypes were indicated as follows: \$$p\leq0.1$; *$p\leq0.05$; **$p\leq0.01$; ***$p\leq0.001$; ****$p\leq0.0001$. Data are represented as ± SEM.

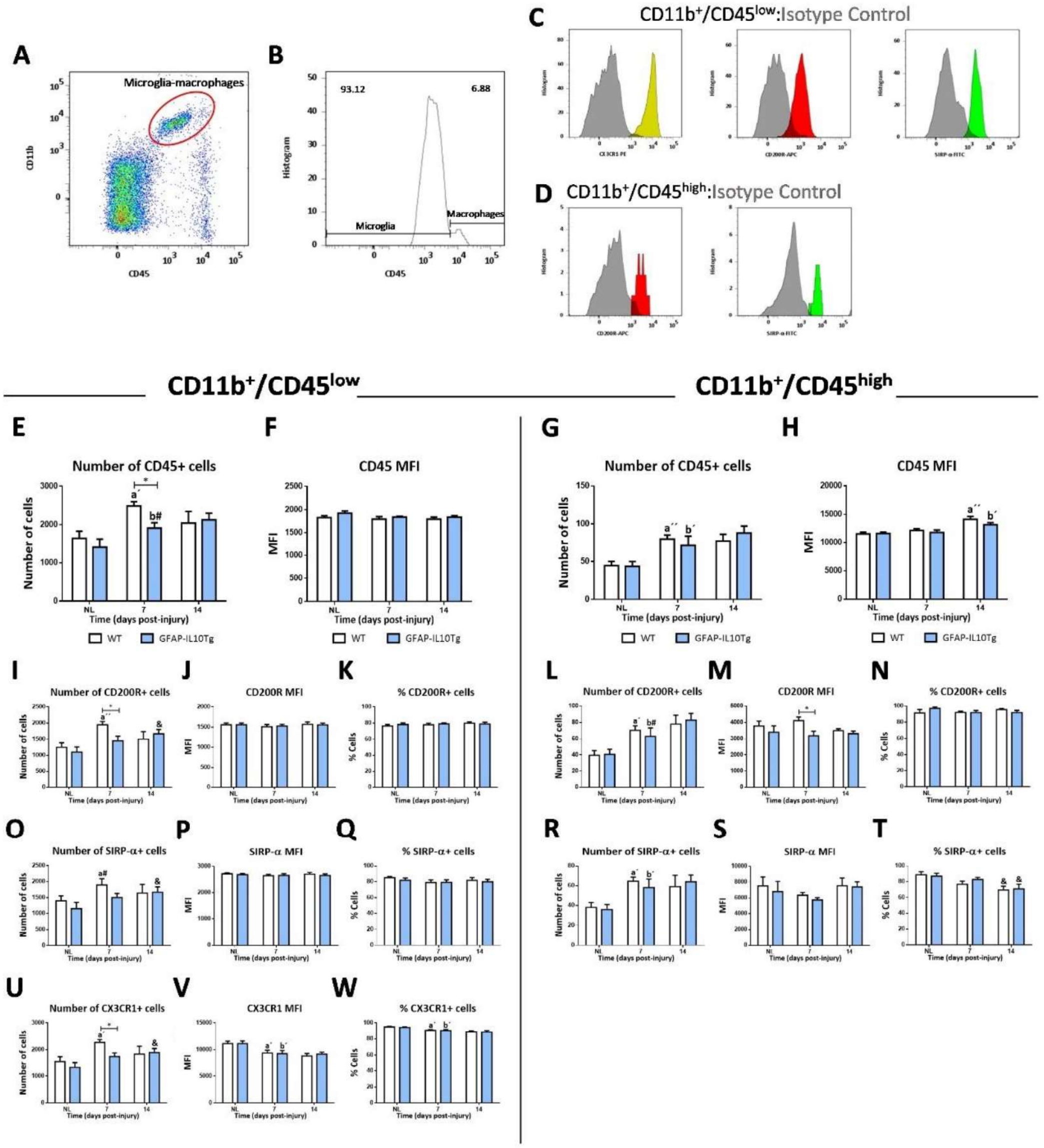

Figure 9. Flow cytometry analysis of "Off" receptors CD200R, SIRP-α and CX3CR1 expression in microglial (CD11b$^+$/CD45^{low}) and macrophage/highly activated microglial (CD11b$^+$/CD45^{high}) populations after FNA in GFAP-IL10Tg mice and the corresponding WT littermates. (A) Representative dot-plot of CD11b/CD45 expression in cells obtained from NL FNs. The population surrounded by a red circle was considered microglia/macrophages. (**B**) Representative histogram showing microglial/macrophage population. From the two peaks detected, it was possible to define two different populations: CD11b$^+$/CD45^{low} considered as microglia and CD11b$^+$/CD45^{high} considered as macrophages/highly activated microglia. **(C-D)** Representative histogram-plot showing the expression of CX3CR1, CD200R and SIRP-α in the population of microglia (C) and macrophages/highly activated microglia (D) in comparison to the corresponding isotype control. **(E-H)** Histograms showing the total number of cells and MFI of CD45 in microglial (E-F) and macrophage/highly activated

microglial (G-H) populations in basal conditions and at 7 and 14dpi in both WT and GFAP-IL10Tg mice. **(I-K, O-Q, U-W)** Histograms showing the total number of cells in microglial populations, MFI, and percentage of cells expressing CD200R (I-K), SIRP-α (O-Q) and CX3CR1 (U-W) in basal conditions and at 7 and 14dpi from both genotypes. **(L-N, R-T)** Histograms showing the total number of macrophages and highly activated microglial cells, MFI, and percentage of cells expressing CD200R (L-N) and SIRP-α (R-T) in basal conditions and at 7 and 14dpi from both genotypes. Differences between time-points were assessed in comparison to the previous time-point in WT (a#p≤0.1; a´p≤0.05; a ´´p≤0.01) and in GFAP-IL10Tg animals, (b#p≤0.1; b´p≤0.05). & (p≤0.05) indicates differences in all genotypes compared to NL. Significant differences between genotypes were indicated as follows: *p≤0.05. Data are represented as ± SEM.

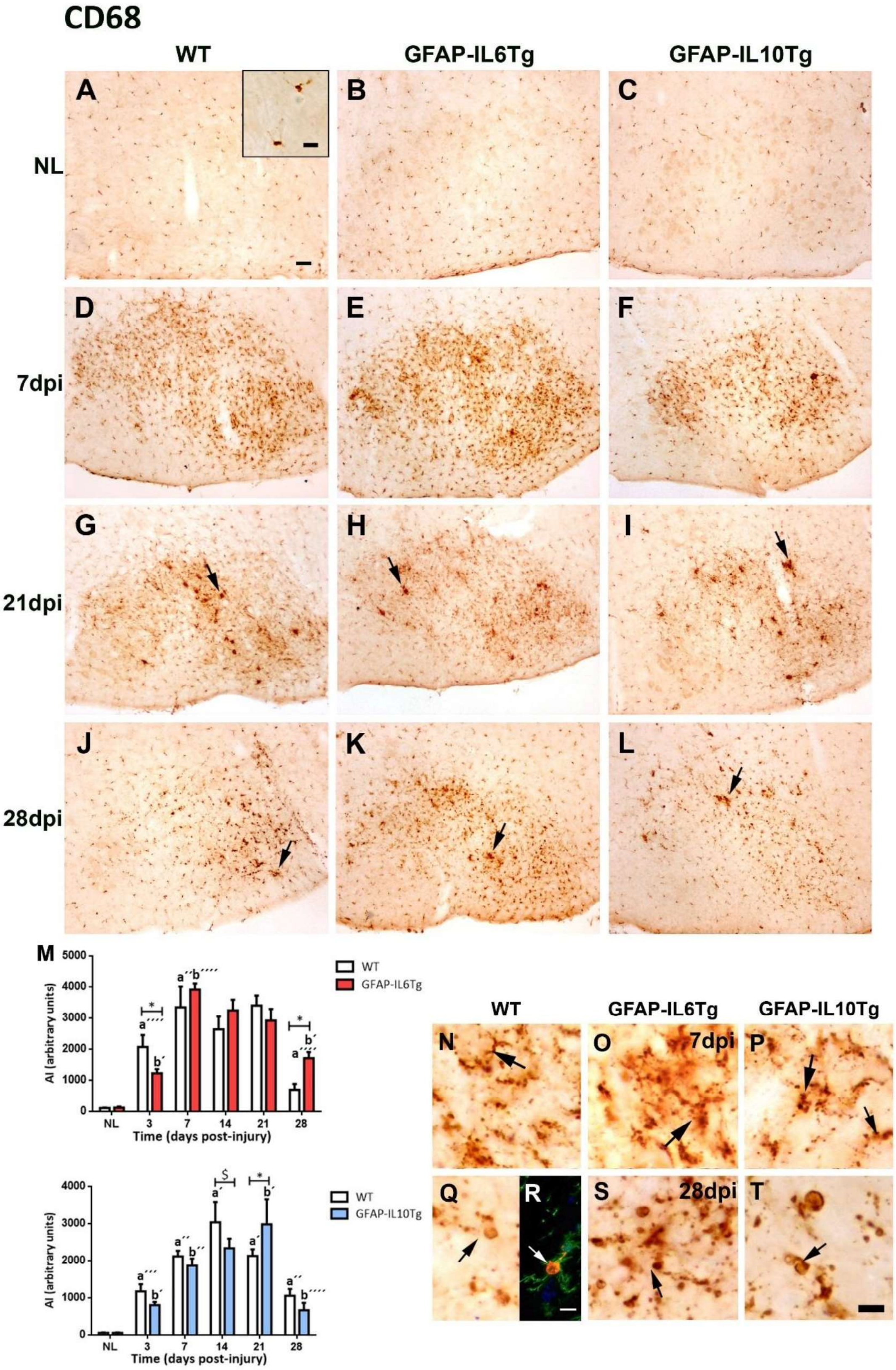
CD68
WT
GFAP-IL6Tg
GFAP-IL10Tg
A
B
C
NL
D
E
F
7dpi
G
H
I
21dpi
J
K
L
28dpi
M
5000
4000
3000
2000
1000
0
AI (arbitrary units)
NL
3
7
14
21
28
Time (days post-injury)
WT
GFAP-IL6Tg
*
a´´´´
b´
a´´b´´´´
*
b´
a´´´´
AI (arbitrary units)
4000
3000
2000
1000
0
NL
3
7
14
21
28
Time (days post-injury)
WT
GFAP-IL10Tg
a´´´
b´
a´´
b´´
$
a´
*
b´
a´
a´´
b´´´´
WT
GFAP-IL6Tg
GFAP-IL10Tg
N
O
7dpi
P
Q
R
S
28dpi
T

Figure 10. Temporal expression pattern of CD68 after FNA in GFAP-IL6Tg, GFAP-IL10Tg and WT mice. (A-L) Representative images of CD68 immunohistochemistry in NL (A-C) and lesioned FN at 7 (D-F), 21 (G-I) and 28dpi (J-L) from WT, GFAP-IL6Tg and GFAP-IL10Tg animals. **(M)** Histograms showing the quantification of CD68 AI time course along the lesion in GFAP-IL6Tg (red), GFAP-IL10Tg (blue) and their corresponding WT littermates. Differences assessed comparing to the previous time-point in WT (a´p≤0.05; a´´p≤0.01; a´´´p≤0.001; a´´´´p≤0.0001) and transgenic mice (b´p≤0.05; b´´p≤0.01; b´´´´p≤0.0001) showed that, there was a significant increase of CD68 reaching a peak between at 7 and 14dpi, followed by a downregulation at 28dpi. Differences between transgenic and WT levels ($p≤0.1; *p≤0.05) were represented in the graphs as well. GFAP-IL6Tg animals had lower CD68 levels at 3dpi and higher levels at 28dpi, whereas GFAP-IL10Tg presented a downregulation of CD68 at 14dpi and an upregulation at 21dpi in comparison with WT mice. **(N-T)** Magnificated images from WT, GFAP-IL6Tg and GFAP-IL10Tg mouse lines showing the morphology of CD68 positive cells (black arrows) in the ipsilateral FN at 7 (N-P) and 28dpi (Q-T). CD68 (orange) col-localized with microglial Iba1 (green) marker (white arrow in R). Data are represented as ± SEM. Scale bar (A-L): 50 µm, (N-T): 10 µm.

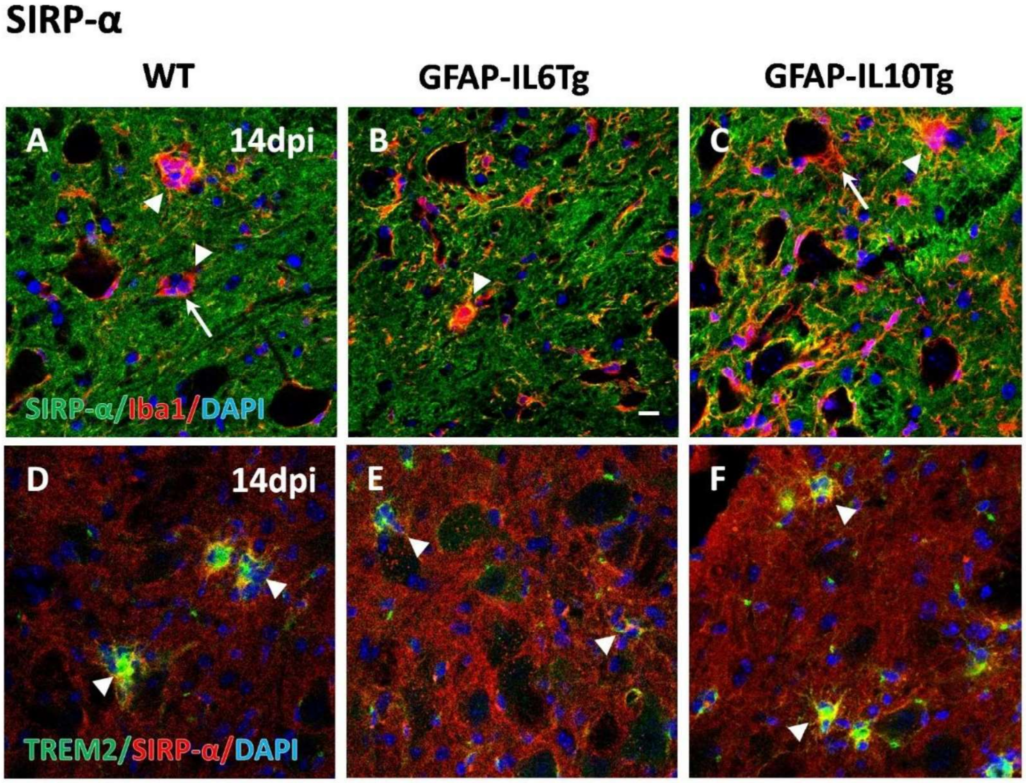

Figure 11. Expression of SIRP-α in phagocytic microglial clusters from GFAP-IL6Tg, GFAP-IL10Tg and WT mice. (A-C) Double immunohistochemical stainings combining SIRP-α (green) and Iba-1 (red) show microglia clusters with elevated levels of SIRP-α (arrowheads) and low expression of SIRP-α (arrows), in WT, GFAP-IL6Tg and GFAP-IL10Tg. **(D-F)** Double immunohistochemical stainings combining SIRP-α (red) and TREM2 (green) demonstrate that microglia clusters contained elevated levels of SIRP-α (arrowheads) in TREM2-positive clusters in WT, GFAP-IL6Tg and GFAP-IL10Tg. (A-F): 10 µm.

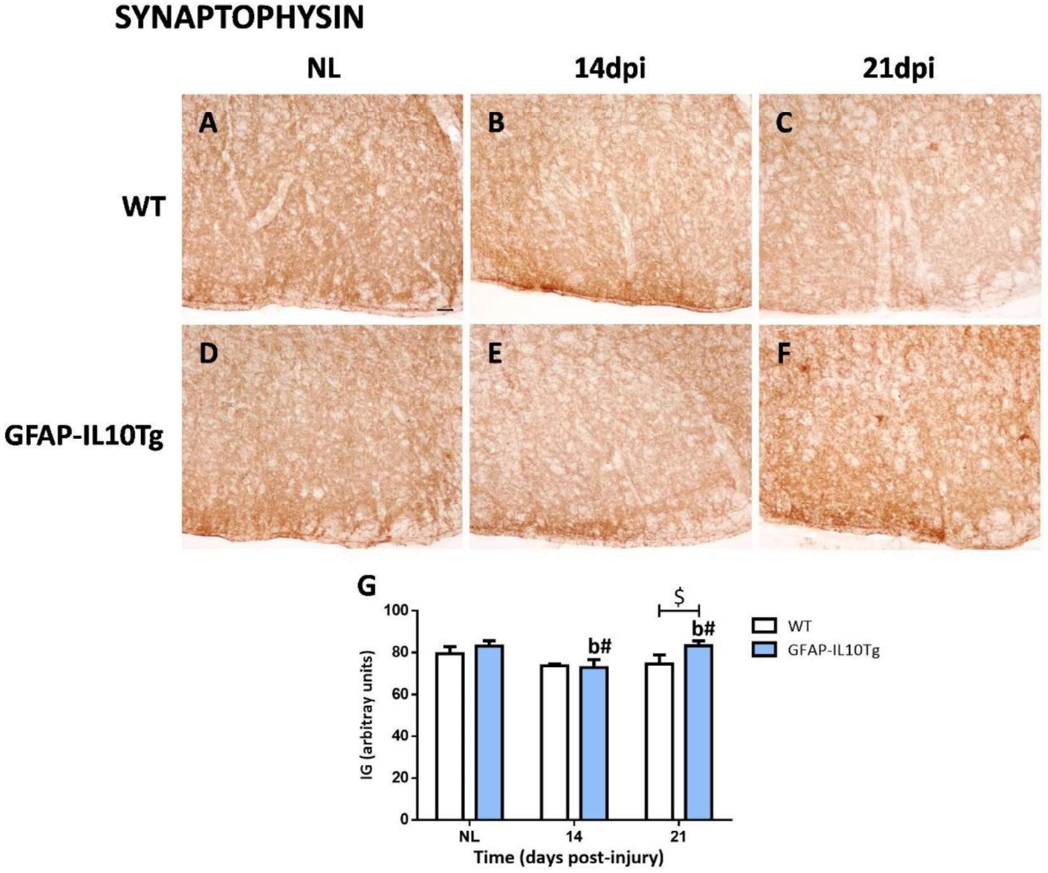
SYNAPTOPHYSIN
NL
14dpi
21dpi
WT
GFAP-IL10Tg
A
B
C
D
E
F
G
$
b#
b#
WT
GFAP-IL10Tg
IG (arbitray units)
100
80
60
40
20
0
NL
14
21
Time (days post-injury)

Figure 12. Temporal expression pattern of Synaptophysin after FNA in GFAP-IL10Tg and WT mice. (A-F) Representative images showing single Synaptophysin staining in the NL (A, D) and lesioned FN at 14 (B, E) and 21dpi (C, F) from WT and GFAP-IL10Tg mice. **(G)** Histogram showing Synaptophysin time course, expressed as IG along all the lesion in both mouse lines. Note that at 21dpi, transgenic mice showed slightly higher Synaptophysin levels ($p≤0.1). Data are represented as ± SEM. Scale bar (A-F): 50 µm.

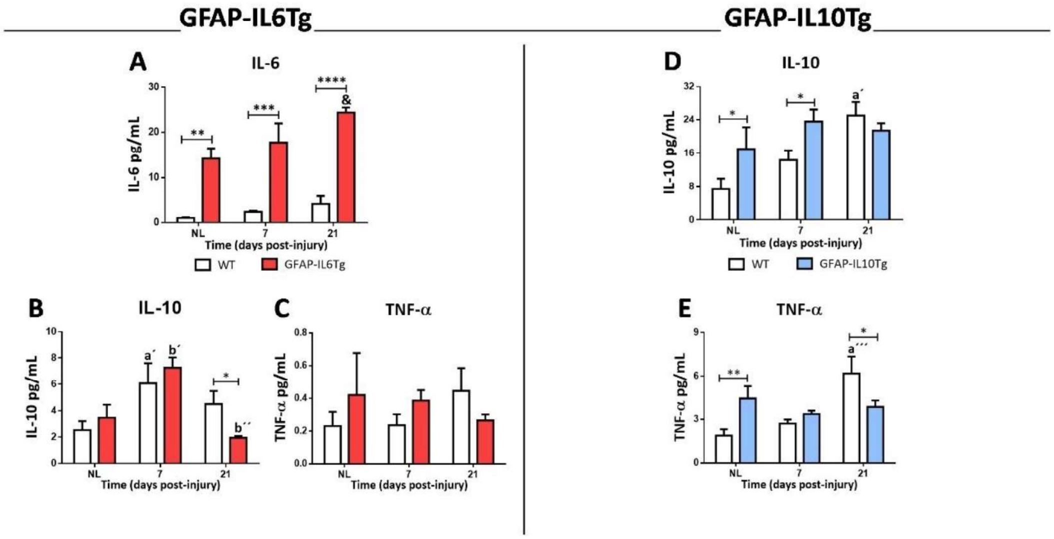

Supplementary Figure 1. Cytokine expression in GFAP-IL6Tg, GFAP-IL10Tg and WT mice. (A-C) Graphs showing the time course of IL-6 (A), IL-10 (B) and TNF-α (C) in the NL and lesioned FN at 7 and 21dpi in both WT and GFAP-IL6Tg animals. **(D-E)** Graphs showing the time course of IL-10 (D) and TNF-α (E) in NL and at 7 and 21dpi in both WT and GFAP-IL10Tg animals. The significance is represented compared to previous time-point in WT mice (a´$p \leq 0.05$; a´´´$p \leq 0.001$) and in transgenic mice (b´≤0.05; b´´≤0.01). & ($p \leq 0.05$) indicates significances respect to NL. Differences between genotypes (*$p \leq 0.05$; **$p \leq 0.01$; ***$p \leq 0.001$; ****$p \leq 0.0001$) were also indicated in the graphs. Data are represented as ± SEM.

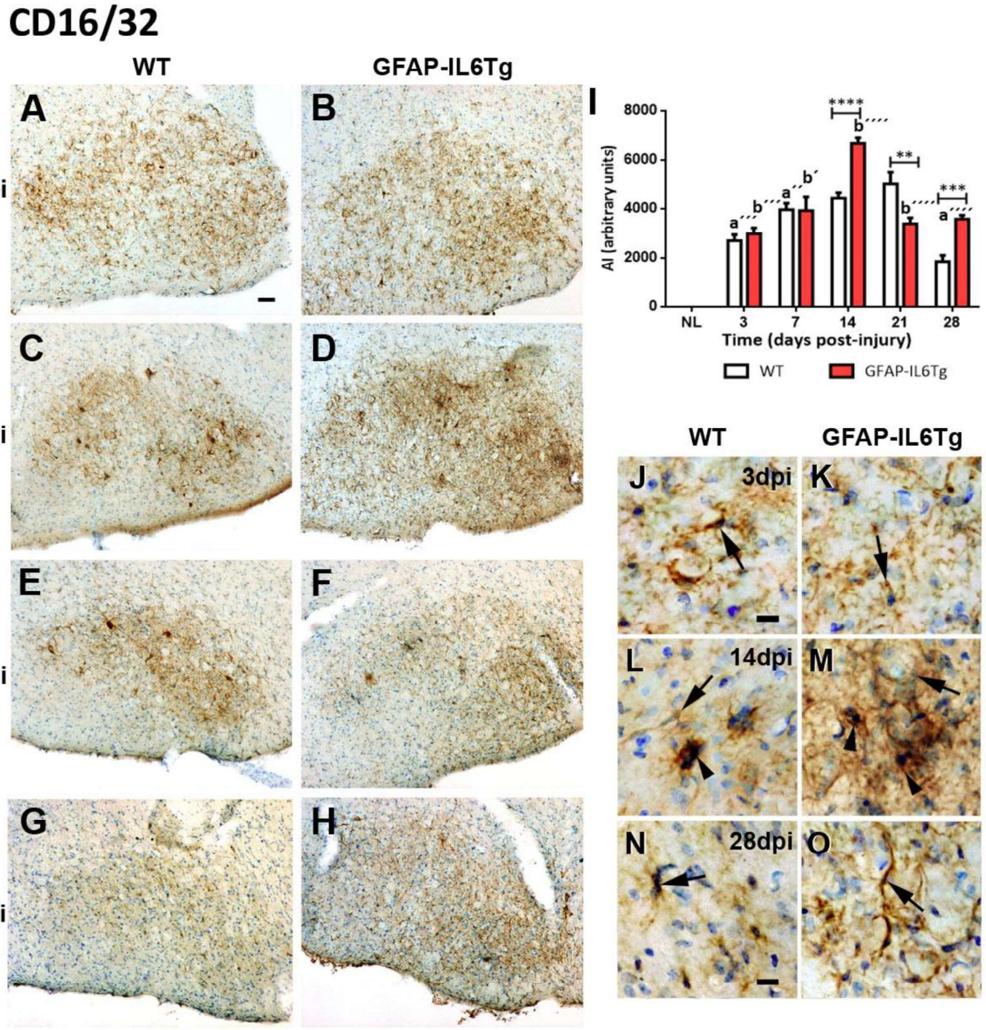
CD16/32
WT
GFAP-IL6Tg
A
B
3dpi
C
D
14dpi
E
F
21dpi
G
H
28dpi
I
8000
6000
4000
2000
0
AI (arbitrary units)
a´´´
b´´´
a´´
b´
****
b´´´´
**
b´´´´
***
a´´´´
NL
3
7
14
21
28
Time (days post-injury)
WT
GFAP-IL6Tg
WT
GFAP-IL6Tg
J
3dpi
K
L
14dpi
M
N
28dpi
O

Supplementary Figure 2. Temporal expression pattern of CD16/32 after FNA in GFAP-IL6Tg and WT mice. (A-H) Representative images of CD16/32 immunohistochemistry in axotomized FN at 3 (A, B), 14 (C, D), 21 (E, F) and 28dpi (G, H) from both WT and GFAP-IL6Tg animals. **(I)** Histogram showing the quantification of CD16/32 AI time course along the lesion in GFAP-IL6Tg and their corresponding WT littermates. Differences assessed comparing to the previous time-point in WT (a´´p≤0.01; a´´´p≤0.001; a´´´´p≤0.0001) and transgenic mice (b´p≤0.05; b´´´p≤0.001; b´´´´p≤0.0001) showed that, there was a significant increase of CD16/32 at 7 and 14dpi, followed by a downregulation at 21 and 28dpi. Differences between transgenic and WT levels (**p≤0.01; ***p≤0.001; ****p≤0.0001) were represented in the graph as well. GFAP-IL6Tg animals showed higher CD16/32 levels at 14 and 28dpi, while they underwent a downregulation at 21dpi compared to WT mice. **(J-O)** Magnification images from WT and GFAP-IL6Tg showing the morphology of CD16/32 positive cells (black arrows) in the ipsilateral FN at 3 (J, K), 14 (L, M) and 28dpi (N, O). At 14dpi, microglial clusters displayed strong CD16/32 staining (black arrowheads in L and M). Data are represented as ± SEM. Scale bar (A-H): 50 µm, (J-O): 10 µm.

TABLES

TABLE 1 Reagents used in immunohistochemistry (IHC)

	Target Antigen/Conjugation	Host/Target	Dilution	Cat Number	Manufacturer
Primary antibodies	CD3	Hamster	1:500	MCA2690	AbD Serotec
	CD16/32	Rat	1:1000	553142	BD Pharmingen
	CD22	Rabbit	1:200	GTX59644	GeneTex
	CD45	Rat	1:1000	MCA1031	Bio-Rad
	CD47	Rat	1:100	127502	BioLegend
	CD68	Rat	1:1000	MCA1957	AbD Serotec
	CD200	Goat	1:250	AF3355	R&D Systems
	CD200	Rat	1:250	MCA1958	AbD Serotec
	CD200R	Goat	1:300	AF2554	R&D Systems
	CX3CL1	Rabbit	1:500	Ab25088	Abcam
	GFAP	Mouse	1:6000	63893	Sigma-Aldrich
	Iba1	Rabbit	1:1000	GTX100042	GeneTex
	MBP	rabbit	1:500	A0623	Dako
	NeuN	Mouse	1:200	MAB377B	Merck Millipore
	SIRP-α	Rat	1:250	144002	BioLegend
	synaptophysin	Mouse	1:6000	837103	BioLegend
Lectin	TL		1:150	L0651	Sigma-Aldrich
Secondary antibodies	Alexa 568	Hamster	1:1000	A21112	Invitrogen
	Alexa 488	Mouse	1:1000	A11029	ThermoFisher
	Alexa 555	Mouse	1:1000	A31570	Invitrogen
	Alexa 488	Rabbit	1:1000	A21206	Invitrogen
	Alexa 555	Rabbit	1:1000	A21428	Invitrogen
	Alexa 488	Rat	1:1000	A11006	ThermoFisher
	Alexa 555	Rat	1:1000	A21434	ThermoFisher
	Alexa 647	Rat	1:1000	A21247	Invitrogen
	Biotinylated	Goat	1:500	BA-9500	Vector Laboratories
	Biotinylated	Rabbit	1:500	BA-1000	Vector Laboratories
	Biotinylated	Rat	1:500	BA-4001	Vector

					Laboratories
	Biotinylated	Mouse IgM	1:500	E0465	DakoCytomation
Alexa Fluor-488 conjugated Streptavidin			1:1000	S11223	ThermoFisher
HRP-conjugated Streptavidin			1:500	SA-5004	Vector Laboratories
DAPI			1:10000	D9542	Sigma-Aldrich

TABLE 2 Reagents used in Flow Cytometry

Target antigen		Format	Dilution	Cat Number	Manufacturer
Fc Blocker	CD16/32	Purified	1:250	553142	BD Biosciences
Primary antibodies	CD11b	APC-Cy7	1:400	557657	BD Biosciences
	CD45	PerCP	1:400	557235	BD Biosciences
	CD200R	Alexa 647	1:50	566345	BD Biosciences
	CX3CR1	PE	1:400	FAB5825P	R&D Systems
	SIRP-α	FITC	1:200	144005	BioLegend
Isotype controls	IgG2b κ	APC-Cy7	1:400	552773	BD Biosciences
	IgG2b κ	PerCP	1:400	552991	BD Biosciences
	IgG2a	AF647	1:50	MCA1212	AbD Serotec
	IgG	PE	1:400	403004	BioLegend
	IgG2a κ	FITC	1:200	553929	BD Biosciences

BIBLIOGRAPHY

Acarin L, Gonzalez B, Castellano B, Castro AJ. Quantitative analysis of microglial reaction to a cortical excitotoxic lesion in the early postnatal brain. Exp. Neurol. (1997) 147:410–417. doi: 10.1006/exnr.1997.6593

Adams S, van der Laan LJ, Vernon-Wilson E, Renardel de Lavalette C, Döpp EA, Dijkstra CD, Simmons DL, van den Berg TK. Signal-regulatory protein is selectively expressed by myeloid and neuronal cells. J Immunol. (1998) 161(4):1853-9

Ahn JH, Kim DW, Park JH, Lee TK, Lee HA, Won MH, Lee CH. Expression changes of CX3CL1 and CX3CR1 proteins in the hippocampal CA1 field of the gerbil following transient global cerebral ischemia. Int J Mol Med. (2019) 44(3):939-948

Almolda B, Villacampa N, Manders P, Hidalgo J, Campbell IL, González B, Castellano B. Effects of Astrocyte-Targeted Production of Interleukin-6 in the Mouse on the Host Response to Nerve Injury. Glia. (2014) 62(7):1142-61

Alvarez-Zarate J, Matlung HL, Matozaki T, Kuijpers TW, Maridonneau-Parini I, van den Berg TK. Regulation of Phagocyte Migration by Signal Regulatory Protein-Alpha Signaling. PLoS One. (2015) 10(6):e0127178. doi: 10.1371/journal.pone.0127178.

Bamberger ME, Harris ME, McDonald DR, Husemann J, Landreth GE. A cell surface receptor complex for fibrillar beta-amyloid mediates microglial activation. J Neurosci. (2003) 23(7):2665-74. doi: 10.1523/JNEUROSCI.23-07-02665.2003. PMID: 12684452; PMCID: PMC6742111.

Bian Z, Shi L, Guo YL, Lv Z, Tang C, Niu S, Tremblay A, Venkataramani M, Culpepper C, Li L, Zhou Z, Mansour A, Zhang Y, Gewirtz A, Kidder K, Zen K, Liu Y. Cd47-Sirpα interaction and IL-10 constrain inflammation-induced macrophage phagocytosis of healthy self-cells. Proc Natl Acad Sci U S A. (2016) 113(37):E5434-43. doi: 10.1073/pnas.1521069113

Biber K, Neumann H, Inoue K, Boddeke HW. Neuronal 'On' and 'Off' Signals Control Microglia. Trends Neurosci. (2007) 30(11):596-602

Burmeister AR, Marriott I. The Interleukin-10 Family of Cytokines and Their Role in the CNS. Front Cell Neurosci. (2018) 12:458. doi: 10.3389/fncel.2018.00458

Butovsky O, Jedrychowski MP, Moore CS, Cialic R, Lanser AJ, Gabriely G, Koeglsperger T, Dake B, Wu PM, Doykan CE, Fanek Z, Liu L, Chen Z, Rothstein JD, Ransohoff RM, Gygi SP, Antel JP, Weiner HL. Identification of a Unique TGF-β Dependent Molecular and Functional Signature in Microglia. Nat Neurosci. (2014) 17(1):131-43. doi: 10.1038/nn.359

Cardona AE, Pioro EP, Sasse ME, Kostenko V, Cardona SM, Dijkstra IM, Huang D, Kidd G, Dombrowski S, Dutta R, Lee JC, Cook DN, Jung S, Lira SA, Littman DR, Ransohoff RM. Control of microglial neurotoxicity by the fractalkine receptor Nat Neurosci. (2006) 9(7):917-24. doi: 10.1038/nn1715

Carter DA, Dick AD. CD200 maintains microglial potential to migrate in adult human retinal explant model. Curr Eye Res. (2004) 28(6):427-36. doi: 10.1080/02713680490503778

Chen H, Lin W, Zhang Y, Lin L, Chen J, Zeng Y, Zheng M, Zhuang Z, Du H, Chen R, Liu N. IL-10 Promotes Neurite Outgrowth and Synapse Formation in Cultured Cortical Neurons after the Oxygen-Glucose Deprivation via JAK1/STAT3 Pathway. Sci Rep. (2016b) 6:30459. doi: 10.1038/srep30459. PMID: 27456198; PMCID: PMC4960594.

Chen P, Zhao W, Guo Y, Xu J, Yin M. CX3CL1/CX3CR1 in Alzheimer's Disease: A Target for Neuroprotection. Biomed Res Int. (2016a) 2016:8090918. doi: 10.1155/2016/8090918

Chitnis T, Imitola J, Wang Y, Elyaman W, Chawla P, Sharuk M, Raddassi K, Bronson RT, Khoury SJ. Elevated neuronal expression of CD200 protects Wlds mice from inflammation mediated neurodegeneration. Am J Pathol. (2007) 170(5):1695-712. doi: 10.2353/ajpath.2007.060677

Cockram TOJ, Dundee JM, Popescu AS, Brown GC. The Phagocytic Code Regulating Phagocytosis of Mammalian Cells. Front Immunol. (2021) 12:629979. doi: 10.3389/fimmu.2021.629979

Colton CA. Heterogeneity of microglial activation in the innate immune response in the brain. J Neuroimmune Pharmacol. (2009) 4(4):399-418. doi: 10.1007/s11481-009-9164-4

Comella Bolla A, Valente T, Miguez A, Brito V, Gines S, Solà C, Straccia M, Canals JM. CD200 is up-regulated in R6/1 transgenic mouse model of Huntington's disease. PLoS One. (2019) 14(12): e0224901

Cosenza-Nashat MA, Kim MO, Zhao ML, Suh HS, Lee SC. CD45 isoform expression in microglia and inflammatory cells in HIV-1 encephalitis. Brain Pathol. (2006) 16(4):256-65. doi: 10.1111/j.1750-3639.2006.00027.x

Cougnoux A, Drummond RA, Collar AL, Iben JR, Salman A, Westgarth H, Wassif CA, Cawley NX, Farhat NY, Ozato K, Lionakis MS, Porter FD. Microglia activation in Niemann–Pick disease, type C1 is amendable to therapeutic intervention. Hum Mol Genet. (2018) 27(12):2076-2089. doi: 10.1093/hmg/ddy112

de Vries HE, Hendriks JJ, Honing H, De Lavalette CR, van der Pol SM, Hooijberg E, Dijkstra CD, van den Berg TK. Signal-regulatory protein alpha-CD47 interactions are required for the transmigration of monocytes across cerebral endothelium. J Immunol. (2002) 168(11):5832-9. doi: 10.4049/jimmunol.168.11.5832

Deczkowska A, Amit I, Schwartz M. Microglial immune checkpoint mechanisms. Nat Neurosci. (2018) 21(6):779-786. doi: 10.1038/s41593-018-0145-x

Ding X, Wang J, Huang M, Chen Z, Liu J, Zhang Q, Zhang C, Xiang Y, Zen K, Li L. Loss of microglial SIRPα promotes synaptic pruning in preclinical models of neurodegeneration. Nat Commun. (2021) 12(1):2030. doi: 10.1038/s41467-021-22301-1

Duan RS, Yang X, Chen ZG, Lu MO, Morris C, Winblad B, Zhu J. Decreased fractalkine and increased IP-10 expression in aged brain of APP(swe) transgenic mice. Neurochem Res. (2008) 33(6):1085-9. doi: 10.1007/s11064-007-9554-z

Elberg G, Liraz-Zaltsman S, Reichert F, Matozaki T, Tal M, Rotshenker S. Deletion of SIRPα (signal regulatory protein-α) promotes phagocytic clearance of myelin debris in Wallerian degeneration, axon regeneration, and recovery from nerve injury. J Neuroinflammation. (2019) 16(1):277. doi: 10.1186/s12974-019-1679-x.

Elward K and Gasque P. "Eat Me" and "Don't Eat Me" Signals Govern the Innate Immune Response and Tissue Repair in the CNS: Emphasis on the Critical Role of the Complement System. Mol Immunol. (2003) 40(2-4):85-94

Erta M, Quintana A, Hidalgo J. Interleukin-6, a Major Cytokine in the Central Nervous System. Int J Biol Sci. (2012) 8(9): 1254–1266

Funikov SY, Rezvykh AP, Mazin PV, Morozov AV, Maltsev AV, Chicheva MM, Vikhareva EA, Evgen'ev MB, Ustyugov AA. FUS(1-359) transgenic mice as a model of ALS: pathophysiological and molecular aspects of the proteinopathy. Neurogenetics. (2018) 19(3):189-204. doi: 10.1007/s10048-018-0553-9

Gautam PK, Acharya A. Suppressed expression of homotypic multinucleation, extracellular domains of CD172α (SIRP-α) and CD47 (IAP) receptors in TAMs upregulated by Hsp70-peptide complex in Dalton's lymphoma. Scand J Immunol. (2014) 80(1):22-35. doi: 10.1111/sji.12180

Gitik M, Liraz-Zaltsman S, Oldenborg PA, Reichert F, Rotshenker S. Myelin down-regulates myelin phagocytosis by microglia and macrophages through interactions between CD47 on myelin and SIRPα (signal regulatory protein-α) on phagocytes. J Neuroinflammation. (2011) 8:24. doi: 10.1186/1742-2094-8-24

Graeber MB, Moran LB. Mechanisms of cell death in neurodegenerative diseases: fashion, fiction, and facts. Brain Pathol. (2002) 12(3):385-90. doi: 10.1111/j.1750-3639.2002.tb00452.x. Erratum in: Brain Pathol. 2002 Oct; 12(4):522. PMID: 12146806; PMCID: PMC8095773.

Grimsley C, Ravichandran KS. Cues for apoptotic cell engulfment: eat-me, don't eat-me and come-get-me signals. Trends Cell Biol. (2003) 13(12):648-56

Han MH, Lundgren DH, Jaiswal S, Chao M, Graham KL, Garris CS, Axtell RC, Ho PP, Lock CB, Woodard JI, Brownell SE, Zoudilova M, Hunt JF, Baranzini SE, Butcher EC, Raine CS, Sobel RA, Han DK, Weissman I, Steinman L. Janus-like opposing roles of CD47 in autoimmune brain inflammation in humans and mice. J Exp Med. (2012) 209(7):1325-34. doi: 10.1084/jem.20101974

Hanisch UK and Kettenmann H. Microglia: Active Sensor and Versatile Effector Cells in the Normal and Pathologic Brain. Nat Neurosci. (2007) 10(11):1387-94

Hanisch UK. Microglia as a source and target of cytokines. Glia. (2002) 40(2):140-55. doi: 10.1002/glia.10161

Harrison JK, Jiang Y, Chen S, Xia Y, Maciejewski D, McNamara RK, Streit WJ, Salafranca MN, Adhikari S, Thompson DA, Botti P, Bacon KB, Feng L. Role for neuronally derived fractalkine in mediating interactions between neurons and CX3CR1-expressing microglia. Proc Natl Acad Sci U S A. (1998) 95(18):10896-901. doi: 10.1073/pnas.95.18.10896

Hoek RM, Ruuls SR, Murphy CA, Wright GJ, Goddard R, Zurawski SM, Blom B, Homola ME, Streit WJ, Brown MH, Barclay AN, Sedgwick JD. Down-regulation of the macrophage lineage through interaction with OX2 (CD200). Science. (2000) 290(5497):1768-71. doi: 10.1126/science.290.5497.1768

Hsieh CP, Chang WT, Lee YC, Huang AM. Deficits in cerebellar granule cell development and social interactions in CD47 knockout mice. Dev Neurobiol. (2015) 75(5):463-84. doi: 10.1002/dneu.22236

Huang AM, Wang HL, Tang YP, Lee EH. Expression of integrin-associated protein gene associated with memory formation in rats. J Neurosci. (1998) 18(11):4305-13. doi: 10.1523/JNEUROSCI.18-11-04305.1998. PMID: 9592107; PMCID: PMC6792811.

Hughes PM, Botham MS, Frentzel S, Mir A, Perry VH. Expression of fractalkine (CX3CL1) and its receptor, CX3CR1, during acute and chronic inflammation in the rodent CNS. Glia. (2002) 37(4):314-27

Hutter G, Theruvath J, Graef CM, Zhang M, Schoen MK, Manz EM, Bennett ML, Olson A, Azad TD, Sinha R, Chan C, Assad Kahn S, Gholamin S, Wilson C, Grant G, He J, Weissman IL, Mitra SS, Cheshier SH. Microglia are effector cells of CD47-SIRPα antiphagocytic axis disruption against glioblastoma. Proc Natl Acad Sci U S A. (2019) 116(3):997-1006. doi: 10.1073/pnas.1721434116

Kettenmann H, Hanisch UK, Noda M, Verkhratsky A. Physiology of microglia. Physiol Rev. (2011) 91(2):461-553

Kloss CU, Werner A, Klein MA, Shen J, Menuz K, Probst JC, Kreutzberg GW, Raivich G. Integrin family of cell adhesion molecules in the injured brain: regulation and cellular localization in the normal and regenerating mouse facial motor nucleus. J Comp Neurol. (1999) 411(1):162-78. doi: 10.1002/(sici)1096-9861(19990816)411:1<162::aid-cne12>3.0.co;2-w. PMID: 10404114.

Koenigsknecht J, Landreth G. Microglial phagocytosis of fibrillar beta-amyloid through a beta1 integrin-dependent mechanism. J Neurosci. (2004) 24(44):9838-46. doi: 10.1523/JNEUROSCI.2557-04.2004. PMID: 15525768; PMCID: PMC6730228.

Koning N, Bö L, Hoek RM, Huitinga I. Downregulation of macrophage inhibitory molecules in multiple sclerosis lesions. Ann Neurol. (2007) 62(5):504-14. doi: 10.1002/ana.21220

Koning N, Swaab DF, Hoek RM, Huitinga I. Distribution of the Immune Inhibitory Molecules CD200 and CD200R in the Normal Central Nervous System and Multiple Sclerosis Lesions Suggests Neuron-Glia and Glia-Glia Interactions. J Neuropathol Exp Neurol. (2009) 68(2):159-67

Kreutzberg GW. Microglia: a sensor for pathological events in the CNS. Trends Neurosci. (1996) 19(8):312-8. doi: 10.1016/0166-2236(96)10049-7

Lago N, Pannunzio B, Amo-Aparicio J, López-Vales R, Peluffo H. CD200 Modulates Spinal Cord Injury Neuroinflammation and Outcome Through CD200R1. Brain Behav Immun. (2018) 73:416-426

Lauro C, Catalano M, Trettel F, Mainiero F, Ciotti MT, Eusebi F, Limatola C. The chemokine CX3CL1 reduces migration and increases adhesion of neurons with mechanisms dependent on the beta1 integrin subunit. J Immunol. (2006)177(11):7599-606. doi: 10.4049/jimmunol.177.11.7599. PMID: 17114429.

Lehrman EK, Wilton DK, Litvina EY, Welsh CA, Chang ST, Frouin A, Walker AJ, Heller MD, Umemori H, Chen C, Stevens B. CD47 Protects Synapses from Excess Microglia-Mediated Pruning During Development. Neuron. (2018) 100(1):120-134

Lim SH, Park E, You B, Jung Y, Park AR, Park SG, Lee JR. Neuronal synapse formation induced by microglia and interleukin 10. PLoS One (2013) 8:e81218. doi: 10.1371/journal.pone.0081218

Lively S, Schlichter LC. Microglia Responses to Pro-inflammatory Stimuli (LPS, IFNγ+TNFα) and Reprogramming by Resolving Cytokines (IL-4, IL-10). Front. Cell. Neurosci. (2018) 12:215

Lyons A, Downer EJ, Crotty S, Nolan YM, Mills KH, Lynch MA. CD200 ligand receptor interaction modulates microglial activation in vivo and in vitro: a role for IL-4. J Neurosci (2007) 27(31):8309-13

Lyons A, McQuillan K, Deighan BF, O'Reilly JA, Downer EJ, Murphy AC, Watson M, Piazza A, O'Connell F, Griffin R, Mills KH, Lynch MA. Decreased neuronal CD200 expression in IL-4-deficient mice results in increased neuroinflammation in response to lipopolysaccharide. Brain Behav Immun. (2009) 23:1020–1027.

Makwana M, Werner A, Acosta-Saltos A, Gonitel R, Pararajasingam A, Ruff C, Rumajogee P, Cuthill D, Galiano M, Bohatschek M, Wallace AS, Anderson PN, Mayer U, Behrens A, Raivich G. Peripheral facial nerve axotomy in mice causes sprouting of motor axons into perineuronal central white matter: time course and molecular characterization. J Comp Neurol. (2010) 518(5):699-721. doi: 10.1002/cne.22240. Erratum in: J Comp Neurol. (2012) 520(8):ii. Pararajasingham, Abirami [corrected to Pararajasingam, Abirami]. PMID: 20034058; PMCID: PMC4491910.

Manich G, Gómez-López AR, Almolda B, Villacampa N, Recasens M, Shrivastava K, González B, Castellano B. Differential Roles of TREM2+ Microglia in Anterograde and Retrograde Axonal Injury Models. Front Cell Neurosci. (2020) 14:567404. doi: 10.3389/fncel.2020.567404

Manich G, Recasens M, Valente T, Almolda B, González B, Castellano B. Role of the CD200-CD200R Axis During Homeostasis and Neuroinflammation. Neuroscience. (2019) 405:118-136. doi: 10.1016/j.neuroscience.2018.10.030

Matozaki T, Murata Y, Okazawa H, Ohnishi H. Functions and molecular mechanisms of the CD47-SIRPalpha signalling pathway. Trends Cell Biol. (2009) 19(2):72-80. doi: 10.1016/j.tcb.2008.12.001

Miyashita M, Ohnishi H, Okazawa H, Tomonaga H, Hayashi A, Fujimoto TT, Furuya N, Matozaki T. Promotion of neurite and filopodium formation by CD47: roles of integrins, Rac, and Cdc42 Mol Biol Cell. (2004) 15(8):3950-63. doi: 10.1091/mbc.e04-01-0019

Möller JC, Klein MA, Haas S, Jones LL, Kreutzberg GW, Raivich G. Regulation of Thrombospondin in the Regenerating Mouse Facial Motor Nucleus. Glia. (1996) 17(2):121-32

Moran LB, Graeber MB. The Facial Nerve Axotomy Model. Brain Res Brain Res Rev. (2004) 44(2-3):154-78

Mott RT, Ait-Ghezala G, Town T, Mori T, Vendrame M, Zeng J, Ehrhart J, Mullan M, Tan J. Neuronal expression of CD22: novel mechanism for inhibiting microglial proinflammatory cytokine production. Glia. (2004) 46(4):369-79. doi: 10.1002/glia.20009

Murata T, Ohnishi H, Okazawa H, Murata Y, Kusakari S, Hayashi Y, Miyashita M, Itoh H, Oldenborg PA, Furuya N, Matozaki T. CD47 promotes neuronal development through Src- and FRG/Vav2-mediated activation of Rac and Cdc42. J Neurosci. (2006) 26(48):12397-407. doi: 10.1523/JNEUROSCI.3981-06.2006.

Nishiyori A, Minami M, Ohtani Y, Takami S, Yamamoto J, Kawaguchi N, Kume T, Akaike A, Satoh M. Localization of fractalkine and CX3CR1 mRNAs in rat brain: does fractalkine play a role in signaling from neuron to microglia?. FEBS Lett. (1998) 429(2):167-72. doi: 10.1016/s0014-5793(98)00583-3

Ohnishi H, Kaneko Y, Okazawa H, Miyashita M, Sato R, Hayashi A, Tada K, Nagata S, Takahashi M, Matozaki T. Differential localization of Src homology 2 domain-containing protein tyrosine phosphatase substrate-1 and CD47 and its molecular mechanisms in cultured hippocampal neurons. J Neurosci. (2005) 25(10):2702-11. doi: 10.1523/JNEUROSCI.5173-04.2005. PMID: 15758180; PMCID: PMC6725182.

Okazawa H, Motegi S, Ohyama N, Ohnishi H, Tomizawa T, Kaneko Y, Oldenborg PA, Ishikawa O, Matozaki T. Negative regulation of phagocytosis in macrophages by the CD47-SHPS-1 system. J Immunol. (2005) 174(4):2004-11. doi: 10.4049/jimmunol.174.4.2004

Oldenborg PA, Gresham HD, Lindberg FP. CD47-signal regulatory protein alpha (SIRPalpha) regulates Fcgamma and complement receptor-mediated phagocytosis. J Exp Med. (2001) 193(7):855-62. doi: 10.1084/jem.193.7.855.

Perry VH, Teeling J. Microglia and macrophages of the central nervous system: the contribution of microglia priming and systemic inflammation to chronic neurodegeneration. Semin Immunopathol. (2013) 35(5):601-12

Petitto JM, Huang Z, Lo J, Streit WJ. IL-2 gene knockout affects T lymphocyte trafficking and the microglial response to regenerating facial motor neurons. J Neuroimmunol. (2003) 134(1-2):95-103. doi: 10.1016/s0165-5728(02)00422-8

Pluvinage JV, Haney MS, Smith BAH, Sun J, Iram T, Bonanno L, Li L, Lee DP, Morgens DW, Yang AC, Shuken SR, Gate D, Scott M, Khatri P, Luo J, Bertozzi CR, Bassik MC, Wyss-Coray T. CD22 blockade restores homeostatic microglial phagocytosis in ageing brains. Nature. (2019) 568(7751):187-192. doi: 10.1038/s41586-019-1088-4

Raivich G, Jones LL, Kloss CU, Werner A, Neumann H, Kreutzberg GW. Immune surveillance in the injured nervous system: T-lymphocytes invade the axotomized mouse facial motor nucleus and aggregate around sites of neuronal degeneration J Neurosci. (1998) 18(15):5804-16. doi: 10.1523/JNEUROSCI.18-15-05804.1998

Raivich G, Liu ZQ, Kloss CU, Labow M, Bluethmann H, Bohatschek M. Cytotoxic Potential of Proinflammatory Cytokines: Combined Deletion of TNF Receptors TNFR1 and TNFR2 Prevents Motoneuron Cell Death After Facial Axotomy in Adult Mouse. Exp Neurol. (2002) 178(2):186-93

Raivich G, Bohatschek M, Kloss CU, Werner A, Jones LL, Kreutzberg GW. Neuroglial Activation Repertoire in the Injured Brain: Graded Response, Molecular Mechanisms and Cues to Physiological Function. Brain Res Brain Res Rev. (1999) 30(1):77-105

Recasens M, Almolda B, Pérez-Clausell J, Campbell IL, González B, Castellano B. Chronic exposure to IL-6 induces a desensitized phenotype of the microglia. J Neuroinflammation. (2021) 18(1):31. doi: 10.1186/s12974-020-02063-1. PMID: 33482848; PMCID: PMC7821504.

Rogers JT, Morganti JM, Bachstetter AD, Hudson CE, Peters MM, Grimmig BA, Weeber EJ, Bickford PC, Gemma C. CX3CR1 deficiency leads to impairment of hippocampal cognitive function and synaptic plasticity. J. Neurosci. (2011) 31:16241–16250. doi: 10.1523/JNEUROSCI.3667-11.2011

Rothaug M, Becker-Pauly C, Rose-John S. The role of interleukin-6 signaling in nervous tissue. Biochim Biophys Acta. (2016) 1863(6 Pt A):1218-27

Sanchez-Molina P, Almolda B, Benseny-Cases N, González B, Perálvarez-Marín A, Castellano B. Specific microglial phagocytic phenotype and decrease of lipid oxidation in white matter areas during aging: Implications of different microenvironments Neurobiol Aging. (2021) 105:280-295. doi: 10.1016/j.neurobiolaging.2021.03.015

Sanchez-Molina P, Almolda B, Giménez-Llort L, González B, Castellano B. Chronic IL-10 overproduction disrupts microglia-neuron dialogue similar to aging, resulting in impaired hippocampal neurogenesis and spatial memory. Brain Behav Immun. (2022) 101:231-245. doi: 10.1016/j.bbi.2021.12.026. Epub ahead of print. PMID: 34990747.

Sato-Hashimoto M, Nozu T, Toriba R, Horikoshi A, Akaike M, Kawamoto K, Hirose A, Hayashi Y, Nagai H, Shimizu W, Saiki A, Ishikawa T, Elhanbly R, Kotani T, Murata Y, Saito Y, Naruse M, Shibasaki K, Oldenborg PA, Jung S, Matozaki T, Fukazawa Y, Ohnishi H. Microglial SIRPα regulates the emergence of CD11c+ microglia and demyelination damage in white matter. Elife (2019) 8:e42025.doi: 10.7554/eLife.42025

Serpe CJ, Sanders VM, Jones KJ. Kinetics of facial motoneuron loss following facial nerve transection in severe combined immunodeficient mice J Neurosci Res. (2000) 62(2):273-8

Shrivastava K, Gonzalez P, Acarin L. The immune inhibitory complex CD200/CD200R is developmentally regulated in the mouse brain. J Comp Neurol. (2012) 520(12):2657-75

Szepesi Z, Manouchehrian O, Bachiller S, Deierborg T. Bidirectional Microglia-Neuron Communication in Health and Disease. Front Cell Neurosci. (2018) 12:323. doi: 10.3389/fncel.2018.00323

Tan J, Town T, Mori T, Wu Y, Saxe M, Crawford F, Mullan M. CD45 opposes beta-amyloid peptide-induced microglial activation via inhibition of p44/42 mitogen-activated protein kinase. J Neurosci. (2000) 20(20):7587-94. doi: 10.1523/JNEUROSCI.20-20-07587.2000

Toth AB, Terauchi A, Zhang LY, Johnson-Venkatesh EM, Larsen DJ, Sutton MA, Umemori H. Synapse maturation by activity-dependent ectodomain shedding of SIRPα. Nat Neurosci. (2013) 16(10):1417-25. doi: 10.1038/nn.3516.

Valente T, Serratosa J, Perpiñá U, Saura J, Solà C. Alterations in CD200-CD200R1 System during EAE Already Manifest at Presymptomatic Stages. Front Cell Neurosci. (2017) 11: 129

Varnum MM, Kiyota T, Ingraham KL, Ikezu S, Ikezu T. The anti-inflammatory glycoprotein, CD200, restores neurogenesis and enhances amyloid phagocytosis in a mouse model of Alzheimer's disease. Neurobiol Aging. (2015) 36(11):2995-3007. doi: 10.1016/j.neurobiolaging.2015.07.027

Villacampa N, Almolda B, Vilella A, Campbell IL, González B, Castellano B. Astrocyte-targeted production of IL-10 induces changes in microglial reactivity and reduces motor neuron death after facial nerve axotomy. Glia. (2015) 63(7):1166-84. doi: 10.1002/glia.22807

Wang J, Ding X, Wu X, Liu J, Zhou R, Wei P, Zhang Q, Zhang C, Zen K, Li L. SIRPα deficiency accelerates the pathologic process in models of Parkinson disease. Glia. (2019) 67(12):2343-2359. doi: 10.1002/glia.23689.

Wang SK, Xue Y, Cepko CL. Augmentation of CD47/SIRPα signaling protects cones in genetic models of retinal degeneration. JCI Insight. (2021) 6(16):e150796. doi: 10.1172/jci.insight.150796.

Wang XJ, Ye M, Zhang YH, Chen SD. CD200-CD200R regulation of microglia activation in the pathogenesis of Parkinson's disease. J Neuroimmune Pharmacol. (2007) 2(3):259-64. doi: 10.1007/s11481-007-9075-1

Xin J, Wainwright DA, Mesnard NA, Serpe CJ, Sanders VM, Jones KJ. IL-10 within the CNS is necessary for CD4+ T cells to mediate neuroprotection. Brain Behav Immun. (2011) 25(5):820-9. doi: 10.1016/j.bbi.2010.08.004. Epub 2010 Aug 17. PMID: 20723599; PMCID: PMC3021103.

Zhang H, Li F, Yang Y, Chen J, Hu X. SIRP/CD47 signaling in neurological disorders. Brain Res. (2015) 1623:74-80. doi: 10.1016/j.brainres.2015.03.012

Zhou X, Xie Q, Xi G, Keep RF, Hua Y. Brain CD47 expression in a swine model of intracerebral hemorrhage. Brain Res. (2014) 1574:70-6. doi: 10.1016/j.brainres.2014.06.003

ANNEX 5 – ARTICLE 2

Differential Roles of TREM2+ Microglia in Anterograde and Retrograde Axonal Injury Models

frontiers in Cellular Neuroscience

ORIGINAL RESEARCH
published: 20 November 2020
doi: 10.3389/fncel.2020.567404

Differential Roles of TREM2+ Microglia in Anterograde and Retrograde Axonal Injury Models

Gemma Manich†, Ariadna Regina Gómez-López†, Beatriz Almolda*, Nàdia Villacampa, Mireia Recasens, Kalpana Shrivastava, Berta González and Bernardo Castellano

Department of Cell Biology, Physiology, and Immunology, Institute of Neuroscience, Universitat Autònoma De Barcelona, Barcelona, Spain

Microglia are the main immune cells of the central nervous system (CNS), and they are devoted to the active surveillance of the CNS during homeostasis and disease. In the last years, the microglial receptor Triggering Receptor Expressed on Myeloid cells-2 (TREM2) has been defined to mediate several microglial functions, including phagocytosis, survival, proliferation, and migration, and to be a key regulator of a new common microglial signature induced under neurodegenerative conditions and aging, also known as disease-associated microglia (DAM). Although microglial TREM2 has been mainly studied in chronic neurodegenerative diseases, few studies address its regulation and functions in acute inflammatory injuries. In this context, the present work aims to study the regulation of TREM2 and its functions after reparative axonal injuries, using two-well established animal models of anterograde and retrograde neuronal degeneration: the perforant pathway transection (PPT) and the facial nerve axotomy (FNA). Our results indicate the appearance of a subpopulation of microglia expressing TREM2 after both anterograde and retrograde axonal injury. TREM2+ microglia were not directly related to proliferation, instead, they were associated with specific recognition and/or phagocytosis of myelin and degenerating neurons, as assessed by immunohistochemistry and flow cytometry. Characterization of TREM2+ microglia showed expression of CD16/32, CD68, and occasional Galectin-3. However, specific singularities within each model were observed in P2RY12 expression, which was only downregulated after PPT, and in ApoE, where *de novo* expression was detected only in TREM2+ microglia after FNA. Finally, we report that the pro-inflammatory or anti-inflammatory cytokine microenvironment, which may affect phagocytosis, did not directly modify the induction of TREM2+ subpopulation in any injury model, although it changed TREM2 levels due to modification of the microglial activation pattern. In conclusion, we describe a unique TREM2+ microglial subpopulation induced after axonal injury, which is directly associated with phagocytosis of specific cell remnants and show different phenotypes, depending on the microglial activation status and the degree of tissue injury.

Keywords: IL-10 (interleukin-10), IL-6 (interleukin-6), phagocytosis, proliferation, neuroinflammation, microglial clusters, P2RY12, APOE

OPEN ACCESS

Edited by:
Veronica Ines Brito,
University of Barcelona, Spain

Reviewed by:
Andrew David Greenhalgh,
The University of Manchester,
United Kingdom
Audrey Lafrenaye,
Virginia Commonwealth University,
United States

***Correspondence:**
Beatriz Almolda
beatriz.almolda@uab.cat

†These authors have contributed equally to this work

Specialty section:
This article was submitted to Non-Neuronal Cells, a section of the journal Frontiers in Cellular Neuroscience

Received: *29 May 2020*
Accepted: *14 October 2020*
Published: *20 November 2020*

Citation:
Manich G, Gómez-López AR, Almolda B, Villacampa N, Recasens M, Shrivastava K, González B and Castellano B (2020) Differential Roles of TREM2+ Microglia in Anterograde and Retrograde Axonal Injury Models. Front. Cell. Neurosci. 14:567404. doi: 10.3389/fncel.2020.567404

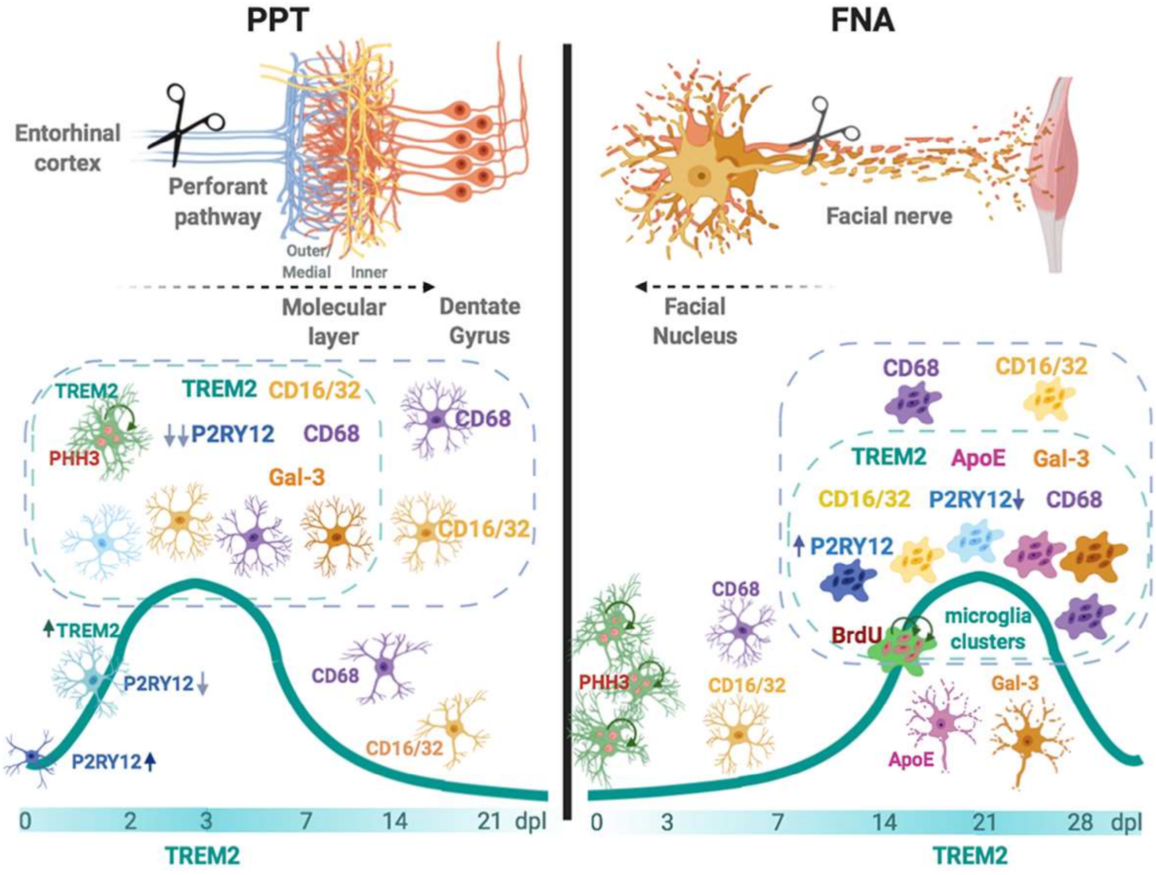

GRAPHICAL ABSTRACT | In the left, after an anterograde axonal injury such as the perforant pathway transection (PPT), TREM2 is rapidly upregulated in a subpopulation of microglia located in the molecular layer. TREM2+ microglia, which can be proliferative, show co-localization with phagocytic CD68 and CD16/32, occasionally with TREM2 phagocytic ligand Galectin-3 (Gal-3), and demonstrates an important P2RY12 downregulation. In the right, after facial nerve axotomy (FNA)—a retrograde axonal injury—TREM2+ microglia is upregulated at late time-points, coinciding with the formation of phagocytic clustered microglia. Microglia clusters can be CD68+ and CD16/32+, may show expression of TREM2 ligands ApoE and Galectin-3, both molecules also observed in the surface of facial motor neurons, and can express variable levels of P2RY12. Overall, our results suggest that TREM2+ microglia is a subpopulation that phagocytes more efficiently specific cell remnants, mainly myelin and degenerating neurons, and its expression prepares the way for injury repair.

INTRODUCTION

Microglial cells are the principal myeloid cells within the central nervous system (CNS), which play an immune surveillance function under homeostasis and after damage or pathological insult (Colonna and Butovsky, 2017; Wolf et al., 2017). A molecule that gained attention in the last years by its involvement in the modulation of microglia is the Triggering Receptor Expressed on Myeloid cells 2 (TREM2), an innate transmembrane type I receptor of the immunoglobulin superfamily that is expressed only by myeloid cells (Colonna, 2003). Several studies have strongly linked variants in the TREM2 gene with increased risk of developing Alzheimer's disease (AD), fronto-temporal dementia, and Nasu-Hakola disease and, to a lesser extent, Parkinson's disease and amyotrophic lateral sclerosis (reviewed in Jay et al., 2017b).

In the brain, TREM2 is exclusively expressed by microglia, with variations depending on the CNS region (Schmid et al., 2002), and is generally upregulated *in vivo* upon inflammatory conditions or in aging (Gratuze et al., 2018). A plethora of ligands bind to TREM2, including anionic ligands, such as phospholipids or sulfatides, lipoproteins like ApoE, β-amyloid, and also DNA (reviewed in Kober and Brett, 2017). Upon ligand binding, TREM2 interacts with DAP12 and results in a wide range of functions, including proliferation, migration, pro-survival signal, lipid sensing, phagocytosis, and energy metabolism (reviewed in Painter et al., 2015; Jay et al., 2017b), mainly aimed at containing and removing apoptotic or degenerated cells produced during neuronal damage (Takahashi et al., 2005, 2007; Hsieh et al., 2009; Krasemann et al., 2017; Deczkowska et al., 2018). Recently, single-cell RNA-sequencing analysis in the CNS tissue linked TREM2 with the differentiation of a newly identified specific microglial subtype appearing in mice in neurodegenerative conditions and aging, the so-called disease-associated microglia (DAM; Keren-Shaul et al., 2017; Deczkowska et al., 2018) or microglia associated to neurodegeneration (Krasemann et al., 2017). These microglia play a key role in chronic neurodegenerative conditions and show a unique transcriptional and functional signature highly differing from homeostatic microglia, characterized by the overexpression of other genes, such as *Clec7a, Lgals3, ApoE*, and the downregulation of microglial homeostatic genes, such as *P2ry12* or *Tmem119*.

The role of TREM2 has been mainly reported in chronic experimental models of AD and other chronic disorders—like experimental autoimmune encephalomyelitis (EAE, reviewed in Karanfilian et al., 2020)—and, to a lesser extent, in different acute neuroinflammatory conditions, including cuprizone-induced demyelination, stroke, and traumatic brain injury, among others (reviewed in Deming et al., 2018). However, little is known about its expression after axonal CNS lesions, and even less about the role of TREM2 in those lesions that are associated with a reparative process. Indeed, studies on microglial TREM2 function after spinal nerve injury (Kobayashi et al., 2016) showed an upregulation of TREM2, which was also detected in the microglial transcriptome after facial nerve injury (Tay et al., 2018). Moreover, in these and other studies based on TREM2KO and DAP12KO mice, reduced secretion of pro-inflammatory cytokines and a lower neuronal death rate were reported after axotomy (Kobayashi et al., 2015; Krasemann et al., 2017), pointing towards an important role of TREM2 in the modulation of the inflammatory response and the resolution of nerve injury (Kobayashi et al., 2016).

In this context, the main objective of our work is to study TREM2 expression and its function in two well-established models of anterograde and retrograde axonal degeneration —with an associated reparative process—: the perforant pathway transection (PPT: transection of the principal pathway that connects the entorhinal cortex with the hippocampus) and the facial nerve axotomy (FNA), respectively. Also, we explored whether changes in microglia activation by local pro-inflammatory or anti-inflammatory microenvironments, using transgenic mice with IL-6 or IL-10 overproduction (Almolda et al., 2014; Villacampa et al., 2015; Recasens et al., 2019), are able to modulate TREM2 expression after PPT and FNA.

MATERIALS AND METHODS

Animals

GFAP-IL6 transgenic (Tg) mice, GFAP-IL10Tg, and their corresponding wild-type (WT) C57BL/6 littermates from both sexes were used in this study. GFAP-IL6Tg was constructed and initially studied by Prof. Iain Campbell (Campbell et al., 1993), while GFAP-IL10Tg has been constructed and characterized by our laboratory (Almolda et al., 2015). All mice were housed and bred in the Institute of Neurosciences of the *Universitat Autònoma de Barcelona* under a 12 h light/dark cycle, with food and water *ad libitum*. All experimental animal work was conducted according to Spanish regulations (Ley 32/2007, Real Decreto 1201/2005, Ley 9/2003 and Real Decreto 178/2004) in agreement with European Union directives (86/609/CEE, 91/628/CEE, and 92/65/CEE) and was approved by the Ethical Committee of the Autonomous University of Barcelona. Every effort was made to minimize the number of animals used to produce reliable scientific data, as well as animal suffering and pain.

Perforant Pathway Transection and Experimental Groups

In the first part of the study, 84 WT animals were used, and in the second part of this study, performed with Tg animals, 27 GFAP-IL6Tg, 45 GFAP-IL10Tg, and a total of 72 corresponding WT mice littermates were used. Animals were subjected to wire-knife unilateral PPT, as already described in Jensen et al. (1999). Briefly, animals were anesthetized with an intraperitoneal injection of a solution of ketamine (80 mg/kg) and xylazine (20 mg/kg) at the dose of 0.01 ml/g body weight. Anesthetized mice were placed in a stereotaxic device (Kopf Instruments®) and a small window in the skull was created by drilling made in the left side of the skull (4.6 mm dorsal to Bregma and 2.5 mm laterally). A folded wire-knife (McHugh Milleux, m121) was inserted at an angle of 15° anterior and 10° lateral. The knife was unfolded at 3.6 mm ventrally and the perforant pathway—formed by fibers from neurons placed in layers II and III from the entorhinal cortex projecting to the hippocampus—was transected retracting the knife 3.3 mm. Finally, the knife was folded and removed from the brain. After surgery, the skin was sutured with 2–0 silk and the wound was cleaned with iodine. Non-lesioned (NL) and lesioned animals were distributed in different experimental groups and euthanized at 2, 3, 7, 14, and 21 days post-lesion (dpl).

Facial Nerve Axotomy and Experimental Groups

In the first part of this work, 110 WT animals were used, and for the second part of this study, specifically performed with Tg animals, 32 GFAP-IL6Tg, 32 GFAP-IL10Tg, and a total of 64 corresponding WT mice littermates were used. Animals were anesthetized with a solution of ketamine (80 mg/kg) and xylazine (20 mg/kg) injected intraperitoneally at a dose of 0.01 ml/g and underwent a unilateral FNA as described in Almolda et al. (2014). The skin behind the right ear was shaved and cleansed with 70% ethanol. A small incision was made in the skin and both the trapezius and the anterior digastric muscles were gently separated to expose the right facial nerve. One millimeter of the facial nerve main branch was resected at the level of the stylomastoid foramen. Following the surgery, the skin was sutured with 5–0 nylon. Corneal dehydration was prevented by the application of Lacri-lube® eye ointment. After anesthesia recovery, the complete whisker paralysis was assessed to ensure that complete facial nerve resection was achieved. NL and axotomized animals were distributed in different experimental groups and euthanized at 3, 7, 14, 21, and 28 dpl.

5′ Bromodeoxyuridine Injections

To determine microglia proliferation in the FNA model, proliferative cells were labeled with 5′ bromodeoxyuridine (BrdU). BrdU is a synthetic thymidine analog that incorporates into the DNA of dividing cells during the S-phase and can be transferred to daughter cells upon replication. Lesioned WT

(n = 4) animals were intraperitoneally injected with BrdU (100 mg/kg) diluted in 0.1 M PBS (pH 7.4) every 24 h, from the day of the lesion to 14 dpl, to be sacrificed afterward.

Tissue Processing for Histological Analysis

Animals were deeply anesthetized with a solution of ketamine (80 mg/kg) and xylazine (20 mg/kg) injected intraperitoneally at a dose of 0.015 ml/g and perfused intracardially with 4% paraformaldehyde in 0.1 M phosphate buffer (pH 7.4). Brains were removed and post-fixed in the same fixative for 4 h at 4°C and, after rinsing in phosphate buffer, cryopreserved for 48 h in a 30% sucrose solution and subsequently frozen in ice-cold 2-methyl butane solution (320404, Sigma–Aldrich). Parallel free-floating coronal sections (30-μm-thick) of the brainstem containing the facial nucleus (FN), in the case of the FNA model, as well as parallel free-floating transversal sections (30-μm-thick) of the brain containing the hippocampus, for the PPT model, were obtained using a CM3050s Leica cryostat, and sections were stored at −20°C in Olmos antifreeze solution until their use. Each experimental group was formed by three to five animals.

Single Immunohistochemistry

Free-floating cryostat sections were processed for the visualization of TREM2, CD16/32, CD68, and phospho-Histone 3 (pHH3). Briefly, after 10 min of endogenous peroxidase blocking with 2% H_2O_2 in 70% methanol and later washes with Tris-buffered saline (TBS, pH 7.4), sections were blocked for 1 h in either blocking solution 1 (BS1), containing 0.2% gelatin (powder food grade, 1.04078, Merck) in TBS with 0.5% Triton X-100 (TBS-T0.5%)—in the case of TREM2 staining—or in blocking solution 2 (BS2), containing 10% fetal bovine serum (FBS) in TBS with 1% Triton X-100 (TBS-T1%)—for CD16/32, CD68 and pHH3–. Then, sections were incubated with sheep anti-TREM2, rat anti-CD16/32, rat anti-CD68, or rabbit anti-pHH3 antibodies (**Table 1**). Incubations were performed overnight (ON) at 4°C plus 1 h at room temperature (RT) in the case of CD16/32, CD68, and pHH3, or 48 h at RT in the case of TREM2. Sections incubated in media lacking the primary antibody were used as negative control and spleen sections as a positive control. After washes with either TBS-T0.5% or TBS-T1%, sections were incubated at RT for 1 h with the corresponding biotinylated secondary antibodies, followed by 1 h at RT with horseradish peroxidase (HRP)-conjugated streptavidin, diluted in the corresponding BS (**Table 1**). After washes with TBS, the final reaction was visualized by incubating sections with a DAB kit (SK-4100; Vector Laboratories Incorporation, Burlingame, CA, USA) following the manufacturer's instructions. Finally, sections were mounted on gelatin-coated slides, counterstained with toluidine blue if considered appropriate, dehydrated in graded alcohols, and, after xylene treatment, coverslipped with DPX.

Double and Triple Immunohistochemistry

Double and triple immunolabeling combining (1) TREM2, ApoE or pHH3 with (2) either Iba1, CD68, CD16/32, Galectin-3, pHH3, P2RY12, GFAP or CD11b, and (3) GFAP were performed as follows: sections were washed and blocked for 1 h with blocking solution 3 (BS3) containing 0.2% gelatin in TBS with 0.1% Triton X-100 (TBS-T0.1%) or with BS2 for pHH3. Later, sections were incubated with sheep anti-TREM2 for 48 h at RT, or either goat anti-ApoE antibody or rabbit anti-pHH3 ON at 4°C plus 1 h at RT. After several washes with TBS-T0.1%, sections were incubated with the corresponding secondary antibody being anti-sheep Alexa-Fluor (AF) 488, anti-goat AF568, anti-goat AF488 in the case of the double immunostaining combining ApoE with GFAP, or anti-rabbit AF488 for 1 h at RT (**Table 1**). Afterward, sections were washed and incubated ON at 4°C plus 1 h at RT with rabbit anti-Iba1, rabbit anti-pHH3, rat anti-CD68, rat anti-CD16/32, rat anti-Galectin-3, rat anti-CD11b antibodies, or mouse anti-GFAP (**Table 1**). After several washes, sections in each combination were incubated for 1 h at RT with the corresponding secondary conjugated antibodies anti-rabbit AF568, anti-rat AF555 anti-rat AF647, or anti-mouse AF555 secondary antibodies (**Table 1**). For the triple IHC protocol, these last steps were repeated using a mouse anti-GFAP antibody and secondary anti-mouse AF488 conjugated antibody (**Table 1**). On the other hand, in the case of TREM2 and P2RY12 double immunohistochemistry, sheep anti-TREM2 and rat anti-P2RY12 primary antibodies were incubated simultaneously 48 h at RT (**Table 1**), and after washes, secondary anti-sheep AF488 antibody was firstly incubated for 1 h at RT, followed by a second incubation with an anti-rabbit AF568 antibody for 1 h at RT (**Table 1**). Finally, in double ApoE and Iba1 or GFAP immunostaining, sections were treated for a diminishing fluorescence background as described in Schnell et al. (1999). Thus, sections were dipped in distilled water, treated with $CuSO_4$ (10 mM) in ammonium acetate buffer (50 mM CH_3COONH_4, pH 5.0) for 90 min, and rinsed again with distilled water before mounting.

Additionally, microglial proliferation was determined by BrdU staining. DNA was denatured by first incubating sections in 0.082 N HCl for 10 min at 4°C and then for 30 min in 0.82 N HCl at 37°C. Sections were subsequently rinsed with borate buffer (pH 8.5) and 0.5% Triton X-100 in TBS. Afterward, sections were incubated for 1 h at RT using BS2, and the anti-BrdU antibody was added and incubated ON at 4°C plus 1 h at RT (**Table 1**). After several washes with TBS-T1%, the corresponding conjugated anti-rat AF555 secondary antibody was added for 1 h at RT (**Table 1**). Then, the anti-Iba1 antibody was incubated ON at 4°C plus 1 h at RT, with a final 1 h incubation at RT of anti-rabbit AF488 conjugated antibody (**Table 1**). All double-labeled sections were nuclei stained with DAPI (**Table 1**) for 5 min, before being coverslipped with Fluorescence Mounting Medium (S-3023; Dako).

Brightfield Microscopy Quantification

Quantitative analysis was performed on sections stained with single immunohistochemistry for TREM2, CD68, CD16/32, and pHH3. For each immunostaining, three to five WT, GFAP-IL6Tg, and GFAP-IL10Tg animals per time post-lesion and experimental lesion model were analyzed.

In the PPT model, images of two central hippocampal sections containing the deafferented molecular layer (ML) of the dentate gyrus (DG) for each lesioned animal, and the

TABLE 1 | List of antibodies and reagents used in immunohistochemistry (IHC).

	Target antigen	Host/conjugation	Dilution	Catalog number	Manufacturer
Primary antibodies	ApoE	Goat	1:2,500	AB947	EMD Millipore
	BrdU	Rat	1:120	Ab6326	Abcam
	CD11b	Rat	1:1,000	MCA74G	AbD Serotec
	CD16/32	Rat	1:1,000	553142	BD Pharmingen
	CD68	Rat	1:1,000	MCA1957	AbD Serotec
	Galectin-3	Rat	1:500	125402	BioLegend
	GFAP	Mouse	1:6,000	G3893	Sigma
	Iba1	Rabbit	1:500	GTX100042	GeneTex
	P2RY12	Rat	1:50	848001	BioLegend
	pHH3	Rabbit	1:500	06-570	EMD Millipore
	TREM2	Sheep	1:400	AF1729	R&D Systems
Secondary antibodies	Goat IgG	Alexa Fluor 568	1:1,000	A11057	Invitrogen
	Goat IgG	Alexa Fluor 488	1:1,000	A11055	Invitrogen
	Mouse IgG	Alexa Fluor 555	1:1,000	A31570	Invitrogen
	Rabbit IgG	Alexa Fluor 488	1:1,000	A21206	Invitrogen
	Rabbit IgG	Alexa Fluor 568	1:1,000	A10042	Invitrogen
	Rat IgG	Alexa Fluor 555	1:1,000	A21434	Invitrogen
	Rat IgG	Alexa Fluor 647	1:1,000	A21247	Invitrogen
	Sheep IgG	Alexa Fluor 488	1:1,000	A11015	Invitrogen
	Goat IgG	Biotinylated	1:500	BA-9500	Vector Laboratories
	Rabbit IgG	Biotinylated	1:500	BA-1000	Vector Laboratories
	Rat IgG	Biotinylated	1:500	BA-4001	Vector Laboratories
	Sheep IgG	Biotinylated	1:500	BA-6000	Vector Laboratories
HRP-conjugated Streptavidin			1:500	SA-5004	Vector Laboratories
DAPI			1:10,000	D9542	Sigma–Aldrich

equivalent area for NL mice, were captured. A total of three photographs were obtained for each hippocampus, at 40× magnification in the case of TREM2 and 20× magnification for CD16/32 and CD68 analysis. For the FNA model, at least three representative sections from the brainstem of each animal, containing the central part of the contralateral and the ipsilateral FN, were photographed at 10× magnification. All images were obtained using a DXM 1200F Nikon digital camera joined to a brightfield Nikon Eclipse 80i microscope and the corresponding ACT-1 2.20 software (Nikon Corporation). In both models, quantification of each photograph was done by using the AnalySIS® software, in which the threshold corresponding to the staining was manually set. In the case of TREM2, the threshold was set to quantify only TREM2 cellular staining, excluding the background staining corresponding to soluble TREM2 (sTREM2). Analysis of each photograph resulted in the percentage of area covered by the immunolabeling (% Area) and the intensity of the immunoreaction (Mean Gray Value Mean). Then, the AI index was calculated by multiplying the percentage of the immunolabeled area and the Mean Gray Value Mean (Acarin et al., 1997). Results of the AI index and intensity were expressed in arbitrary units.

In the case of PPT, quantification of microglial cell proliferation was carried out on hippocampal sections immunostained for the mitotic marker pHH3 in NL and lesioned animals at 2, 3, and 7 dpl. The number of pHH3+ microglial cells in the whole ML of the DG were manually counted using a 20× objective. Data were averaged and represented as pHH3+ cells/mm^2.

For the FNA model, pHH3 quantification was done in NL and lesioned animals at 3, 7, 14, 21, and 28 dpl. The number of pHH3+ cells in the FN were manually counted using a 20× objective. Then, all FN counted were photographed at 10×, and the area of each FN was quantified using ImageJ software (Wayne Rasband, National Institute of Health, Bethesda, MD, USA). pHH3 cell density was calculated from the total pHH3+ cells/FN area for each animal, and results were expressed as pHH3+ cells/mm^2.

Confocal Microscopy Quantification

To evaluate the percentage of ramified microglial TREM2+ cells for the PPT model, sections immunostained with Iba1 and TREM2 were used. A minimum of three WT, GFAP-IL6Tg, and GFAP-IL10Tg animals euthanized at 3 dpl were quantified. In this case, the total ML of DG was photographed at 40× magnification with a Zeiss LSM 700 confocal microscope. From the total amount of microglial Iba1+ cells contained in the deafferented ML of the DG, ramified microglial TREM2+ cells were counted using the "Cell counter" plug-in from ImageJ software. Results were expressed as a percentage of Iba1+ cells containing TREM2 in their ramifications from the total number of Iba1+ cells (% TREM2 + Iba1+ cells/total Iba1+ cells).

In the FNA model, quantification of microglial clusters expressing TREM2 and microglial TREM2 ramified clusters was performed by analyzing the double immunofluorescence for Iba1 and TREM2. A minimum of three WT, GFAP-IL6Tg, and GFAP-IL10Tg animals at 14 and 21 dpl were used. The number of total microglial clusters in the FN, identified by Iba1+ staining, expressing TREM2 in microglial ramifications were manually counted using a 40× and 63× objective with a Zeiss LSM 700 confocal microscope. Results were expressed in percentage as TREM2 + Iba1+ microglial clusters from the total amount of Iba1+ clusters (% TREM2 + Iba1+ microglial clusters/total Iba1+ clusters).

Tissue Processing for Protein Quantification

For quantifying sTREM2, NL, 3 dpl after PPT (*n* = 6–8) and 21 dpl axotomized WT animals (*n* = 10) were used. Animals were deeply anesthetized with a solution of ketamine (80 mg/kg) and xylazine (20 mg/kg) injected intraperitoneally at a dose of 0.015 ml/g and perfused intracardially for 1 min with cold 0.1 M DPBS (pH 7.4, 14190-094; Thermo Fisher Scientific, Waltham, MA, USA). Then, the brain was removed from the skull, and for NL and PPT-lesioned animals, the hippocampus, was dissected out. For FNA-lesioned animals, the brain was excised and two 0.5-mm-thick coronal slices were obtained from the brain trunk using a Mouse Brain Matrix (Zivic Instruments). For each slice, the dorsal inferior half was cut with sterile knives, and tissue containing the contralateral and ipsilateral FN was divided. Samples were immediately snap-frozen individually in liquid nitrogen, and stored at −80°C. The tissue of two hippocampi or three FN was pooled for protein extraction. Briefly, protein extraction was performed by using a mechanical homogenizer to disrupt tissue in lysis buffer, containing 25 mM HEPES, 2% Igepal, 5 mM $MgCl_2$, 1.3 mM EDTA, 1 mM EGTA, 0.1 M PMSF, and protease (1:100, P8340; Sigma–Aldrich) and phosphatase inhibitor cocktails (1:100, P0044; Sigma–Aldrich), and allowing solubilization for 2 h at 4°C. Afterward, samples were centrifuged at 6,500 *g* for 10 min at 4°C in a microcentrifuge (5415R centrifuge, Eppendorf) and the supernatants were collected and frozen.

For separating the soluble protein fraction, each protein lysate was ultracentrifuged at 107,000 *g* for 30 min at 4°C in a Sorvall MTX 150 Series Micro-Ultracentrifuge. After ultracentrifugation, supernatants were collected and concentrated by using microcentrifuge cellulose filter units (MRCPRT010, Merck Millipore). Resulting protein lysates were collected and total protein concentration was determined with a commercial Pierce BCA Protein Assay kit (#23225; Thermo Fisher Scientific, Waltham, MA, USA) according to manufacturer's protocol.

Enzyme-Linked Adsorbent Immunoassay for sTREM2 Detection

Quantification of sTREM2 was performed by following the manufacturer's instructions of a Mouse TREM2 ELISA kit (ABIN429539, Antibodies-online). Briefly, standards and the corresponding samples were incubated at 2.5 μg/μl in a pre-coated TREM2 ELISA plate. After reagent incubations, and the addition of TMB substrate and Stop solution, results were read at 450 nm in the microplate reader Varioskan^{TM} Lux (Thermo Fisher Scientific, Waltham, MA, USA).

Isolation of Myelin and Fluorescent Labeling With pHrodo^{TM} Green STP Ester

Myelin was isolated following the protocol described by Rolfe et al. (2017). Briefly, six WT animals were dislocated under the effects of anesthesia (dose of 0.015 ml/g of 80 mg/kg ketamine and 20 mg/kg xylazine solution, injected intraperitoneally). Brains were removed quickly and cut into little pieces in a cold 0.32 M sucrose solution prepared in 0.1 M Tris.Cl buffer. After homogenization with a mechanical homogenizer, myelin was separated by using a sucrose gradient in an ultracentrifuge at 105,000 *g* for 45 min at 4°C (70Ti Rotor, Sorvall). Myelin was isolated from the interphase, and after a hypoosmotic shock using Tris.Cl buffer and 0.32 M sucrose, pelleted myelin was weighted and reconstituted in PBS at a 100 mg/ml (w/v) suspension.

For myelin fluorescent labeling, conjugation with pHrodo-STP Ester Green® (P35369, Thermo Fisher Scientific, Waltham, MA, USA)—with excitation at 505 nm and emission at 525 nm—was used following the procedure described by Greenhalgh et al. (2018). Briefly, the pHrodo dye was dissolved in 75 μl dimethyl sulfoxide (DMSO, Sigma–Aldrich), and afterward, 18.5 μl of myelin in a concentration of 15 mg/ml was mixed with 25 μl of pHrodo and resuspended in 206.5 μl of PBS (pH 8.0). After 45 min of incubation at RT, with agitation and protected from light, labeled myelin was spun down, resuspended in PBS (pH 7.4), and stored at −80°C.

Myelin Phagocytosis Assay and Flow Cytometry

The capacity of TREM2+ microglia in PPT-lesioned animals (at 3 dpl) and axotomized animals (21 dpl) to phagocyte myelin debris was analyzed by isolating cells with Percoll and performing a myelin phagocytosis assay followed by a flow cytometry procedure (Almolda et al., 2009; Greenhalgh et al., 2018). Briefly, anesthetized animals (dose of 0.015 ml/g of an 80 mg/kg ketamine and 20 mg/kg xylazine solution, injected intraperitoneally) were intracardially perfused for 1 min with 0.1 M DPBS. The brain was removed and the area of interest, either hippocampus or FN, was dissected out as described above. For each tube, an individual lesioned hippocampus, two NL hippocampus, or a pool of two either lesioned or contralateral NL FN were used. To obtain a cell suspension, samples were dissociated through 160 and 70 μm meshes and digested for 30 min at 37°C using type IV collagenase (17104-019; Life Technologies, Carlsbad, CA, USA) and DNAsa I (D5025; Sigma–Aldrich, St. Louis, MO, USA). Subsequently, each cellular suspension was centrifuged at RT for 20 min at 2,400 rpm in a discontinuous density Percoll gradient (17-0891-02; Amersham-Pharmacia, UK) between 1.03 and 1.08 g/ml using a Heareus Multifuge 3L-R centrifuge (ThermoFisher). Myelin in the upper layer was removed, and cells in the interphase and the clear upper-phase were collected and washed in PBS + 2% FBS. Afterward, the myelin phagocytosis assay was performed as follows: cells were resuspended in DMEM-F12 medium (ref. 31330-038; Thermo Fisher Scientific, Waltham, MA, USA) + 10% FBS, then 3 μg of pHrodo Green-labeled myelin were added, and samples were incubated at 37°C for 4 h. For negative controls, the same procedure was performed without adding myelin, or by resuspending cells in PBS + 2% FBS and preserving at 4°C. After myelin incubation, cells were washed one time with PBS + 2% FBS at 1,200 rpm for 10 min. Then, cells were blocked for Fc receptors by incubating them in a

TABLE 2 | List of antibodies used in flow cytometry.

Target antigen		Format	Dilution	Catalog number	Manufacturer
Fc blocker	CD16/32	Purified	1:250	553142	BD Biosciences
Primary antibodies	CD11b	APC-Cy7	1:400	557657	BD Biosciences
	CD45	PerCP	1:400	557235	BD Biosciences
	TREM2	PE	1:400	FAB17291P	R&D Company

solution of purified CD16/32 diluted in PBS + 2% FBS, for 10 min at 4°C (**Table 2**). Afterward, cells were labeled for 30 min at 4°C with the combination of the following surface antibodies: anti-CD11b-APCCy7, anti-CD45-PerCPCy5, and anti-TREM2-PE (**Table 2**). In parallel, isotype-matched control antibodies for the different fluorochromes (BD Pharmingen, Switzerland) and samples that were not incubated with myelin were used as the negative control, while a cell suspension of splenocytes and cerebellum of GFAP-IL6Tg animals as the positive control. Finally, cells were acquired using a FACS Canto flow cytometer (Becton Dickinson, San Jose, CA, USA) in the corresponding fluorescent channels, and pHrodo-Green labeled myelin phagocytosed by microglia could be captured in the FITC channel. Results were analyzed using the FlowJo^{TM} software (FlowJo LLC).

Statistical Analysis

Statistics were performed using Graph Pad Prism® software (Graph Pad Software Inc.) and results were expressed as Mean ± Standard error of the mean (SEM). Appropriate statistical tests were used for each condition: for time-course dynamics, one-way ANOVA with multiple comparison *post hoc* Tukey's test was used, for microglial cell density Dunnet's *post hoc* test was used instead, for sTREM2 comparison and flow cytometry analysis either unpaired or paired Student's *t*-test was used, and finally, two-way ANOVA with multiple comparison *post hoc* Sidak's test was used to compare Tg mouse lines with their corresponding WT.

RESULTS

TREM2 Is Upregulated in the Denervated ML of the DG After PPT

The immunohistochemical study of TREM2 expression after PPT showed that, in comparison to the low to undetectable TREM2 expression in the ML of NL animals, a significant upregulation in TREM2 immunolabeling in both the medial molecular layer (MML) and the outer molecular layer (OML) of the DG was observed (**Figures 1A–F**). A notable increase in TREM2 immunolabeling was found between 2 and 3 dpl, which sharply declined afterward, at 7 and 14 dpl. At 21 dpl, levels of TREM2 were comparable to basal conditions (**Figure 1G**).

Co-localization studies indicated that all TREM2+ cells corresponded to microglia/macrophages, as they co-labeled with Iba1 at all time-points analyzed (**Figures 1H,I**). Moreover, variations in the cellular location of TREM2 after injury were observed. Whereas in basal conditions TREM2 was found concentrated in the cytoplasm, in a position adjacent to the nucleus of microglial cells (arrowheads in **Figure 1H**); at 2 and 3 dpl, a subpopulation of microglial cells showed TREM2 expression in their ramifications (**Figure 1I**). Quantification of TREM2+/Iba1+ microglia cells at 3 dpl revealed that approximately half of microglia co-expressed TREM2 and Iba1 in their ramifications (48.1 ± 1.96%, in **Figure 1J**). From 3 dpl onwards, microglial cells expressing TREM2 in their ramifications decreased progressively. Interestingly, at 7 and 14 dpl, only a few scattered microglial processes were labeled, being TREM2 expression mostly restricted again into the region next to the nucleus. At 21 dpl, TREM2 was completely restricted in a position adjacent to the nucleus, like in basal conditions (**Figure 1F**). Notably, from 2 to 14 dpl, also a diffuse staining of sTREM2 covering the neuropil of both the MML and the OML was observed (**Figures 1B–E**). Quantification of sTREM2 at 3 dpl showed an increase of this protein fraction in the lesioned compared to the NL hippocampus (**Figure 1K**).

TREM2 Is Upregulated In the Lesioned FN After FNA

After FNA, the immunohistochemical study of TREM2 expression showed an upregulation of TREM2 in the ipsilateral FN along the different time points, in comparison to the NL contralateral side, where the levels of TREM2 were very low (**Figures 2A–F**). TREM2 immunolabeling increased from 3 dpl onwards, showed a maximum at 21 dpl, and decreased thereafter at 28 dpl, although levels were still higher than in the contralateral NL FN (**Figure 2J**).

Double-immunolabeled sections with TREM2 and Iba1 demonstrated that, in the NL contralateral side, TREM2 expression was concentrated in the cytoplasm of microglia, in a position adjacent to the nucleus (arrowheads in **Figure 2G**). In the ipsilateral side, at 3 and 7 dpl, TREM2 expression remained located like in basal conditions although levels of expression were higher (arrowheads in **Figure 2H**). In contrast, at 14 and 21 dpl, TREM2 staining was additionally found in the ramifications of a subpopulation of microglial cells, forming part of the so-called microglial clusters or microglial nodules (arrows in **Figure 2I**), which consist of accumulations of three to four microglial cells commonly described in the time-course of FNA injury (Moran and Graeber, 2004). At these time-points, almost all microglial clusters in the FN showed TREM2+ ramified microglia (**Figure 2K** and arrows in **Figure 2I**). In a similar way to the observations of PPT injury, low diffuse staining of sTREM2 covering the neuropil of the FN was observed, especially at 14 and 21 dpl. A comparison of the amount of sTREM2 fraction between NL and 21 dpl animals

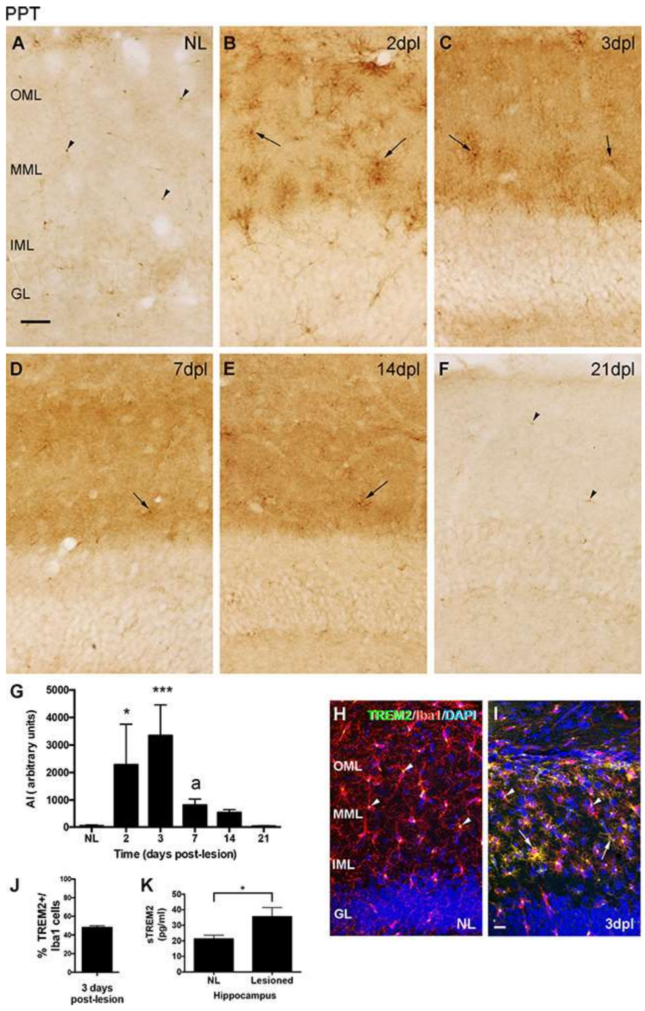

FIGURE 1 | Temporal pattern of Triggering Receptor Expressed on Myeloid cells-2 (TREM2) changes in microglial cells after perforant pathway transection (PPT). **(A–F)** Representative images showing TREM2 staining in the granular (GL) as well as the inner, medial and outer molecular layers (IML, MML, and OML, respectively) of the dentate gyrus (DG) in non-lesioned (NL) **(A)** and PPT-lesioned mice from 2 to 21 dpl **(B–F)**. Note that, while in NL and at 21 dpl TREM2 was only depicted as small rounded morphologies (arrowheads), from 2 to 14 dpl ramified TREM2+ cells were also observed (arrows). **(G)** Graph showing the quantification of the AI index for TREM2 along the different time-points. Note the higher level of TREM2 at 2 and 3 dpl compared to NL and the posterior decrease from 3 to 7 dpl (one-way ANOVA, time effect $p < 0.0001$; *post hoc* Tukey's test $^{*}p < 0.05$, $^{***}p < 0.001$ respect to NL, a $p < 0.01$ respect to the previous time-point). **(H,I)** Double immunohistochemistry showing microglial cells labeled with Iba1 (red) and TREM2 (green). Note that in NL animals, TREM2 is confined to areas around the nucleus of some Iba1+ cells (arrowheads), whereas at 3 dpl, additionally, some prolongations of Iba1+ microglial cells (arrows) were also observed. **(J)** Graph showing the quantification of the percentage of TREM2+ cells, -those showing TREM2 staining in ramifications-, from total Iba1+ cells at 3 dpl. **(K)** Graph showing the quantification of sTREM2 (pg/ml) in the hippocampus of NL and PPT-lesioned mice at 3 dpl. A significant increase in the amount of sTREM2 is detected in the lesioned hippocampus (unpaired Student's *t*-test, $^{*}p < 0.05$). Scale bar **(A–F)** = 50 μm; **(H,I)** = 50 μm.

did not show a statistically significant increase in this protein fraction after lesion (**Figure 2L**).

Phenotypic and Functional Characterization of TREM2+ Microglial Cells After PPT and FNA

TREM2 has been principally associated with microglial proliferation, phagocytosis, and DAM-triggering (Takahashi et al., 2005, 2007; Wang et al., 2015; Keren-Shaul et al., 2017; Krasemann et al., 2017). To determine if TREM2 microglial expression after PPT and FNA was related to these functions, we studied the dynamics of microglial proliferation (pHH3) and phagocytosis (CD16/32, CD68) in both models, and we compared it to the time course of TREM2 expression. We also performed co-localization studies with TREM2+ microglia using specific markers related to proliferation (pHH3, BrdU), phagocytosis (CD16/32, CD68, ApoE, Galectin-3), and DAM-triggering (Galectin-3, ApoE, and P2RY12), as well as a functional myelin phagocytosis assay. In this part of the study, we described as TREM2+ microglia the population appearing after both lesions that show an increase of TREM2 in microglial ramifications, according to our results.

Expression of Proliferation Markers

In the PPT paradigm, a subpopulation of TREM2+ cells in the MML and OML expressed pHH3, a mitotic marker, at both 2 and 3 dpl (**Figures 3A–F**), coinciding with the peak of microglial proliferation observed in this paradigm (**Figure 3G**). Despite all proliferative cells were TREM2+, the total amount of proliferating cells within the TREM2+ subpopulation was low.

After FNA, pHH3 cell counting showed a peak of proliferation at 3 dpl, when TREM2 was located intracytoplasmatically. The study of TREM2 with pHH3 showed that, at 14 and 21 dpl, a low number of proliferating pHH3+ microglial cells was detected (**Figures 4A,B**). Also, accumulative BrdU for 14 dpl indicated the presence of BrdU+ microglial cells in both the parenchyma and within clusters where, as previously described, TREM2+ cells were located. Proliferating cells showed variable BrdU intensity in the nucleus, indicating an uneven number of mitosis (**Figures 4C–E**).

Expression of the Phagocytic Markers CD16/32 and CD68

The study of Fc-receptors CD16/32 and lysosomal CD68 expression in microglia during PPT and FNA time-courses provided a general assessment of changes in these phagocytic molecules. In the NL hippocampus, microglia express low levels of CD16/32, being not fully coincident with microglia expressing intracellular TREM2 (**Figures 5A–C**). After the PPT lesion, the majority of TREM2+ cells observed at 3 dpl, in the peak of microglia activation, presented variable CD16/32 staining (arrowheads and arrows in **Figures 5D–F**). At later time-points, 14 dpl, when TREM2 was restricted to the cytoplasm in a position adjacent to the nucleus, some microglia cells still maintained CD16/32 expression (**Figures 5G–I**). Furthermore, in NL hippocampus, CD68 and TREM2 were both located intracellularly and mostly coincident in microglia cells (**Figures 5K–M**). At 3 dpl, all TREM2+ microglia contained CD68, although CD68 expression was

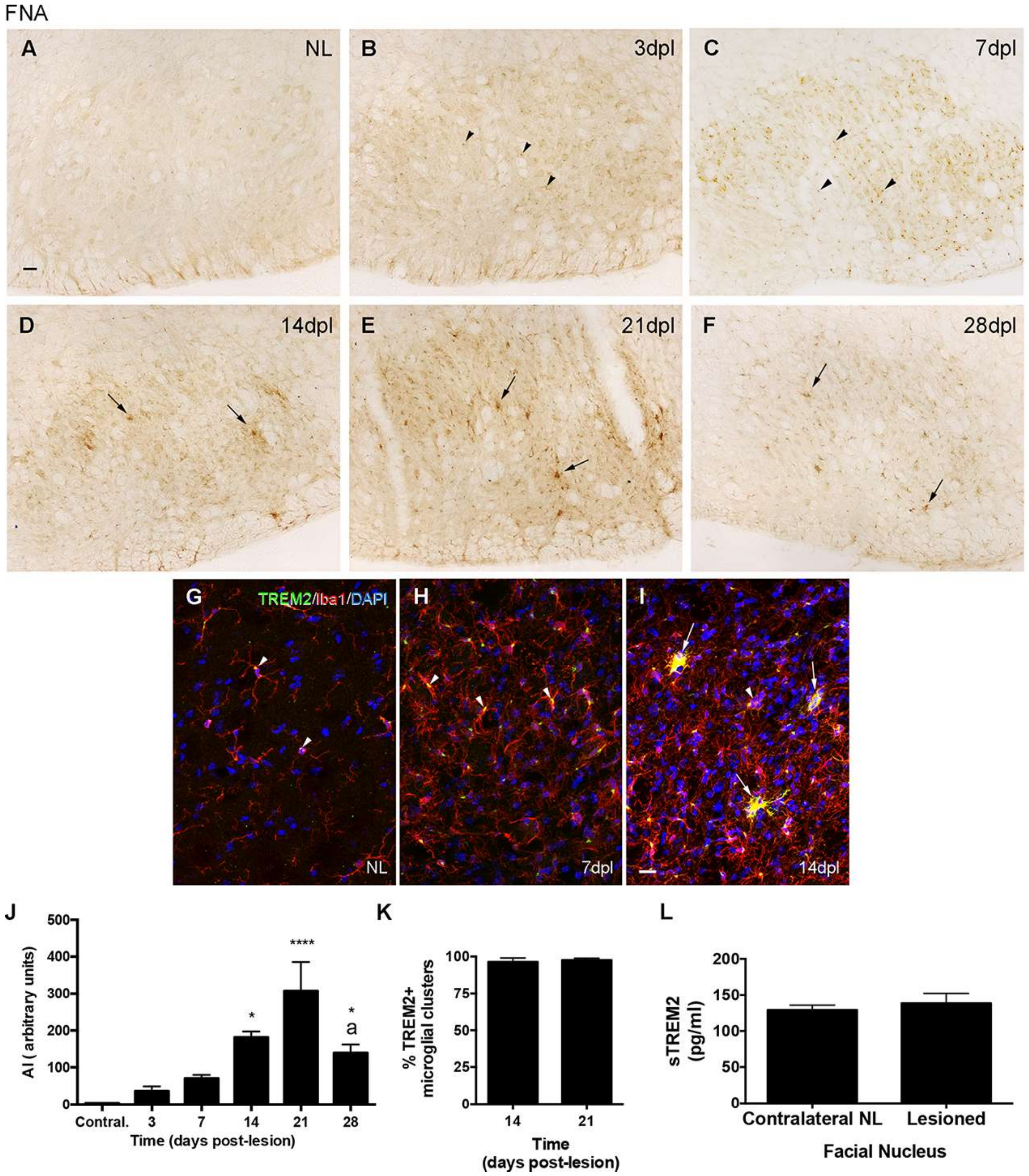
FNA
A
NL
B
3dpl
C
7dpl
D
14dpl
E
21dpl
F
28dpl
G
TREM2/Iba1/DAPI
NL
H
7dpl
I
14dpl
J
AI (arbitrary units)
500
400
300
200
100
0
****
*
*
a
Contral.
3
7
14
21
28
Time (days post-lesion)
K
% TREM2+ microglial clusters
100
75
50
25
0
14
21
Time (days post-lesion)
L
sTREM2 (pg/ml)
200
150
100
50
0
Contralateral NL
Lesioned
Facial Nucleus

FIGURE 2 | Temporal pattern of TREM2 changes in microglial cells after facial nerve axotomy (FNA). **(A–F)** Representative images showing TREM2 staining in the contralateral NL, as well as the ipsilateral sides of the FN from 3 to 28 dpl. From NL to 7 dpl TREM2 is mainly restricted to a perinuclear location (arrowheads), whereas from 14 dpl onwards TREM2 is extended to microglia ramifications and clusters (arrows). **(G–I)** Double immunohistochemistry showing microglial cells positive for TREM2 (green) and Iba1 (red). Note that in both the NL side and at 7 dpl, TREM2 is confined to areas around the nucleus of some Iba1+ cells (arrowheads), whereas at 14 dpl expression was detected in microglial prolongations in some microglial clusters (arrows). It is important to note that occasional Iba1 + TREM2-clusters were found at this time-point (arrowheads in **I**). **(J)** Graph showing the quantification of the AI index for TREM2 along the different time-points.

(*Continued*)

FIGURE 2 | Continued
Note the increase of TREM2 until 21 dpl and the later decrease (one-way ANOVA, time effect $p < 0.0001$; *post hoc* Tukey's test $^{*}p < 0.05$, $^{****}p < 0.001$ compared to NL; a $p < 0.01$ compared to the previous time-point). **(K)** Graph showing the percentage of microglial clusters containing TREM2+ microglial cells with expression in their ramifications at 14 and 21 dpl. **(L)** Graph showing the quantification of sTREM2 (pg/ml) in the FN of contralateral NL and the corresponding ipsilateral FN of mice lesioned at 21 dpl. No significant differences in the amount of sTREM2 are detected (paired Student's *t*-test, $p = 0.61$). Scale bar **(A–F)** = 30 μm; **(G–I)** = 50 μm.

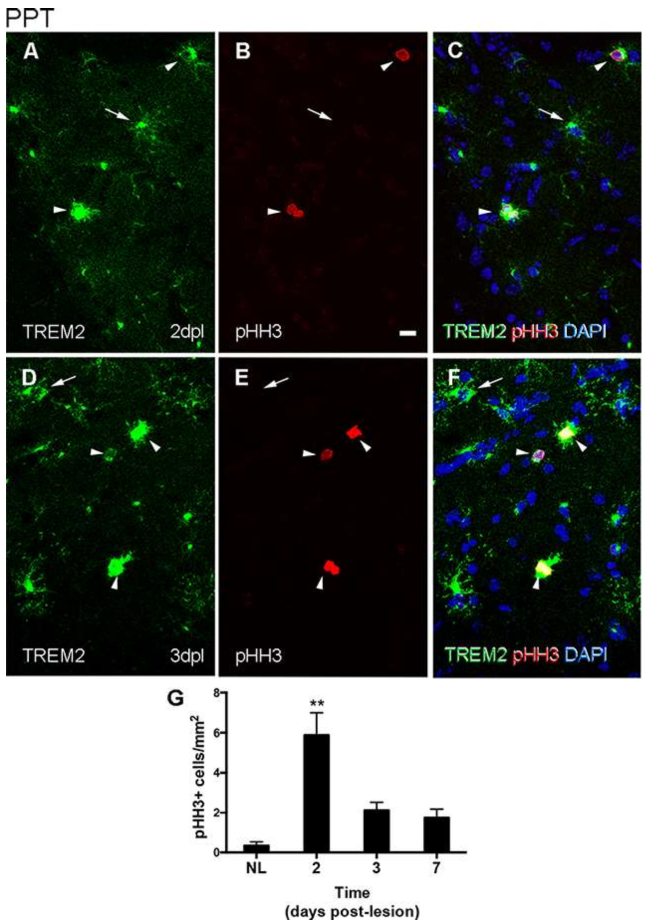

FIGURE 3 | Determination of the proliferative activity of TREM2+ microglial cells after PPT. **(A–F)** Representative double-immunolabeled images combining TREM2 (green) and PHH3 (red) in the DG of PPT-lesioned animals at 2 dpl **(A–C)** and 3 dpl **(D–F)**. Note that at both time points PHH3+ cells showed membranal TREM2 expression in the ramifications and soma of microglial cells (arrowheads). However, not all TREM2+ microglial cells with expression in their ramifications were undergoing mitosis (arrows). **(G)** Graph of PHH3+ cell density (cell/mm^2) in NL and PPT lesioned animals after 2, 3, and 7 dpl (one-way ANOVA, time effect $p < 0.0001$; *post hoc* Tukey's compared to NL $^{**}p < 0.01$). Scale bar **(A–F)** = 10 μm.

also found in other microglia, that is, CD68 is not exclusive to TREM2+ microglial subpopulation (arrowheads in **Figures 5N–P**). At 14 dpl, CD68 and TREM2 were again expressed intracellularly and mostly coincident in microglia (**Figures 5Q–S**).

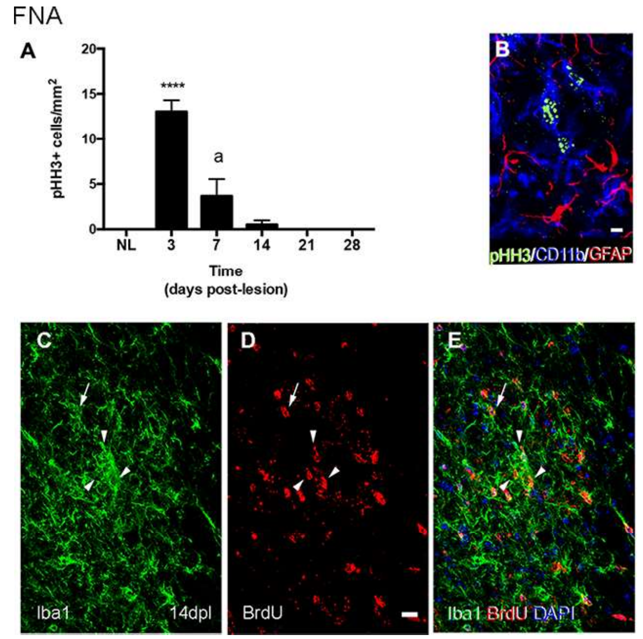

FIGURE 4 | Determination of the proliferative activity in microglial clusters after FNA. **(A)** Graph showing the quantification of PHH3+ cell density in the FN after FNA. Note the massive increase of proliferative cells at 3 dpl, followed by a later decrease at 7 and 14 dpl, and the disappearance of proliferative cells from 21 dpl onwards (one-way ANOVA, time effect $p < 0.0001$; *post hoc* Tukey's $^{****}p < 0.001$ compared to NL, a $p < 0.001$ compared to the previous time-point). **(B)** Representative triple immunofluorescence image combining PHH3 (green) with CD11b (blue) and GFAP (red). Note that all PHH3+ cells counted in the FN corresponded to microglia cells (CD11b+), but not astrocytes (GFAP). **(C–E)** Representative double-immunolabeled images combining TREM2 (green) and BrdU (red) in the FN of 14 dpl animals administered daily with BrdU. Proliferative BrdU+ microglial cells were observed inside microglial clusters (arrowheads) and outside them (arrows). Scale bar **(B)** = 5 μm; **(C–E)** = 10 μm.

In line with the above-mentioned observations, the dynamics of CD16/32 expression in the PPT lesion was sharply upregulated until 7 dpl and decreased thereafter at 14 dpl, although at this time point, levels of expression were still around 100-times higher than in NL animals (**Figure 5J**). In contrast, CD68 expression also was upregulated at 3 dpl but then progressively decreased from 7 to 14 dpl. At this later time-point, CD68 levels were still around two-times higher than NL mice (**Figure 5T**).

In the contralateral NL FN, CD16/32 was not expressed in microglial cells (**Figures 6A–C**), while CD68 was located intracellularly and colocalized with intracellular TREM2 expression (**Figures 6H–J**). After FNA, the majority of clusters containing TREM2+ microglia also co-expressed both CD16/32 and CD68 (arrows in **Figures 6D–F,K–M**). However, the few microglial clusters that were TREM2- also contained microglial staining for CD16/32 and CD68 (arrowheads in **Figures 6D–F,K–M**).

When we studied the microglial expression pattern of CD16/32 and CD68 along the different time-points after FNA

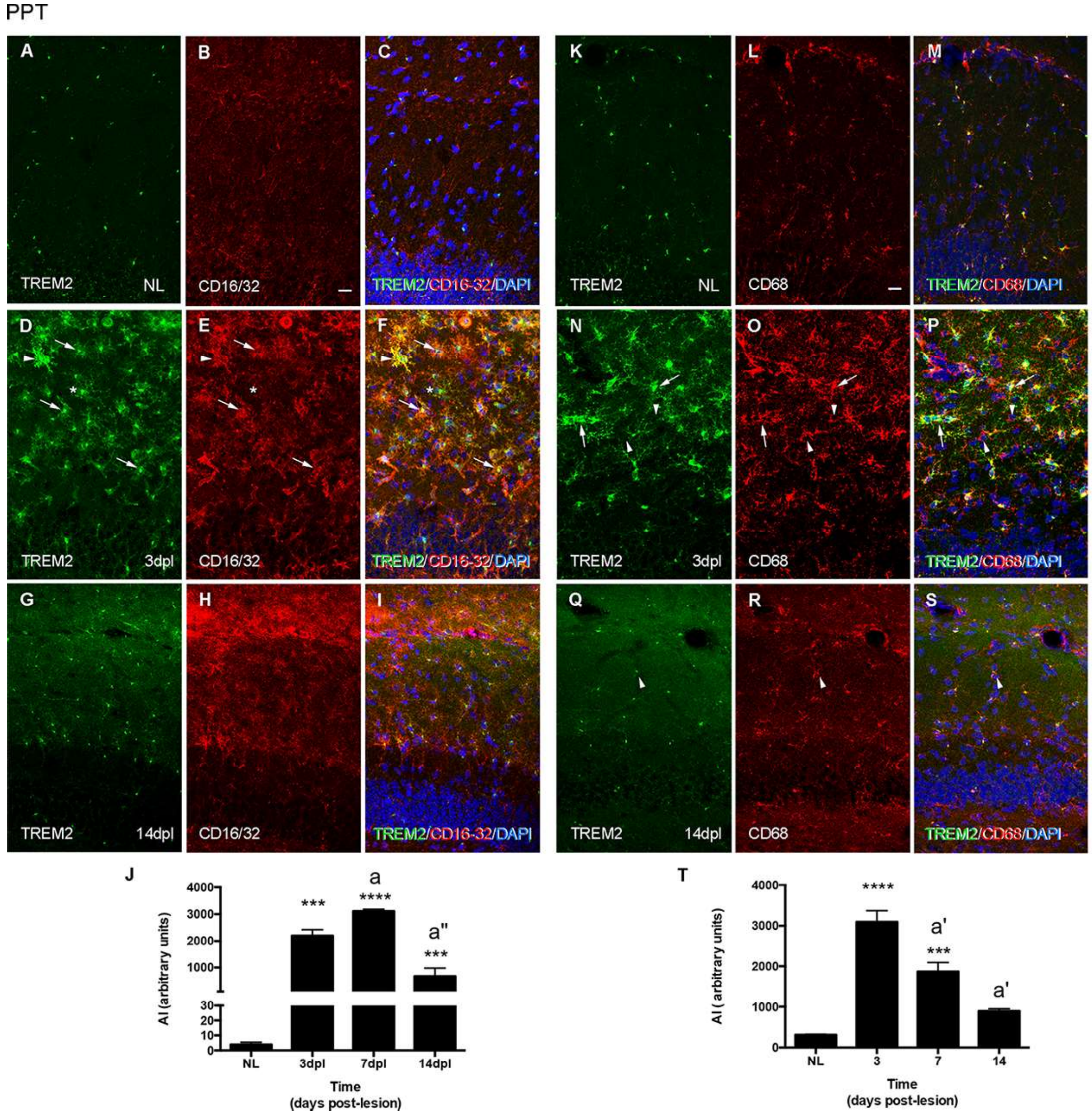
PPT
A
TREM2
NL
B
CD16/32
C
TREM2/CD16-32/DAPI
K
TREM2
NL
L
CD68
M
TREM2/CD68/DAPI
D
TREM2
3dpl
E
CD16/32
F
TREM2/CD16-32/DAPI
N
TREM2
3dpl
O
CD68
P
TREM2/CD68/DAPI
G
TREM2
14dpl
H
CD16/32
I
TREM2/CD16-32/DAPI
Q
TREM2
14dpl
R
CD68
S
TREM2/CD68/DAPI
J
AI (arbitrary units)
4000
3000
2000
1000
30
20
10
0
***
a
****
a''
***
NL
3dpl
7dpl
14dpl
Time
(days post-lesion)
T
AI (arbitrary units)
4000
3000
2000
1000
0
****
a'
***
a'
NL
3
7
14
Time
(days post-lesion)

FIGURE 5 | Analysis of CD16/32 and CD68 expression in TREM2+ microglial cells after PPT. **(A–I)** Representative double-immunolabeled images combining TREM2 (green) and CD16/32 (red) in the ML of the DG in NL **(A–C)** at 3 dpl **(D–F)** and 14 dpl **(G–I)**. Note that both TREM2 + CD16/32+ (arrows), some of them very intensely stained (arrowheads) and TREM2+ CD16/32- (asterisk) microglial cells were observed. **(J)** Graph showing the AI index of CD16/32 expression in NL and PPT-lesioned mice at 3, 7, and 14 dpl (One-way ANOVA, time effect $p < 0.0001$; *post hoc* Tukey's test compared to NL $^{***}p < 0.001$, $^{****}p < 0.0001$; a $p < 0.01$, a$''$ $p < 0.001$ compared to previous time point). **(K–S)** Representative double-immunolabeled images combining TREM2 (green) and CD68 (red) in the DG of NL **(K–M)** and PPT-lesioned animals at 3 **(N–P)** and 14 dpl **(Q–S)**. Note that similarly to CD16/32, most TREM2+ ramified cells expressed also CD68 (arrows in **N–P**) at 3 dpl, whereas at 14 dpl TREM2 expression was restricted to the perinuclear area of CD68+ cells (arrowheads in **Q–S**). Also, some TREM2-CD68+ cells were found at 3 dpl (arrowheads in **N–P**). **(T)** Graph showing the AI index of CD68 expression in NL and PPT-lesioned mice at 3, 7, and 14 dpl (one-way ANOVA, time effect $p < 0.0001$; *post hoc* Tukey's test compared to NL $^{***}p < 0.001$, $^{****}p < 0.0001$; a$'$ $p < 0.01$ compared to previous time point). Scale bar **(A–I,K–S)** = 50 μm.

(**Figures 6G,N**), we found that both CD16/32 and CD68 levels increased rapidly at 3 and 7 dpl, respectively, remained elevated until 21 dpl, and decreased at 28 dpl (**Figures 6G,N**).

Expression of the Phagocytic Ligands ApoE and Galectin-3

According to results obtained in previous sections, we studied ApoE and Galectin-3 expression, both specific phagocytic ligands of TREM2 and DAM-associated molecules. The study was centered on the peak of TREM2 expression after PPT, around 3 dpl, and after FNA, at 14 and 21 dpl, compared to basal conditions.

In the NL hippocampus, no expression of ApoE was observed in microglia, like similarly observed in the PPT paradigm at any time-point (**Figures 7A–I**), as its expression was in all cases restricted to astrocytes (**Supplementary**

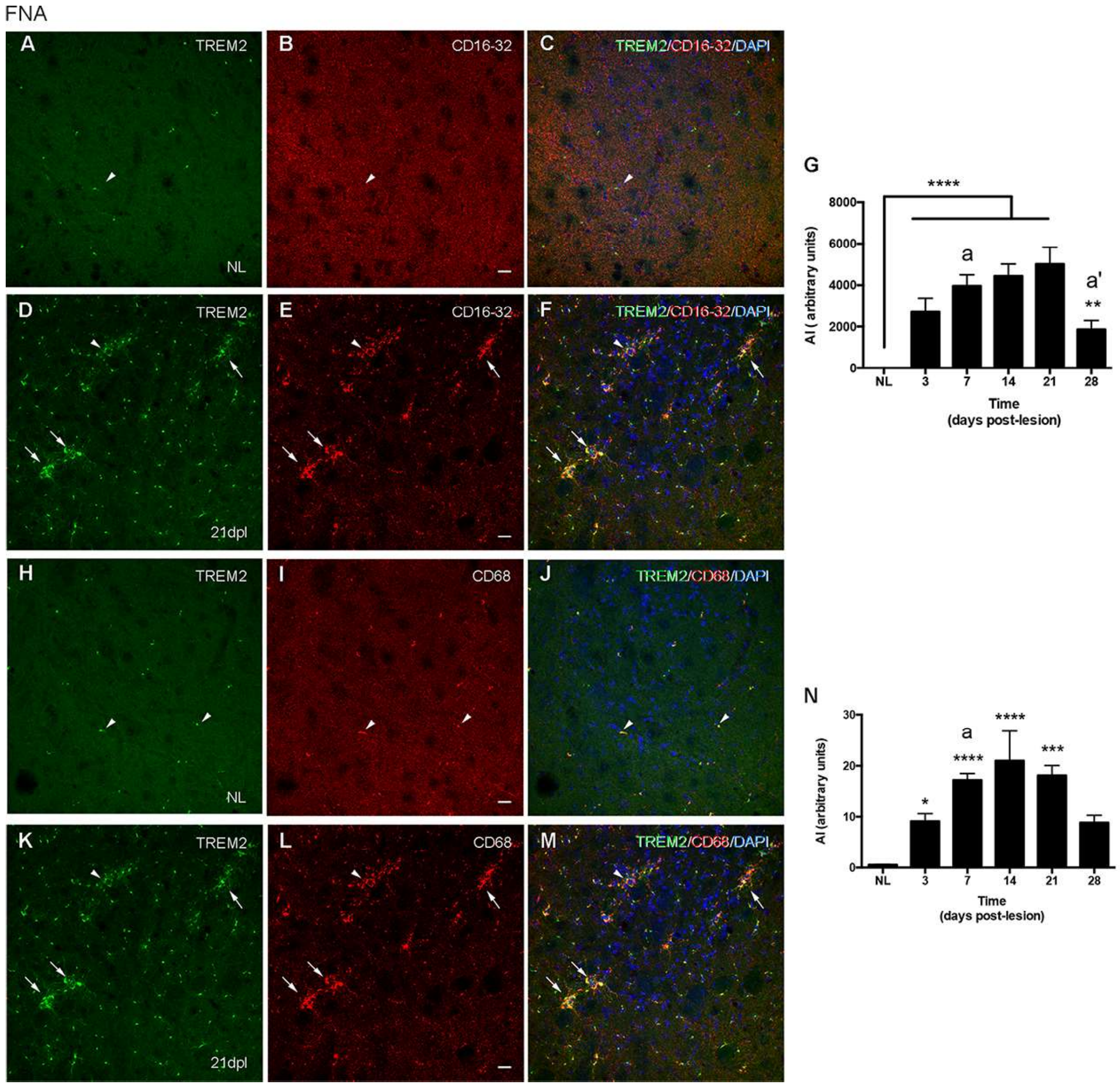
FNA
A
TREM2
NL
B
CD16-32
C
TREM2/CD16-32/DAPI
D
TREM2
21dpl
E
CD16-32
F
TREM2/CD16-32/DAPI
G
AI (arbitrary units)
8000
6000
4000
2000
0
****
a
a'
**
NL
3
7
14
21
28
Time
(days post-lesion)
H
TREM2
NL
I
CD68
J
TREM2/CD68/DAPI
K
TREM2
21dpl
L
CD68
M
TREM2/CD68/DAPI
N
AI (arbitrary units)
30
20
10
0
*
a
****
****
***
NL
3
7
14
21
28
Time
(days post-lesion)

FIGURE 6 | Analysis of CD16/32 and CD68 expression in TREM2+ microglial cells after FNA. **(A–F)** Representative double-immunolabeled images combining TREM2 (green) and CD16/32 (red) in the NL **(A–C)** and ipsilateral FN at 21 dpl **(D–F)**. Note that microglial clusters with low (arrowheads) or high (arrows) TREM2+ expression in their ramifications being CD16/32+ could be observed. **(G)** Graph showing the AI index of CD16/32 expression in the contralateral, NL, and the ipsilateral sides of the FN from 3 to 28 dpl (one-way ANOVA, time effect $p < 0.0001$; *post hoc* Tukey's test compared to NL $^{**}p < 0.01$, $^{****}p < 0.0001$, compared to the previous time-point a $p < 0.05$, a′ $p < 0.0001$). **(H–M)** Representative double-immunolabeled images combining TREM2 (green) and CD68 (red) in the NL **(H–J)** and ipsilateral FN of lesioned animals at 21 dpl **(K–M)**. Note that similarly to CD16/32, most CD68+ microglial clusters express high levels of TREM2 (arrows in **K–M**), but also some clusters with low levels of TREM2 were found to be CD68+ (arrowheads in **K–M**). **(N)** Graph showing the AI index of CD68 expression in NL and FNA-lesioned mice from 3 to 28 dpl (one-way ANOVA, time effect $p < 0.01$; *post hoc* Tukey's test compared to NL $^{*}p < 0.05$, $^{***}p < 0.001$, $^{****}p < 0.0001$, respect to the previous time-point a $p < 0.05$). Scale bar **(A–F,H–M)** = 50 μm.

Figure 1). Moreover, *de novo* expression of Galectin-3 in some TREM2+ microglial cells was reported at 2 and 3 dpl (**Figures 8A–F**).

After FNA, the expression of ApoE was restricted to astrocytes in the contralateral NL side (**Figures 9A–C**; **Supplementary Figure 2**), but on the ipsilateral side, ApoE staining was observed in cells of TREM2+ microglial clusters at both 14 and 21 dpl (**Figures 9D–I**). Moreover, ApoE+ facial motor neurons (FMN, dashed line circles in **Figures 9D–I**) were observed. As far as Galectin-3 is concerned, *de novo* expression of this marker was found in some TREM2+ microglial clusters, although no clear relationship between Galectin-3 and TREM2 intensities was observed, since clusters with high TREM2 levels presented variable Galectin-3 intensity staining (arrows and arrowheads, **Figures 10A–F**). Additionally, Galectin-3 staining on the surface of isolated FMN was found at 14 and 21 dpl (dashed line circles in **Figures 10A–F**).

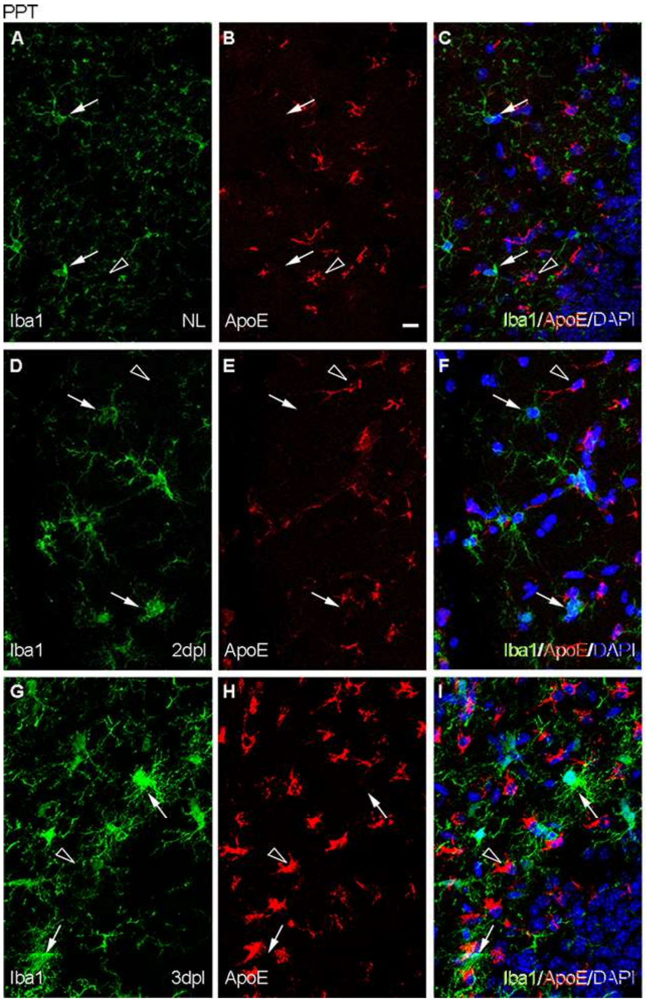

FIGURE 7 | Analysis of the expression of TREM2 ligand ApoE after PPT. **(A–I)** Representative images of double immunofluorescence combining ApoE (red) and Iba1 (green) in the NL DG **(A–C)** and at 2 dpl **(D–F)** and 3 dpl **(G–I)** after PPT. Note that ApoE expression could be observed on astrocyte-like cells (empty arrowheads), but not in microglia (white arrows) in all the time-points. Scale bar **(A–I)** = 10 μm.

Expression of the Homeostatic Microglial Marker P2RY12

Because ApoE and Galectin-3 molecules were upregulated, as it is seen in DAM, we were interested to observe whether the homeostatic receptor P2RY12 was downregulated, to further confirm similarities with the DAM phenotype. After PPT, in contrast to the high P2RY12 expression observed in all microglia of the NL DG; a gradual downregulation of P2RY12 levels was observed in TREM2+ microglial cells of the OML and MML until 3 dpl (arrowheads, **Figure 11**). However, in the FNA model, different levels of P2RY12 were reported in TREM2+ microglial clusters at both 14 and 21 dpl. Indeed, TREM2+ clusters showing either low or high P2RY12 were observed. Few TREM2- clusters located within the same region showed high P2RY12 levels (**Figures 12A–O**).

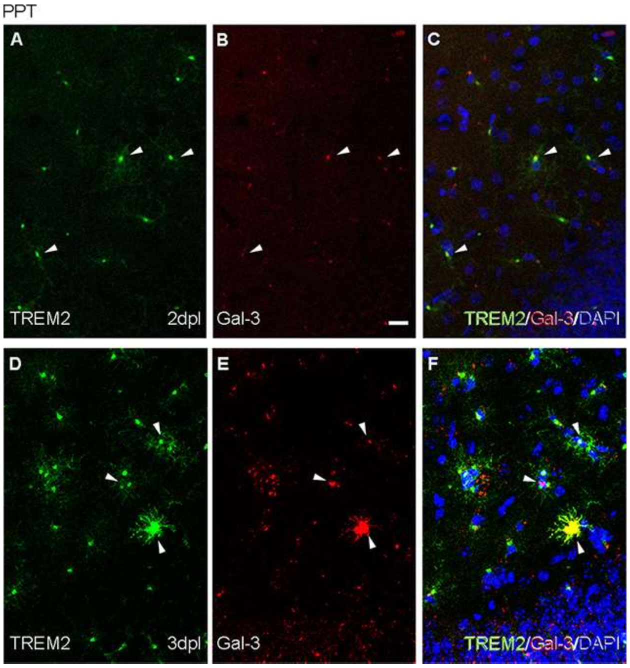

FIGURE 8 | Analysis of the expression of TREM2 ligand Galectin-3 after PPT. **(A–F)** Representative double immunofluorescence images combining Galectin-3 (red) and TREM2 (green) at 2 dpl **(A–C)** and 3 dpl **(D–F)** after PPT. Occasional microglial cells showing TREM2 expression in their ramifications contained Galectin-3 (white arrowheads) as perinuclear staining in both time-points. Note that at 3 dpl some microglial cells also presented Galectin-3 in their ramifications, indicating an increase of Galectin-3 compared to 2 dpl. Scale bar **(A–F)** = 10 μm.

Microglial Phagocytosis of Myelin by TREM2+ Microglia After PPT and FNA

To study the functional phagocytosis capacity of both TREM2+ and TREM2- microglia after PPT and FNA, we performed a myelin phagocytosis assay and flow cytometry analysis of CD11b+/CD45^{low} and CD11b+/CD45^{high} populations (**Figures 13A–D**). Our results show that in the CD11b+CD45^{low} population of NL hippocampus and FN, formed by microglia, TREM2- cells are phagocytosing myelin debris in low percentages, in all cases below 20% (**Figures 13E,M**). Interestingly, similar percentages are maintained after lesion (**Figures 13G,O**), despite the number of cells is increased in these conditions. Therefore, our results indicate that phagocytosis is not exclusive of TREM2+ cells within CD11b+/CD45^{low} cells but is a minor function within this population. On the contrary, when we studied CD11b+/CD45^{low}/TREM2+ cells in NL hippocampus and FN, we could observe that phagocytosis by microglial cells is increased, and differences between Myelin- and Myelin+ cells observed within the TREM2- population are hardly maintained (**Figures 13F,N**). Furthermore, in the lesioned hippocampus, 50% of cells are phagocyting myelin (**Figure 13H**), whereas after FNA there is a tendency to show a higher percentage of phagocytic TREM2+ cells (**Figure 13P**). In the case of CD11b+/CD45^{high} populations, formed by macrophages or highly activated microglia, TREM2- cells show a similar

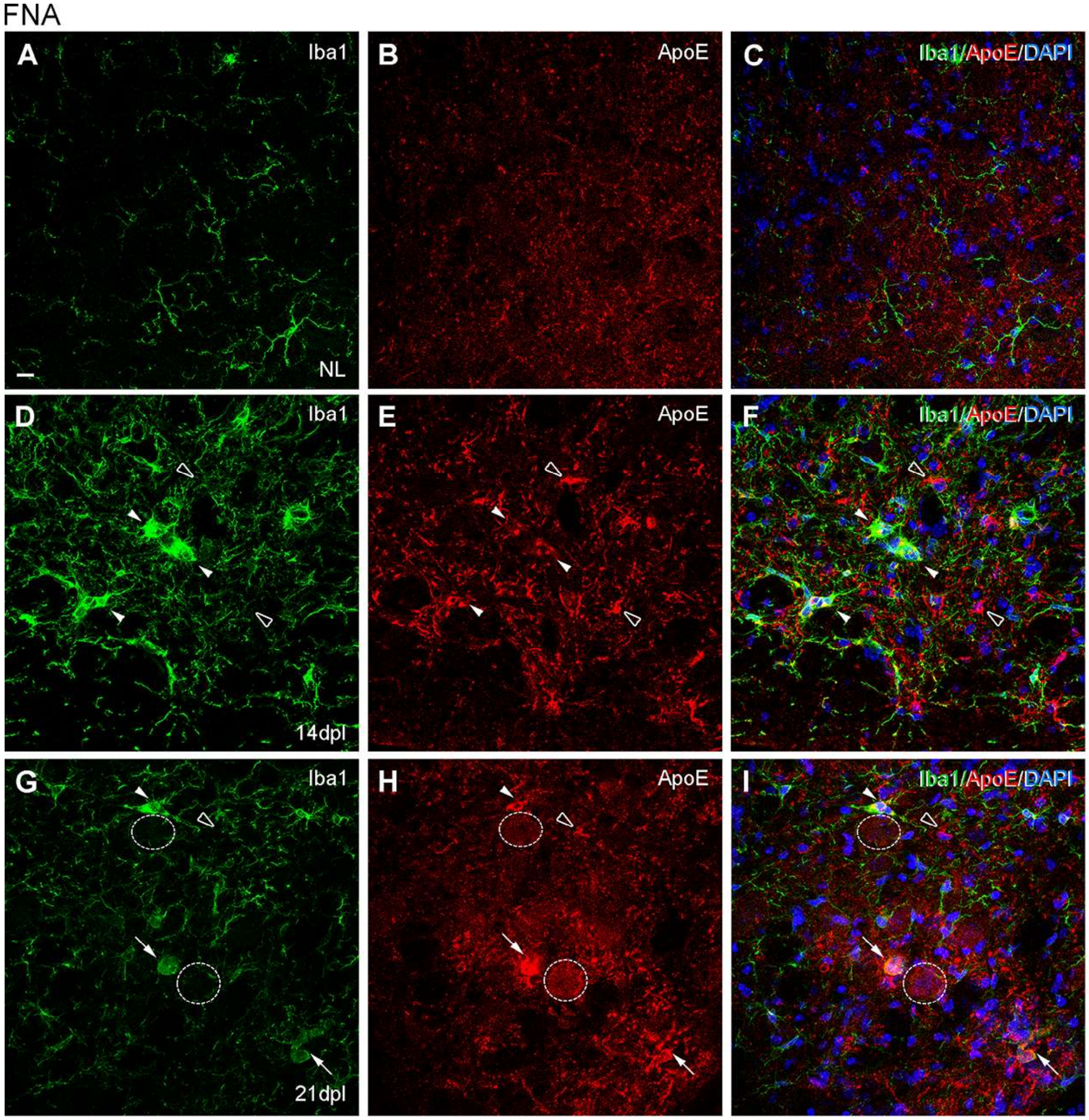

FIGURE 9 | Analysis of ApoE expression in microglial clusters after FNA. **(A–I)** Representative double-immunolabeled images combining Iba1 (green) and ApoE (red) in the NL FN **(A–C)** and at 14 dpl **(D–F)** and 21 dpl **(G–I)**. In the lesioned FN, astrocyte-like cells were easily identified by strong ApoE staining (empty arrowheads). Note that at 14 and 21 dpl, ApoE was also present in microglial clusters (white arrowheads), and in some of them with high levels of ApoE staining (white arrows), although not all clusters were positive for ApoE (data not shown). Additionally, at 21 dpl, some FMN showed ApoE staining on their surface (dashed line circles). Scale bar **(A–I)** = 10 μm.

phagocytic capacity than the one observed in CD11b+/CD45^{low} cells: high percentages of non-phagocytic cells are found in NL and lesioned hippocampus and FN (**Figures 13I,K,Q,S**). Observation of phagocytosis in CD11b+/CD45^{high}/TREM2+ population showed a completely opposed behavior, as NL and lesioned hippocampus and FN contained elevated percentages, over 70%, of phagocytic cells (**Figures 13J,L,R,T**). Altogether, our results indicate that TREM2 is a receptor preferentially found on phagocytotic cells but it is not exclusive of them, as also TREM2- cells can phagocytose myelin.

Transgenic Overproduction of Either IL-6 or IL-10 Modifies TREM2 Expression, Especially After Anterograde Degeneration (PPT Model)

Previous studies in our laboratory (Almolda et al., 2014; Villacampa et al., 2015; Recasens et al., 2019) using two Tg animal lines with an astrocyte-targeted expression of the pro-inflammatory cytokine IL-6 (GFAP-IL6Tg) and the anti-inflammatory cytokine IL-10 (GFAP-IL10Tg),

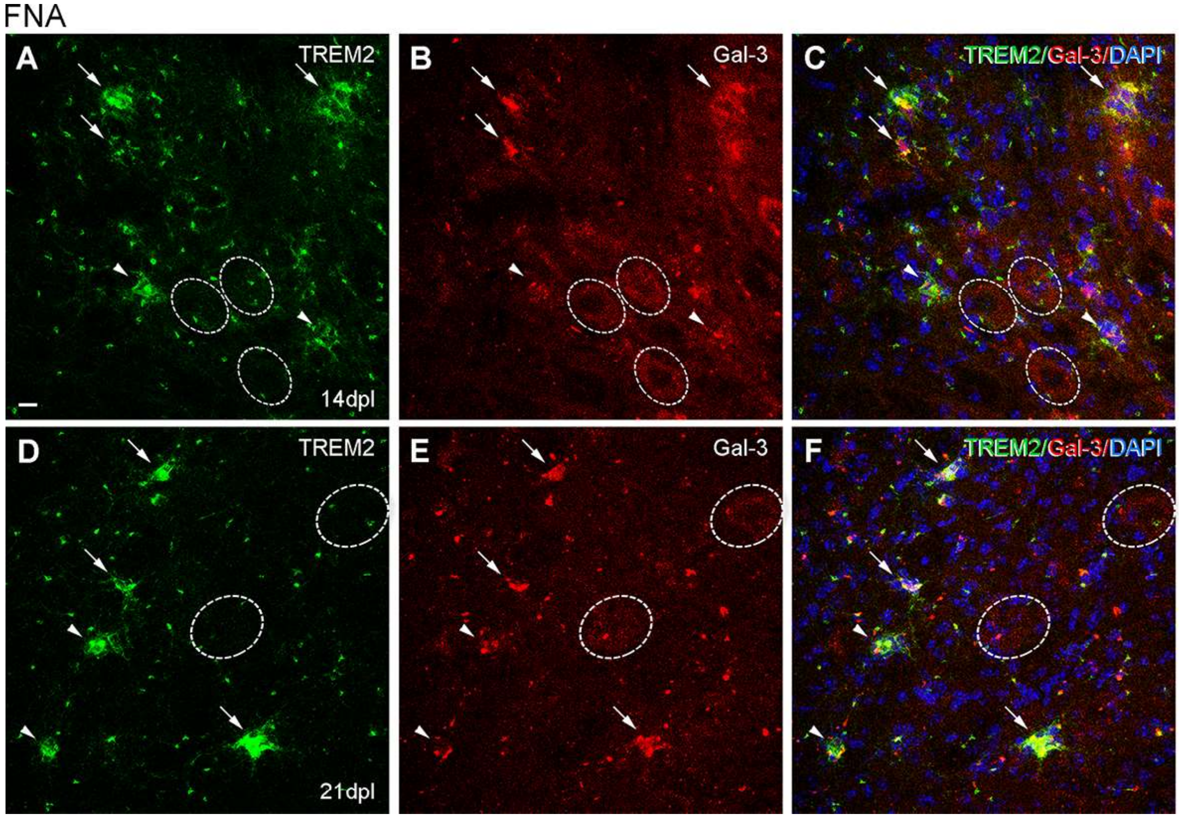

FIGURE 10 | Analysis of Galectin-3 expression in microglial clusters after FNA. **(A–F)** Representative double-immunolabeled images combining TREM2 (green) and Galectin-3 (red) in the ipsilateral FN at 14 dpl **(A–C)** and 21 dpl **(D–F)**. Note that at 14 and 21 dpl, clusters displaying high intensity for Galectin-3 (white arrows) could show either high or low intensity for TREM2. Likewise, clusters presenting low Galectin-3 (white arrowheads) presented variable TREM2 intensity as well. No differences in microglial cluster Galectin-3 staining were seen between 14 and 21 dpl. FMN were also positive for Galectin-3 at 14 and 21 dpl, being more easily detectable at 14 dpl (dashed line circles). Scale bar **(A–F)** = 10 μm.

demonstrated significant differences in the microglial activation pattern after PPT and FNA. These differences correlated with important modifications in lesion outcomes, either neuronal survival or axonal sprouting. Considering that the effect of cytokines into TREM2 expression is not known and that neuronal survival and axonal sprouting are conditioned to the microglial phagocytic activity which, according to our results, can be modified by TREM2 expression, we found of great interest to assess the regulation of cellular TREM2 expression in these Tg animals after both experimental models.

In NL conditions, we detected a qualitative increase of TREM2 intensity levels in the OML and MML of the hippocampus of both GFAP-IL6Tg and GFAP-IL10Tg mice; but no modifications were observed in the NL FN (**Figures 14B,D,F,H**; **Supplementary Figures 3A,E,I,L**).

After PPT, a higher percentage of area occupied by TREM2 in the deafferented area of the ML was detected at 3 dpl in both Tg mice (**Figures 14A,C**; **Supplementary Figures 3B,F**). These differences were more pronounced in the GFAP-IL6Tg mice than in GFAP-IL10Tg mice compared to their respective WT. In line with these observations, at 3 dpl, a higher percentage of ramified TREM2+/Iba1+ microglial cells was found in GFAP-IL10Tg (74.7 ± 1.91%) and in GFAP-IL6Tg (61.97 ± 2.58%) concerning WT animals (48.1 ± 1.96%; **Figures 15A–D**).

After FNA, a significantly lower percentage of TREM2 stained area was observed at 21 dpl in GFAP-IL6Tg mice compared to WT mice (**Figure 14E**; **Supplementary Figure 3K**). Similar to WT mice, in GFAP-IL6Tg and GFAP-IL10Tg mice, all or almost all microglial clusters showed TREM2 staining in microglial ramifications at 14 dpl and at 21 dpl (**Figure 15E**).

DISCUSSION

In this work, we studied TREM2 regulation in microglia after axonal injury, in both anterograde and retrograde neurodegeneration models: the PPT and the FNA respectively. Results obtained demonstrate an upregulation of TREM2 expression in both models of axonal injury but following different patterns. In the PPT, TREM2+ cells appeared at early time-points (2 and 3 dpl), whereas after FNA TREM2+ microglia were observed mainly forming clusters at 14 and 21 dpl. Also, we identified singular subpopulations of TREM2+ microglia expressing CD16/32, CD68 as well as showing *de novo* expression of ApoE or Galectin-3 and diverse levels of the homeostatic P2RY12 molecule. Finally, using Tg animals,

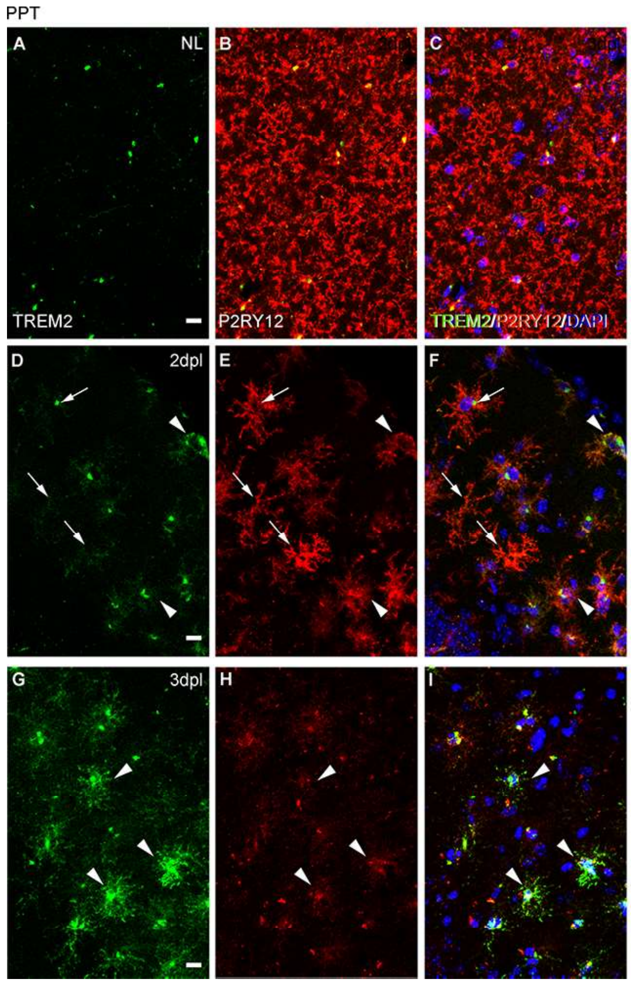

FIGURE 11 | Analysis of P2RY12 expression in microglial cells after PPT. **(A–I)** Representative images showing P2RY12 expression in the DG of the hippocampus in NL conditions **(A–C)**, at 2 dpl **(D–F)**, and 3 dpl **(G–I)** after PPT. In NL conditions, TREM2 (in green) is expressed accumulated adjacent to the nucleus, and high levels of P2RY12 (in red) are found in all microglial cells. After lesion, at 2 dpl, most microglia show low levels of TREM2 in ramifications and high levels of P2RY12 expression in all microglial cells (arrows). Also, some microglia with high levels of TREM2 expression and low levels of P2RY12 microglia are observed (arrowheads), being the latter the microglial phenotype mostly seen at 3 dpl. Scale bar **(A–I)** = 10µm.

we demonstrated that the cytokine microenvironment, which modifies microglial activation, influenced TREM2 expression, especially in the PPT paradigm and under IL-6 overexpression. In the following paragraphs, we will discuss our findings with the current literature.

TREM2 Is Increased in Activated Microglial Cells After Both PPT and FNA

TREM2 is a receptor found in the membrane of myeloid immune cells such as macrophages, osteoclasts, and microglia (Schmid et al., 2002; Colonna, 2003). Under basal conditions, TREM2 has been reported in microglial cells, both *in vitro* and *in vivo*, during development and in adulthood (Schmid et al., 2002; Chertoff et al., 2013). In agreement, we observed constitutive TREM2 expression in microglia in the FN and hippocampus of NL animals. In these regions most TREM2 labeling was restricted to a concentrated area in the cytoplasm, in a position adjacent to the nucleus of the microglial cells, coinciding with a previous study where the intracellular distribution was shown in two pools: a deposit in the Golgi complex and a population of exocytic vesicles, that would facilitate a continuous translocation to and recycled from the cell surface (Prada et al., 2006). This storage of intracellular TREM2 favors the continuous functional adaptation of these cells to the microenvironment and their rapid response to microglial activation. However, the fact that TREM2 shall be exposed to the membrane to interact with their ligands, lead us to study the TREM2+ microglial population appearing after lesions, showing elevated levels of TREM2 expression in ramifications, and according to our flow cytometry study, at least with partial TREM2 expression at the level of the cytoplasmic membrane.

In our study, upregulation of TREM2 expression could be observed in both models of axonal injury, being coincident with the previous general *in vivo* data in chronic (Jay et al., 2017a; Sayed et al., 2018) and acute CNS inflammatory injuries (Saber et al., 2017; Scott-Hewitt et al., 2017; Wu et al., 2017), as well as in other axonal injury models (Kobayashi et al., 2016; Tay et al., 2018). Additionally, an increase in sTREM2 could be found at the peak of TREM2 microglial expression after PPT, which was not detected after FNA. sTREM2 is the result of proteolytic TREM2 cleavage by ADAM10 and ADAM17 at H157–S158 peptide bond, resulting in its liberation. Despite little is known about the role of sTREM2, this fraction has been related to the potentiation of several microglial functions including pro-inflammatory cytokine production, migration, survival, and phagocytosis (Zhong et al., 2017, 2019).

Although both injury models presented expression of TREM2 in microglia, differences in the pattern of expression of this molecule were found between anterograde and retrograde degeneration models. Concretely, after PPT, TREM2 expression followed a pattern coincident with microglia activation (Recasens et al., 2019), but after FNA, TREM2 levels increased at 14–21 dpl and were restricted to microglial clusters that do not coincide with microglial activation, which starts at 3 dpl, peaks from 7 to 14 dpl, and is downregulated afterward (Villacampa et al., 2015). These results suggest that not all activated microglia express TREM2 and pointed towards a specific role of this receptor in microglial function. Differences in TREM2 expression could be related to the nature of the lesion (anterograde vs. retrograde) and microglial cell function along the time-course of both models. On one hand, PPT is a model that involves the complete transection of the perforant pathway, that produces an anterograde axonal and terminal degeneration of these axons in the outer 2/3 of the ML in the hippocampal DG. Due to this lesion, a rapid and robust microglial activation is induced in the DG at 2–5 dpl (Lynch et al., 1972; Jensen et al., 1999; Ladeby et al., 2005), whose principal function is to phagocyte myelin and neuronal debris (Nielsen et al., 2009), contributing to the structural reorganization and axonal collateral sprouting initiated around 7 dpl and being complete at 14 dpl (Deller et al., 2007). On the other hand, the FNA model involves a mechanical transection of the facial nerve,

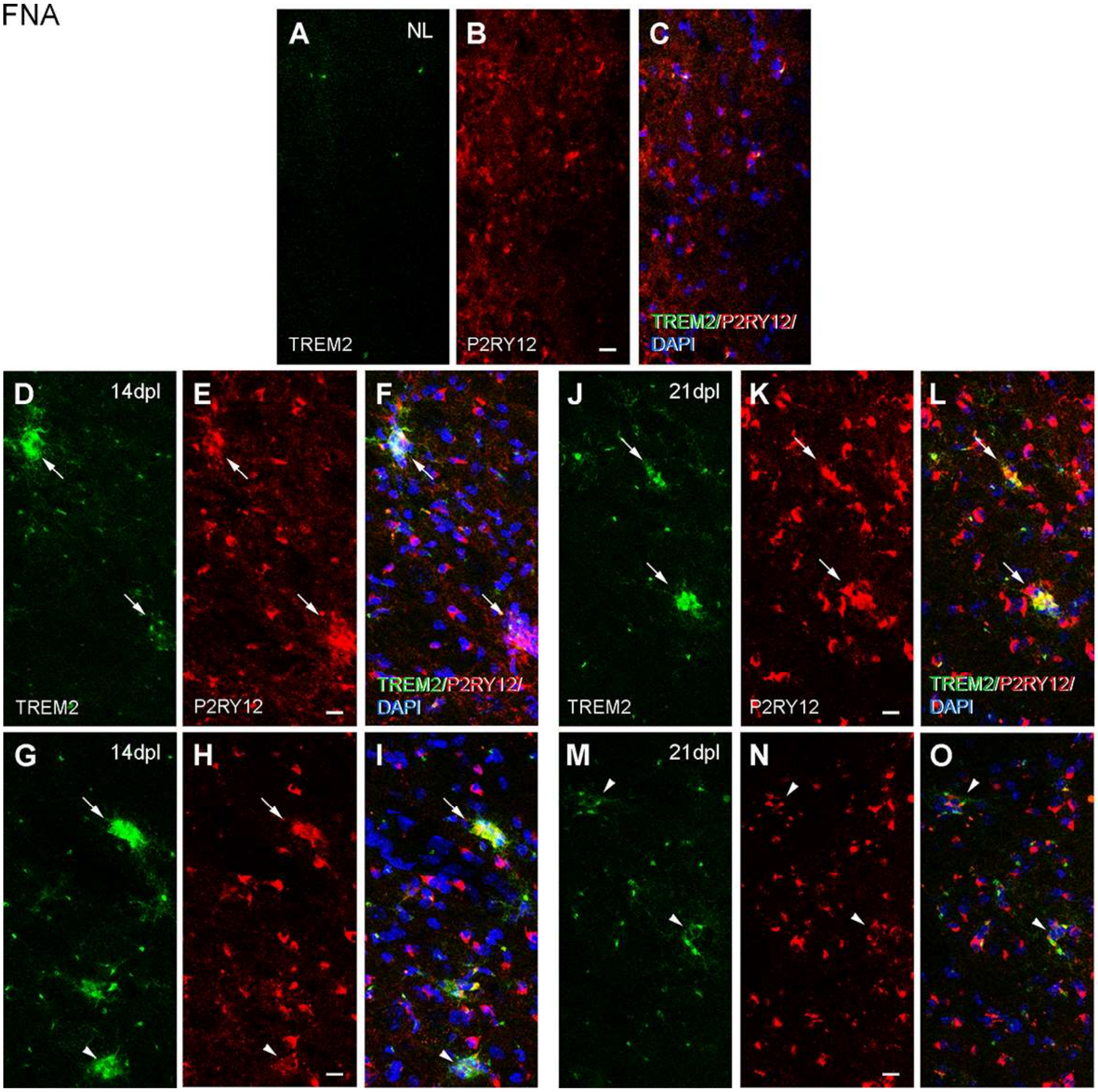

FIGURE 12 | Analysis of P2RY12 expression in microglial clusters after FNA. **(A–O)** Representative double-immunolabeled images combining TREM2 (green) and P2RY12 (red) in the ipsilateral NL FN **(A–C)** and at 14 **(D–I)** and 21 dpl **(J–O)**. Note that clusters with high levels of P2RY12 (arrows) can present both high and low levels of TREM2. In the same way, clusters with low levels of P2RY12 (arrowheads) show high and low levels of TREM2. No differences were detected between all the time-points in terms of P2RY12 staining. Scale bar **(A–O)** = 10 μm.

that leads to retrograde neuronal degeneration accompanied by a dramatic microglial activation. During early microglia activation and proliferation, from 3 to 7 dpl, TREM2 expression is mainly intracytoplasmatic and does not increase its expression in ramifications. Importantly, we observe an increase in intracellular TREM2 in this period, which could suggest a role for the intracellular TREM2 pool in microglia. Later, TREM2 is upregulated in specific structures called microglial clusters, first appearing at 14 dpl, located around FMN and involved in phagocytosis (Moran and Graeber, 2004).

The fact that TREM2 increases its expression in microglia coinciding in both models with the specific time-point related to phagocytosis, together with the expression of different markers, CD16/32, and CD68, involved in this function, points out to an especially relevant role of TREM2+ microglia after axonal injury in this function.

TREM2+ Cells Expressed Markers Related to Proliferation and Phagocytosis After FNA and PPT

The phenotypic characterization of TREM2+ microglial cells showed expression of both proliferation and phagocytic markers after PPT, but only phagocytic markers after FNA.

In terms of proliferation, our results showed that, after PPT, all proliferating microglia were TREM2+. In previous reports in DAP12KO mice, a reduced microglial increase

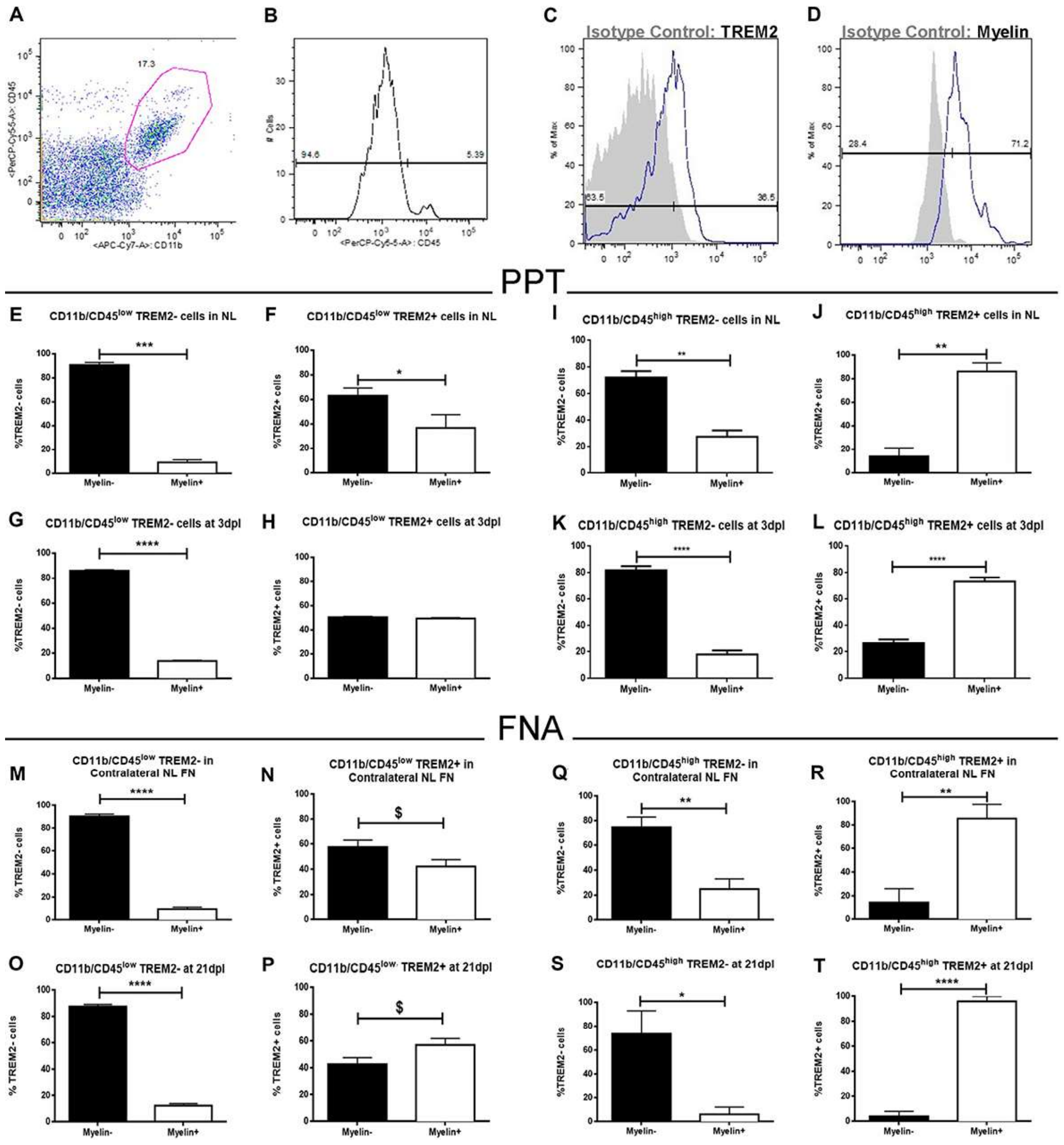

FIGURE 13 | Flow cytometry analysis of myelin phagocytosis by TREM2+ microglia and macrophages from NL and lesioned hippocampus and FN after PPT and FNA. **(A)** Representative dot-plot of CD11b/CD45 expression in cells obtained from the hippocampus of NL animals. The selected region was the population of cells used in this study. **(B)** Representative histogram where populations of CD11b+/CD45$^{\text{low}}$ cells (microglia) and CD11b+/CD45$^{\text{high}}$ cells (macrophages) were defined. **(C,D)** Representative histogram-plot showing the expression of TREM2 **(C)** and Myelin **(D)** in the population of microglia/macrophages in comparison to the corresponding isotype control. **(E–H)** Graphs showing the percentage of TREM2− and TREM2+ cells phagocyting myelin in NL **(E,F)** and at 3 dpl **(G,H)** in CD11b+/CD45$^{\text{low}}$ population after PPT. **(I–L)** Graphs showing the percentage of TREM2− and TREM2+ cells phagocyting myelin in NL **(I,J)** and at 3 dpl **(K,L)** in CD11b+/CD45$^{\text{high}}$ population after PPT. **(M–P)** Graphs showing the percentage of TREM2− and TREM2+ cells phagocyting myelin in contralateral NL FN **(M,N)** and at 21 dpl **(O,P)** in CD11b+/CD45$^{\text{low}}$ population after FNA. **(Q–T)** Graphs showing the percentage of TREM2− and TREM2+ cells phagocyting myelin in contralateral NL FN **(Q,R)** and at 21 dpl **(S,T)** in CD11b+/CD45$^{\text{high}}$ population after FNA. **(E–T)** Results were represented as ± SEM (Unpaired Student's *t*-test, ****$p \leq 0.0001$, ***$p \leq 0.001$, **$p \leq 0.01$, *$p \leq 0.05$, $^{\$}p \leq 0.08$).

after spinal nerve transection (Kobayashi et al., 2016) was found. Also, TREM2KO mice showed reduced microglia proliferation during homeostasis and after injury (Cantoni et al., 2015; Poliani et al., 2015; Zheng et al., 2017), and impaired proliferation was observed in AD mouse models without TREM2 or harboring dysfunctional TREM2 variants (Jay et al., 2017a; Cheng-Hathaway et al., 2018; Meilandt et al., 2020). On the other hand, some authors demonstrated that lack of TREM2 did not affect microglia proliferation in microglial cell cultures (Noto et al., 2010) or after spinal nerve

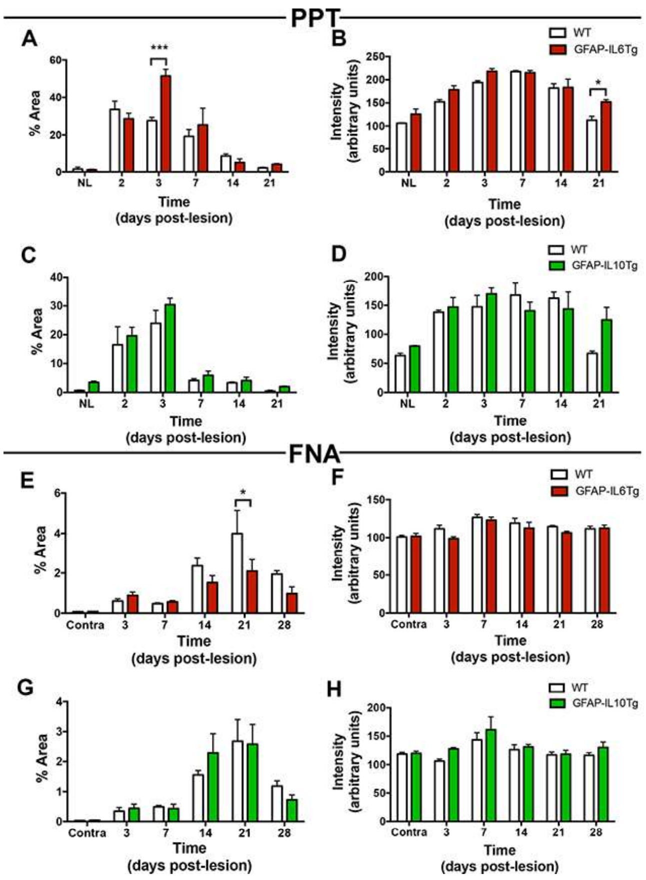

FIGURE 14 | Temporal pattern of TREM2 expression in microglial cells in mice with astrocyte-targeted overexpression of IL-6 (GFAP-IL6Tg) or IL-10 (GFAP-IL10Tg) compared to their corresponding wild-type (WT) after PPT and FNA. **(A–D)** Graphs showing either the percentage of Area **(A,C)** or intensity **(B,D)** of TREM2 expression in the OML and MML of the DG of PPT-lesioned GFAP-IL6Tg, GFAP-IL10Tg, and their corresponding WT littermates. Statistically significant differences are observed between GFAP-IL6Tg and WT animals in the percentage of Area of TREM2 expression at 3 dpl (two-way ANOVA, time effect $p < 0.0001$, genotype $p = 0.07$; interaction time-genotype $p < 0.01$; Sidak's multiple comparison test, $^{***}p < 0.001$) as well as the intensity of TREM2 expression (two-way ANOVA, time effect $p < 0.0001$, genotype $p < 0.01$; Sidak's multiple comparison test, $^{*}p < 0.05$). Also, differences between GFAP-IL10Tg and WT mice are shown in the percentage of Area of TREM2 expression (two-way ANOVA, time effect $p < 0.0001$, genotype $p = 0.08$; no significant differences were found with Sidak's multiple comparison test) and the intensity of TREM2 expression (two-way ANOVA, time effect $p < 0.0001$, genotype $p = 0.308$; no significant differences were found with Sidak's multiple comparison test). **(E–H)** Graphs showing either the percentage of Area **(E,G)** or intensity **(F,H)** of TREM2 expression in the ipsilateral FN of GFAP-IL6Tg and GFAP-IL10Tg lesioned animals, and their corresponding WT littermates. Differences in the percentage of Area (two-way ANOVA, time effect $p < 0.0001$, genotype effect $p < 0.05$; Sidak's multiple comparison test, $^{*}p < 0.01$) and intensity (two-way ANOVA, time effect $p < 0.0001$, genotype effect $p = 0.06$; no significant differences detected with Sidak's multiple comparison test) of TREM2 in GFAP-IL6Tg compared to WT were found. In the case of GFAP-IL10Tg, no statistically significant differences between time-points were observed at neither the percentage of Area (two-way ANOVA, time effect $p < 0.0001$, genotype effect $p = 0.883$, no significant differences detected with Sidak's multiple comparison test) nor the intensity (two-way ANOVA, time effect $p < 0.01$, genotype effect $p = 0.06$; no significant differences detected with Sidak's multiple comparison test).

transection in DAP12KO (Guan et al., 2016). From our point of view, our current study demonstrates that the increase in TREM2+ microglia depends on the specific features of microglial response to axonal injury. In PPT, proliferation is coincident with microglia activation, and the lesion is rapidly rectified; while after FNA, activation and proliferation are immediately triggered, and phagocytosis of late degenerating FMN and injury resolution are delayed. Our BrdU study demonstrated that cells that were previously proliferating after FNA, and were not showing TREM2 expression at that time, were forming phagocytic microglial clusters, which are mainly TREM2+. Yet, further studies are needed to demonstrate a clear relationship between TREM2 expression and proliferation in axonal lesions.

Despite TREM2 phagocytic role has been extensively studied in acute and chronic neurodegenerative diseases models as AD or multiple sclerosis (reviewed in Deming et al., 2018; Karanfilian et al., 2020); to the best of our knowledge, this is the first study showing a link of TREM2 with phagocytic microglia after direct or primary acute axonal injury. As far as the possible role of TREM2+ microglial cells in phagocytosis is concerned, our results indicate an important implication of TREM2 in phagocytosis in both models, thus coinciding with the view of TREM2 as a receptor involved in the triggering of an "eat-me" signal (Neumann et al., 2009). After both PPT and FNA, most TREM2+ cells also expressed the phagocytic-associated molecules CD16/32 and CD68, and the myelin phagocytosis assay in TREM2+ microglia showed higher percentages of phagocytosis of myelin debris compared to TREM2- cells. In our results, the pattern of expression of TREM2 in microglia and its specific location, especially in microglial clusters, lead us to speculate that, after FNA, TREM2+ microglia are involved in the phagocytosis of degenerating FMN close to microglial clusters, whereas in the PPT paradigm TREM2 is recognizing myelin debris, that appears at early time-points in this lesion (Jensen et al., 1999). Certain specificity of TREM2 for phagocytosis of myelin debris and apoptotic neurons has already been suggested based also on TREM2 ligands (Gervois and Lambrichts, 2019). In the case of myelin phagocytosis, similarly to our observations, TREM2 increases its expression correlating to myelin debris appearance in demyelinating models (Piccio et al., 2007; Takahashi et al., 2007; Scott-Hewitt et al., 2017). Overexpression of TREM2 in administered bone-marrow-derived cells improved myelin clearance in EAE-induced mice (Takahashi et al., 2005), while TREM2 blockade increased demyelination (Piccio et al., 2007). TREM2KO microglia showed diminished microglia activation and was unable to degrade myelin in cuprizone models (Cantoni et al., 2015; Poliani et al., 2015; Nugent et al., 2020), and accordingly, the treatment with an agonistic antibody against TREM2 enhanced microglial clearance and digestion of myelin, facilitated remyelination and preserved axonal integrity (Cignarella et al., 2020). Our results also suggest that TREM2+ microglia phagocyte myelin debris more efficiently, which may facilitate a rapid lesion resolution after PPT, and the proper axonal collateral sprouting.

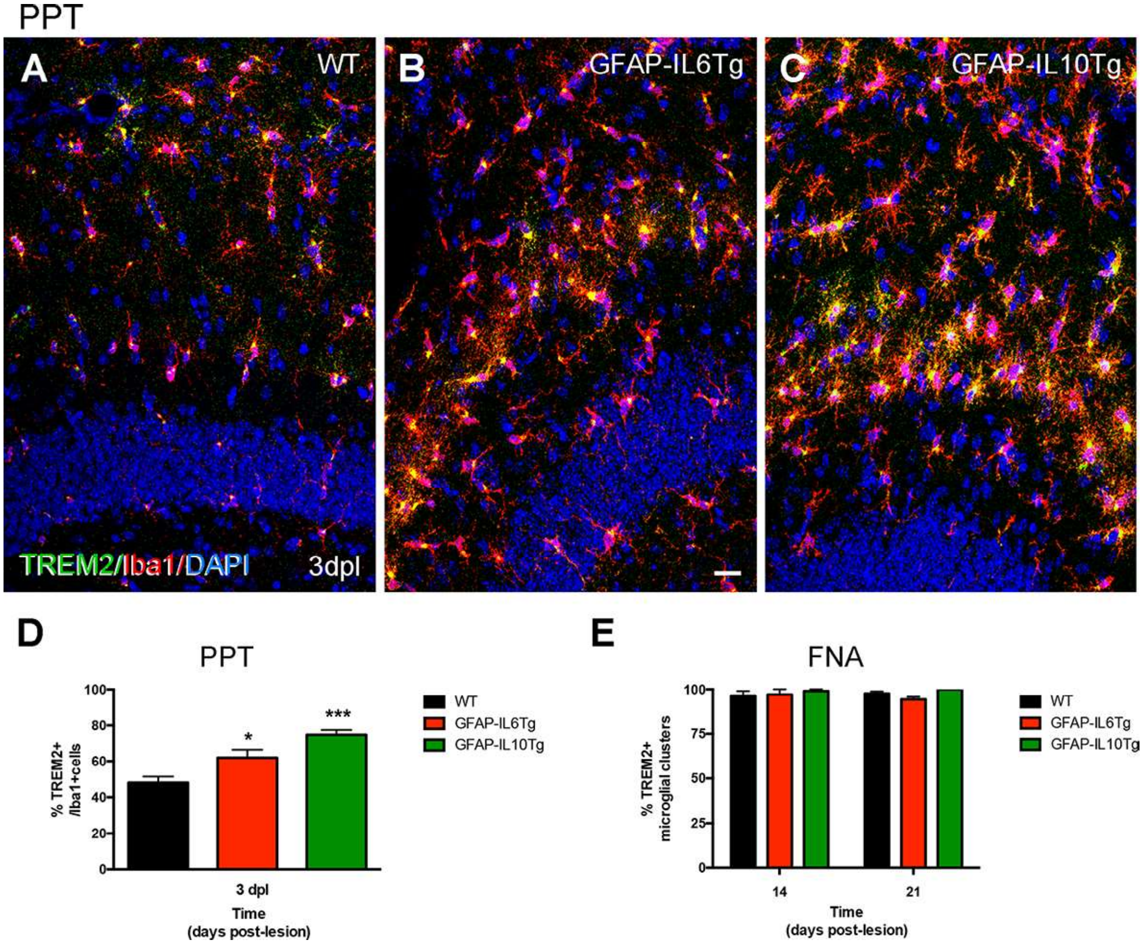

FIGURE 15 | Quantification of TREM2+ microglia subpopulation after PPT and TREM2+ microglial clusters after FNA in GFAP-IL6Tg, GFAP-IL10Tg, and WT mice. **(A–C)** Representative double-immunolabeled images combining TREM2 (green) and Iba1 (red) in the ML of the DG at 3 dpl in WT **(A)**, GFAP-IL6Tg **(B)**, and GFAP-IL10Tg **(C)**. **(D)** Graph showing the percentage of TREM2+ ramified cells concerning the total number of Iba1 cells at 3 dpl in WT (48.1 ± 1.96%), GFAP-IL6Tg (61.97 ± 2.58%), and GFAP-IL10Tg (74.7 ± 1.91%). A higher percentage of TREM2/Iba1 cells are found in Tg mice concerning WT at 3 dpl (one-way ANOVA, $*p < 0.01$; *post hoc* Dunnet's test, GFAP-IL6Tg vs. WT $*p = 0.01$, and GFAP-IL10Tg vs. WT $***p = 0.001$). **(E)** Graph showing the percentage of microglial clusters with TREM2+ expression in their ramifications at 14 and 21 dpl after FNA in WT, GFAP-IL6Tg, and GFAP-IL10Tg. Scale bar **(A–C)** = 50 μm.

On the other hand, a higher avidity in phagocytosis has been established for apoptotic or degenerating cells. *In vitro* studies showed inhibition of phagocytosis of apoptotic neurons after TREM2 knockdown, while on the contrary, apoptotic neurons were cleared more efficiently by TREM2+ BV2 cultured cells (Takahashi et al., 2005; Hsieh et al., 2009). TREM2KO microglia showed also decreased phagocytic capacity, and possibly related to this fact, a reduced age-associated neuron loss was found in TREM2KO aged mice (Linnartz-Gerlach et al., 2019). In our study, TREM2 was mainly expressed in microglial clusters, reported to phagocytose degenerating FMN (Moran and Graeber, 2004), which reinforces the role of TREM2+ cells in neuronal phagocytosis in this model. As reported for PPT, TREM2+ microglia after FNA showed higher phagocytic activity of myelin compared to TREM2- microglia, and suggested that, despite being two different axonal lesions with two different targets, the phagocytic capacity of TREM2+ microglia in both models is independent of their specific lesion particularities.

In line with these results, ApoE, a phagocytic ligand of TREM2, was found in TREM2+ microglia after FNA, but not after PPT. ApoE has been reported to be upregulated after FNA in microglia, as we and other transcriptomic studies found (Tay et al., 2018). Moreover, the ApoE staining in FMN could indicate a role of this molecule as a ligand in TREM2-mediated phagocytosis in clusters, as demonstrated in other studies (Krasemann et al., 2017). Apoptotic neurons can bind to ApoE, and Atagi et al. (2015) demonstrated that its expression enhanced microglial phagocytosis, acting as an opsonin. Consequently, studies on ApoE-KO animals showed decreased FMN death after FNA (Krasemann et al., 2017). To our knowledge, ApoE upregulation has been described in DAM microglia, which has been associated with axonal dystrophy in AD models but is not induced in neuropathic pain (Krasemann et al., 2017; Deczkowska et al., 2018). Given our results, microglial ApoE may not be induced, in specific circumstances, in TREM2+ microglia of injuries affecting only axons, and consequently, TREM2+ microglia could be phagocyting axonal debris after PPT in an ApoE-independent manner.

In this work, we additionally studied another recently described TREM2 ligand, Galectin-3 (Boza-Serrano et al., 2019). In our observations, we found that Galectin-3 was expressed in TREM2+ microglial cells after both types of axonal injuries. Galectin-3 is a molecule extensively related to microglial myelin phagocytosis and clearance (Puigdellivol et al., 2020), which reinforces this role in PPT TREM2+ microglia. Also, after FNA, we observed the expression of Galectin-3 in microglia and on the surface of some FMN, as occurred with ApoE. Galectin-3 is similarly described in the surface of neurons after traumatic brain injury, where it has been suggested to act as an alarmin (Yip et al., 2017; Boza-Serrano et al., 2019) or an opsonizing molecule in the phagocytosis of desialylated neurons (Nomura et al., 2017; Puigdellivol et al., 2020), thus reinforcing this phagocytic role for TREM2+/Galectin-3+ microglia after FNA.

Apart from the phagocytic particularities, TREM2-mediated phagocytosis has been qualified as an "anti-inflammatory," because it results in the production of anti-inflammatory cytokines (Takahashi et al., 2007; Hsieh et al., 2009) due to an antagonistic role of TREM2 upon NF-κB activation (Yao et al., 2019). Cuprizone studies showed that the absence of TREM2 expression in microglia increases axonal injury and impairs a proper repair (Cantoni et al., 2015; Poliani et al., 2015) that can be rescued with TREM2 activating antibodies (Cignarella et al., 2020). In our study, in both injury models, inflammation is downregulated around the peak of TREM2 expression (Gehrmann et al., 1991; Moran and Graeber, 2004), which indicates a reparatory role for this receptor. As suggested by the above-mentioned studies, the reparatory effect could be the result of the efficient TREM2-mediated phagocytosis accompanied by the secretion of anti-inflammatory cytokines, that could facilitate either axonal sprouting or effective FMN clearance and neuronal regeneration, depending on the model.

Although we centered our attention on microglial TREM2-mediated phagocytosis, it is important to note also that CD16/32+ and CD68+ microglial cells without TREM2 expression were found in both injury models. Our study shows that TREM2 is only triggered in a subpopulation of phagocytic microglial cells and strongly suggests a TREM2-independent microglial phagocytosis. Indeed, some reports indicate that TREM2 is not strictly required for microglia to produce the engulfment of cellular remnants, but it increases the efficient phagocytosis of apoptotic neurons (Hsieh et al., 2009; Cantoni et al., 2015). These results are following our phagocytosis study, where lower percentages of TREM2-independent microglial phagocytosis are observed in all conditions when compared to TREM2+ phagocytosis of myelin. Interestingly, a recent work assigned a role for TREM2 in lipid digestion, excluding its involvement in the uptake of myelin debris during microglial phagocytosis which—according to cell cultures assays performed with TREM2KO bone-marrow-derived cells in this work—may be rescued by high levels of M-CSF (Nugent et al., 2020). Given these results, the relevance of TREM2-mediated phagocytosis may be dependent on the microenvironment in which phagocytosis takes place. On the other hand, the role of sTREM2 in phagocytosis mediated by TREM2- cells may not be excluded. Interestingly, PPT showed increased levels of sTREM2 after lesion, that is not observed after FNA, and are concomitant with high CD68 levels. sTREM2 has been involved in the stimulation of β-amyloid phagocytosis and lysosomal pathways, and it also increased CD68 expression in the AD model (Zhong et al., 2019). Therefore it could be interesting to further explore the role of sTREM2 in the phagocytic function of this model.

Finally, we explored the possibility that TREM2+ cells presented a downregulation of the homeostatic microglial receptor P2RY12. Downregulation of this receptor, together with the expression of TREM2, CD68, CD16/32, Galectin-3, and ApoE has been defined by transcriptomic studies to be associated with the induction of a DAM-phenotype in microglia (Keren-Shaul et al., 2017; Krasemann et al., 2017; Boza-Serrano et al., 2019). In line with these works, our results showed a general P2RY12 downregulation in microglia after PPT in the peak of activation, which is not restricted to TREM2+ microglia. However, after FNA, different patterns of P2RY12 expression were observed in TREM2+ clusters, including clusters with high P2RY12 levels, which suggested the induction of diverse microglial phenotypes within the TREM2+ microglia subpopulation. Similarly, other reports also found activated microglia with high P2RY12 expression in pre-active and chronic white matter lesions of multiple sclerosis and in diffuse β-amyloid plaques in human samples (van Wageningen et al., 2019; Walker et al., 2020). Still, the significance of TREM2 microglia with high P2RY12 levels remain to be explored.

Altogether, the phenotypic characterization of TREM2+ microglia after PPT and FNA indicates a clear involvement of this molecule in a subpopulation of phagocytosing microglia, probably aimed at recognizing myelin debris and degenerating neurons, that could clear more efficiently these cell remnants. In the PPT paradigm, TREM2+ microglia were CD16/32+, CD68+, Galectin 3+, ApoE-, whereas, in the FNA model, TREM2+ microglia in clusters was CD16/32+, CD68+, Galectin-3+, ApoE+ and showed P2RY12 variable expression.

Pro-inflammatory Rather Than Anti-Inflammatory Local Microenvironments Influence Microglial TREM2 Expression Mainly After PPT but Also After FNA

The final part of this work was to analyze possible modifications of TREM2 in both GFAP-IL6Tg and GFAP-IL10Tg animals after PPT and FNA. To our knowledge, few *in vitro* and *in vivo* data are available on the effect of cytokines on the regulation of microglial TREM2 expression (Petković et al., 2016; Zhai et al., 2017; Zhong et al., 2019). Moreover, our previous studies demonstrated in both Tg animals and after both injury models, differences in microglial activation pattern and injury outcome, which are importantly related to phagocytic.

In the PPT, a higher percentage of microglial cells expressing TREM2 was observed in both GFAP-IL10Tg and GFAP-IL6Tg compared to WT. However, this result did not match with differences in terms of microglial proliferation observed between Tg animals (Recasens et al., 2019), suggesting that other mechanisms related to microglial activation, and possibly related to phagocytosis, are originating differences in delayed axonal sprouting.

In our previous studies in the FNA model, GFAP-IL6Tg showed increased neuronal death and less microglial clusters (Almolda et al., 2014), and GFAP-IL10Tg presented more neuronal survival and microglial clusters (Villacampa et al., 2015) compared to WT. The significant reduction in the TREM2+ area observed in GFAP-IL6Tg mice at 21 dpl could be explained by the lower microglia cluster formation, although our results also indicate that TREM2 expression in microglial clusters is not directly affected by cytokine overproduction, as almost all clusters are TREM2+ in all mouse lines. Indeed, the reduced TREM2 expression in GFAP-IL6Tg due to lower cluster numbers could be explained by a deficient phagocytic capacity in microglia, as already observed in cuprizone-treated GFAP-IL6Tg (Petković et al., 2016). Thus, our results suggest that IL-6 overproduction downregulates TREM2 expression due to changes in the microglial activation pattern, which affect cluster formation, and may not to be a direct effect of IL-6 on TREM2 levels. Moreover, in our study, we did not find a direct link between injury outcome and TREM2 after FNA.

As a whole, TREM2 expression in Tg animals seems to be more influenced by changes in microglial activation pattern that indirectly affects TREM2 expression, than by a direct effect of IL-6 or IL-10 overproduction in phagocytic capacity due to changes in TREM2 microglial expression.

CONCLUSIONS

In conclusion, the results obtained in this work show that TREM2 expression is upregulated after both anterograde and retrograde axonal injury in a specific subpopulation of microglia. Although we have not found a temporal relationship between the induction of proliferation and TREM2 expression in microglial cells, this unique TREM2+ microglia are associated with a more efficient phagocytosis of specific cell remnants, such as myelin and degenerated neurons. However, it is important to highlight that the phenotypic profile of TREM2+ microglial cells in the two models studied present specific characteristics linked to the degree of tissue injury. Concretely, the expression of P2RY12 is only downregulated in microglia after PPT, whereas ApoE expression in TREM2+ cells is exclusively observed in retrograde axotomy, where the axonal injury causes neuronal death. Finally, pro-inflammatory and anti-inflammatory local CNS microenvironments by IL-6 or IL-10 overproduction modified TREM2 expression, mainly after PPT and under pro-inflammatory conditions, due to changes in differential microglial activation but not to a direct cytokine effect.

DATA AVAILABILITY STATEMENT

The original contributions presented in the study are included in the article/**Supplementary Materials**, further inquiries can be directed to the corresponding author.

ETHICS STATEMENT

All experimental animal work was conducted according to Spanish regulations (Ley 32/2007, Real Decreto 1201/2005, Ley 9/2003, and Real Decreto 178/2004) in agreement with European Union directives (86/609/CEE, 91/628/CEE, and 92/65/CEE) and was approved by the Ethical Committee of the Autonomous University of Barcelona.

AUTHOR CONTRIBUTIONS

GM, AG-L, NV, and MR designed and performed the experiments, including acquiring data and analyzing data; and wrote and revised the manuscript. BA designed experiments, analyzed data; wrote and revised manuscript. KS contributed to design the experiments, analyzed data, and revised the manuscript. BC and BG designed the research and revised the manuscript. All authors contributed to the article and approved the submitted version.

FUNDING

This work was supported by the Ministerio de Ciencia e Innovación (BFU2014-55459 and BFU2017-87843-R) to BC.

ACKNOWLEDGMENTS

We would like to thank Miguel A. Martil and Isabella Appiah for their outstanding technical help, and Núria Barba for her help on confocal microscopy. The graphical abstract was created with BioRender.com.

SUPPLEMENTARY MATERIAL

The Supplementary Material for this article can be found online at: https://www.frontiersin.org/articles/10.3389/fncel.2020.567404/full#supplementary-material.

SUPPLEMENTARY FIGURE 1 | Analysis of ApoE expression in astrocytes after perforant pathway transection (PPT). **(A–F)** Representative double-immunolabeled images combining ApoE (green) and GFAP (red) in the non-lesioned (NL) dentate gyrus (DG) of the hippocampus **(A–C)** and at 2 dpl **(D–F)** after PPT. Note that ApoE expression was easily found on astrocyte-like cells in each condition (white arrows). Scale bar **(A–F)** = 10 μm.

SUPPLEMENTARY FIGURE 2 | Analysis of ApoE expression in astrocytes after facial nerve axotomy (FNA). **(A–I)** Representative double-immunolabeled images combining ApoE (green) and GFAP (red) in the ipsilateral NL FN **(A–C)** and at

14 dpl **(D–F)** and 21 dpl **(G–I)**. Note that, in all the time-points, ApoE was detected in astrocytes (white arrows). Scale bar **(A–I)** = 10 μm.

SUPPLEMENTARY FIGURE 3 | Temporal pattern of TREM2 changes in microglial cells in GFAP-IL6Tg and GFAP-IL10Tg after PPT and FNA. **(A–H)** Representative images showing TREM2 staining in the granular (GL) as well as the inner, medial and outer molecular layers (IML, MML, and OML, respectively) of the DG in NL and PPT-lesioned mice at 3, 7, and 21 dpl of GFAP-IL6Tg **(A–D)** and GFAP-IL10Tg mice **(E–H)**. Note that, while in NL TREM2 was only depicted as small rounded morphologies (arrowheads), also found at 21 dpl, at 3 and 7 dpl ramified and occasionally at 21 dpl TREM2+ cells were also observed (arrows). **(I–N)** Representative images showing TREM2 staining in the contralateral NL, as well as the ipsilateral sides of the FN at 14 and 21 dpl of GFAP-IL6Tg **(I–K)** and GFAP-IL10Tg **(L–N)**. In NL TREM2 is mainly restricted to a perinuclear location (arrowheads), whereas at 14 and 21 dpl TREM2 is extended to microglia ramifications and clusters (arrows). Scale bar **(A–H)** = 50 μm; **(I–N)** = 30 μm.

REFERENCES

Acarin, L., Gonzalez, B., Castellano, B., and Castro, A. J. (1997). Quantitative analysis of microglial reaction to a cortical excitotoxic lesion in the early postnatal brain. *Exp. Neurol.* 147, 410–417. doi: 10.1006/exnr.1997.6593

Almolda, B., Costa, M., Montoya, M., Gonzalez, B., and Castellano, B. (2009). CD4 microglial expression correlates with spontaneous clinical improvement in the acute Lewis rat EAE model. *J. Neuroimmunol.* 209, 65–80. doi: 10.1016/j.jneuroim.2009.01.026

Almolda, B., de Labra, C., Barrera, I., Gruart, A., Delgado-Garcia, J. M., Villacampa, N., et al. (2015). Alterations in microglial phenotype and hippocampal neuronal function in transgenic mice with astrocyte-targeted production of interleukin-10. *Brain Behav. Immun.* 45, 80–97. doi: 10.1016/j.bbi.2014.10.015

Almolda, B., Villacampa, N., Manders, P., Hidalgo, J., Campbell, I. L., Gonzalez, B., et al. (2014). Effects of astrocyte-targeted production of interleukin-6 in the mouse on the host response to nerve injury. *Glia* 62, 1142–1161. doi: 10.1002/glia.22668

Atagi, Y., Liu, C.-C., Painter, M. M., Chen, X.-F., Verbeeck, C., Zheng, H., et al. (2015). Apolipoprotein E is a ligand for triggering receptor expressed on myeloid cells 2 (TREM2). *J. Biol. Chem.* 290, 26043–26050. doi: 10.1074/jbc.M115.679043

Boza-Serrano, A., Ruiz, R., Sanchez-Varo, R., Garcia-Revilla, J., Yang, Y., Jimenez-Ferrer, I., et al. (2019). Galectin-3, a novel endogenous TREM2 ligand, detrimentally regulates inflammatory response in Alzheimer's disease. *Acta Neuropathol.* 138, 251–273. doi: 10.1007/s00401-019-02013-z

Campbell, I. L., Abraham, C. R., Masliah, E., Kemper, P., Inglis, J. D., Oldstone, M. B., et al. (1993). Neurologic disease induced in transgenic mice by cerebral overexpression of interleukin 6. *Proc. Natl. Acad. Sci. U S A* 90, 10061–10065. doi: 10.1073/pnas.90.21.10061

Cantoni, C., Bollman, B., Licastro, D., Xie, M., Mikesell, R., Schmidt, R., et al. (2015). TREM2 regulates microglial cell activation in response to demyelination *in vivo*. *Acta Neuropathol.* 129, 429–447. doi: 10.1007/s00401-015-1388-1

Cignarella, F., Filipello, F., Bollman, B., Cantoni, C., Locca, A., Mikesell, R., et al. (2020). TREM2 activation on microglia promotes myelin debris clearance and remyelination in a model of multiple sclerosis. *Acta Neuropathol.* 140, 513–534. doi: 10.1007/s00401-020-02193-z

Colonna, M. (2003). TREMs in the immune system and beyond. *Nat. Rev. Immunol.* 3, 445–453. doi: 10.1038/nri1106

Colonna, M., and Butovsky, O. (2017). Microglia function in the central nervous system during health and neurodegeneration. *Annu. Rev. Immunol.* 35, 441–468. doi: 10.1146/annurev-immunol-051116-052358

Cheng-Hathaway, P. J., Reed-Geaghan, E. G., Jay, T. R., Casali, B. T., Bemiller, S. M., Puntambekar, S. S., et al. (2018). The Trem2 R47H variant confers loss-of-function-like phenotypes in Alzheimer's disease. *Mol. Neurodegener.* 13:29. doi: 10.1186/s13024-018-0262-8

Chertoff, M., Shrivastava, K., Gonzalez, B., Acarin, L., and Gimenez-Llort, L. (2013). Differential modulation of TREM2 protein during postnatal brain development in mice. *PLoS One* 8:e72083. doi: 10.1371/journal.pone.0072083

Deczkowska, A., Keren-Shaul, H., Weiner, A., Colonna, M., Schwartz, M., and Amit, I. (2018). Disease-associated microglia: a universal immune sensor of neurodegeneration. *Cell* 173, 1073–1081. doi: 10.1016/j.cell.2018.05.003

Deller, T., Del Turco, D., Rappert, A., and Bechmann, I. (2007). Structural reorganization of the dentate gyrus following entorhinal denervation: species differences between rat and mouse. *Prog. Brain Res.* 163, 501–528. doi: 10.1016/S0079-6123(07)63027-1

Deming, Y., Li, Z., Benitez, B. A., and Cruchaga, C. (2018). Triggering receptor expressed on myeloid cells 2 (TREM2): a potential therapeutic target for Alzheimer disease? *Expert Opin. Ther. Targets* 22, 587–598. doi: 10.1080/14728222.2018.1486823

Gehrmann, J., Schoen, S. W., and Kreutzberg, G. W. (1991). Lesion of the rat entorhinal cortex leads to a rapid microglial reaction in the dentate gyrus. A light and electron microscopical study. *Acta Neuropathol.* 82, 442–455. doi: 10.1007/BF00293378

Gervois, P., and Lambrichts, I. (2019). The emerging role of triggering receptor expressed on myeloid cells 2 as a target for immunomodulation in ischemic stroke. *Front. Immunol.* 10:1668. doi: 10.3389/fimmu.2019.01668

Gratuze, M., Leyns, C. E. G., and Holtzman, D. M. (2018). New insights into the role of TREM2 in Alzheimer's disease. *Mol. Neurodegener.* 13:66. doi: 10.1186/s13024-018-0298-9

Greenhalgh, A. D., Zarruk, J. G., Healy, L. M., Baskar Jesudasan, S. J., Jhelum, P., Salmon, C. K., et al. (2018). Peripherally derived macrophages modulate microglial function to reduce inflammation after CNS injury. *PLoS Biol.* 16:e2005264. doi: 10.1371/journal.pbio.2005264

Guan, Z., Kuhn, J. A., Wang, X., Colquitt, B., Solorzano, C., Vaman, S., et al. (2016). Injured sensory neuron-derived CSF1 induces microglial proliferation and DAP12-dependent pain. *Nat. Neurosci.* 19, 94–101. doi: 10.1038/nn.4189

Hsieh, C. L., Koike, M., Spusta, S. C., Niemi, E. C., Yenari, M., Nakamura, M. C., et al. (2009). A role for TREM2 ligands in the phagocytosis of apoptotic neuronal cells by microglia. *J. Neurochem.* 109, 1144–1156. doi: 10.1111/j.1471-4159.2009.06042.x

Jay, T. R., Hirsch, A. M., Broihier, M. L., Miller, C. M., Neilson, L. E., Ransohoff, R. M., et al. (2017a). Disease progression-dependent effects of TREM2 deficiency in a mouse model of Alzheimer's disease. *J. Neurosci.* 37, 637–647. doi: 10.1523/JNEUROSCI.2110-16.2016

Jay, T. R., von Saucken, V. E., and Landreth, G. E. (2017b). TREM2 in neurodegenerative diseases. *Mol. Neurodegener.* 12:56. doi: 10.1186/s13024-017-0197-5

Jensen, M. B., Hegelund, I. V., Poulsen, F. R., Owens, T., Zimmer, J., and Finsen, B. (1999). Microglial reactivity correlates to the density and the myelination of the anterogradely degenerating axons and terminals following perforant path denervation of the mouse fascia dentata. *Neuroscience* 93, 507–518. doi: 10.1016/s0306-4522(99)00139-6

Karanfilian, L., Tosto, M. G., and Malki, K. (2020). The role of TREM2 in Alzheimer's disease; evidence from transgenic mouse models. *Neurobiol. Aging* 86, 39–53. doi: 10.1016/j.neurobiolaging.2019.09.004

Keren-Shaul, H., Spinrad, A., Weiner, A., Matcovitch-Natan, O., Dvir-Szternfeld, R., Ulland, T. K., et al. (2017). A unique microglia type associated with restricting development of Alzheimer's disease. *Cell* 169, 1276.e17–1290.e17.doi: 10.1016/j.cell.2017.05.018

Kobayashi, M., Konishi, H., Sayo, A., Takai, T., and Kiyama, H. (2016). TREM2/DAP12 signal elicits proinflammatory response in microglia and exacerbates neuropathic pain. *J. Neurosci.* 36, 11138–11150. doi: 10.1523/JNEUROSCI.1238-16.2016

Kobayashi, M., Konishi, H., Takai, T., and Kiyama, H. (2015). A DAP12-dependent signal promotes pro-inflammatory polarization in microglia following nerve injury and exacerbates degeneration of injured neurons. *Glia* 63, 1073–1082. doi: 10.1002/glia.22802

Kober, D. L., and Brett, T. J. (2017). TREM2-ligand interactions in health and disease. *J. Mol. Biol.* 429, 1607–1629. doi: 10.1016/j.jmb.2017.04.004

Krasemann, S., Madore, C., Cialic, R., Baufeld, C., Calcagno, N., El Fatimy, R., et al. (2017). The TREM2-APOE pathway drives the transcriptional phenotype of dysfunctional microglia in neurodegenerative diseases. *Immunity* 47, 566.e9–581.e9. doi: 10.1016/j.immuni.2017.08.008

Ladeby, R., Wirenfeldt, M., Garcia-Ovejero, D., Fenger, C., Dissing-Olesen, L., Dalmau, I., et al. (2005). Microglial cell population dynamics in the injured adult central nervous system. *Brain Res. Brain Res. Rev.* 48, 196–206. doi: 10.1016/j.brainresrev.2004.12.009

Linnartz-Gerlach, B., Bodea, L.-G., Klaus, C., Ginolhac, A., Halder, R., Sinkkonen, L., et al. (2019). TREM2 triggers microglial density and age-related neuronal loss. *Glia* 67, 539–550. doi: 10.1002/glia.23563

Lynch, G., Matthews, D. A., Mosko, S., Parks, T., and Cotman, C. (1972). Induced acetylcholinesterase-rich layer in rat dentate gyrus following entorhinal lesions. *Brain Res.* 42, 311–318. doi: 10.1016/0006-8993(72)90533-1

Meilandt, W. J., Ngu, H., Gogineni, A., Lalehzadeh, G., Lee, S. H., Srinivasan, K., et al. (2020). Trem2 deletion reduces late-stage amyloid plaque accumulation, elevates the Aβ42:Aβ40 ratio, and exacerbates axonal dystrophy and dendritic spine loss in the PS2APP Alzheimer's mouse model. *J. Neurosci.* 40, 1956–1974. doi: 10.1523/JNEUROSCI.1871-19.2019

Moran, L. B., and Graeber, M. B. (2004). The facial nerve axotomy model. *Brain Res. Brain Res. Rev.* 44, 154–178. doi: 10.1016/j.brainresrev.2003.11.004

Neumann, H., Kotter, M. R., and Franklin, R. J. (2009). Debris clearance by microglia: an essential link between degeneration and regeneration. *Brain* 132, 288–295. doi: 10.1093/brain/awn109

Nielsen, H. H., Ladeby, R., Fenger, C., Toft-Hansen, H., Babcock, A. A., Owens, T., et al. (2009). Enhanced microglial clearance of myelin debris in T cell-infiltrated central nervous system. *J. Neuropathol. Exp. Neurol.* 68, 845–856. doi: 10.1097/NEN.0b013e3181ae0236

Nomura, K., Vilalta, A., Allendorf, D. H., Hornik, T. C., and Brown, G. C. (2017). Activated microglia desialylate and phagocytose cells *via* neuraminidase, galectin-3, and mer tyrosine kinase. *J. Immunol.* 198, 4792–4801. doi: 10.4049/jimmunol.1502532

Noto, D., Takahashi, K., Miyake, S., and Yamada, M. (2010). *In vitro* differentiation of lineage-negative bone marrow cells into microglia-like cells. *Eur. J. Neurosci.* 31, 1155–1163. doi: 10.1111/j.1460-9568.2010.07152.x

Nugent, A. A., Lin, K., van Lengerich, B., Lianoglou, S., Przybyla, L., Davis, S. S., et al. (2020). TREM2 regulates microglial cholesterol metabolism upon chronic phagocytic challenge. *Neuron* 105, 837.e9–854.e9.doi: 10.1016/j.neuron.2019.12.007

Painter, M. M., Atagi, Y., Liu, C.-C., Rademakers, R., Xu, H., Fryer, J. D., et al. (2015). TREM2 in CNS homeostasis and neurodegenerative disease. *Mol. Neurodegener.* 10:43. doi: 10.1186/s13024-015-0040-9

Petković, F., Campbell, I. L., Gonzalez, B., and Castellano, B. (2016). Astrocyte-targeted production of interleukin-6 reduces astroglial and microglial activation in the cuprizone demyelination model: implications for myelin clearance and oligodendrocyte maturation. *Glia* 64, 2104–2119. doi: 10.1002/glia.23043

Piccio, L., Buonsanti, C., Mariani, M., Cella, M., Gilfillan, S., Cross, A. H., et al. (2007). Blockade of TREM-2 exacerbates experimental autoimmune encephalomyelitis. *Eur. J. Immunol.* 37, 1290–1301. doi: 10.1002/eji.200636837

Poliani, P. L., Wang, Y., Fontana, E., Robinette, M. L., Yamanishi, Y., Gilfillan, S., et al. (2015). TREM2 sustains microglial expansion during aging and response to demyelination. *J. Clin. Invest.* 125, 2161–2170. doi: 10.1172/JCI77983

Prada, I., Ongania, G. N., Buonsanti, C., Panina-Bordignon, P., and Meldolesi, J. (2006). Triggering receptor expressed in myeloid cells 2 (TREM2) trafficking in microglial cells: continuous shuttling to and from the plasma membrane regulated by cell stimulation. *Neuroscience* 140, 1139–1148. doi: 10.1016/j.neuroscience.2006.03.058

Puigdellivol, M., Allendorf, D. H., and Brown, G. C. (2020). Sialylation and Galectin-3 in microglia-mediated neuroinflammation and neurodegeneration. *Front. Cell. Neurosci.* 14:162. doi: 10.3389/fncel.2020.00162

Recasens, M., Shrivastava, K., Almolda, B., Gonzalez, B., and Castellano, B. (2019). Astrocyte-targeted IL-10 production decreases proliferation and induces a downregulation of activated microglia/macrophages after PPT. *Glia* 67, 741–758. doi: 10.1002/glia.23573

Rolfe, A. J., Bosco, D. B., Broussard, E. N., and Ren, Y. (2017). *In vitro* phagocytosis of myelin debris by bone marrow-derived macrophages. *J. Vis. Exp.* 130:56322. doi: 10.3791/56322

Saber, M., Kokiko-Cochran, O., Puntambekar, S. S., Lathia, J. D., and Lamb, B. T. (2017). Triggering receptor expressed on myeloid cells 2 deficiency alters acute macrophage distribution and improves recovery after traumatic brain injury. *J. Neurotrauma* 34, 423–435. doi: 10.1089/neu.2016.4401

Sayed, F. A., Telpoukhovskaia, M., Kodama, L., Li, Y., Zhou, Y., Le, D., et al. (2018). Differential effects of partial and complete loss of TREM2 on microglial injury response and tauopathy. *Proc. Natl. Acad. Sci. U S A* 115, 10172–10177. doi: 10.1073/pnas.1811411115

Scott-Hewitt, N. J., Folts, C. J., Hogestyn, J. M., Piester, G., Mayer-Proschel, M., and Noble, M. D. (2017). Heterozygote galactocerebrosidase (GALC) mutants have reduced remyelination and impaired myelin debris clearance following demyelinating injury. *Hum. Mol. Genet.* 26, 2825–2837. doi: 10.1093/hmg/ddx153

Schmid, C. D., Sautkulis, L. N., Danielson, P. E., Cooper, J., Hasel, K. W., Hilbush, B. S., et al. (2002). Heterogeneous expression of the triggering receptor expressed on myeloid cells-2 on adult murine microglia. *J. Neurochem.* 83, 1309–1320. doi: 10.1046/j.1471-4159.2002.01243.x

Schnell, S. A., Staines, W. A., and Wessendorf, M. W. (1999). Reduction of lipofuscin-like autofluorescence in fluorescently labeled tissue. *J. Histochem. Cytochem.* 47, 719–730. doi: 10.1177/002215549904700601

Takahashi, K., Prinz, M., Stagi, M., Chechneva, O., and Neumann, H. (2007). TREM2-transduced myeloid precursors mediate nervous tissue debris clearance and facilitate recovery in an animal model of multiple sclerosis. *PLoS Med.* 4:e124. doi: 10.1371/journal.pmed.0040124

Takahashi, K., Rochford, C. D., and Neumann, H. (2005). Clearance of apoptotic neurons without inflammation by microglial triggering receptor expressed on myeloid cells-2. *J. Exp. Med.* 201, 647–657. doi: 10.1084/jem.20041611

Tay, T. L., Sagar, Dautzenberg, J., Grun, D., and Prinz, M. (2018). Unique microglia recovery population revealed by single-cell RNAseq following neurodegeneration. *Acta Neuropathol. Commun.* 6:87. doi: 10.1186/s40478-018-0584-3

van Wageningen, T. A., Vlaar, E., Kooij, G., Jongenelen, C. A. M., Geurts, J. J. G., and van Dam, A. M. (2019). Regulation of microglial TMEM119 and P2RY12 immunoreactivity in multiple sclerosis white and gray matter lesions is dependent on their inflammatory environment. *Acta Neuropathol. Commun.* 7:206. doi: 10.1186/s40478-019-0850-z

Villacampa, N., Almolda, B., Vilella, A., Campbell, I. L., Gonzalez, B., and Castellano, B. (2015). Astrocyte-targeted production of IL-10 induces changes in microglial reactivity and reduces motor neuron death after facial nerve axotomy. *Glia* 63, 1166–1184. doi: 10.1002/glia.22807

Walker, D. G., Tang, T. M., Mendsaikhan, A., Tooyama, I., Serrano, G. E., Sue, L. I., et al. (2020). Patterns of expression of purinergic receptor P2RY12, a putative marker for non-activated microglia, in aged and Alzheimer's disease brains. *Int. J. Mol. Sci.* 21:678. doi: 10.3390/ijms21020678

Wang, Y., Cella, M., Mallinson, K., Ulrich, J. D., Young, K. L., Robinette, M. L., et al. (2015). TREM2 lipid sensing sustains the microglial response in an Alzheimer's disease model. *Cell* 160, 1061–1071. doi: 10.1016/j.cell.2015.01.049

Wolf, S. A., Boddeke, H. W., and Kettenmann, H. (2017). Microglia in physiology and disease. *Annu. Rev. Physiol.* 79, 619–643. doi: 10.1146/annurev-physiol-022516-034406

Wu, R., Li, X., Xu, P., Huang, L., Cheng, J., Huang, X., et al. (2017). TREM2 protects against cerebral ischemia/reperfusion injury. *Mol. Brain* 10:20. doi: 10.1186/s13041-017-0296-9

Yao, H., Coppola, K., Schweig, J. E., Crawford, F., Mullan, M., and Paris, D. (2019). Distinct signaling pathways regulate TREM2 phagocytic and NFκB antagonistic activities. *Front. Cell. Neurosci.* 13:457. doi: 10.3389/fncel.2019.00457

Yip, P. K., Carrillo-Jimenez, A., King, P., Vilalta, A., Nomura, K., Chau, C. C., et al. (2017). Galectin-3 released in response to traumatic brain injury acts as an alarmin orchestrating brain immune response and promoting neurodegeneration. *Sci. Rep.* 7:41689. doi: 10.1038/srep41689

Zhai, Q., Li, F., Chen, X., Jia, J., Sun, S., Zhou, D., et al. (2017). Triggering receptor expressed on myeloid cells 2, a novel regulator of immunocyte phenotypes, confers neuroprotection by relieving neuroinflammation. *Anesthesiology* 127, 98–110. doi: 10.1097/ALN.0000000000001628

Zheng, H., Jia, L., Liu, C. C., Rong, Z., Zhong, L., Yang, L., et al. (2017). TREM2 promotes microglial survival by activating Wnt/β-catenin pathway. *J. Neurosci.* 37, 1772–1784. doi: 10.1523/JNEUROSCI.2459-16.2017

Zhong, L., Chen, X.-F., Wang, T., Wang, Z., Liao, C., Wang, Z., et al. (2017). Soluble TREM2 induces inflammatory responses and enhances microglial survival. *J. Exp. Med.* 214, 597–607. doi: 10.1084/jem.20160844

Zhong, L., Xu, Y., Zhuo, R., Wang, T., Wang, K., Huang, R., et al. (2019). Soluble TREM2 ameliorates pathological phenotypes by modulating microglial functions in an Alzheimer's disease model. *Nat. Commun.* 10:1365. doi: 10.1038/s41467-019-09118-9

Conflict of Interest: The authors declare that the research was conducted in the absence of any commercial or financial relationships that could be construed as a potential conflict of interest.

Copyright © 2020 Manich, Gómez-López, Almolda, Villacampa, Recasens, Shrivastava, González and Castellano. This is an open-access article distributed under the terms of the Creative Commons Attribution License (CC BY). The use, distribution or reproduction in other forums is permitted, provided the original author(s) and the copyright owner(s) are credited and that the original publication in this journal is cited, in accordance with accepted academic practice. No use, distribution or reproduction is permitted which does not comply with these terms.

ANNEX 6 – ARTICLE 3

Evaluation of Myelin Phagocytosis by Microglia/Macrophages in Nervous Tissue Using Flow Cytometry

Evaluation of Myelin Phagocytosis by Microglia/Macrophages in Nervous Tissue Using Flow Cytometry

Ariadna Regina Gómez-López,[1] Gemma Manich,[1,2] Mireia Recasens,[1]
Beatriz Almolda,[1] Berta González,[1] and Bernardo Castellano[1]

[1]Department of Cell Biology, Physiology and Immunology, Institute of Neuroscience,
Universitat Autònoma de Barcelona, Barcelona, Spain
[2]Corresponding author: *Gemma.Manich@uab.cat*

Determination of microglial phagocytosis of myelin has acquired importance in the study of demyelinating diseases. One strategy to determine microglial phagocytosis capacity consists of assaying microglia with fluorescently labeled myelin; however, most approaches are performed in cell culture, where microglia usually show important phenotypic differences compared with in vivo conditions. In this article we describe an adapted flow cytometry protocol to assay myelin phagocytosis by microglia obtained directly from in vivo tissue of the central nervous system. Key steps for a first analysis of phagocytic microglia are provided. Additionally, we describe how to fluorescently label myelin using a pH-sensitive tag, pHrodo^{TM} Green STP Ester. © 2021 Wiley Periodicals LLC.

Basic Protocol: Assay for determination of myelin phagocytosis by microglia/macrophages using flow cytometry
Support Protocol 1: Conjugation of isolated and purified myelin with pHrodo Green STP Ester
Support Protocol 2: Quantification of phagocytic cell number by flow cytometry

Keywords: flow cytometry • microglia • myelin • phagocytosis • pHrodo

How to cite this article:
Gómez-López, A. R., Manich, G., Recasens, M., Almolda, B., González, B., & Castellano, B. (2021). Evaluation of myelin phagocytosis by microglia/macrophages in nervous tissue using flow cytometry. *Current Protocols*, *1,* e73. doi: 10.1002/cpz1.73

INTRODUCTION

Microglia are the resident macrophages of the central nervous system (CNS), and they participate in shaping the brain in physiologic and pathologic conditions (Lloyd & Miron, 2019). Neuroinflammation is mainly modulated by these cells, as they first detect and clear cell debris resulting from tissue damage and later promote repair of the tissue to reestablish homeostasis. In demyelinating diseases or CNS lesions that disturb white matter, microglia exert a central role by phagocyting myelin debris. Clearance of myelin is key in the injury time course due to the fact that myelin debris is highly toxic and a source of oxidative mediators (Lampron et al., 2015). In addition, the presence of myelin debris inhibits oligodendrocyte progenitor cell migration, maturation, and de novo myelin formation, consequently delaying remyelination (Kotter, Li, Zhao, & Franklin, 2006). As a result, microglial capacity and efficiency in myelin phagocytosis will have a decisive impact in the recovery of demyelinating injuries and diseases (Peferoen, Kipp, van der

CURRENT PROTOCOLS
A Wiley Brand

Current Protocols e73, Volume 1
Published in Wiley Online Library (wileyonlinelibrary.com).
doi: 10.1002/cpz1.73
© 2021 Wiley Periodicals LLC

Valk, van Noort, & Amor, 2014). In recent years, the study of microglia has shown that modulation of their phenotype could influence recovery by performing a more efficient clearance of myelin debris and also by having a trophic effect on oligodendrocyte remyelination. All these studies center around the modulation of microglial phenotypes as a possible therapeutic strategy for remyelination therapies (Lloyd & Miron, 2019; Miron et al., 2013). In this context, assays for evaluating myelin phagocytosis by microglia are an important tool for studying microglial phenotypes.

Microglial phagocytosis has been characterized for years by several methods, ranging the most simple—involving the detection of an increase in lysosomal proteins (macrosyalin or CD68), Fc receptors (CD16 or CD32), or phagocytic receptors such as CD206 (Galloway, Phillips, Owen, & Moore, 2019)—to more complex procedures in which an in vivo assessment of microglial phagocytosis capacity is determined by, for example, quantifying engulfed polymer carboxylate microspheres, β-amyloid, or apoptotic neurons (Beccari, Diaz-Aparicio, & Sierra, 2018; Pul, Chittappen, & Stangel, 2013; Ramesha, Rayaprolu, & Rangaraju, 2020). The latter method provides a precise characterization of the entire microglia phagocytosis capacity because phagocytosis can be affected at several different steps, from particle uptake to its internalization or lysosomal digestion. However, when studying myelin phagocytosis, two important aspects affecting the results may be taken into account: (1) the conditions in which microglia phagocytosis are assayed, since results obtained in vitro, depending on culture conditions, could be significantly altered from the phenotype observed in vivo and (2) the cellular material to be engulfed in the assay, as phagocytosis may be specific for a type of receptor, and therefore, the material to be phagocytosed could lead to different results.

Currently, protocols for assaying microglial or macrophage phagocytosis of myelin debris consist, in general, of assays detecting fluorescently labeled myelin engulfed by microglia (Diaz-Lucena et al., 2018; Hendrickx, Schuurman, van Draanen, Hamann, & Huitinga, 2014; Hendriks et al., 2008; Maheshwari et al., 2013; Rolfe, Bosco, Broussard, & Ren, 2017; van der Laan et al., 1996). All protocols, with only one exception to our knowledge (Greenhalgh et al., 2018), perform the assay with cultured microglia but not directly with microglia obtained from CNS tissue. With this background, we adapted a flow cytometry protocol (Almolda, Costa, Montoya, Gonzalez, & Castellano, 2009) to assay myelin phagocytosis by microglia obtained from in vivo CNS tissue (Manich et al., 2020). Briefly, the Basic Protocol describes dissection of mouse healthy or lesioned CNS tissue, isolation of cells by Percoll® gradient, incubation of fluorescently labeled myelin with the isolated cells to assay phagocytosis, and antibody incubation for detecting and characterizing microglia together with internalized fluorescent myelin by flow cytometry (Fig. 1). We describe in Support Protocol 1 how to fluorescently label isolated and purified myelin obtained according to a *Current Protocols* article by Larocca and Norton (2007), using a pH-sensitive tag, pHrodo™ Green STP Ester (pHrodo-Green), as previously described for other phagocytosis assays with apoptotic cells (Aziz, Yang, & Wang, 2013). Support Protocol 2 specifies how to use fluorescent beads in the final steps of the flow cytometry protocol to obtain a whole cell count for each sample, as well as key steps to analyze these results.

STRATEGIC PLANNING

Before starting, the experiment should be thoroughly planned, especially taking into consideration the following aspects: (1) the combination of fluorochromes conjugated to antibodies being used; (2) controls (positive and negative) that should be included; and (3) the number of samples to use in the assay.

To plan the combination of fluorochromes, antibodies and conjugated myelin should emit fluorescence at different wavelengths being separated, as much as possible, in the light

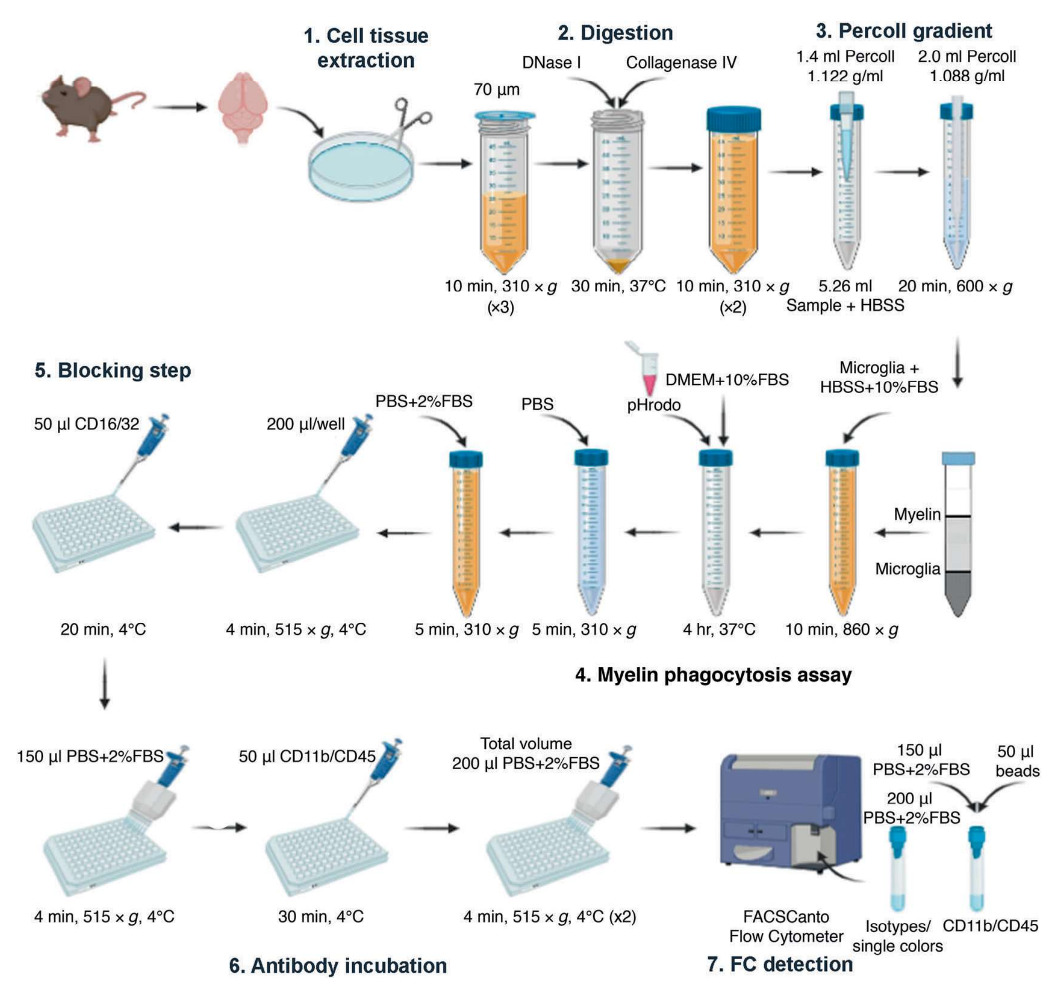
1. Cell tissue extraction
2. Digestion
DNase I
Collagenase IV
70 µm
3. Percoll gradient
1.4 ml Percoll 1.122 g/ml
2.0 ml Percoll 1.088 g/ml
10 min, 310 × g (×3)
30 min, 37°C
10 min, 310 × g (×2)
5.26 ml Sample + HBSS
20 min, 600 × g
5. Blocking step
50 µl CD16/32
200 µl/well
PBS+2%FBS
PBS
pHrodo
DMEM+10%FBS
Microglia + HBSS+10%FBS
Myelin
Microglia
20 min, 4°C
4 min, 515 × g, 4°C
5 min, 310 × g
5 min, 310 × g
4 hr, 37°C
10 min, 860 × g
4. Myelin phagocytosis assay
150 µl PBS+2%FBS
50 µl CD11b/CD45
Total volume 200 µl PBS+2%FBS
150 µl PBS+2%FBS
50 µl beads
200 µl PBS+2%FBS
4 min, 515 × g, 4°C
30 min, 4°C
4 min, 515 × g, 4°C (x2)
FACSCanto Flow Cytometer
Isotypes/ single colors
CD11b/CD45
6. Antibody incubation
7. FC detection

Figure 1 Summary of the myelin phagocytosis assay. Briefly, after perfusing mice with ice-cold PBS, (1) brain regions of interest are extracted, cut in small pieces, and passed through a 160-µm membrane. (2) After transferring samples through a 70-µm filter into 50-ml conical tubes, samples are washed three times, first with Hank's buffered-saline solution containing 10% fetal bovine serum (HBSS+10%FBS) and then with HBSS. Next, samples are digested at 37°C for 30 min. After stopping the digestion by washing samples with HBSS+10%FBS and HBSS, the interphase layer with microglia/macrophages is obtained by (3) centrifuging samples with a Percoll gradient. Following centrifugation, (4) the interphase layer is transferred into a new 15-ml conical tube and washed with HBSS+10%FBS. Thereafter, samples are incubated with myelin conjugated to pHrodo Green STP Ester for 4 hr at 37°C. Then, samples are washed twice with phosphate-buffered saline (PBS) and PBS containing 2% FBS (PBS+2%FBS). Subsequently, (5) samples are transferred to a 96-well conical-bottom plate, diluted in PBS+2%FBS, and incubated for 20 min at 4°C with CD16/32 to block Fc receptors. (6) After washing samples, wells are incubated with CD11b and CD45 antibodies, their corresponding isotype controls, and single colors for 30 min at 4°C. Finally, wells are washed twice with PBS+2%FBS. (7) At this point they are ready to be analyzed on a flow cytometer (FC).

spectrum from each other. For further insight in this topic, a *Current Protocols* article by Maciorowski, Chattopadhyay, and Jain (2017) provides more information. In this article we conjugate myelin with pHrodo-Green, which emits in the FITC spectrum. However, it should be taken into account that other conjugation options are available, such as pHrodo Red SE (pHrodo-Red) emitting in the TRITC spectrum.

Appropriate flow cytometry controls are essential to ensure correct interpretation of the results (Fig. 2). For the specific study of microglia, as an immune cell, positive control tissues should include lymphoid tissues such as spleen and CNS tissue with known myeloid

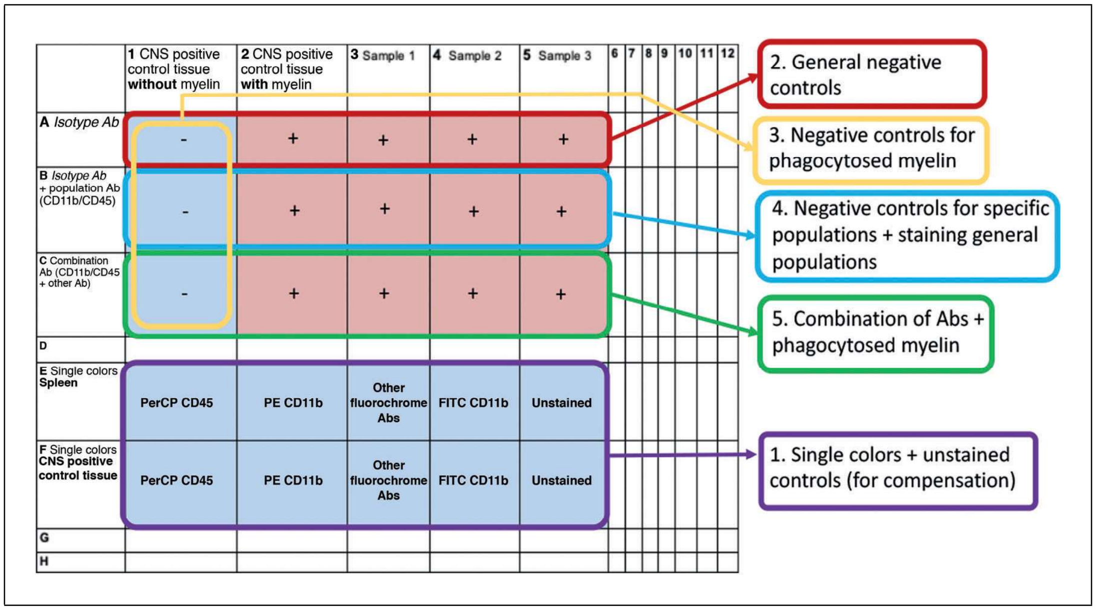

	1 CNS positive control tissue **without** myelin	**2** CNS positive control tissue **with** myelin	**3** Sample 1	**4** Sample 2	**5** Sample 3	**6**	**7**	**8**	**9**	**10**	**11**	**12**
A *Isotype Ab*	-	+	+	+	+							
B *Isotype Ab* + population Ab (CD11b/CD45)	-	+	+	+	+							
C Combination Ab (CD11b/CD45 + other Ab)	-	+	+	+	+							
D												
E Single colors **Spleen**	**PerCP CD45**	**PE CD11b**	**Other fluorochrome Abs**	**FITC CD11b**	**Unstained**							
F Single colors **CNS positive control tissue**	**PerCP CD45**	**PE CD11b**	**Other fluorochrome Abs**	**FITC CD11b**	**Unstained**							
G												
H												

2. General negative controls
3. Negative controls for phagocytosed myelin
4. Negative controls for specific populations + staining general populations
5. Combination of Abs + phagocytosed myelin
1. Single colors + unstained controls (for compensation)

Figure 2 Schematic of the experimental design of a plate for flow cytometry, showing samples used in a study. Positive controls, such as the spleen and central nervous system (CNS) tissue, are stained with antibodies (Abs) for each single fluorochrome used in the study (rows E and F) to be used for flow cytometry compensation. All remaining samples are incubated with isotype control antibodies (row A), used as general negative controls; cell population antibodies plus remaining isotype antibodies (row B) to identify microglia/macrophages and detect possible interferences with other antibodies; and antibody combinations (row C) for the whole antibody staining of interest. Additionally, CNS tissue used as a positive control is incubated without and with myelin (columns 1 and 2, respectively). Comparison of both conditions allows for identification of the fluorescence captured in the FITC spectrum and emitted by phagocytosed myelin.

activation and/or leukocyte infiltration (e.g., lipopolysaccharide-injected animal). For each sample, comprising spleen and CNS tissue, at least three negative controls should be included: (1) the general negative control, corresponding to cells incubated with all the isotype control antibodies (antibodies with a coincident isotype carrying the same fluorochromes as the antibodies of interest); (2) the specific negative control of the population of interest, corresponding to cells incubated with the antibodies used to identify the population of interest (i.e., CD45 and CD11b, in the case of microglia/macrophages) plus isotype controls for the other markers of interest; and (3) the unstained control, corresponding to cells incubated without any antibody and used to discard autofluorescence emitted by the cells or tissue analyzed. Additionally, an extra negative control lacking the incubation with myelin should be added to the study to discard the fluorescence emitted at the same wavelength as pHrodo-Green derived from other fluorochromes.

Finally, spleen and CNS tissue are incubated in separate wells with antibodies conjugated to fluorochromes in combination (directed against a common epitope such as CD45 or CD11b). All fluorochromes contained in the combination should be included in the experiment. These positive controls are used for flow cytometry compensation to correctly analyze positive staining.

BASIC PROTOCOL

ASSAY FOR DETERMINATION OF MYELIN PHAGOCYTOSIS BY MICROGLIA/MACROPHAGES USING FLOW CYTOMETRY

In this protocol (summarized in Fig. 1), we isolate cells from CNS tissue of interest (e.g., whole brain, spinal cord, or part of either), and we incubate the tissue with pHrodo-conjugated myelin. Then, we detect the microglia/macrophage population using antibodies directed against CD45 and CD11b. However, it is possible to use or add any antibody that is of interest in the study. Cells are passed through the flow cytometer to detect populations and cells containing intracellular phagocytosed myelin.

Materials

Healthy or lesioned C57Bl/6J mice (e.g., The Jackson Laboratory, ref. 000664, or other similar strain not carrying fluorescent reporters)
0.1 M Dulbecco's phosphate-buffered saline (PBS), pH 7.2 (e.g., Thermo Fisher Scientific, 14190-094)
Hank's buffered saline solution (HBSS; e.g., Thermo Fisher Scientific, 14025-050)
10% (v/v) fetal bovine serum (FBS; e.g., VWR, S181BH-500)
Collagenase IV (e.g., Life Technologies, 17104-019)
DNase I (e.g., Sigma-Aldrich, D5025)
1.088 and 1.122 g/ml Percoll (see recipe)
Dulbecco's modified Eagle medium (DMEM) F-12 (e.g., Thermo Fisher Scientific, D8437)
pHrodo-conjugated myelin (see Support Protocol 1)
Anti-CD16/32 antibody (e.g., BD Biosciences, 553142)
Anti-CD11b APC-Cy7-conjugated antibody (e.g., BD Biosciences, 557657)
Anti-CD11b FITC-conjugated antibody (e.g., BD Biosciences, 557396)
Anti-CD45 PerCP-conjugated antibody (e.g., BD Biosciences, 557235)
APC-Cy7 rat IgG2b κ isotype control antibody (e.g., BD Biosciences 552773)
PerCP rat IgG2b κ isotype control antibody (e.g., BD Biosciences 552991)
10% bleach

15- and 50-ml conical tubes (e.g., VWR, 525-0636 and 525-0304, respectively)
90 × 14–mm petri dish (e.g., Deltalab, 200209)
160-μm nylon membrane (e.g., Nylon Net Filter; Millipore Sigma, NY6H00010)
Tweezers
70-μm cell strainer (e.g., Life Sciences, 352350)
Refrigerated centrifuge with swinging-bucket rotor, round buckets, and microplate carriers (e.g., Thermo Heraeus Multifuge 3L-R or similar)
37°C incubator with variable shaking
5-ml automatic pipette
Glass Pasteur pipette (e.g., Normax, 5426023)
96-well conical-bottom plate (e.g., Thermo Fisher Scientific, 277143)
12 × 75–mm round-bottom polystyrene tubes (e.g., Fisher Scientific, 352052)
Flow cytometer (e.g., BD FACSCanto™)
Vortex mixer
Computer running FlowJo™ software (available at *https://www.flowjo.com/*)

Additional reagents and equipment for anesthesia (see *Current Protocols* article: Donovan & Brown, 2001), animal perfusion (see *Current Protocols* article: Miller, Karpus, and Davidson, 2010), removal of lymphoid organs (see *Current Protocols* article: Reeves & Reeves, 2001), CNS tissue dissection (see *Current Protocols* article: Manglani, Gossa, & McGavern, 2018), and flow cytometric preparation and cell analysis (see *Current Protocols* articles: Maciorowski et al., 2017; McKinnon, 2018).

NOTE: All protocols involving live animals must first be reviewed and approved by an Institutional Animal Care and Use Committee (IACUC) or conform to local guidelines regarding the care and use of laboratory animals.

NOTE: Special care must be taken throughout the protocol to avoid contamination between samples. All instruments should be cleaned and sterilized after use to avoid cross-contamination between different samples.

Tissue disaggregation

1. Anesthetized mouse and then transcardially perfuse using cold PBS for 20 to 60 s to remove blood.

   For details on mouse perfusion, see Miller et al. (2010). This protocol should be performed by an experienced researcher and according to IACUC-approved protocols.

   We have tested this protocol with several CNS areas (e.g., cerebellum, hippocampus, facial nucleus, cortex). Depending on the size and number of cells recovered for each area, samples may be pooled. A spleen and positive tissue control of CNS origin should always be added to ensure adequate flow cytometry controls (see Strategic Planning for more details).

   An N of at least 4 to 5 mice for each experimental group is required to obtain good statistical results.

2. Quickly dissect CNS region of interest, and immerse in 20 ml cold HBSS containing 10% (v/v) FBS (HBSS+10%FBS) in a 50-ml conical tube. Also, dissect tissues that will be used as flow cytometry controls (spleen and CNS tissue), and place samples in their respective sample tubes. Repeat step for each sample.

   Possible CNS regions of interest include brain, cerebellum, and spinal cord or subregions such as the hippocampus and cortex. Assays with small samples such as the facial nucleus can be performed by pooling two or three samples per tube.

3. In a petri dish, add sample and HBSS+10%FBS contained in one tube. Place sample within 160-µm membrane, and very gently and carefully press sample with tweezers to pass through the mesh.

   For large samples, cut tissue in small pieces using a scalpel before passing through meshes.

   Cut nylon membrane in squares of ~5 cm; size should be adapted to sample volume.

   It is important to pass the tissue through the mesh as gently as possible. This step is crucial to obtain maximal cell numbers.

4. Collect cell suspension with a pipette, and pass through a 70-µm filter placed in the top of a 50-ml conical tube. Add HBSS+10%FBS to clean any remaining cells from the surface of the petri dish. Pass sample through the 70-µm filter, and collect in the same 50-ml conical tube.

5. Repeat steps 3 and 4 for all samples. Change petri dish, gloves, and pipettes between samples, and clean tweezers to avoid contamination.

6. Equilibrate all samples to the same volume in 50-ml conical tubes by adding HBSS+10%FBS.

7. Centrifuge 50-ml conical tubes 10 min at 310 × *g*, 24°C, and maximum brake speed.

8. Discard supernatant of each tube.

9. Add 1 ml HBSS+10%FBS, and gently resuspend pellet with a pipette. Then add more HBSS+10%FBS to 20 ml. Avoid contamination between samples.

   Cell survival is reduced when cells are in pellets for long periods. Avoid large delays, and resuspend cells in this and all subsequent steps as soon as possible.

10. Repeat steps 7 and 8. Carefully resuspend each sample in 1 ml HBSS (room temperature) using a pipette. Add more HBSS (e.g., to 20 ml), and equilibrate between tubes with HBSS.

    Here it is important to change to HBSS, as tissue digestion should be done without serum.

11. Centrifuge tubes 10 min at 310 × *g*, 24°C, and maximum brake speed.

Tissue digestion

12. Prepare digestion solution that will be used in step 13 (0.5% [v/v] collagenase IV, 1.25% [v/v] DNase I in HBSS). For 10 ml, combine 50 µl collagenase IV, 125 µl DNase I, and 10 ml HBSS.
13. Discard supernatant of each 50-ml conical tube. Add 10 ml digestion solution. Carefully resuspend each sample in the digestion solution. Incubate all samples at 37°C for 30 min. Agitate constantly at low speed, or at least manually move samples every 10 min.
14. Bring each sample tube to 50 ml with HBSS+10%FBS.

    Addition of serum in this step is important to stop the digestion quickly.

15. Centrifuge tubes 10 min at 310 × *g*, 24°C, and maximum brake speed.
16. Discard supernatant of each tube.
17. Add 1 ml HBSS, and gently resuspend pellet with a pipette. Then add HBSS to 50 ml.
18. Centrifuge tubes 10 min at 310 × *g*, 24°C, and maximum brake speed.
19. Discard supernatant of each tube.
20. Add 1 ml HBSS, and gently resuspend pellet with a pipette.

Cell isolation with Percoll gradient

21. Using a 5-ml automatic pipette, measure how much sample (in ml) is contained in each tube. Transfer to a 15-ml conical tube.
22. Add enough HBSS to obtain a final volume of 5.26 ml for each tube.
23. Add 1.4 ml of 1.122 g/ml Percoll to each tube, and mix gently by inverting the tube two to three times.
24. Insert a glass Pasteur pipette into the tube until the tip of the pipette reaches the bottom of the 15-ml conical tube. Slowly add 2 ml of 1.088 g/ml Percoll into the top of the Pasteur pipette and allow it to reach the bottom of the tube.

    Be careful to not accidentally mix the two phases.

25. Once the two Percoll phases are generated, centrifuge tubes 20 min at 600 × *g*, 24°C, with no brake. Set rotor deceleration to its minimum value.

    In this step it is important to avoid the brake in order to maintain a correct Percoll gradient and good separation of the different density phases.

26. Collect interphase layer with an automatic pipette, and place in another 15-ml conical tube. If the sample contains few cells or aggregates, collect the whole top phase (with exception of the myelin, which is seen as a white cloud at the top of the tube).

    If the Percoll phases are not clearly separated, repeat centrifugation (step 25), ensuring that the brake is turned off.

27. Add HBSS+10%FBS to each tube to a total volume of 15 ml.
28. Centrifuge tubes 10 min at 860 × *g*, 24°C, with maximum brake speed.
29. Discard supernatant.

    At this step you should have a pellet of isolated cells samples in each sample tube.

Incubation of pHrodo-conjugated myelin with isolated cells

30. Resuspend pellet in each tube in 250 µl DMEM F-12 containing 10% (v/v) FBS.

31. Thaw pHrodo-conjugated myelin, and then vortex for 1 min.

32. Add 10 µl (3 µg) pHrodo-conjugated myelin to each tube. Do not add pHrodo-conjugated myelin to tubes used as negative controls for phagocytosis.

    Sample tubes containing negative tissue controls should first be resuspended in 1 to 2 ml HBSS+10%FBS using a pipette and then brough to 15 ml with HBSS+10%FBS. Samples should be stored at 4°C until the phagocytosis protocol ends.

    Although a higher percentage of cells with phagocytized myelin has been obtained when using conical tubes for myelin incubation, it is also possible to incubate samples with myelin in plain-bottom microplates coated with 10 µg/µl poly-L-lysine.

33. Incubate tubes for 4 hr at 37°C in a cell culture incubator without agitation. Avoid long periods of contact with light.

Transfer of cells to microplate for staining

34. Fill each sample tube with PBS to 15 ml.

35. Centrifuge tubes 5 min at 310 × *g*, 24°C, using maximum brake speed.

36. Discard supernatant of tube.

37. Add 1 ml PBS containing 2% (v/v) FBS (PBS+2%FBS), and gently resuspend pellet using a pipette. Then add PBS+2%FBS to 15 ml.

38. Centrifuge tubes 5 min at 310 × *g*, 24°C, using maximum brake speed.

39. Discard supernatant of each tube.

40. Prepare a 96-well plate with conical bottom.

41. Calculate total required volume to transfer all samples to all plate wells, including wells incubated with isotype antibodies, those to identify cell populations, and those incubated with all other antibodies (rows A, B, and C in Fig. 2). When calculating total volume, take into account that each well will contain 200 µl sample.

    If your sample has a reduced pellet (low number of cells), you can consider adding 100 µl into the isotype and cell population wells (rows A and B in Fig. 2) instead of 200 µl.

42. Resuspend each sample in the calculated volume of PBS+2%FBS, and transfer samples to plate wells.

    If you added only 100 µl into the isotype and cell population wells, add 100 µl PBS+2%FBS to reach a final volume of 200 µl in each well.

43. Centrifuge 96-well plate 4 min at 515 × *g*, 4°C, using maximum brake speed.

Blocking of unspecific epitopes

44. Prepare Fc blocking solution by diluting Fc-blocking CD16/32 antibody (1:250 dilution) in PBS+2%FBS.

45. Discard supernatant by decanting the plate. Remove remaining liquid by tapping the plate on a clean paper towel.

    Cell survival is reduced when cells are preserved in pellets for long periods. After discarding supernatant, cells should be resuspended as soon as possible in this and all subsequent steps.

46. Resuspend pellets in each well with 50 µl Fc blocking solution, and incubate for 20 min at 4°C without shaking.

47. Add 150 µl PBS+2%FBS to each well.

48. Centrifuge 96-well plate 4 min at 515 × *g*, 4°C, using maximum brake speed.

49. Discard supernatant by decanting the plate. Remove remaining liquid by tapping the plate on a clean paper towel.

Staining of cell populations

50. Prepare CD11b and CD45 antibodies (1:400 dilutions), as well as other antibodies in the combination of interest for the experiment, corresponding isotype controls (1:400), and positive single-color controls (1:400) in PBS+2%FBS (see Strategic Planning for more details).

    Antibody solutions can be prepared 1 or 2 hr in advance (e.g., during step 46) and stored at 4°C until use.

51. Resuspend pellet of each well in 50 µl prepared antibody combinations, isotype control, and positive single-color control, and incubate for 30 min at 4°C without shaking and protected from light.

52. Add 150 µl PBS+2%FBS to each well.

53. Centrifuge 96-well plate 4 min at 515 × *g*, 4°C, using maximum brake speed.

54. Discard supernatant by decanting the plate. Remove remaining liquid by tapping the plate on a clean paper towel.

55. Resuspend pellet of each well in 200 µl PBS+2%FBS.

56. Centrifuge 96-well plate 4 min at 515 × *g*, 4°C, and maximum brake speed.

57. Discard supernatant by decanting the plate. Remove remaining liquid by tapping the plate on a clean paper towel.

58. Resuspend pellet of each well in 200 µl PBS+2%FBS, and transfer samples to round-bottom polystyrene tubes.

Flow cytometry data acquisition

59. Before starting, wash flow cytometer acquisition needle with 10% bleach for 3 min to remove any remaining particles from previous experiments.

60. To remove bleach, rinse with distilled water for 3 min.

61. Vortex sample tube for 5 s to resuspend cells just before starting sample acquisition.

62. Start acquisition with samples containing single colors and negative controls to compensate the cytometer and to test that all lasers work properly before acquiring samples of interest. Then acquire samples of interest.

    More information on compensation of the flow cytometer can be found in a Current Protocols article by Maciorowski et al. (2017).

    Depending on the expected quantity of events, the acquisition speed may be from fast to moderate. During sample acquisition, keep the awaiting samples at 4°C and protected from light.

Gating strategy

63. In FlowJo, use the side scatter area (SSC-A) versus forward scatter area (FSC-A) axes, and select the lower half population corresponding to myeloid and lymphoid populations containing microglia/macrophages (Fig. 3A).

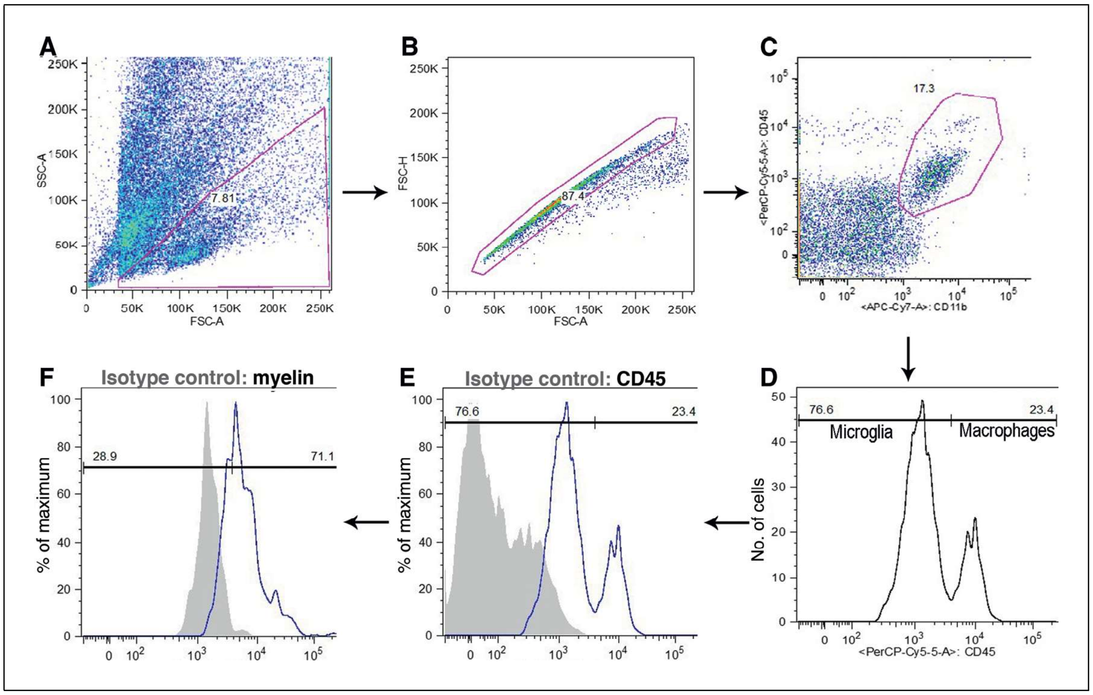

Figure 3 Gating strategy to identify phagocytic microglia/macrophages. (**A**) Side scatter area (SSC-A) versus forward scatter area (FSC-A) gating to obtain microglia/macrophages based on size and granularity. (**B**) Live cells selected by expressing FSC height (FSC-H) versus FSC-A gating. (**C**) Representative dot plot of CD11b/CD45 expression. The selected area delimits the CD11b+/CD45+ microglial/macrophage population. (**D**) Representative histogram where the populations of CD11b+/CD45$^{\text{low}}$ cells (microglia) and CD11b+/CD45$^{\text{high}}$ cells (macrophages) were defined. (**E**, **F**) Representative histograms showing expression of CD45 (mean fluorescence intensity) and myelin in the microglia/macrophage populations compared with the corresponding isotype control in which positive staining was defined.

64. Within the defined population, select only live cells by gating the population observed on the diagonal when FSC height (FSC-H) intersects with FSC-A (Fig. 3B).

65. Select axes corresponding to CD11b versus CD45 staining, and use the isotype controls for both markers to discard the negative population (Fig. 3C).

    Within the CD11b+/CD45+ population, two subpopulations are easily noticeable: microglia (CD11b+/CD45^{low}) and macrophages (CD11b+/CD45^{high}). From this point forward, these two populations can be analyzed together or separately, depending on the purpose of the study.

66. To better distinguish microglia and macrophage populations, use the histogram of CD45.

    The population with lower CD45 expression corresponds to microglia, and the population with higher CD45 expression contains macrophages.

67. Display the histogram of FITC fluorochrome (myelin) within the gated population to be analyzed (microglia: CD11b+CD45$^{\text{low}}$; macrophages: CD11b+CD45$^{\text{high}}$; microglia/macrophages: CD11b+CD45+; Fig. 3F).

    If other additional antibodies of interest are included in the staining combination by the user, the gating strategy will depend on the kind of expected data. This analysis will usually include selection of the specific population in the histogram before detecting myelin+ or myelin– cells in the FITC channel histogram.

CONJUGATION OF ISOLATED AND PURIFIED MYELIN WITH pHrodo GREEN STP ESTER

SUPPORT PROTOCOL 1

This protocol describes the conjugation of pHrodo-Green, a pH-sensitive fluorescent dye (excitation = 505 nm; emission = 525 nm), with previously isolated myelin obtained according to a *Current Protocol* article by Larocca and Norton (2007). Under acidic conditions pHrodo increases its fluorescence, and therefore pHrodo-conjugated myelin will emit at a higher intensity when found in lysosomal compartments of microglia/macrophages. This enhances the detection of phagocytosed myelin due to both the increase of pHrodo-fluorescent emission and a reduced background of possible remaining unengulfed myelin debris in the medium. Engulfed myelin are easily detected by a flow cytometer in the FITC channel.

Materials

15 mg/ml isolated and purified myelin (see *Current Protocols* article: Larocca & Norton, 2007).
pHrodo-Green (see recipe)
PBS, pH 7.2 and 8 (e.g., Thermo Fisher Scientific, 14190-094)

1.5-ml microcentrifuge tube
Laboratory rocker
Refrigerated centrifuge

1. Mix 18.5 µl of 15 mg/ml purified myelin with 25 µl pHrodo-Green in a 1.5-ml microcentrifuge tube. Resuspend in 206.5 µl PBS, pH 8.
2. Incubate reaction for 45 min at room temperature protected from light on a rocker at low speed.
3. Centrifuge 10 min at 4000 × *g*, 4°C. Discard supernatant.
4. Resuspend in 950 µl PBS, pH 7.2, to obtain a final concentration of 0.3 µg/µl purified myelin labeled with pHrodo-Green.

   PBS can be adjusted to obtain the most convenient concentration of labeled myelin required by the user.

5. Store conjugated myelin at −80°C for up to 6 months.

   When conjugated myelin is stored for long-term periods, the efficacy should be assayed following the manufacturer's instructions.

QUANTIFICATION OF PHAGOCYTIC CELL NUMBER BY FLOW CYTOMETRY

SUPPORT PROTOCOL 2

Analysis using FlowJo software will provide the percentage of the different cell populations. Addition of fluorescent beads to the different samples before acquisition will allow quantification of total cell numbers for each sample. In this protocol, we detail how to quantify cells and how to analyze the results to obtain the total cell number.

Additional Materials (also see Basic Protocol)

Samples of interest (see Basic Protocol)
Precision Count Beads^{TM} (e.g., BioLegend, 424902)

Addition of beads to samples

1. Resuspend pellet of each well (obtained in Basic Protocol step 57) in 200 µl PBS+2%FBS, and transfer to flow cytometer tubes. Resuspend wells that contain

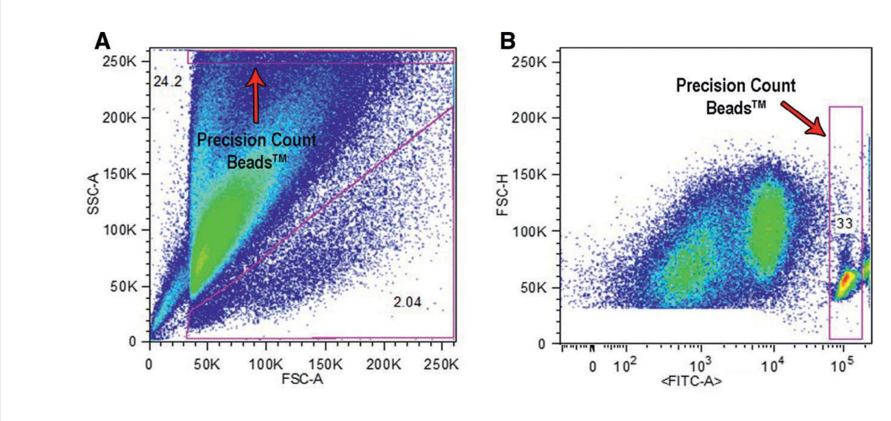

Figure 4 Detection of fluorescent beads in the flow cytometer for cell counting. (**A**) Side scatter area (SSC-A) versus forward scatter area (FSC-A) gating to obtain bead profiles. Note that beads are located at the top of the graph. (**B**) Inside this population, beads are highly fluorescent in all channels. Here, beads are selected with the FITC channel.

the antibody combination of interest in a final volume of 150 µl, since 50 µl Precision Count Beads will be added later.

Flow cytometry acquisition

2. Follow Basic Protocol steps 59 and 60.

3. Vortex sample tube for 5 s to resuspend cells just before starting sample acquisition.

4. In the case of samples with antibody combination staining, add 50 µl Precision Count Beads to each tube just before acquisition. Begin sample acquisition. During sample acquisition, keep awaiting samples at 4°C and protected from light.

   Addition of Precision Count Beads before acquisition can reduce the yield of cells recovered. Add beads to each tube just before the moment of acquisition.

   Depending on the expected quantity of events, the acquisition speed may be fast to moderate.

Bead quantification

5. Select Precision Count Beads in the initial graph (FSC-A vs. SSC-A) where the cell population is selected.

   Precision Count Beads have a high SSC and low FSC profile. Thus, SSC should be adjusted in such a way that the cells are optimally visible. This can be done by acquiring a sample of Precision Count Beads alone and comparing the results to the cell profiles (Fig. 4).

6. In the SSC-A versus FSC-A graph, where microglial/macrophage populations are selected from the lower half of the graph, select a small area in the upper part of the graph.

   Beads are located in this region.

7. Inside the selected bead area, plot the graph with one of the fluorescent channels. Work with the channel where the beads are more easily identifiable (Fig. 4).

   This can be done because Precision Count Beads are highly fluorescent in all channels.

8. With the help of FlowJo, once the population of beads is analyzed, view the number of recovered beads in each sample in the Statistics column.

9. Calculate the exact number of Precision Count Beads added to each tube using the following formula and values:

$$\text{Precision Count Beads added } = \frac{50\ \mu\text{l} \times \text{N particles}}{1000\ \mu\text{l}},$$

where the amount of beads added is 50 µl and the bead concentration (indicated on the product vial) is N particles/ml.

When calculating total bead number, we usually acquire around 50,000 beads per tube. This number should be similar in all sample tubes, and great variations in one tube may indicate inaccurate pipetting or mixing. However, the total bead number of an assay (in our case, 50,000 beads) can vary greatly depending on the speed of acquisition and lot number of your product and should be determined by the user.

10. To calculate the exact cell number of a specific population corresponding to each tube, apply the following formula:

$$\text{Number of cells} = \frac{\text{cell count recovered per population} \times \text{Precision Count Beads added}}{\text{Precision Count Beads recovered in the tube}}.$$

REAGENTS AND SOLUTIONS

Percoll, 1.088 g/ml

31.2 ml Percoll (e.g., GE Healthcare, 17-0891-01)
5 ml of 10× PBS
13.8 ml distilled deionized water
Store at 4°C for up to 6 months

Percoll, 1.122 g/ml

44.4 ml Percoll (e.g., GE Healthcare, 17-0891-01)
5 ml of 10× PBS
0.6 ml distilled deionized water
Store at 4°C for up to 6 months

pHrodo-Green

500 µg pHrodo-Green lyophilized powder (e.g., Thermo Fisher Scientific, P35369)
75 µl dimethyl sulfoxide, 99% pure (e.g., Sigma-Aldrich, D8418)
Store at –80°C for up to 6 months

It is best to use pHrodo-Green stock solution fresh. If stored at −80°C, test the efficacy of fluorescently labeled myelin upon conjugation as described by the manufacturer's instructions.

COMMENTARY

Background Information

Phagocytosis assays with fluorescence-conjugated myelin

Assays for evaluating myelin phagocytosis in microglia/macrophage populations have been frequently used in the study of this cell population. Most assays have been performed in cell cultures with specific cell lines such as BV-2 (Hendrickx et al., 2014; Maheshwari et al., 2013; Van der Goes, Kortekaas, Hoekstra, Dijkstra, & Amor, 1999), in macrophage cultures obtained from bone marrow–derived macrophages (Diaz-Lucena et al., 2018; Rolfe et al., 2017), in peritoneal macrophages (da Costa, van der Laan, Dijkstra, & Bruck, 1997; Garcia-Mateo et al., 2014; Hendriks et al., 2008; van der Laan et al., 1996), and in microglial cultures from rodents or human tissue

(Greenhalgh et al., 2018; Hendrickx et al., 2014). To our knowledge, only Greenhalgh et al. (2018) have analyzed microglia obtained from tissue, in their case after separation of microglia by magnetic columns. While the use of cultured cells is an approach that can give additional data with respect to myelin phagocytosis, microglia suffer phenotypic modifications when cultured that can modify the results compared with those observed with uncultured tissue microglia (Dubbelaar, Kracht, Eggen, & Boddeke, 2018). Here we analyze microglial phagocytosis capacity a short time after extraction from CNS tissue, which facilitates obtaining data more closely reflecting in vivo conditions.

Microglia/macrophage phagocytosis has been analyzed with different approaches. Here we describe a flow cytometry approach that allows for accurate and fast quantification of the phagocytic population. In these protocols we only identify the microglia and macrophage populations, but additional antibodies can be used to further characterize the expression of other receptors or molecules in the analyzed phagocytic populations (Greenhalgh et al., 2018; Manich et al., 2020).

Conjugation of myelin with fluorescence for detection

Several conjugation options with fluorescence have been used for myelin detection. In general, myelin conjugation is performed through linkage of fluorophores with proteins at their amino terminus, as in the case for pHrodo-Green, pHrodo-Red, and carboxyfluorescein succinimidyl ester (Greenhalgh et al., 2018; Hendrickx et al., 2014; Rolfe et al., 2017). Lipophilic staining with, for example, Dil, which binds to the lipids of myelin and emits in the TRITC spectrum, has also been used (da Costa et al., 1997; Diaz-Lucena et al., 2018; Garcia-Mateo et al., 2014; Hendriks et al., 2008; van der Laan et al., 1996). Other lipophilic dialkylcarbocyanines that offer different features and emission and excitation spectra, including DiO, DiD, or DiR, may be interesting candidates for myelin conjugation.

Here we used pHrodo because of the advantages offered by this fluorophore. Among them is the increase in fluorescence when pHrodo is placed in an acidic environment (Hendrickx et al., 2014), which enhances detection of pHrodo internalized in phagolysosomes and reduces possible background generated by an excess of conjugated myelin in the samples. On the other hand, detection is minimized of myelin particles that are bound to receptors or that have been internalized but are not yet in phagolysosomes.

Myelin phagocytosis assay after cell isolation from tissue

Time is one of the most critical factors in myelin phagocytosis assays. As a matter of fact, differences between populations may not be detected due to insufficient incubation time or, oppositely, too long of an incubation time, as differences in the kinetics of phagocytic uptake between two cell populations may not be detected. In Garcia-Mateo et al. (2014) and Hendrickx et al. (2014), we can find examples with cell culture assays of differences in myelin phagocytosis kinetics between, for example, microglia and macrophage populations. Most studies performed with cultured cells suggest incubation times of ∼1.5 hr. In isolated tissue, we and others have studied myelin phagocytosis with 4 hr of incubation (Greenhalgh et al., 2018; Manich et al., 2020), in our case due to increased myelin phagocytosis compared with 1.5 hr.

Critical Parameters and Troubleshooting

During the Basic Protocol, several key points can determine good cell number recovery and myelin phagocytosis assay. Among the most important points, the following should be highlighted: (1) cell tissue extraction using mesh, which is important for good cell recovery; (2) time of tissue digestion, which allows for good cell recovery but if too lengthy can activate microglial cells; (3) obtaining cells from the interphase layer and upper phase layer of the Percoll gradient, which should be performed by the same user to obtain consistent results and to ensure good myelin separation; (4) time of myelin incubation (4 hr suggested based on our experience but longer or shorter times as determined by the user); (5) staining controls (positive and negative controls to properly evaluate positive staining); and (6) appropriate flow cytometer compensation with single colors for detection.

Critical points should be specially monitored; possible problems that arise in the experiment might be related to the management of these critical points. We provide a troubleshooting guide to detect and solve the most common problems related to this protocol (Table 1).

Understanding Results

Flow cytometric analysis will indicate the percentage of cells within the CD11b/CD45

Table 1 Troubleshooting Guide for Myelin Phagocytosis Assay

Problem	Possible cause	Solution
Low cell recovery	Insufficient extraction of cells when passing through membranes	Spend more time passing samples through 160- and 70-μm membranes
		Ensure collection of all remaining sample
	Incomplete digestion	Check calculations for digestion solution
		Check state of reagents used, as well as temperature and agitation conditions
	Increased cell death	Practice protocol more
		Shorten time spent performing the protocol
		Avoid rough and abrupt cell manipulation
		Avoid elevated room temperatures while performing the protocol; maintain cells at 4°C from Percoll separation until acquisition
		Avoid maintaining cells in pellet
Percoll gradient does not clearly separate in phases	Percoll solutions are not correctly prepared or are expired	Check calculations and reagent state of Percoll solutions
	Percoll has mixed after centrifugation	Manipulate Percoll tubes carefully after centrifugation
		Check brake speed, which should be at minimum values
		Centrifuge tubes again at same speed and time indicated in the protocol
Low myelin phagocytosis	Incorrect myelin conjugation	Check myelin efficiency in fluorescence emission according to manufacturer's instructions
	Low myelin quantity	Vortex myelin well before placing conjugated myelin into sample tubes
		Increase amount of total myelin used in experiment
	Insufficient time of myelin incubation	Increase time of myelin incubation
	Incomplete myelin withdrawal during Percoll gradient	Carefully remove top myelin phase formed after Percoll gradient centrifugation before cell isolation
Significant variations in bead recovery	Variation in amount of beads added to sample tubes	Vortex well before adding beads in each sample tube
		Use the same vial of beads for the entire experiment
		Clean pipette tips before adding beads to tubes to avoid volume errors
	Variations in amount of beads recovered	Vortex sample tubes well immediately before acquisition
Graphs with high background levels	Insufficient washing steps	Increase washing steps between incubations
	Too much myelin creating nonspecific staining	During Percoll centrifugation, avoid myelin recovery as much as possible; if needed, recover less sample

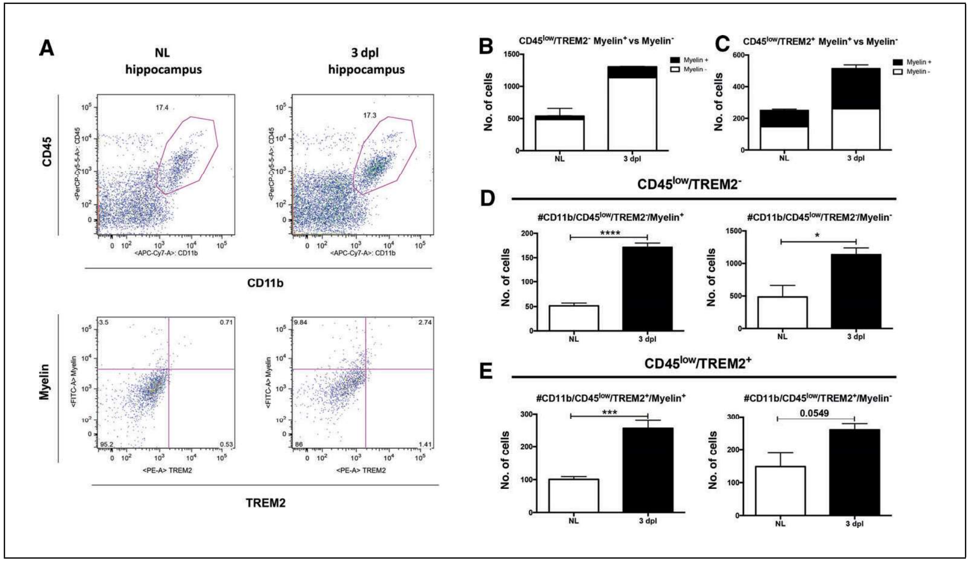

Figure 5 Results obtained after myelin phagocytosis assay. An example of analysis of microglia TREM2+ phagocytic capacity is shown. (**A**) Top diagrams indicate selection of the microglial population in the nonlesioned (NL) and lesioned hippocampus (after perforant pathway transection [PPT]; 3 days post lesion [dpl]). Bottom diagrams show CD11b+/CD45+ cell populations gated for pHrodo Green STP Ester–conjugated myelin and TREM2 staining in both NL and PPT-lesioned hippocampus. (**B–E**) Results of phagocytic microglia (CD11b/CD45^{low}) in TREM2+ and TREM2– populations obtained after calculating the total number of cells for each population. TREM2– microglia show a decreased proportion of phagocytosis compared with TREM2+ microglia in both NL and 3 dpl hippocampus (B, C). In panels D and E, comparison of TREM2– and TREM2+ microglia show a statistically significant increase in the number of phagocytic cells, whereas this increase is less pronounced in the microglial TREM2– and TREM2+ phagocytic populations (unpaired Student's *t*-test; *$P < 0.05$, ***$P < 0.001$, ****$P < 0.0001$).

population or, if specified during the analysis, within the CD11b+/CD45^{high} and/or CD11b+/CD45^{low} populations that have phagocytized myelin, as well as other populations studied by the user through additional antibody staining. One example of results achieved with additional antibody staining is illustrated in Figure 5, in which TREM2+ microglia and/or macrophage myelin phagocytosis was evaluated in lesioned and nonlesioned hippocampus. In this assay, additional antibodies were included in the specific incubation steps (Basic Protocol step 50): (1) anti-TREM2-PE-conjugated antibody (1:400 dilution; R&D Company, FAB17291P) in the whole antibody combination; (2) isotype antibody (1:400 dilution; rat IgG2B PE-conjugated antibody; R&D Company, IC013P) for negative controls; and (3) single-color antibody (anti-CD11b-PE; BD Biosciences, 557397) for compensation. Proper analysis of these populations was performed by plotting within CD11b+/CD45^{high} or CD11b+/CD45^{low} populations of TREM2+ and TREM2– cells (i.e., CD11b+/CD45^{low}/TREM2– or CD11b+/CD45^{low}/TREM2+ populations) and then detecting myelin+ and myelin– cells, as explained in Basic Protocol steps 63 to 67 (specific plotting strategy found in Manich et al., 2020). In both general or specific stainings, differences in the percentage of cells between groups or conditions could indicate higher or lower efficiency in myelin phagocytosis capacity (as seen in the phagocytic TREM2+ population; Figure 5B,C; Manich et al., 2020). Also, if Support Protocol 2 has been used, the user will obtain additional information on the total number of phagocytic cells, as we also observed in phagocytic TREM2+ cells (Fig. 5). In addition, other parameters, such as mean fluorescence intensity (Maheshwari et al., 2013; van der Laan et al., 1996) or geometric mean fluorescence intensity (Hendrickx et al., 2014; Van der Goes et al., 1999) can provide information on the estimated average of myelin phagocytized by cells and the total amount of myelin phagocytized by cells, respectively. When analyzing results, the time of incubation should be considered as a factor that may affect the results obtained in the experiment. This fact also may prevent the user from making general conclusions from data obtained from the nonphagocytic population as, depending on the conditions of the experiment, one cannot confirm if certain microglia/macrophages will either not phagocytize myelin or have not done so yet.

Time Considerations

The time required to perform the entire protocol is ∼16 hr. The total time of the experiment can be reduced or extended depending on the number of samples analyzed and user experience. Time is a critical parameter for cell survival, and therefore it should be reduced to the minimum possible. Also, the time used for myelin incubation should be critically assayed and determined before executing this experiment.

Acknowledgments

The authors thank Dr. Manuela Costa for help on the flow cytometer. Some illustrative figures were created with BioRender. This work was supported by the Ministerio de Ciencia e Innovación (BFU2017-87843-R) to BCL.

Conflicts of Interest

The authors declare no conflicts of interest.

Author Contributions

Ariadna Regina Gómez-López: Conceptualization, Data curation, Formal analysis, Methodology, Software, Supervision, Validation, Visualization, Writing-original draft, **Gemma Manich**: Conceptualization, Data curation, Investigation,Methodology, Supervision, Validation, Visualization, Writing-original draft, **Mireia Recasens**: Conceptualization, Data curation, Formal analysis, Methodology, Software, Supervision, Validation, Visualization, Writing-review & editing, **Beatriz Almolda**: Conceptualization, Data curation, Formal analysis, Investigation, Methodology, Software, Supervision, Validation, Writing-review & editing, **Berta González**: Conceptualization, Funding acquisition, Investigation, Project administration, Resources, Supervision, Validation, Writing-review & editing, **Bernardo Castellano**: Conceptualization, Funding acquisition, Investigation, Project administration, Resources, Supervision, Validation, Writing-review & editing

Data Availability Statement

Data sharing not applicable – no new data generated

Literature Cited

Almolda, B., Costa, M., Montoya, M., Gonzalez, B., & Castellano, B. (2009). CD4 microglial expression correlates with spontaneous clinical improvement in the acute Lewis rat EAE model. *Journal of Neuroimmunology*, *209*, 65–80. doi: 10.1016/j.jneuroim.2009.01.026.

Aziz, M., Yang, W. L., & Wang, P. (2013). Measurement of phagocytic engulfment of apoptotic cells by macrophages using pHrodo succinimidyl ester. *Current Protocols in Immunology*, *100*, 14.31.1–14.31.8. doi: 10.1002/0471142735.im1431s100.

Beccari, S., Diaz-Aparicio, I., & Sierra, A. (2018). Quantifying microglial phagocytosis of apoptotic cells in the brain in health and disease. *Current Protocols in Immunology*, *122*, e49. doi: 10.1002/cpim.49.

da Costa, C. C., van der Laan, L. J., Dijkstra, C. D., & Bruck, W. (1997). The role of the mouse macrophage scavenger receptor in myelin phagocytosis. *European Journal of Neuroscience*, *9*, 2650–2657. doi: 10.1111/j.1460-9568.1997.tb01694.x.

Diaz-Lucena, D., Gutierrez-Mecinas, M., Moreno, B., Martinez-Sanchez, J. L., Pifarre, P., & Garcia, A. (2018). Mechanisms involved in the remyelinating effect of sildenafil. *Journal of Neuroimmune Pharmacology*, *13*, 6–23. doi: 10.1007/s11481-017-9756-3.

Donovan, J., & Brown, P. (2001). Anesthesia. *Current Protocols in Immunology*, *27*, 1.4.1–1.4.5. doi: 10.1002/0471142735.im0104s27.

Dubbelaar, M. L., Kracht, L., Eggen, B. J. L., & Boddeke, E. (2018). The kaleidoscope of microglial phenotypes. *Frontiers in Immunology*, *9*, 1753. doi: 10.3389/fimmu.2018.01753.

Galloway, D. A., Phillips, A. E. M., Owen, D. R. J., & Moore, C. S. (2019). Phagocytosis in the brain: Homeostasis and disease. *Frontiers in Immunology*, *10*, 790. doi: 10.3389/fimmu.2019.00790.

Garcia-Mateo, N., Ganfornina, M. D., Montero, O., Gijon, M. A., Murphy, R. C., & Sanchez, D. (2014). Schwann cell-derived apolipoprotein D controls the dynamics of post-injury myelin recognition and degradation. *Frontiers in Cellular Neuroscience*, *8*, 374. doi: 10.3389/fncel.2014.00374.

Greenhalgh, A. D., Zarruk, J. G., Healy, L. M., Baskar Jesudasan, S. J., Jhelum, P., Salmon, C. K., … David, S. (2018). Peripherally derived macrophages modulate microglial function to reduce inflammation after CNS injury. *PLoS Biology*, *16*, e2005264. doi: 10.1371/journal.pbio.2005264.

Hendrickx, D. A., Schuurman, K. G., van Draanen, M., Hamann, J., & Huitinga, I. (2014). Enhanced uptake of multiple sclerosis-derived myelin by THP-1 macrophages and primary human microglia. *Journal of Neuroinflammation*, *11*, 64. doi: 10.1186/1742-2094-11-64.

Hendriks, J. J., Slaets, H., Carmans, S., de Vries, H. E., Dijkstra, C. D., Stinissen, P., & Hellings,

N. (2008). Leukemia inhibitory factor modulates production of inflammatory mediators and myelin phagocytosis by macrophages. *Journal of Neuroimmunology*, *204*, 52–57. doi: 10.1016/j.jneuroim.2008.07.015.

Kotter, M. R., Li, W. W., Zhao, C., & Franklin, R. J. (2006). Myelin impairs CNS remyelination by inhibiting oligodendrocyte precursor cell differentiation. *Journal of Neuroscience*, *26*, 328–332. doi: 10.1523/JNEUROSCI.2615-05.2006.

Lampron, A., Larochelle, A., Laflamme, N., Prefontaine, P., Plante, M. M., Sanchez, M. G., … Rivest, S. (2015). Inefficient clearance of myelin debris by microglia impairs remyelinating processes. *Journal of Experimental Medicine*, *212*, 481–495. doi: 10.1084/jem.20141656.

Larocca, J. N., & Norton, W. T. (2007). Isolation of myelin. *Current Protocols in Cell Biology*, *33*, 3.25.1–3.25.19. doi: 10.1002/0471143030.cb0325s33.

Lloyd, A. F., & Miron, V. E. (2019). The pro-remyelination properties of microglia in the central nervous system. *Nature Reviews Neurology*, *15*, 447–458. doi: 10.1038/s41582-019-0184-2.

Maciorowski, Z., Chattopadhyay, P. K., & Jain, P. (2017). Basic multicolor flow cytometry. *Current Protocols in Immunology*, *117*, 5.4.1–5.4.38. doi: 10.1002/cpim.26.

Maheshwari, A., Janssens, K., Bogie, J., Van Den Haute, C., Struys, T., Lambrichts, I., … Hellings, N. (2013). Local overexpression of interleukin-11 in the central nervous system limits demyelination and enhances remyelination. *Mediators of Inflammation*, *2013*, 685317. doi: 10.1155/2013/685317.

Manglani, M., Gossa, S., & McGavern, D. B. (2018). Leukocyte isolation from brain, spinal cord, and meninges for flow cytometric analysis. *Current Protocols in Immunology*, *121*, e44. doi: 10.1002/cpim.44.

Manich, G., Gómez-López, A. R., Almolda, B., Villacampa, N., Recasens, M., Shrivastava, K., … Castellano, B. (2020). Differential roles of TREM2+ microglia in anterograde and retrograde axonal injury models. *Frontiers in Cellular Neuroscience*, *14*, 567404. doi: 10.3389/fncel.2020.567404.

McKinnon, K. M. (2018). Flow cytometry: An overview. *Current Protocols in Immunology*, *120*, 5.1.1–5.1.11. doi: 10.1002/cpim.40.

Miller, S. D., Karpus, W. J., & Davidson, T. S. (2010). Experimental autoimmune encephalomyelitis in the mouse. *Current Protocols in Immunology*, *88*, 15.1.1–15.1.20. doi: 10.1002/0471142735.im1501s88.

Miron, V. E., Boyd, A., Zhao, J. W., Yuen, T. J., Ruckh, J. M., Shadrach, J. L., … ffrench-Constant, C. (2013). M2 microglia and macrophages drive oligodendrocyte differentiation during CNS remyelination. *Nature Neuroscience*, *16*, 1211–1218. doi: 10.1038/nn.3469.

Peferoen, L., Kipp, M., van der Valk, P., van Noort, J. M., & Amor, S. (2014). Oligodendrocyte-microglia cross-talk in the central nervous system. *Immunology*, *141*, 302–313. doi: 10.1111/imm.12163.

Pul, R., Chittappen, K. P., & Stangel, M. (2013). Quantification of microglial phagocytosis by a flow cytometer-based assay. *Methods in Molecular Biology*, *1041*, 121–127. doi: 10.1007/978-1-62703-520-0_14.

Ramesha, S., Rayaprolu, S., & Rangaraju, S. (2020). Flow cytometry approach to characterize phagocytic properties of acutely-isolated adult microglia and brain macrophages in vitro. *Journal of Visualized Experiments*, *160*, e61467. doi: 10.3791/61467.

Reeves, J. P., & Reeves, P. A. (2001). Removal of lymphoid organs. *Current Protocols in Immunology*, *1*, 1.9.1–1.9.3. doi: 10.1002/0471142735.im0109s01.

Rolfe, A. J., Bosco, D. B., Broussard, E. N., & Ren, Y. (2017). In vitro phagocytosis of myelin debris by bone marrow-derived macrophages. *Journal of Visualized Experiments*, *130*, e56322. doi: 10.3791/56322.

Van der Goes, A., Kortekaas, M., Hoekstra, K., Dijkstra, C. D., & Amor, S. (1999). The role of anti-myelin (auto)-antibodies in the phagocytosis of myelin by macrophages. *Journal of Neuroimmunology*, *101*, 61–67. doi: 10.1016/s0165-5728(99)00133-2.

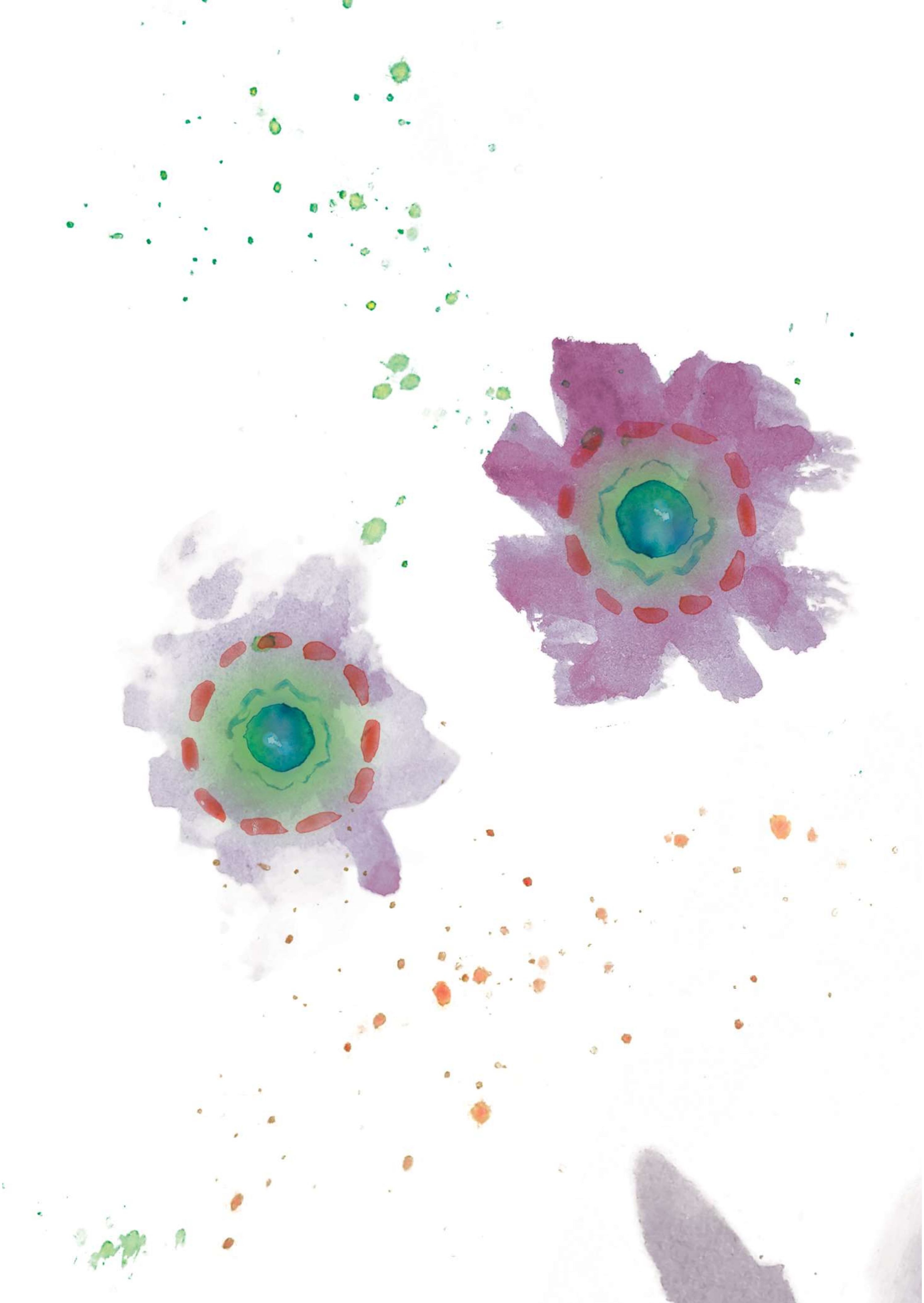van der Laan, L. J. W., Ruuls, S. R., Weber, K. S., Lodder, I. J., Döpp, E. A., & Dijkstra, C. D. (1996). Macrophage phagocytosis of myelin in vitro determined by flow cytometry: Phagocytosis is mediated by CR3 and induces production of tumor necrosis factor-α and nitric oxide. *Journal of Neuroimmunology*, *70*, 145–152. doi: 10.1016/s0165-5728(96)00110-5.